

**PERFORMANCE OF BAFFLES IN A
SWAY EXCITED SLOSHING
RECTANGULAR TANK**

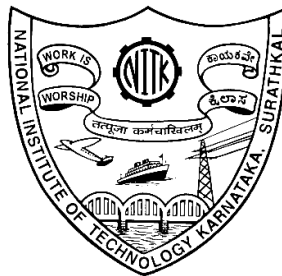
Thesis

Submitted in partial fulfilment of the requirements for the degree of

DOCTOR OF PHILOSOPHY

by

**SAHAJ K. V.
165075AM16F11**



**DEPARTMENT OF WATER RESOURCES & OCEAN ENGINEERING
NATIONAL INSTITUTE OF TECHNOLOGY KARNATAKA**

SURATHKAL, MANGALURU – 575025

DECEMBER 2022

PERFORMANCE OF BAFFLES IN A SWAY EXCITED SLOSHING RECTANGULAR TANK

Thesis

Submitted in partial fulfilment of the requirements for the degree of
DOCTOR OF PHILOSOPHY

by

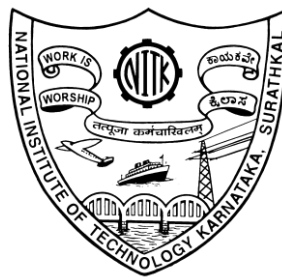
SAHAJ K.V.

165075AM16F11

Under the guidance of

Dr. T. NASAR

Associate Professor



**DEPARTMENT OF WATER RESOURCES AND OCEAN ENGINEERING
NATIONAL INSTITUTE OF TECHNOLOGY KARNATAKA,
SURATHKAL, MANGALORE - 575025
DECEMBER 2022**

DECLARATION

By the Ph.D. Research Scholar

I hereby *declare* that the Research Thesis entitled **"PERFORMANCE OF BAFFLES IN A SWAY EXCITED SLOSHING RECTANGULAR TANK"**, which is being submitted to the **National Institute of Technology Karnataka, Surathkal** in partial fulfilment of the requirements for the award of the Degree of **Doctor of Philosophy** in the **Department Of Water Resources & Ocean Engineering** is a *bonafide report of the research work carried out by me*. The material contained in this Research Thesis has not been submitted to any University or Institution for the award of any degree.



165075AM16F11, SAHAJ K V

(Register Number, Name & Signature of the Research Scholar)

Department of Water Resources and Ocean Engineering

National Institute of Technology Karnataka, Surathkal

Place: NITK-Surathkal

Date:

CERTIFICATE

This is to certify that the Research Thesis entitled
**"PERFORMANCE OF BAFFLES IN A SWAY EXCITED
SLOSHING RECTANGULAR TANK"** submitted by **SAHAJ K V**
(Register Number: 165075 AM16F11) as the record of the
research work carried out by him, is *accepted as the Research
Thesis submission* in partial fulfilment of the requirements for
the award of degree of **Doctor of Philosophy**.

T. Nasar
26/12/22

Dr. T. Nasar

Associate Professor
Research Supervisor



B. M. Dodamani
Prof. B. M. Dodamani

Chairman - DRPC

Department of Water Resources and Ocean Engineering
National Institute of Technology Karnataka, Surathkal

Chairman (DRPC)
Dept. of Water Resources & Ocean Engineering

ACKNOWLEDGEMENT

With deep sense of gratitude, I express my heartfelt thanks to my research supervisor Dr. T. Nasar, Associate Professor, Department of Water Resources and Ocean Engineering, NITK for his invaluable guidance, encouragement and motivation throughout my research work. I am indebted to him for his wholehearted interest and keenness in every phase of research work and thesis preparation. His moral support, guidance, interactions, discussions and precious suggestions have greatly helped me to complete this research work. It has been my greatest opportunity and pleasure to work under him. His crucial comments have guided me to publish my research work in acclaimed International Journals. I am grateful to Prof. B. M. Dodamani, Head of the Department of Water Resources and Ocean Engineering, NITK, Surathkal for his continuous support during the thesis submission.

I acknowledge my sincere thanks to Research Progress Assessment Committee members, Dr. A. S. Balu, Department of Civil Engineering and Prof. Subba Rao, Department of Water Resources and Ocean Engineering for providing valuable suggestions, comments and encouragement at various stages of my research work.

I wish to thank Prof. Amba Shetty, former HOD of Department of Water Resources and Ocean Engineering NITK, Surathkal for her support and permitting me to use the departmental laboratory facilities that helped in completing my research work. I am grateful to Prof. Subba Rao, for his indispensable help and suggestions during my journey. I also extend my heartfelt gratitude to Prof. G. S. Dwarakish former Head of the Department and all the faculty members of Water Resources and Ocean Engineering Department for their help and support.

My special thanks to Mr. Balakrishna, GIS Lab, who made sure that laboratory facilities were working fine all the time and helped me out whenever in trouble. My sincere thanks to Mr. Seetharam Sir, Mr. Anil Kumar for their help in department facilities. I wish to appreciate the efforts and co-operation rendered by non-teaching staff Mr. Gopal Krishna, Mr. Padmanabha, Mr. Harish (FM Lab), Ananda, Shashidhar, Shailesh, Harish (SOM), Niranjana Shetty and Ashwini & office staff Ms.

Sweekritha bhandary and Ramu of Water Resources and Ocean Engineering Department.

I gratefully acknowledge the emotional support and encouragement provided by my dear colleagues Dr. Pramod Kumar Kappadi, Mr. Pruthvin Shetty, Mr. Pandu Shetty Mr. Puneethraj, Mr. Niranjan, Mr. Sumanth and other fellow lab-mates, who pushed me every time to walk extra-mile towards the goal. I am indebted to the support, technical suggestions and all the help rendered by Mr. Kumaran V., Mr. Raveesh R M and Mr. Murugan N. whose contributions during Ansys Simulation is incredible.

I would like to express my sincere thanks to Dr. Vijay K. G. Assistant Professor IITM Chennai and Dr. PramodKumar Kappadi Assistant Professor DSCE Bengaluru for their support in rectifying errors in my journal papers. I sincerely recognize the role of Mr. Manjunath Madikeari, Assistant Professor GITAM University Bengaluru in constantly motivating me in this wonderful journey.

My special thanks to Mithun P C, Kishan Salian, Puneeth Naik, Harsha H S, Basavaraj N H, Avinash K L and Hithesh Poojary best friend of mine who stood by me throughout this journey with their support, suggestions and timely help extended at NITK. I would like to cherish the love and support shown by my NITK friends Praveen K M, Vishwanath mane, Surakshitha, Ayilobeni Kikon, Vijay Suryavamshi, Shaik Abdul shareef, Shaik Salma, Sai Charan and Sandeep Reddy during my stay at NITK.

I am forever grateful to my father Sri. Kanthappa Alangar, mother Smt. Vimala K and my elder sister Mrs. Nisha Kiran K V who provided me the best available education and encouraged in all my endeavors. I am grateful to my wife Mrs. Ramya Kulal who has been influential in motivating me in this journey with her moral support and cooperation & also extended the necessary financial aid during the extension period. I would like to thank my father-in-law Mr. Sanjeeva Moolya & brother-in-law's Mr. Manoj Kumar and Mr. Sushanth for their support and encouraging me in every possible way.

I lovingly acknowledge the moral support and help extended by my best friends during this journey. Their informal support and encouragement have been very crucial. I am grateful to everybody who helped and encouraged me during this memorable journey of research work.

SAHAJ K V

Dedication

I dedicate this thesis to my beloved parents, my kind-hearted
elder sister and my caring wife,
for their eternal love

&

My loving mother-in-law Late Jayalaxmi,
who stays in my heart forever

Along with those close to my heart
Family members and Friends

ABSTRACT

The liquid in partially filled tanks tends to slosh when subjected to external disturbances. The safety of liquid transportation system necessitates the liquid sloshing problem with great practical importance. The knowledge of liquid sloshing frequency and hydrodynamic force on the wall is essential for seismic design of liquid storage tanks. Liquid motion in partially filled tanks may cause large structural loads if the period of tank motion is close to the natural period of fluid inside the tank. The large liquid movement in tanks creates highly localized impact pressure on tank walls and also displays a violent disturbance in the fluid. Hence, this highly nonlinear nature of the problem is the greatest interference in solving such a problem analytically and even computationally. Ship structures are likely subjected to impact pressure actions arising from sloshing, slamming, and green seas while in service. The accelerations arising from the motions of a ship in a sea way produce sloshing loads, that is, inertial reactions, on partially filled liquid cargo tank structures of the ship. Motions of liquid cargo vessels such as oil tankers often produce severe sloshing loads. Sloshing implies movement of a free liquid surface inside a vessel. A shake-table experiment for various depths of water is investigated to examine the effect of sloshing. The shake table is designed and devised to measure the sloshing force and the concept is tried for patentability as well. An experimental program is performed to study the phenomena of liquid sloshing and to assess the sloshing oscillation expected on the side walls in a partially filled rectangular tank. The sloshing tank of model scale 1:43 (Nasar et al. 2008) is fitted into the horizontal shake table. In order to examine the sloshing effects, a liquid fill level with an aspect ratio (h_s/l , where h_s is static liquid depth, l is tank length) of 0.163, 0.325 and 0.488 is considered which corresponds to 25% and 50% and 75% liquid fill levels. In view of suppressing sloshing oscillation and baffle wall configurations which is made up of acrylic sheets materials with different porosities of 4.4%, 6.8% and 9.2% and by placing baffle at a distance of $L/2$ conditions and $L/3$ & $2L/3$ conditions in a rectangular tank are studied. The movement of fluid in a rectangular tank has been studied using another set of experimental approach with mild steel plates materials and different baffle configurations were adopted for analysing the sloshing oscillation, natural frequencies and variation in wave deflection. The adopted

porosities in the present study are 15%, 20% and 25 %. Porous screen is placed inside the tank at $L/2$ location and $L/3$ & $2L/3$ locations and study is extended for single and double porous screen for better energy absorption. The parametric studies were carried out to show the liquid sloshing effects in terms of slosh frequencies, maximum free surface elevation and hydrodynamic forces acting on the tank walls. Capacitance wave probes have been placed at tank ends to record the free surface water elevation. At distinct locations along the length of the tank, time histories of sloshing oscillations (η) are recorded. The behaviour of sloshing oscillation is observed for the excitation. The frequencies of excitation ranges from 0.4566 Hz to 1.9757 Hz which covers up to fifth mode sloshing frequencies and the amplitude of 8mm is adopted.

Sloshing force is captured by load cells and it is also analysed. Linear Variable Displacement Transducers (LVDT) are used to measure the displacement of the shake table. In the present study single and dual porous screen under the action of wave signals were analysed to understand the wave control performance due to porosity parameters. The results of maximum free surface elevation (η_{max}), root mean square surface elevation (η_{rms}), Sloshing Dynamics, sloshing forces (F'_{max} , F'_{av} and F_s), energy dissipation (E_w) and spectral moments (m_o) are presented here. The suppression of resonant sloshing motion by porous baffle is analysed. A higher sloshing oscillation is observed for the aspect ratio (h_s/l) of 0.325 than compared with other two fill levels. The tank with a water depth of $h_s/l= 0.325$ and porous baffle of 15% porosity shows attenuation in sloshing force of about 32.78% whereas the 20% and 25% porosities of baffles show attenuation of 39.74% and 38.86% respectively in comparison with no baffle condition at $L/3$ & $2L/3$ locations.

The sloshing of liquid in containers is a ubiquitous phenomenon that represents one of the most fundamental fluid-structure interaction problems. By virtue, the liquid in a partially filled tank tends to slosh when subjected to external disturbances and is a vicious resonant fluid motion in a moving tank. In view of this difficulty, the sloshing effects are analysed by employing Computational Fluid Dynamics (CFD) and is validated with experimental tests. The fill levels of the sloshing tanks are varied for three different fill levels of aspects ratios (h_s/l - 0.163, 0.325 and 0.488). Further, a comparative study is performed with porous and no porous presence of baffle

conditions. The results from CFD correlate well with the experimental measurements on the sloshing effect. The numerical study shows a good correlation with the experiment results and the deviation of numerical simulation in comparison with experimental findings is found to be 9.24%. Results presented in this study can be used in the ship tanks in view of dynamic stability, reduction of sloshing energy and avoidance of roof impact.

Keywords: Sloshing Oscillation, Fluid-Structure Interaction, Computational Fluid Dynamics, Spectral Moments, Energy Dissipation and Excitation Frequencies.

TABLE OF CONTENTS

	Page No.
ABSTRACT	i
TABLE OF CONTENTS	iv
LIST OF FIGURES	vii
LIST OF TABLES	xvii
LIST OF ABBREVIATIONS	xviii
CHAPTER 1	
INTRODUCTION	1
1.1 GENERAL	1
1.2 SLOSHING IN LIQUID STORAGE TANKS	6
1.3 SLOSHING IN RECTANGULAR TANKS	7
1.4 SHREDS OF EVIDENCE OF SLOSHING	7
1.5 PROBLEM DEFINITION	8
1.6 ORGANIZATION OF THE THESIS	8
1.7 OBJECTIVES	9
CHAPTER 2	
LITERATURE REVIEW	11
2.1 INTRODUCTION	11
2.2 SIGNIFICANCE OF LIQUID SLOSHING	11
2.3 COMPUTATIONAL STUDIES	11
2.4 NUMERICAL AND EXPERIMENTAL STUDIES	14
2.5 CLOSURE	26
CHAPTER 3	
PROBLEM DEFINITION AND METHODOLOGY	27
3.1 GENERAL	27
3.2 PROBLEM DEFINITION	27
3.3 METHODOLOGY	27
3.4 EXPERIMENTAL SETUP	29
3.4.1 Sloshing Tank Description	30

3.5	INSTRUMENTATION	30
3.6	POROUS BAFFLE	35
	3.6.1 Acrylic Sheet	35
	3.6.2 Mild Steel Plate	37
3.7	BASE SHEAR FORCE	38
3.8	SHAKE TABLE MOTION	39
CHAPTER 4		
EXPERIMENTAL INVESTIGATION WITHOUT BAFFLES		41
4.1	RESULTS AND DISCUSSION	41
	4.1.1 Sloshing Oscillation Time Histories (η)	41
	4.1.2 Maximum Free Surface Response (η_{max})	43
	4.1.3 Root Mean Square Surface Elevation (η_{rms})	46
	4.1.4 Sloshing Dynamics	47
	4.1.5 Sloshing Force	50
4.2	CLOSURE	52
CHAPTER 5		
EXPERIMENTAL INVESTIGATION WITH BAFFLES		55
5.1	RESULTS AND DISCUSSION	55
5.2	FREE SURFACE RESPONSE	55
	5.2.1 Acrylic Sheet	55
	5.2.2 Mild Steel Plate	64
5.3	MAXIMUM FREE SURFACE ELEVATION	72
	5.3.1 Acrylic Sheet	72
	5.3.2 Mild Steel Plate	79
5.4	ENERGY DISSIPATION	84
	5.4.1 Acrylic Sheet	85
	5.4.2 MS Plate	89
5.5	SCREEN FORCE (F_x)	93
5.6	SLOSHING FORCE (F_S)	100
5.7	SPECTRAL MOMENT (m_0)	112

CHAPTER 6	
NUMERICAL PERFORMANCE CHARACTERISTICS OF SLOSHING RECTANGULAR TANK	119
6.1 BACKGROUND	119
6.2 COMPUTATIONAL FLUID DYNAMICS	119
6.2.1 Ansys- Fluent CFD Platform	121
6.3 MATHEMATICAL FORMULATION AND NUMERICAL SIMULATION	121
6.4 SOLVER CONTROLS	124
6.5 PRELIMINARY INVESTIGATION	126
6.5.1 Modelling of geometry	126
6.5.2 Meshing details	128
6.5.3 Boundary Conditions	131
6.5.4 Influence of the numerical wave sloshing tank	132
6.5.5 Validation between ANSYS Fluent and Experimental Results	134
6.5.6 Relative error calculation	141
6.6 CLOSURE	145
CHAPTER 7	
CONCLUSIONS	147
7.1 SUMMARY	147
7.2 CONCLUSIONS	147
7.3 FUTURE SCOPES	149
REFERENCES	151
APPENDIX A	159
LIST OF PUBLICATIONS	163

LIST OF FIGURES

Figure No.	Particular	Page No.
Figure 3.1	The flowchart of the experimental procedure	29
Figure 3.2	Photographic view of the rectangular tanks	30
Figure 3.3	Cross-section of the liquid tank on the shake table	31
Figure 3.4	Schematic sketch of the liquid tank on the shake table	32
Figure 3.5	Experimental setup of shake table with liquid sloshing tank	32
Figure 3.6	Photographic view of (a) Data Acquisition System b) Hydraulic actuator, (c) LVDT, (d) S-Type load cell and (e) Accelerometer	33
Figure 3.7	Calibration charts for wave probes	34
Figure 3.8	Staggered Position of 4.4%, 6.8% and 9.2% Porosities (a) (Enlarged View) (b) Staggered position porosities	35
Figure 3.9	Photographic of porous baffles (a) 6.8%, (b) 4.4% and c) 9.2%	36
Figure 3.10	Size of pores in baffles wall for different staggered position of 15%, 20% and 25% porosities	37
Figure 3.11	Photographic of porous baffles (a) 15%, (b) 20% and, (c) 25%	38
Figure 4.1	Time histories of sloshing oscillation corresponding to excitation amplitudes of 4 mm and 8 mm: (a) $h_s/l = 0.163$, (b) $h_s/l = 0.325$, (c) $h_s/l = 0.488$ respectively	42
Figure 4.2	Variation of η_{max}/A no porous baffle with various frequencies ratio for $h_s/l = 0.163$, 0.325 and 0.488	44
Figure 4.3	Variation of η_{max}/A with different frequencies ratio (f/f_1) for a) $h_s/l = 0.163$; b) $h_s/l = 0.325$ and (c) $h_s/l = 0.488$	45
Figure 4.4	Comparison of η_{rms}/A with different frequencies ratio (f/f_1) for (a) $h_s/l=0.163$; (b) $h_s/l=0.325$, (c) $h_s/l=0.488$	46

Figure 4.5	Sloshing oscillation spectra corresponding to excitation amplitude of 4 mm for $h_s/l = 0.163$, (a) $f = f_1 = 0.6059$, (b) $f = f_3 = 1.4603$, (c) $f = f_5 = 1.9637$, $h_s/l = 0.325$, (d) $f = f_1 = 0.7755$ (e) $f = f_3 = 1.5270$, (f) $f = f_5 = 1.9757$ Hz and $h_s/l = 0.488$, (g) $f = f_1 = 0.8432$, (h) $f = f_3 = 1.5302$ and (i) $f = f_5 = 1.9757$ Hz	48
Figure 4.6	Sloshing oscillation spectra corresponding to excitation amplitude of 8 mm for $h_s/l = 0.163$, (a) $f = f_1 = 0.6059$, (b) $f = f_3 = 1.4603$, (c) $f = f_5 = 1.9637$, $h_s/l = 0.325$, (d) $f = f_1 = 0.7755$, (e) $f = f_3 = 1.5270$, (f) $f = f_5 = 1.9757$ and $h_s/l = 0.488$, (g) $f = f_1 = 0.8432$, (h) $f = f_3 = 1.5302$ and (i) $f = f_5 = 1.9757$ Hz	49
Figure 4.7	Comparison of F'_{max} with different frequency ratios (f/f_1) for (a) $h_s/l = 0.163$, (b) $h_s/l = 0.325$ and (c) $h_s/l = 0.488$	51
Figure 4.8	Comparison of average of 10 largest sloshing peaks, F'_{av} with different frequency ratios (f/f_1) for (a) $h_s/l = 0.163$, (b) 0.325, and (c) 0.488	52
Figure. 5.1	Experimental free surface elevation response at $L/2$ location and excitation at natural sloshing frequencies $h_s/l = 0.163$, (a) $f = 0.6059$ Hz (f_1), (b) $f = 1.0967$ Hz (f_2), (c) $f = 1.4604$ Hz (f_3), (d) $f = 1.7376$ Hz (f_4) and (e) $f = 1.9637$ Hz (f_5)	57
Figure 5.2	Experimental free surface elevation response at $L/2$ locations and excitation at natural sloshing frequencies $h_s/l = 0.325$, (a) $f = 0.7755$ Hz (f_1), (b) $f = 1.2277$ Hz (f_2), (c) $f = 1.5270$ Hz (f_3), (d) $f = 1.7666$ Hz (f_4) and (e) $f = 1.9756$ Hz (f_5)	58

Figure 5.3	Experimental free surface elevation response at $L/2$ location and excitation at natural sloshing frequencies $h_s/l=0.488$, (a) $f= 0.8432 \text{ Hz}$ (f_1), (b) $f= 1.2468 \text{ Hz}$ (f_2), (c) $f= 1.5302 \text{ Hz}$ (f_3), (d) $f= 1.7671 \text{ Hz}$ (f_4) and (e) $f= 1.9757 \text{ Hz}$ (f_5)	59
Figure 5.4	Experimental free surface elevation response at $L/3$ and $2L/3$ locations and excitation at natural sloshing frequencies $h_s/l = 0.163$, (a) $f= 0.6059 \text{ Hz}$ (f_1), (b) $f= 1.0967 \text{ Hz}$ (f_2), (c) $f= 1.4604 \text{ Hz}$ (f_3), (d) $f= 1.7276 \text{ Hz}$ (f_4) and (e) $f= 1.9637 \text{ Hz}$	60
Figure 5.5	Experimental free surface elevation response for $L/3$ and $2L/3$ locations and excitation at natural sloshing frequencies $h_s/l = 0.325$, (a) $f= 0.7755 \text{ Hz}$ (f_1), (b) $f= 1.2277 \text{ Hz}$ (f_2), (c) $f= 1.5270 \text{ Hz}$ (f_3), (d) $f= 1.7666 \text{ Hz}$ (f_4) and (e) $f= 1.9756 \text{ Hz}$	61
Figure 5.6	Experimental free surface elevation response for baffle at $L/3$ and $2L/3$ location and excitation at natural sloshing frequencies $h_s/l=0.488$, (a) $f= 0.8432 \text{ Hz}$ (f_1), (b) $f= 1.2468 \text{ Hz}$ (f_2), (c) $f= 1.5302 \text{ Hz}$ (f_3), (d) $f= 1.7671 \text{ Hz}$ (f_4) and (e) $f= 1.9757 \text{ Hz}$ (f_5)	62
Figure 5.7	Time histories of free surface elevation with various frequency ratios at $L/2$ location for $h_s/l = 0.163$, (a) $f= 0.6059 \text{ Hz}$ (f_1), (b) $f= 1.0967 \text{ Hz}$ (f_2), (c) $f= 1.4604 \text{ Hz}$ (f_3), (d) $f= 1.7376 \text{ Hz}$ (f_4) and (e) $f= 1.9637 \text{ Hz}$ (f_5)	66
Figure 5.8	Time histories of free surface elevation with various frequency ratios at $L/2$ location for $h_s/l = 0.325$, (a) $f= 0.7755 \text{ Hz}$ (f_1), (b) $f= 1.2287 \text{ Hz}$ (f_2), (c) $f= 1.5270 \text{ Hz}$ (f_3), (d) $f= 1.7666 \text{ Hz}$ (f_4) and (e) $f= 1.9757 \text{ Hz}$ (f_5)	67

Figure 5.9	Time histories of free surface elevation with various frequency ratios at $L/2$ location for $h_s/l = 0.488$, a) $f = 0.8432 \text{ Hz}$ (f_1), (b) $f = 1.2468 \text{ Hz}$ (f_2), (c) $f = 1.5302 \text{ Hz}$ (f_3), (d) $f = 1.7671 \text{ Hz}$ (f_4) and (e) $f = 1.9757 \text{ Hz}$ (f_5)	68
Figure 5.10	Time histories of free surface elevation with various frequency ratios at $L/3$ & $2L/3$ locations for $h_s/l = 0.163$, a) $f = 0.6059 \text{ Hz}$ (f_1), (b) $f = 1.0967 \text{ Hz}$ (f_2), (c) $f = 1.4604 \text{ Hz}$ (f_3), (d) $f = 1.7376 \text{ Hz}$ (f_4) and (e) $f = 1.9637 \text{ Hz}$ (f_5)	69
Figure 5.11	Time histories of free surface elevation with various frequency ratios $L/3$ & $2L/3$ locations for $h_s/l = 0.325$, (a) $f = 0.7755 \text{ Hz}$ (f_1), (b) $f = 1.2287 \text{ Hz}$ (f_2), (c) $f = 1.5270 \text{ Hz}$ (f_3), (d) $f = 1.7666 \text{ Hz}$ (f_4) and (e) $f = 1.9757 \text{ Hz}$ (f_5)	70
Figure 5.12	Time histories of free surface elevation with various frequency ratios $L/3$ & $2L/3$ locations for $h_s/l = 0.488$, (a) $f = 0.8432 \text{ Hz}$ (f_1), (b) $f = 1.2468 \text{ Hz}$ (f_2), (c) $f = 1.5302 \text{ Hz}$ (f_3), (d) $f = 1.7671 \text{ Hz}$ (f_4) and (e) $f = 1.9757 \text{ Hz}$ (f_5)	71
Figure 5.13	Variation of η_{\max} / A no porous baffle with various frequencies ratio for $h_s/l = 0.163, 0.325$ and 0.488	73
Figure 5.14	Variation of η_{\max} / A with and without porous baffle for frequencies ratios (f/f_1), at $L/2$ location (a) $h_s/l = 0.163$ and, (b) $h_s/l = 0.325$	74
Figure 5.15	Variation of η_{\max} / A with and without porous baffle for frequencies ratios (f/f_1), at $L/2$ location (c) $h_s/l = 0.488$	75
Figure 5.16	Variation of η_{\max} / A with and without porous baffle to different frequencies ratio (f/f_1), at $L/3$ & $2L/3$ locations (a) $h_s/l = 0.163$ and, (b) $h_s/l = 0.325$	76
Figure 5.17	Variation of η_{\max} / A with and without porous baffle to different frequencies ratio (f/f_1), at $L/3$ & $2L/3$ (c) $h_s/l = 0.488$	77

Figure 5.18	Variation of η_{\max} / A with and no porous baffle with various frequencies ratio for $h_s/l = 0.163$ for $L/2$ locations	80
Figure 5.19	Variation of η_{\max} / A with and no porous baffle with various frequencies ratio for $h_s/l = 0.325$ for $L/2$ locations	80
Figure 5.20	Variation of η_{\max} / A with and no porous baffle with various frequencies ratio for $h_s/l = 0.488$ for $L/2$ locations	81
Figure 5.21	Variation of η_{\max} / A with and no porous baffle with various frequencies ratio for $h_s/l = 0.163$ for $L/3$ and $2L/3$ locations	81
Figure 5.22	Variation of η_{\max} / A with and no porous baffle with various frequencies ratio for $h_s/l = 0.325$ for $L/3$ and $2L/3$ locations	82
Figure 5.23	Variation of η_{\max} / A with and no porous baffle with various frequencies ratio for $h_s/l = 0.488$ for $L/3$ and $2L/3$ locations	82
Figure 5.24	Dimensionless dissipated energy for excitation amplitude of 8 mm no porous baffles for $h_s/l = 0.163, 0.325$ and 0.488	85
Figure 5.25	Comparison Of energy for with and without porous baffle at $L/2$ location for (a) $h_s/l = 0.163$ and, (b) $h_s/l = 0.325$	86
Figure 5.26	Comparison Of energy for with and without porous baffle at $L/2$ locations for (c) $h_s/l = 0.488$	87
Figure 5.27	Comparison of energy for with and without baffle at $L/3$ & $2L/3$ locations for (a) $h_s/l = 0.163$ and (b) $h_s/l = 0.325$	87
Figure 5.28	Comparison of Energy for with and without baffle at $L/3$ and $2L/3$ locations for (c) $h_s/l = 0.488$	88
Figure 5.29	Dimensionless dissipated energy for excitation amplitude of 8 mm with and no porous baffles for $h_s/l = 0.163$ at $L/2$ location	90

Figure 5.30	Dimensionless dissipated energy for excitation amplitude of 8mm with and no porous baffles for $h_s/l= 0.325$ at $L/2$ location	87
Figure 5.31	Dimensionless dissipated energy for excitation amplitude of 8mm with and no baffles for $h_s/l= 0.488$ at $L/2$ locations	91
Figure 5.32	Dimensionless dissipated energy for excitation amplitude of 8 mm with and no porous baffles for $h_s/l= 0.163$ at $L/3$ & $2L/3$ locations	91
Figure 5.33	Dimensionless dissipated energy for excitation amplitude of 8 mm with and no porous baffles for $h_s/l= 0.325$ at $L/3$ & $2L/3$ locations	92
Figure 5.34	Dimensionless dissipated energy for excitation amplitude of 8 mm with and no baffles for $h_s/l= 0.488$ at $L/3$ & $2L/3$ locations	92
Figure 5.35	Baffle with Load Cell (top view)	93
Figure 5.36	Experimental screen force for $h_s/l = 0.163$ and excitation at natural sloshing frequencies at $L/2$ locations (a) $f= 0.6059$ Hz (f_1), (b) $f= 1.0967$ Hz (f_2), (c) $f= 1.4604$ Hz (f_3), (d) $f= 1.7276$ Hz (f_4) and (e) $f= 1.9637$ Hz (f_5)	94
Figure 5.37	Experimental screen force for $h_s/l = 0.325$ and excitation at natural sloshing frequencies at $L/2$ locations (a) $f= 0.7755$ Hz (f_1), (b) $f= 1.2277$ Hz (f_2), (c) $f=1.5270$ Hz (f_3), (d) $f= 1.7666$ Hz (f_4) and (e) $f= 1.9756$ Hz (f_5)	95
Figure 5.38	Experimental screen force for $h_s/l = 0.488$ and excitation at natural sloshing frequencies at $L/2$ locations (a) $f= 0.8432$ Hz (f_1), (b) $f= 1.2468$ Hz (f_2), (c) $f= 1.5302$ Hz (f_3), (d) $f= 1.7671$ Hz (f_4) and (e) $f= 1.9757$ Hz (f_5)	96

Figure 5.39	Experimental screen force for $h_s/l = 0.163$ and excitation at natural sloshing frequencies at $L/3$ & $2L/3$ location (a) $f= 0.6059$ Hz (f_1), (b) $f= 1.0967$ Hz (f_2), (c) $f= 1.4604$ Hz (f_3), (d) $f= 1.7276$ Hz (f_4) and (e) $f= 1.9637$ Hz (f_5)	97
Figure 5.40	Experimental screen force for $h_s/l = 0.325$ and excitation at natural sloshing frequencies at $L/3$ & $2L/3$ locations (a) $f=0.7755$ Hz (f_1), (b) $f= 1.2277$ Hz (f_2), (c) $f=1.5270$ Hz (f_3), (d) $f= 1.7666$ Hz (f_4) and (e) $f= 1.9756$ Hz (f_5)	98
Figure 5.41	Experimental screen force for $h_s/l = 0.488$ and excitation at natural sloshing frequencies at $L/3$ & $2L/3$ locations (a) $f= 0.8432$ Hz (f_1), (b) $f= 1.2468$ Hz (f_2), (c) $f= 1.5302$ Hz (f_3), (d) $f= 1.7671$ Hz (f_4) and (e) $f= 1.9757$ Hz (f_5)	99
Figure 5.42	Dimensionless maximum sloshing force for excitation amplitude of 8mm no porous baffles for $h_s/l = 0.163$, 0.325 and 0.488	102
Figure 5.43	Time histories of sloshing force corresponding to excitation amplitude for no baffle $h_s/l= 0.163$ (a) $f = 0.6059$ Hz (f_1), $f = 1.4604$ Hz (f_3), $f = 1.9637$ Hz (f_5), $h_s/l= 0.325$ (b) $f = 0.7755$ Hz (f_1), $f = 1.5270$ Hz (f_3), $f = 1.9757$ Hz (f_5), and $h_s/l= 0.488$ (c) $f = 0.8432$ Hz (f_1), $f = 1.5302$ Hz (f_3), and $f = 1.9757$ Hz (f_5)	103
Figure 5.44	Variation of sloshing forces for with baffle and no baffle (a) and (b) for 25% fill level at $L/2$ locations	104
Figure 5.45	Variation of sloshing forces for with baffle and no baffle (a) and (b) for 50% fill level at $L/2$ locations	105
Figure 5.46	Variation of sloshing forces for with baffle and no baffle (a) and (b) for 75% fill level at $L/2$ locations	106
Figure 5.47	Variation of sloshing forces for with baffle and no baffle (a) and (b) for 25% fill level at $L/3$ & $2L/3$ locations	108
Figure 5.48	Variation of sloshing forces for with baffle and no baffle (a) and (b) for 50% fill level at $L/3$ & $2L/3$ locations	109

Figure 5.49 (a) and (b)	Variation of sloshing forces for with baffle and no baffle for 75% fill level at $L/3$ & $2L/3$ locations	110
Figure 5.50	Variation of spectral energy (m_0) with different frequencies ratio (f/f_1); for $h_s/l = 0.163$ for $L/2$ locations	113
Figure 5.51	Variation of spectral energy (m_0) with different frequencies ratio (f/f_1); for (a) $h_s/l = 0.325$ for $L/2$ locations	114
Figure 5.52	Variation of spectral energy (m_0) with different frequencies ratio (f/f_1); for (a) $h_s/l = 0.488$ for $L/2$ locations	114
Figure 5.53	Variation of spectral energy (m_0) with different frequencies ratio (f/f_1); for $h_s/l = 0.163$ for $L/3$ & $2L/3$ locations	115
Figure 5.54	Variation of spectral energy (m_0) with different frequencies ratio (f/f_1); for $h_s/l = 0.325$ for $L/3$ & $2L/3$ locations	115
Figure 5.55	Variation of spectral energy (m_0) with different frequencies ratio (f/f_1); for (a) $h_s/l = 0.488$ for $L/3$ & $2L/3$ locations	116
Figure 6.1	Geometry of the shake table model	121
Figure 6.2	Non-Iterative Time Advancement flow chart (ANSYS Fluent User Guide, 2020)	125
Figure 6.3	Schematic numerical sloshing tanks with three different fill levels with boundary conditions	127
Figure 6.4	Workflow in numerical simulations Ansys-Fluent	128
Figure 6.5	The fluent meshing for mild steel plate (a) single case porous baffles and (b) Double case porous baffle	129
Figure 6.6	Fluent meshing closer to the test model	130
Figure 6.7	Variation of free surface elevation (η) between experimental and computational results for the aspect ratio of $h_s/l = 0.163$	133

Figure 6.8	Variation of free surface elevation (η) between experimental and computational results for the aspect ratio of $h_s/l= 0.325$	133
Figure 6.9	Variation of free surface elevation (η) between experimental and computational results aspect ratio of $h_s/l= 0.488$	134
Figure 6.10	Time histories of free surface elevation with baffle frequency ratios $0.6059 \text{ Hz} (f_1)$ for $h_s/l = 0.163$ at single baffle conditions ($L/2$)	135
Figure 6.11	Time histories of free surface elevation with baffle frequency ratios $0.7755 \text{ Hz} (f_1)$ for $h_s/l = 0.325$ at single baffle conditions ($L/2$)	136
Figure 6.12	Time histories of free surface elevation with baffle frequency ratios $0.8432 \text{ Hz} (f_1)$ for $h_s/l = 0.488$ at single baffle conditions ($L/2$)	137
Figure 6.13	Time histories of free surface elevation with baffle frequency ratios $0.6059 \text{ Hz} (f_1)$ for $h_s/l = 0.163$ at double baffle conditions ($L/3$ and $2L/3$)	138
Figure 6.14	Time histories of free surface elevation with baffle frequency ratios $0.7755 \text{ Hz} (f_1)$ for $h_s/l = 0.325$ at double baffle conditions ($L/3$ and $2L/3$)	139
Figure 6.15	Time histories of free surface elevation with baffle frequency ratios $0.8432 \text{ Hz} (f_1)$ for $h_s/l = 0.488$ at double baffle conditions ($L/3$ and $2L/3$)	140
Figure 6.16	(a)Wave propagation in numerical sloshing oscillation at $t= 5\text{sec}$ (b) Peak sloshing oscillation at $t= 20\text{sec}$ for baffle at $L/2$ location for 25% fill level case	142
Figure 6.17	(a) Wave propagation in numerical sloshing oscillation at $t= 5\text{sec}$ (b) Peak sloshing oscillation at $t= 20\text{sec}$ for baffle at $L/2$ location for 50% fill level case	143

Figure 6.18	(a) wave propagation in numerical sloshing oscillation at $t= 5\text{sec}$ (b) Peak sloshing oscillation at $t= 20\text{sec}$ for baffle at $L/2$ location for 75% fill level case	143
Figure 6.19	(a) Wave propagation in numerical sloshing oscillation at $t= 5\text{sec}$ (b) Peak sloshing oscillation at $t= 20\text{sec}$ for baffle at $L/3$ & $2L/3$ locations for 25% fill level case	144
Figure 6.20	(a) Wave propagation in numerical sloshing oscillation at $t= 5\text{sec}$ (b) Peak sloshing oscillation at $t= 20\text{sec}$ for baffle at $L/3$ & $2L/3$ locations for 50% fill level case	144
Figure 6.21	(a) Wave propagation in numerical sloshing oscillation at $t= 5\text{sec}$ (b) Peak sloshing oscillation at $t= 20\text{sec}$ for baffle at $L/3$ & $2L/3$ locations for 75% fill level case	144

LIST OF TABLES

Table No.	Particular	Page No.
Table 3.1	Dimensions of liquid sloshing tank	30
Table 3.2	Excitation frequencies for shake table experiments	39
Table 6.2	Grids Parameters	131
Table A.1	Calibration readings for a run-up probe	161
Table A.2	Percentage error for various instruments	162

LIST OF ABBREVIATIONS

A	Excitation amplitude
E_d	Energy dissipated
E_w'	Normalized energy
f_n	Sloshing frequency
f	Excitation frequency
g	Acceleration due to gravity
m_w	Mass of the liquid
η	Free surface elevation
η'	Normalized free surface elevation
n	Surface mode number
h_s	Static liquid depth
l	Length of the tank
m_w	Mass of the liquid
η_{max}	Maximum free surface elevation
F'_{max}	Normalised peak sloshing force
t	Time period
m_o	Area under the curve
F_x	Screen forces
F'_{av}	Normalised average sloshing force
F_s	Sloshing force
M	Number of linear waves

A_j	Amplitude of the j^{th} wave
K_j	Wave number of the j^{th} wave
Ω_j	Angular wave frequency
θ_j	Phase of the j^{th} wave assumed to be uniformly distributed over the interval $(0, 2\pi)$
$S\eta(\omega_j)$	Spectral density function corresponding to the frequency ω_j for sea surface (η)
$\Delta\omega$	frequency step

Common Acronyms

FSI	Fluid Structure Interaction
VOF	Volume of Fluid
RMS	Root Mean Square
TLD	Tuned Liquid Damper
CFD	Computational Fluid Dynamics

CHAPTER 1

INTRODUCTION

1.1 GENERAL

Sloshing can be defined as any movement of the free liquid surface inside a partially filled liquid container which can be caused by external disturbance. The dynamics of liquid interacts with a container and alter the system dynamics significantly. The movement of liquid due to its structure and containment interactions is a crucial factor in various engineering disciplines, such as those related to the design and construction of spacecraft tanks and rockets. It is also important in the transportation of liquid, especially when there is an earthquake. In addition to this, the movement of liquid in a reservoir can additionally be caused by the effects of water oscillation. These are the types of tanks that are commonly used in the oil and gas industries. The effects of liquid sloshing on moving containers are a major concern for engineers and scientists working in the aerospace, civil, and nuclear industries. During earthquake-induced ground motion, sloshing in oil tanks, large dams and elevated water towers are an alarm for seismologists and engineers. In moving containers like tank trucks on highways and liquid cargo vessels in the ocean, liquid sloshing creates problems affecting the safety of transportation. The problem is also significant for aerospace engineering which involves the design and development of aircraft and large rockets with fuel tanks. Because of the arbitrary orientation created by liquid volume near-zero gravity, it becomes difficult to handle and manage the liquid flow.

Since 1950, the attention on liquid sloshing in a partially filled tank has a great deal in many fields of engineering such as naval architecture, aerospace applications, ocean engineering and civil engineering. It is important to know the dynamic performance of the sloshing with respect to the safety of transportation systems and human life.

The study of a partially filled tanks sloshing motion is of practical importance. Firstly, the sloshing problem is gained importance in aerospace liquid fuel tanks. In maritime applications, the motion of free surface liquid can cause instability of the ship and

structural damage. Over the years, the studies on the sloshing have been carried out by researchers by using different analytical methods and experimental techniques, which are discussed in the literature review (Chapter 2). The study of the movement of liquid in a reservoir involves the estimation of its natural frequencies, its amplitude, and its forces. It also takes into account the various hydrodynamic and pressure distributions (Ibrahim, 2005). The various factors that affect the movement of liquid in a container are also studied to determine its dynamic stability and performance. Due to the nature of the liquid's motion, the frequency of its forced harmonics is often studied. This process is carried out to find the lowest natural frequency for the given liquid (Ibrahim, 2005).

It has been observed that sloshing oscillations behave in a non-linear manner even when excited with regular harmonic excitations (Nasar et al., 2008). The effects of non-linear factors such as amplitude jumps, chaotic liquid surface motion, and parametric resonance are also studied to determine the maximum response frequency. These factors can be used to determine the movement of liquid in a container. The shape and disturbance of a container are also influenced by the free surface motion's nature. There are various types of free-surface motions that can be used to describe the movement of liquid in a tank, such as asymmetric, non-planar, chaotic, and symmetric. The severity of the spill can be determined depending on the tank's geometry, liquid properties, and the frequency of its motion.

In moving containers, sloshing phenomena are described by considering the two-dimensional flow of fluid. In cylindrical or spherical tanks, the sloshing phenomenon is considered for three-dimensional fluid flow. In partially filled containers, the liquid sloshing dynamics are based on fluid field equations and estimation of the hydrodynamic moments and forces. Direct solutions are possible for rectangular containers and upright cylindrical tanks. Usually, the boundary value problems are used to trace mode shapes and the fluid response characteristics due to external excitations. For containers that are partially filled, the free surface motion analysis determines the natural frequencies of the liquid. This process is performed in order to estimate the corresponding mode shapes and their frequency. In aerospace vehicles, the knowledge of natural frequency is very important in the design of the tanks' active control system.

When a rectangular tank moves, different types of sloshing waves can be generated depending on the level of oscillation and the depth of the tank. These can be caused by various factors such as hydraulic jump, travelling wave, or a combination of these. In shallow liquid conditions, the formation of a standing wave can be triggered by the lower natural frequency of the liquid (Akyildiz and Unal 2005). The increasing frequency of oscillation causes the standing wave to transform into a series of short-wave travelling waves. The hydraulic jump will occur when a small disturbance is encountered near the resonance frequency. This will cause the wave to become a solitary wave. For extremely deep liquid conditions, the formation of large-amplitude standing wave patterns is observed. This phenomenon is caused by the combination of traveling and asymmetric waves.

The free liquid surface dynamic behaviour depends on its frequency and the type of excitation. The type of excitation includes periodic, sinusoidal, random and impulsive. Further, the orientation with respect to the tank can be parametric, lateral, roll, pitching/yawing excitation or their combination. The free liquid surface will exhibit two types of linearity under lateral harmonic excitation. The first one is different forms of liquid behaviour and the second involves a large amplitude response. The most significant among these is swirl motion (rotary sloshing) and this type of motion is observed closer to the lowest natural frequency.

When the tank's motion frequency is close to that of a fluid-filled tank, large amplitudes are expected. This phenomenon occurs when the two frequencies become sufficiently close. The resulting free liquid surface motion decays because of the forces generated by the boundary layer's damping. The damping factor can be influenced by the tank's liquid height, liquid kinematics, and liquid volume.

The rapid acceleration of the liquid can cause its hydrodynamic pressure to increase on the tank walls. Although the exact effects of the liquid on the tank's structure and containment are not well known, experimental studies have shown that it can cause significant impact pressure. When a hydraulic jump or travelling wave is present, the tank's supporting structure and containment can be affected.

The presence of the flowing liquid can also cause non-impulsive and unpredictable pressure. These conditions can be caused by the rapid movement of the liquid between the solid surface and the tank's surface. The most significant impact pressures are generated near the free surface and the tank walls. Even though the pressure variation is not harmonic or periodic, it can be caused by a harmonic external excitation. Impulsive pressures are usually associated with hydraulic jumps and travelling waves. On the other hand, non-impulsive pressures are produced by oscillating fluids. These are dynamic pressures that are produced slowly and are usually produced from standing waves.

When a container is disturbed by external forces, such as a moving vehicle, it can cause the container to slosh. However, this condition can only occur if the container has a free surface of liquid. These conditions can be caused by the rapid movement of the liquid between the solid surface and the tank's surface. The effects of the liquid on a moving vehicle's stability and steering performance can be caused by the interactions between the liquid and its surroundings. The effects of the liquid on different types of cargo ships and rockets are also known to be caused by the presence of the flowing liquid.

The dynamic behavior of a free liquid surface can be influenced by its excitation type, container shape, and liquid motion. For instance, the excitation of a tank can be random, periodic, or sinusoidal. This type of movement can also create various non-planar and asymmetrical movements of the liquid. The presence of the flowing liquid can also cause non-linearity in the liquid surface. In lateral harmonic excitation, the surface exhibits two types of non-linear behaviour. One of these is a large amplitude response, while the other is caused by the various modes of sloshing.

The study of fluid sloshing has been conducted for a long time and continues to attract a lot of attention due to its importance in the field of computational fluid dynamics. Usually, the multiple approaches used to study the effects of the liquid on the tank's structure and containment are performed through a theoretical/analytical approach, experimental approach, and computational approach. The presence of a free liquid surface can also cause a container to get disturbed by external forces. This condition can lead to safety issues since it can cause the liquid to move uncontrollably. Even

though the frequency of the movement can be small, it can still cause a large amount of force to be generated. The liquid motion can also become non-linear, with surface slopes approaching infinity. One of the most important factors that can be considered when it comes to the design of a tank's liquid surface is the frequency of its sloshing. Usually, a good result can be obtained by calculating the frequency of the movement, but it is not always possible to achieve a reasonable result.

On the one hand, the presence of the flowing liquid can cause its flow dynamics to change, while on the other hand, it can cause the container to get affected by its movement. This phenomenon can be caused by the forces generated by the vehicle's unavoidable motion.

There are many engineering problems that can arise due to the effects of a liquid's flow on a vessel's stability. These include ship instability, turbulence in a rocket or spaceship, and the storage of tanks under water. When a wall moves, the energy exchange between the two takes place. The fluid can show various types of motions, such as rotation, chaotic, and planar. Depending on the external excitation, the fluid can also have multiple other motions. To avoid the spill of the fluids and the structural damage caused by the container's partial fill, it is important that the container is handled carefully. If the container has a free surface, its oscillations or liquid sloshing can occur as the vessel gets subjected to excitations. The various parameters that affect the performance of moving containers are also taken into account to determine the optimal solution. The lowest frequency that a liquid can have is usually excited by the external frequencies. This is why most studies are focused on finding out how forced harmonic oscillations can occur near the lowest natural frequency.

This can be done with either solid or porous baffles. The effects of liquid sloshing on highway container trucks are severe. It can cause a variety of issues, such as reduced stability and safety performance. The effects of liquid cargo oscillations on the steering and braking systems of partially-filled tanks can also affect the overall stability of the vehicles. The presence of liquid surface tension can affect the geometry of satellites, especially those that orbit Earth. During the early stages of life, a significant portion of a satellite's mass is composed of liquid propellant. This can negatively affect satellite

performance. Although ship motion stimulates the flow of cargo, it also affects the motion of the vessel. This coupling effect can be used in various ways, such as ship design and motion control. In addition to accurately predicting the loads on a tank structure, studies have shown that the effects of sloshing can be studied in real-time. The presence of liquid propellant can also affect the end walls of ships. Knowing the effects of liquid cargo on the design of transit truck and oil carrying ships will allow engineers to improve the performance of these vehicles. The calculation of the hydrodynamic pressure in moving containers is usually performed by two different components. The first one is caused by the movement of the fluid with the same velocity, while the second one is due to the free-surface-liquid motion.

In real life and as well as real-life circumstances, some are:

- Sloshing in LNG carrier
- Sloshing in storage tanks
- Sloshing in oil tanks
- Sloshing in trucks of railway compressors
- Sloshing in dams
- Sloshing in fuel tanks

1.2 SLOSHING IN LIQUID STORAGE TANKS

liquid storage tank is an essential component of industrial facilities. There are various types of tanks that can be built depending on their structure, construction, and storage condition. Usually, concrete or steel tanks are used for storage. Steel tanks can suffer extreme damages due to corrosion. In environmental engineering, reinforced concrete is commonly used as sewage treatment tanks and water reservoirs. These are commonly used for various applications, such as fire suppression, drinking water, and agricultural farming. Due to the unpredictable failure of a container, the environment and human life are greatly affected by liquid sloshing. This phenomenon can cause soil contamination and toxic substances to spill from the tanks in industries. It is therefore important that the various factors that affect the structure and function of a liquid

storage tank are studied. Researchers and engineers are trying to develop effective ways to prevent the effects of liquid sloshing on the environment. Researchers and engineers are working on developing new ways to reduce the impact of the sloshing phenomenon on structures. They are also trying to develop structures that can endure the effects of the force.

The presence of seismic excitation during the fluid sloshing process can cause a serious issue in a liquid storage tank. For instance, if a fire occurs in one of the tanks, it could cause the roof to collapse. To minimize the effects of the force, the maximum height of the sloshing wave should be used to provide a freeboard for the liquid surface. The main cause of the phenomenon is the large amplitude slosh waves. These waves appear when the frequency components of seismic waves coincide with the natural period of an earthquake. When the wave amplitude exceeds the threshold that can create dynamic effects on a fluid tank, it should be considered as a non-linear phenomenon. This means that the free surface boundary condition should be continuously updated. This method can be carried out by taking into account the non-linear effects of the liquid.

1.3 SLOSHING IN RECTANGULAR TANKS

The goal of this study is to find out the dynamics of the sloshing in tanks. In order to do so, the experimental work is performed on a rectangular tank with the help of a simulation of the behavior. According to the Section 1.1, the shape and geometry of the tank are the factors that influence the behavior of the tank are modeled and fabricated for the present experimental work with reference to Nasar et al., (2008). The free liquid surface's motion is usually caused by the presence of viscous boundary layers. The damping forces generated by these layers can be influenced by the various tank dimensions and liquid height. To explore the effects of these factors on the behavior of a partially filled tank, a variety of tank excitation frequencies, fill levels, and rectangular tank shapes are studied.

1.4 SHREDS OF EVIDENCE OF SLOSHING

When a seismic excitation takes place, the liquid in a storage tank tends to move and cause severe structural problems. These include the buckling of the ground supported

tank, the collapse of the supporting tower of an elevated tank, the failure of the tank's joints with pipes, and the corrosion of the tank's outer shell. In the Alaska earthquake, many tanks experienced these problems. Fire also damaged the roofs of the tanks, and the tanks' structural systems failed. In Japan, many petroleum storage tanks were spoiled due to the effects of the 1964 Niigata earthquake, the 1983 Chubu earthquake, and the 2003 Tokachi-Oki earthquake. This suggests that the tanks should be thoroughly checked before they are used.

1.5 PROBLEM DEFINITION

The proposed research work aims at exploring the damping characteristics of porous baffle wall for liquid sloshing. In this proposed work it is thought to introduce porous baffle wall which helps to reduce the effect of sloshing on the tanks. An optimum design of porous baffles can be achieved by selecting the optimum diameter of the pores for higher energy dissipation. The present proposal aims to explore the additional damping offered by porous screen through experimental investigation. Porous screen is serving as a promising buffer in many engineering systems to dissipate kinetic energy of liquid, and in turn, increase the damping of the system with which it involves.

1.6 ORGANIZATION OF THE THESIS

Chapter 1, gives a general introduction to liquid sloshing and its effect. The basic theory which is used in the present study and computational background is also discussed.

Chapter 2, deals with available work of literature review which has been done in the field of sloshing and is used in the present work. The literature has been focused on the sloshing dynamics, sloshing forces and energy dissipation due to action of wave and sloshing of fluid.

Chapter 3, explains the problem formulation and the details of the experiment's setup of the present study. Details of testing model, instrumentation, calibration probes and data acquisition are discussed.

Chapter 4, Sloshing dynamics, sloshing forces, and maximum free surface elevation are compared with the experimental conducted for no baffle conditions.

Chapter 5, the assessment of sloshing dynamics and maximum free surface elevation are compared with the experimental conducted for both acrylic and mild steel plate materials. Analysing the sloshing oscillation measured by resistance probes fixed inside the partially filled tank. Performance of baffles responses has been explored.

Chapter 6, discusses the numerical models by mathematical formulation and governing equations which are solved to obtain the solution by computational fluid dynamics.

Chapter 7, presents the summary of the thesis and conclusion drawn from the present study and some scope of future work which can be done in the field of sloshing.

1.7 OBJECTIVES

1. To study the sloshing dynamics in a sway excited tank for three different fill levels.
2. To evaluate the performance of porous baffles in the sway excited rectangular tank in comparison with no baffle tank.
3. To develop a numerical model using Computational Fluid Dynamics (CFD) approach and validate with experimental findings.

CHAPTER 2

LITERATURE REVIEW

2.1 INTRODUCTION

This section aims to provide an overview of the various fields of interest that are involved in the research carried out in these areas. The review literature will provide the necessary background information to enable the reader to make informed decisions regarding the project. In addition, computational and numerical work have also been presented.

2.2 SIGNIFICANCE OF LIQUID SLOSHING

Over the years, the issue of how to deal with the effects of fuel on the surfaces of partially filled vessels has been studied in various engineering disciplines. One of the most common applications of this research is in the stabilization of aircraft. Initially, this was focused on the tanks in rockets. The current trend is focused on the motion of liquids in naval applications. This includes studies on the effects of fuel flow on the structural and acoustical properties of storage tanks and fuel tanks. Also, the seismic and aerodynamic equilibrium of tall structures were studied.

In 1952, Rodriguez and Graham conducted a study on the effects of the liquid's free surface oscillations on the tank wall. They then developed a model that takes into account the various components of the tank, such as springs. The researchers then tested this model with a fixed rigid mass and a depth specified.

2.3 COMPUTATIONAL STUDIES

Warnitchai and pinkaew (1998) studied the effects of flow damping devices on the liquid movement in a rectangular tank. The results indicated that the devices greatly increase the dissipation rate and reduce the modal frequency. The researchers also found that the devices can introduce a new type of damping to the liquid movement.

Kingsley and Craig (2007) The researchers focused on the effects of volume of fluid on the design and optimization of a 3-D rectangular tank. Through a k- turbulence model, they were able to obtain the necessary information about the liquid movement. A user-defined function was then used to perform a numerical simulation.

Godderidge et al. (2009) analyzed the effects of volume of fluid on the design and optimization of a 3-D rectangular tank. Through a k- turbulence model, they were able to obtain the necessary information about the liquid movement. They then used a user-defined function to perform a numerical simulation.

Hou et al. (2012) studied the effects of liquid movement on the performance of a 2-D rectangular tank. Through the use of ANSYS-FLUENT software, they were able to perform transient analysis on two different frequencies. These two frequencies are coupled with external sway and roll. To determine the movement of the free surface of the liquid, the researchers used a dynamic mesh technique known as the Volume of Fluid method. The results of the study revealed that the severe effects of the liquid movement can be experienced at near resonant and excitation frequencies.

Jung et al. (2012) The study was performed on a semi-filled tank with a minimum liquid height of 30 centimeters. The researchers found that the vertical height of the tank's baffles can affect the liquid's sloshing performance in a three-dimensional tank with a 70% water fill level. The researchers used the volume of fluid as a stimulus to stimulate the flow in a two-phase liquid system. The results of the study indicated that the free liquid surface exhibited linear behaviour when compared to the liquid fill levels.

Niraj Kumar (2013) carried out study of sloshing effects in a cylindrical tank with and without baffles under linear acceleration. The aim of the present simulation to study the variation of force and moment caused by sloshing, when the tank is subjected to longitudinal and combined longitudinal and lateral acceleration, with transverse and transverse baffle with hole. In the present study a 3-D transient analysis of a fuel tank to acceleration field is done by using ANSYS-FLUENT v13.0. The model used in the simulation is multiphase with Volume of Fluid (VOF) for tracing of interface. The study

concluded that the increase in filling level in the tank increases the magnitude of the forces and moment due to the large mass of fuel.

Singal et al. (2014) researchers conducted a computation study to analyse the effects of earthquake frequency content on a rectangular water storage tanks seismic behaviour. They also studied the variation in the height of the tank's baffles relative to its initial liquid fill level. Through the use of the software ANSYS-FLUENT, the researchers were able to perform multiple simulations on different fill levels and seismic excitation conditions. The researchers used the volume of fluid as a stimulus to stimulate the flow in a two-phase liquid system. Through the use of the finite volume method, they were able to perform a simulation of the two-phase flow in a 3-D tank. The results indicated that the liquid's behaviour can become extreme and cause severe impact on the tank's top walls. The results of the study revealed that the free surface behaviour of the tank was almost linear when the vertical height of the tank's baffles was equal to the liquid fill level.

Zhang et al. (2014) performed a study on the effects of force on the performance of a two-dimensional rectangular tank's smoothed particle hydrodynamics. The study was carried out using a SPH simulation. The researchers were able to check the accuracy and stability of the simulation by applying a suitable boundary condition. The study was conducted on the effects of smooth particle hydrodynamics on the design and optimization of a three-dimensional tank. The results of the study revealed that the surging and swaying of the tank can affect its performance. The study also aims to provide a foundation for future studies on the effects of liquid movement on ship motions.

Jung et al. (2015) studied the effects of natural frequency modes on the performance of a rectangular tank's sloshing phenomena. The researchers used a set method to perform the simulations. They found that the free surface's deformation becomes weaker when the frequency modes are higher. The results of the study revealed that the irregular deformation of the free surface can be caused by the waves generated by the natural frequency.

Lin et al. (2019) studied the effects of liquid movement on the performance of a two-dimensional tank's sloshing phenomena. They used a meshless method to develop a two-dimensional numerical model that takes into account the response of the container to the stimulus. The results of the study revealed that the increasing number of resonant and single frequency bands can cause the overall displacements of the liquid to increase.

Park et al. (2020) developed an analytical method that can predict the movement of a rectangular pool's liquid during its various phases of excitation. The researchers were able to develop a method that can be used to estimate the maximum amount of water that can be lost due to the effects of the pool's excessive flow.

Zhang et al. (2022) carried out numerical simulations of sloshing waves in vertically excited square tank by improved MPS method. In the present study, the phenomenon of faraday wave in a pure heave excited square tank is numerically simulated through the moving particle semi-implicit (MPS) method. Numerical results show that the surface instabilities depend on the forcing amplitude, the surface instability is more likely when the forced amplitude is increased.

2.4 NUMERICAL AND EXPERIMENTAL STUDIES

Evans and McIver (1987) studied the effects of vertical and bottom-mounted baffles on the water waves' resonance frequencies in a rectangular container. The results indicated that a half-immersed vertical baffle can reduce the lowest resonance wave number by about half, while a bottom-mounted one can no longer affect the same number. The linear water-wave theory allows the computation of eigen frequencies for various vertical and bottom-mounted tank designs.

Armenio and La Rocca (1996) studied the effects of vertical and unmounted baffles on the water's movement in a rectangular open tank. The results indicated that the presence of a vertical wall at the middle of the tank significantly changes the response of the water to the movement in the tank. This effect, which is referred to as a jump-like effect, also results in a reduction of the dynamic loads on the walls.

Isaacson and Premasiri (2001) presented a theoretical model that predicted the effects of vertical and bottom-mounted baffles on the water's movement in a fluid-filled tank

or reservoir during horizontal oscillations. In order to validate the model, experimental measurements were performed on the effects of different baffle configurations. The results indicated that the damping coefficient of vertical and horizontal baffles increases with the relative length and depth of the tank. They found that the vertical and horizontal types of baffles are more effective at damping the liquid motions in tall tanks. In terms of their use in near resonance conditions, the researchers recommend using both types of baffles.

Pal et al. (2001) conducted a finite element analysis to study the effects of different baffle configurations on the water's movement in a liquid-filled container. They then used a sensor device to measure the free surface wave heights. The results of the experiments were compared with the theoretical results.

Biswal et al. (2004) conducted a dynamic response analysis of a cylindrical tank with an annular-baffle. Their results indicated that the flexibility of the tank and the design of the baffle can help in studying the effects of the interaction between the tank and the water on the movement in the tank. To perform the analysis, the researchers used a finite element code to study both the structural and liquid domains. The researchers studied the effects of rigid and flexible baffles on the water's movement in a liquid-filled container. They found that the flexible version of the design can reduce the amplitude of the water's flow by placing the device close to the free surface. The results indicated that the flexible version of the design performs better than the rigid one when it comes to controlling the water's flow.

Frandsen (2004) conducted a computational study on the effects of the water's movement on a two-dimensional tank. The results of the study were used to develop a non-linear finite difference model that takes into account the inviscid flow equations. The simulations were performed on a single water depth and were limited to a single tank aspect ratio. In this paper, the researchers discuss the relationship between the non-linear behaviour of a solution and the wave steepness. They found that when the steepness reaches around 0.1, the importance of this relationship increases.

Akyildiz and Unal (2005) performed a series of experiments to study the effects of the vertical and bottom-mounted baffles on the walls of a tank. The results of the study

revealed that the vertical version of the design was less effective in reducing the pressure on the walls as the filling level increased. The results of the study revealed that the side-rebounds of solid-baffle tanks are subjected to high impact loads due to the shallow water effect. It is also believed that the sudden hydrodynamic loads caused by solid-baffle configurations can cause structural failure.

Akyildiz and Unal (2006) conducted a series of experiments to study the effects of different baffle configurations on the movement in a liquid-filled container. They then used a numerical simulation technique to study the effects of liquid sloshing. The results of the study revealed that the water's response to increasing the amplitude of the excitation can cause various effects. The researchers noted that the rolling amplitude of the tank and the frequency of its movement directly affected the non-linearity of the liquid's movement.

Cho et al. (2005) researchers were able to perform a numerical analysis to study the effects of liquid sloshing in a two-dimensional baffled tank. Through their study, the researchers were able to determine the overall damping characteristics of the tank. They were able to perform the analysis by taking into account the various factors that affect the design of the tank's baffles.

Maleki and Ziyaeifar (2008) conducted a study to study the effects of different types of horizontal ring and vertical blade baffles on the movement of a liquid-filled container. The researchers found that the damping ratio increased with the increasing relative sloshing height and the height of the baffles at the bottom of the tank.

Nasar et al. (2008) conducted another study to study the effects of liquid on the movement of a partially filled tank that's mounted on a barge. The tank's various ratios are analyzed to determine the effects of the wave oscillation and the response of the vessel to the changes in its position. The researchers also studied the effects of the wave height and frequency on the oscillation.

Nasar et al. (2009) researchers were able to study the effects of liquid on the movement of a partially filled tank that's mounted on a barge. Through their simulations, they were able to determine the various factors that affect the tank's internal and external damping properties. The researchers were able to observe the movement of the tank through the

combined excitation degrees of sway, roll, and sway. The four liquid fill levels that were analyzed were: h_s/l , 0.325, 0.488, and 0.585. The study also analyzed the effects of peak wave excitation on the variation in the pressure.

Panigrahy et al. (2009) conducted another experiment to study the effects of liquid on the movement of a partially filled tank that's mounted on a barge. Through their study, they were able to determine the various factors that affect the tank's internal and external damping properties. One of the main factors that they were able to analyze was the free surface displacement of the water from the mean static level.

Belakroum et al. (2010) conducted another study to study the effects of liquid on the movement of a partially filled tank that's mounted on a barge. Through their simulations, they were able to determine the various factors that affect the tank's internal and external damping properties. One of the main factors that they were able to study was the effect of the use of a normal to the free-surface design of the tank's baffles.

Goudarzi et al. (2010) the researchers conducted another study to analyze the effects of horizontal ring and vertical blade baffles on the movement of a slender tank. They found that the wall-bound design of the tank's baffles is more effective than the vertical ones. The researchers also noted that the efficiency of the horizontal ring and vertical blade baffles decreases with the decreasing liquid depth.

Faltinsen and Timokha (2011) revealed that the analytical expression of natural sloshing on a surface type screen is a complex function due to the various factors that affect its performance. For instance, the number of submerged perforations and the solidity ratio can affect the natural sloshing mode. On the other hand, the secondary resonance phenomenon can occur at a frequency close to primary resonance.

Akyildiz (2012) conducted another study to study the effects of liquid on the movement of a partially filled tank that's mounted on a barge. Through their numerical method, they were able to analyze the behavior of the liquid in the tank. The researchers were able to use the Volume of Fluid technique to study the effects of liquid on the movement of the tank. The numerical model was able to solve the complete equations of the

Navier-Stokes equations by implementing the finite difference approximations of the moving coordinate system.

Goudarzi and Sabbagh-Yazdi (2012) conducted another study to analyze the effects of liquid on the movement of a partially filled tank that's mounted on a barge. Through their analytical methods, they were able to determine the various factors that affect the tank's internal and external damping properties. They were able to come up with an estimate of the hydrodynamic damping ratio for the upper and lower mounted vertical and horizontal blade baffles. The researchers were able to use the Miles approach to study the effects of horizontal ring and vertical blade baffles on the movement of a slender tank. Through their experiments, they were able to validate the analytical models and investigate the effectiveness of different configurations.

Nasar et al. (2012) studied the effects of liquid on the movement of a partially filled tank that's mounted on a barge. Through their experimental program, they were able to determine the exact characteristics of the liquid's movement. The researchers analyzed the effects of liquid on the movement of a partially filled tank by determining its relative liquid depths. They were able to measure the sloshing oscillation along the tank's length using a variety of methods. The researchers were also able to study the effect of the peak wave frequency on the oscillation's amplitude. The researchers found that the dominant energy source is the lowest n th phase sloshing frequency. In addition, the secondary peaks are also observed at higher order in the process. They also noted that the sacrifice of the second phase is observed when the peak excitation frequency is close to its primary resonance.

Saghi and Ketabdari (2012) developed a numerical code to study the effects of liquid on the movement of a partially filled tank. The code was able to solve the Laplace equation and the free surface boundary conditions of the tank by implementing the FEM-BEM method. Through their study, the researchers were able to identify the various factors that can affect the movement of a rectangular tank. They were able to suggest the best aspect ratios for the tank to minimize the pressure on its perimeter. The results of the study revealed that the rectangular tank with a maximum surrounded volume can reduce the overall sloshing pressure.

Ning et al. 2012 studied the boundary elements of liquid sloshing in the combined vertical and horizontal excitation. To avoid possible instabilities, they applied a smooth technique to the free surface at every step. The results of the study revealed that the horizontal and vertical wave load decreases with the increasing length of the unbaffled tank's vertical blade. However, the vertical blade does not affect the vertical wave load.

Saoudi et al. (2013) conducted a study in 2013 to study the effects of forced sloshing on the free surface of a tank. Through their numerical method, they were able to come up with a robust estimate of the free surface displacement due to the frequency of the external turbulence. The results of the study revealed that the amplitude of the displacement decreases with the resonance condition and the frequency of the liquid's movement increases with the harmonic excitation. The results of the study revealed that the presence of a certain type of baffle can affect the free surface displacement and the frequency of the liquid's sloshing. The study revealed that the presence of the screen can also affect the free surface displacement. It eliminates the beating phenomenon and decreases the amplitude of the free surface displacement.

Xue et al. (2013) carried out with a robust estimate of the free surface displacement due to the frequency of the external turbulence. Through their numerical method, the researchers were also able to study the effects of the vertical and horizontal blade baffles on the movement of a rectangular tank. In order to perform a spectral analysis of the free surface elevation, the researchers used the Fast Fourier Transformation. They were able to conclude that the vertical blade's damping effect is more effective at reducing the free surface displacement at lower external frequencies. The researchers found that the vertical blade's damping effect is more effective at reducing the external turbulence at lower excitation frequencies.

Jin et al. (2014) researchers were able to study the effects of a horizontal perforated plate on the movement of a tank. The results of the study revealed that the horizontal plate can restrain the violent outbursts caused by horizontal excitation. The characteristics of a horizontal-perforated tank, which are commonly used in first- and third-order models, revealed that the structure can reduce the free surface displacement by up to 50%. To effectively restrain the movement of water between the

compartments, the researchers recommend that the total area of the perforations be less than 10%.

Dong (2015) conducted a simulation and modelling study on the effects of liquid on the movement of a partially filled tank. Through the use of STAR-CCM+, the researchers were able to simulate the multiple tank motions. The four types of tank motions that are considered are pitch, sway, surge, and roll. The results of the study were validated by an external journal. The numerical method was able to show an acceptable agreement with the results of the study before and after impact load. The increase in the liquid depth will also increase the liquid motion's nonlinearity. For pitch motion, the reduction rate is 83.3%.

Nayak and Biswal (2015) studied the effects of various internal objects, such as the vertical and horizontal blade baffles, on the movement of a tank. Through their experimental program, the researchers were able to conclude that the relative position of the submerged and the horizontal blade baffles affects the damping ratio. It is also believed that the increasing height of the submerged portion of the tank increases the damping ratio as it moves toward the free surface.

Kumar and Sinhamahapatra (2016) performed a study on the dynamic characteristics of surface-piercing and bottom-mounted hollow-core tank casings. The researchers were able to perform a variety of studies on the effects of various internal objects on the movement of a tank by calculating the effective slosh damping, overturning moment, and base shear force. The researchers were able to study the effects of various internal objects, such as the vertical and horizontal blade baffles, on the movement of a tank. They were able to find the optimal configuration of the tank's partially-perforated plate to achieve the best possible dynamic response.

Neves et al. (2016) studied on the effects of the various mass transfer processes on the movement of a tank. Through their numerical method, the researchers were able to compare the results of their simulations with those of their experimental results. The study was performed on the two different methods, namely, the lagrangian and the moving particle semi-implicit. The researchers were able to study the various hydrodynamic features of the rolling and sway motion of a tank under different water

levels. Through their various methods, they were able to come up with a robust estimate of the overall flow rate. The Moving Particle Semi-Implicit and the Lumped Mass methods performed well in the initial stages. However, the MPS model is preferred in the last phase due to wave breaking.

Wang et al. (2016) studied the effects of liquid on the movement of a partially filled tank. Through their numerical method, they were able to come up with a robust estimate of the free surface displacement due to the frequency of the external turbulence. The results of the study revealed that the proposed method has better convergence and accuracy than the existing methods.

Cavalagli et al (2017) investigated the effects of energy dissipation in a type of liquid-carrying blanket known as a sloshing absorber. Through their numerical method, the researchers were able to come up with a robust estimate of the energy dissipation. The paper also noted that the computational tool used in the study is very useful in the design of low-cost materials for civil structures.

Cho et al. (2017) performed robust estimate of the energy dissipation in a tank that was moving at a moderate speed. Through their numerical method, they were able to come up with a solution that is based on the linear potential theory's MEEM method. Another method that is used for analyzing the effects of liquid on the movement of a tank is the BEM. This is an independent method that can be used for double checking and general applications. The researchers were able to conclude that the wall-attached type of the ceramic-based blanket can suppress the flow of liquid better than the cantered type. Since the reduction in the porosity of the material causes the forces to increase, the optimal design of the blanket needs to be studied simultaneously.

Wang et al. (2017) studied the effects of liquid on the movement of a partially filled tank. Through their numerical method, they were able to come up with a solution that is based on the scale boundary finite element method. The results of the study revealed that the proposed method is very useful for the study of complex 3D sloshing phenomena. It allows for the simulation of a wide range of fluids with a small number of degrees of freedom.

Xue et al. (2017) focused on the computational study of the effects of liquid on the movement of a cubic tank. They were able to achieve their results by developing a two-phase fluid flow model that was able to solve the Navier-Stokes equations. The use of non-conventional computational methods such as the combination of non-conventional baffles allowed the researchers to reduce the dynamic impact pressures and the amplitude of the tank wall. They were also able to shift the natural frequency of the liquid storage system. Although the use of an appropriate orifice can help increase the payload of a large tanker, it is still important to carefully consider the design of the tank's outer casing. This can be done through the use of numerical simulation and experimental procedures.

Hu et al. (2018) investigated the natural frequencies of the liquid movement in two-dimensional baffled tanks. The results of the study were presented using the Boundary Element Method. The governing equations of the tank were also solved using the method. The researchers were additionally able to study the effects of vertical and horizontal baffles on the natural frequencies of the tank.

Kim et al. (2018) conducted on the effects of the reduction of the flow rate of a liquid through the use of a type of spring system known as a baffle. The results of the study revealed that the system had a different damping effect when compared to the results of the study with the other types of spring systems. During the course of the experiment, the large force generated by the liquid near the free surface was continuously repeated.

Hejazi and Mohammadi (2019) studied the effects of liquid on the movement of a tank under seismic excitations. Through a series of shaking-table tests, they were able to determine the various characteristics of the tank's response to different excitation amplitudes and water levels. The results of the study revealed that the free vertical displacement of the tank depends on the acceleration of the response in the first phase of the process.

Radnic et al. (2018) conducted on the effects of water flowing through a small rectangular water tank under dynamic excitation. The results of the study revealed that the tank's side tank walls are more responsive to the changes in the water's flow rate.

By increasing the rigidity of the side tank walls, the forces on the side tank walls are also increased.

Liu et al. (2019) developed a numerical model that was able to study the hydrodynamic performance of a liquid hydrogen tank that was subjected to a sinusoidal excitation. The model was able to capture the free surface's fluctuations during the process. The author noted that the amplitudes of the side pressure points' fluctuations are around 300 Pa and the middle pressure point's is less than 50 Pa.

Liu et al. (2019) conducted on the performance of a liquid oxygen tank that was subjected to a sinusoidal excitation, the researchers were able to determine the various characteristics of the tank's movement under different amplitudes. They were able to achieve their results by developing a user-defined VOF method. The study revealed that the varying profiles of the moments of the excitation can be attributed to the different fluctuation elevations.

Nasar et al. (2019) conducted on the performance of a liquid oxygen tank that was subjected to a sinusoidal excitation, the researchers were able to determine the various characteristics of the tank's movement under different amplitudes. They were also able to explore the effectiveness of a type of liquid tank's internal structure that's made of a combination of fiberglass and polyurethane. The author of the study noted that the use of a flexible and resilient surface can be used as an alternative to improve the performance of the ship tanks.

Stephen et al. (2019) conducted on the interaction between a semi-filled liquid tank and a barge, Stephen and his colleagues were able to perform a numerical analysis of the effects of the liquid's movement on the vessel's stability. The study was conducted on a partially filled tank that's mounted on a rigidly-mounted platform. The researchers found that the sacrifice of second mode during the second modal resonance is significant for the 50% and 75% fill levels. The contribution of secondary modes is also insignificant for the third modal resonance.

Qin et al. (2019) conducted to analyze the structural response of the anti-sloshing components of a semi-filled liquid tank that were subjected to varying configurations. Through a series of simulations, the researchers were able to determine the various factors that influence the structural response of the tank's components. They were also able to determine the amplitude and frequency of the natural and forced vibrations of the vertical and horizontal baffles. The researchers noted that the increased vertical and horizontal baffle length can increase the forced vibration amplitude.

Wang et al. (2019) performed an isogeometric boundary element analysis to determine the optimal configuration of the multiple porous tanks' anti-sloshing components. The three different types of tanks that were subjected to the study were the top-mounted, bottom-mounted, and annular models. A zoning method was then performed to study the arrangement of the tanks' multiple functional components. The results of the study revealed that the first natural frequency of the tank decreased significantly due to the increasing radius ratio. On the other hand, the natural frequencies of the higher order modes increased significantly.

Yu et al. (2019) focused on the effects of vertical slat screens on the reduction of shallow water sloshing in a tank that was subjected to horizontal excitation. The researchers were able to test the effectiveness of these screens by exposing the tank to varying excitation frequencies. One of the most important factors that the researchers considered when it came to optimizing the performance of the anti-sloshing components of the tanks was the position of the screens. They discovered that two screens can effectively suppress the wakening effect of the higher mode frequency excitation.

Liu et al. 2019 conducted a study on the performance of a non-isothermal liquid oxygen tank that was subjected to various liquid filling levels. They were able to develop a numerical model that was able to predict the hydrodynamic performance of the tank under different conditions. Through a combination of heat transfer and fluid sloshing, the researchers were able to obtain a detailed understanding of the movement of the liquid-vapor interface during the sloshing process. The side monitors of a liquid tank are mainly affected by the movement of the liquid, which can lead to significant

interface changes. In addition, the increasing liquid filling level can cause substantial elevation fluctuations.

Liu et al. (2020) conducted a study on the performance of a fuel storage tank that was subjected to sinusoidal excitations. They were able to obtain a detailed understanding of the movement of the liquid-vapor interface during the sloshing process. The results of the study revealed that the volume of fluid method was able to capture the interface's variability. The force that the liquid oxygen tank exerts against external excitation is different from its internal force. Its sloshing force can decrease with fluctuations in its amplitude and direction. The interfacial moment monitor has a stable and fluctuating profile due to its different amplitudes.

Saghi et al. (2020) performed an optimization study on the performance of a fuel storage tank that was subjected to a combination of open foam and sinusoidal excitations. They discovered that the increase in the amplitude can lead to a decrease in the horizontal force and the maximum pressure exerted on the tank. The researchers also noted that the increasing motion sway amplitude can cause the vertical force exerted on the tank to increase.

Saghi et al. (2021) focused on the influence of dual-baffles on the sway-induced tank sloshing dynamics. Through a combination of mathematical and computational methods, they were able to improve the performance of the tank by up to 15%. The results of the study revealed that the use of optimized dual-baffles can reduce the overall sloshing loads by up to 15%.

Tsao and Huang (2021) presented a study on the performance of a rectangular tank that was subjected to a combination of open foam and sinusoidal excitations. The results of the study revealed that the analytical solution was able to provide a useful tool for the design of linear-flow systems. The numerical method was also able to predict the performance of the tank under different conditions.

Cho (2021) carried out liquid sloshing in a swaying/rolling rectangular tank with a flexible porous elastic baffle. The matched eigenfunction expansion method (MEEM) with the green function for the liquid sloshing interaction with the porous elastic baffle were studied. With the decrease in the flexural rigidity of the baffle, the wall

amplification factor increases significantly at the resonance frequencies but the sloshing induced bending moments and shear forces decreases.

2.5 Closure

The literature review includes computational study, numerical and experimental works. From the computational study it is observed that to study sloshing under resonant excitation ANSYS-fluent is useful and to study large deformation smoothed particle hydrodynamics are effective. From experimental work, it is observed that sloshing effect is studied for different fill levels with no baffle and with porous baffle conditions. Few literatures have varied the baffle height with fill levels and concluded that when baffle height is same as that of fill level linear behaviour is observed. Comparison of horizontal and vertical baffles is also done. Computational work and numerical analysis are validated with experimental work. From the above literature it is observed that the sloshing behaviour is severe and it will apply impact load to the structure. The impact load is varying with the different fluid fill levels. Hence the experiment or computational study should be carried out for different fill levels. The analytic solutions were able to capture the essential physics of the sloshing responses with horizontal porous baffles, and thus can be used for the initial design and optimization of such baffles. The present study focuses attention on the sloshing frequency of liquid contained in tanks of rectangular shapes with internal obstructions for with and without porous baffles.

The lowest porosity baffle appears to be the most effective when only the wall free surface amplification factor is taken into account. However, the sloshing forces increase as porosity decreases i.e., there is a trade-off between free-surface amplification factors and sloshing force on tank walls and baffles. The best baffle porosity for the given scenario must therefore be determined while concurrently examining the amplification factor and sloshing force. Impact pressure on the walls is significantly reduced by the usage of baffle walls.

PROBLEM DEFINITION AND METHODOLOGY

3.1 GENERAL

The present study discusses about Computational, Numerical and Experimental studies in the area of sloshing dynamics. By studying the literature review, one deduces the problem for the present study. The problem is defined, objectives and methodology are arrived from the above literature.

3.2 PROBLEM DEFINITION

The proposed research work aims at exploring the damping characteristics of porous baffle wall for liquid sloshing. In this proposed work it is thought to introduce porous baffle wall which helps to reduce the effect of sloshing on the tanks. An optimum design of porous baffles can be achieved by selecting the optimum diameter of the pores for higher energy dissipation. The present proposal aims to explore the additional damping offered by porous screen through experimental investigation. Porous screen is serving as a promising buffer in many engineering systems to dissipate kinetic energy of liquid, and in turn, increase the damping of the system with which it involves.

3.3 METHODOLOGY

The work is carried out in the Department of Water Resources & Ocean Engineering, National Institute of Technology Karnataka, Surathkal. Experiments are conducted using Shake table for three aspect ratios (h_s/l , h_s = static liquid depth and l = length of the tank) of 0.163, 0.325, 0.488 which corresponds to 25%, 50% and 75% fill levels, respectively. For each of the fill level, two excitation amplitudes and seventeen discrete frequencies are used. The flowchart of the experimental procedure is shown in Figure 3.1.

Natural frequency for the different fill levels are calculated using mathematical expression. Ibrahim (2005) gave the linear approximation of resonant liquid sloshing frequencies (f_n in Hz) for the n^{th} sloshing mode in a rectangular tank as:

$$f_n = \frac{1}{2\pi} \sqrt{\frac{n\pi g}{l} \tanh\left(\frac{n\pi h_s}{l}\right)} \quad n=1, 2, 3, \dots \quad (3.1)$$

where, n is the surface mode number, l is the length of the tank and h_s is the static liquid depth.

Where,

h = height of sloshing tank.

a = excitation amplitude.

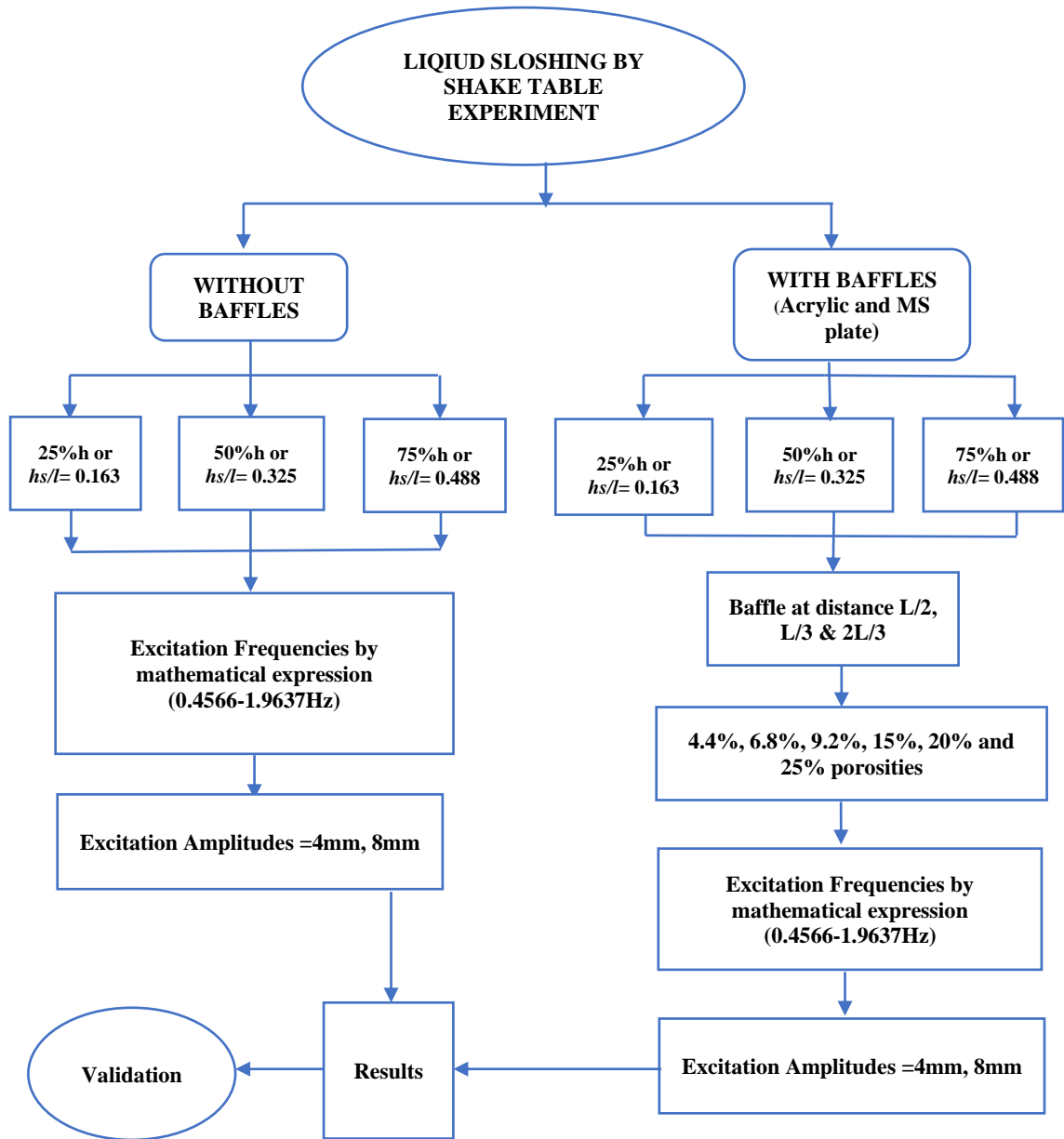


Figure 3.1 The flowchart of the experimental procedure

3.4 EXPERIMENTAL SETUP

The details of sloshing tanks used for the present study and discussion of instrumentation which is used to capture the sloshing response, sloshing forces and shake table displacement are mentioned below.

3.4.1 Sloshing Tank Description

A rectangular tank is fabricated for the present experimental work. The dimensions of the rectangular tanks are tabulated below in Table 3.1. The sloshing tank is made up of 12 mm thick acrylic sheets. The photographic view of the tank is shown below in figure 3.2.

Table 3.1 Dimensions of liquid sloshing tank

Sl. No.	Designation of tank	Dimensions in mm Tank (1:43)
1.	Length (l)	1000
2.	Width (b)	400
3.	Height (h)	650



Figure 3.2 Photographic view of the rectangular tanks

3.5 INSTRUMENTATION

A Series of experiments are conducted on a uniaxial servo-hydraulic shake table. The shake table consists of a base frame which is bolted to a strong floor. The payload capacity of the shake table is 500 kgf with an operating frequency up to 10 Hz. It consists of two platforms; a bigger platform of size 110 cm x 65 cm on the left side and a smaller platform of size 40 cm x 65 cm on the right side, a Data Acquisition System (DAQ) and

a hydraulic power pack. The liquid tank is placed on the bigger platform (Plate 1) and the ballast mass is placed on the smaller platform (Plate 2). A cradle frame is placed above the shake table platform to fix the capacitance probes. The DAQ consists of 16 channels of 16-bit resolution data logger. The channels are used to connect with transducers such as load cells, accelerometers, Linear Variable Displacement Transducer (LVDT) and capacitance (wave probes). Two S-type load cells are used to measure the sloshing forces and the load cells having a capacity of 100 kgf are mounted below the shake table platforms. The horizontal displacement of the shake table is measured using LVDT. Two capacitance-type wave probes are used to trace the free surface response and are fixed on the end walls of the tank. The concept of ballast mass is used to measure the forces and dynamic sloshing force. The typical cross-section of the liquid tank on the shake table arrangement is shown in Figure 3.3. Schematic sketch of the liquid tank on the shake table is illustrated in figure 3.4. The photographic view of the experimental setup is shown in Figure 3.5. Photographic view of (a) Data Acquisition System, (b) Hydraulic actuator, (c) LVDT, (d) S-Type load cell and, (e) Accelerometer are shown in figure 3.6. Calibration charts for wave probes, Load cell and LVDT is illustrated in Figure 3.7(a) and 3.7(b).

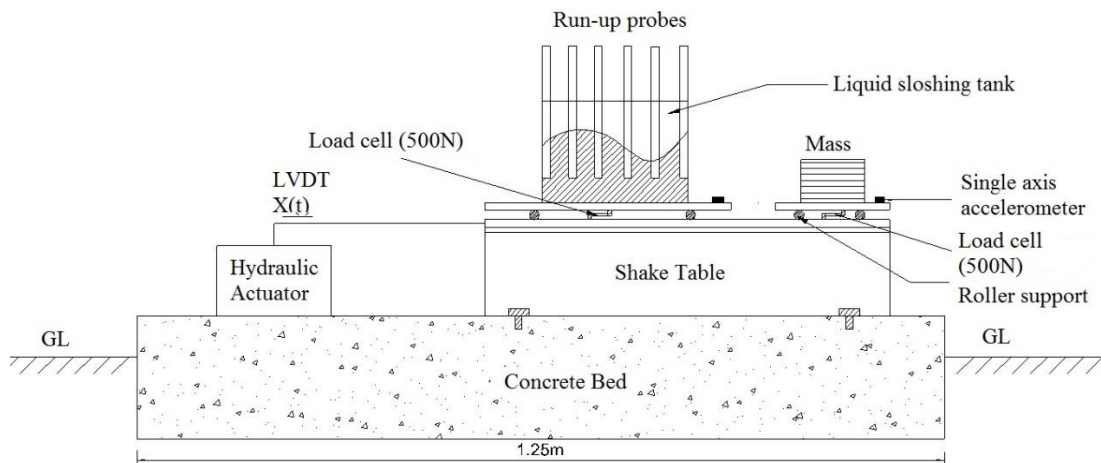


Figure 3.3 Cross-section of the liquid tank on the shake table

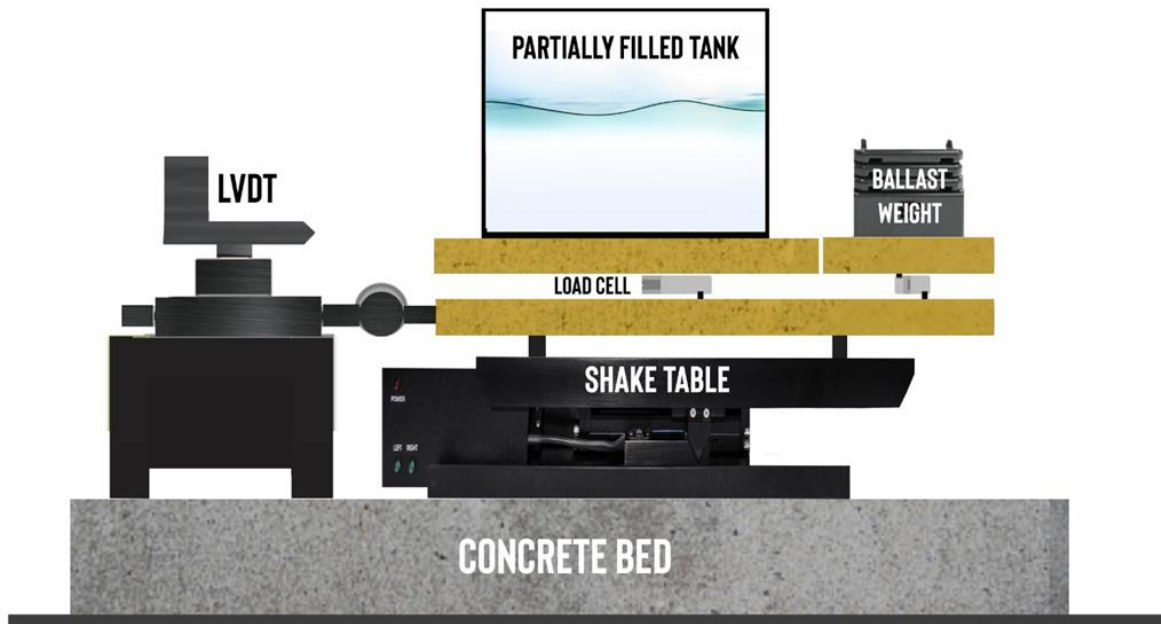


Figure 3.4 Schematic sketch of the liquid tank on the shake table



Figure 3.5 Experimental setup of shake table with liquid sloshing tank



(a)



(b)



(c)



(d)



(e)

Figure 3.6 Photographic view of (a) Data Acquisition System, (b) Hydraulic actuator, (c) LVDT, (d) S-Type load cell and, (e) Accelerometer

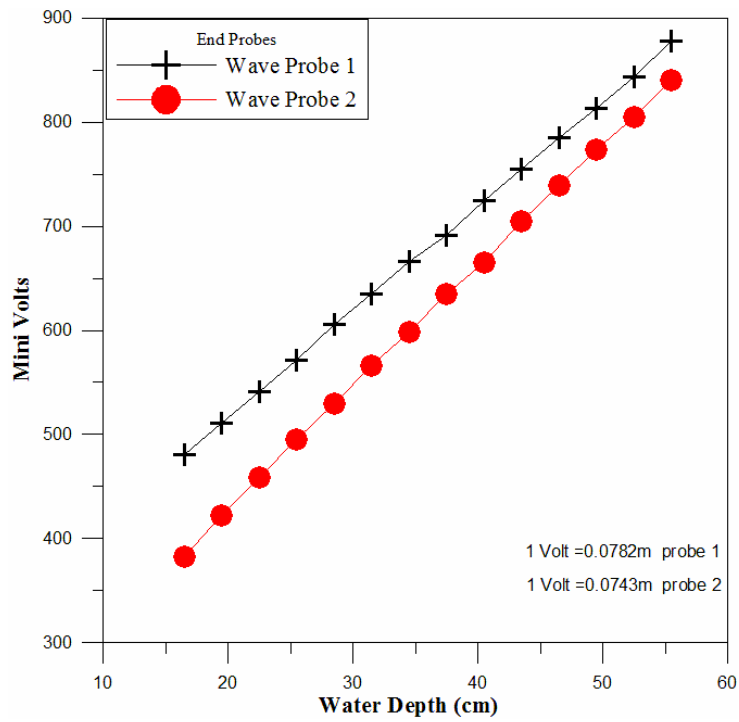


Figure 3.7 (a) Calibration chart for wave probes

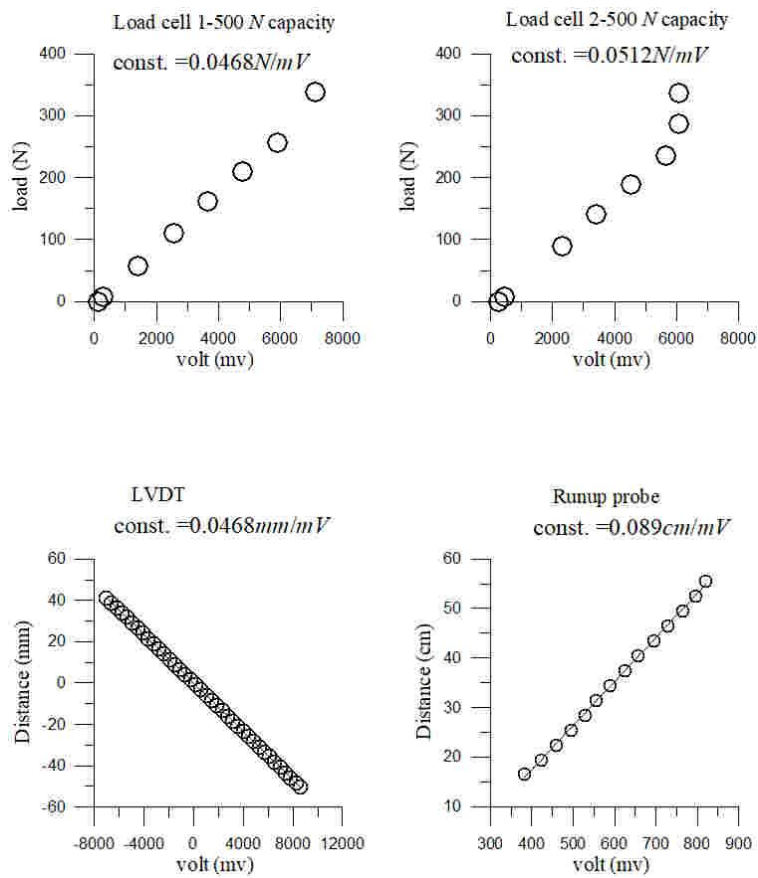


Figure 3.7 (b) Calibration charts: (i) Load cells (ii) LVDT and, (iii) Runup Probe

3.6 POROUS BAFFLE

3.6.1 Acrylic Sheet

The porous baffles with different porosities 4.4%, 6.8% and 9.2% were made using acrylic sheet of 5 mm thickness and the pores of size 15 mm diameter is adopted for all the porosities and the center-to-center distances are 90 mm, 72 mm and 62 mm for 4.4%, 6.8% and 9.2% porosity. The dimensions of porous screens are 0.39 m (*b*) x 0.6 m (*h*). The baffles were positioned where there is a high fluid velocity. When fluid velocity is higher, energy dissipation simultaneously rises. Typically, the first sloshing mode maximum velocity occurs at a distance of $L/2$. The best places to install a baffle are thus $L/3$ and $2L/3$. However, Tait (2004) demonstrated that a sloshing tank with only one baffle screen is unable to decrease the non-linear response as effectively as a tank with multiple baffles. In the present study, baffles were placed at $L/2$ location for first case and at $L/3$ and $2L/3$ locations for second case in rectangular tank. The staggered pores arrangement is shown in Figure 3.8(a) and 3.8(b) and the fabricated porous baffles are shown in the Figure 3.9.

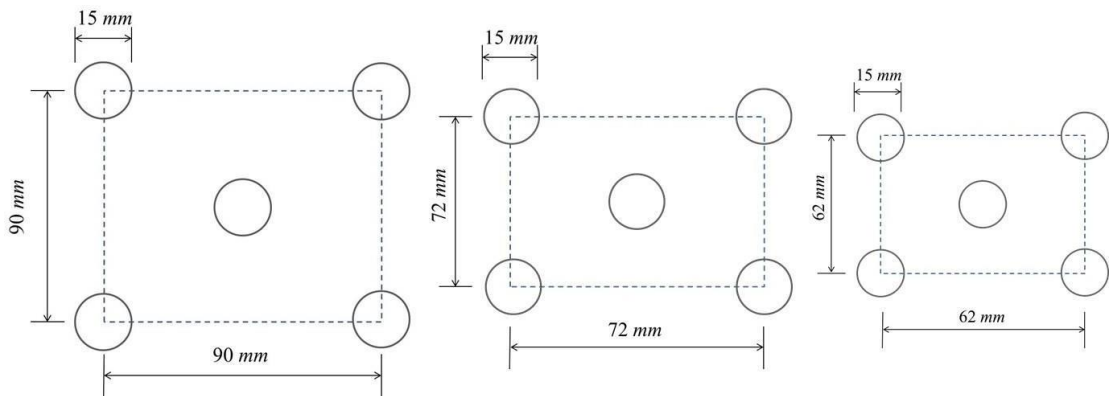


Figure 3.8 (a) Staggered Position of 4.4%, 6.8% and 9.2% Porosities (Enlarged View)

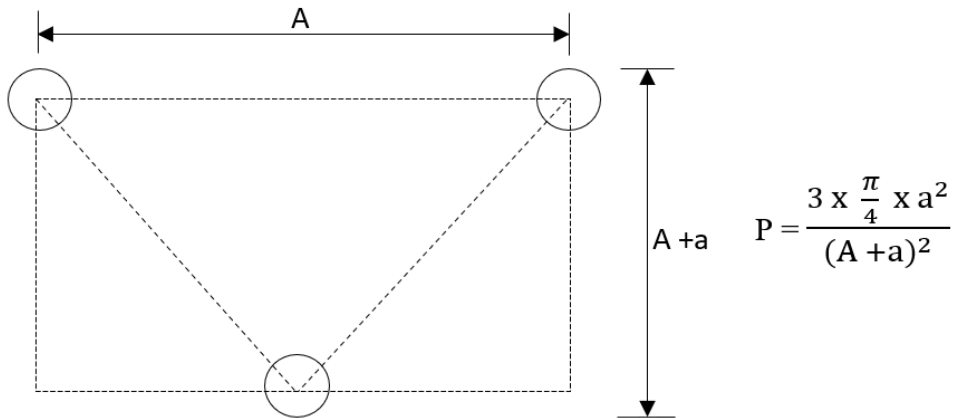


Figure 3.8 (b) Staggered Position of Porosities



Figure 3.9 Photographic of porous baffles (a) 6.8%, (b) 4.4% and, (c) 9.2%

The staggered pores arrangement is adopted. The porosity of baffles was calculated using,

$$p = \frac{v_v}{V} \quad (3.2)$$

where

p is the porosity of baffle

v_v is the hole area

V is the total area.

The porous baffles having fixity at the top and free standing inside the submerged portion of water as shown in Figure 3.9.

3.6.2 Mild Steel Plate

The dimensions of porous screens are 0.39 m (b) x 0.6 m (h). The three different porosities (15%, 20% and 25%) which is made of mild steel plate of 2mm thickness. The pores of size 15mm diameter is adopted for all the porosities and the centre-to-centre distances are 48.5mm, 42 mm and 37.5 mm for 15%, 20%, and 25% porosity, respectively. For different placement of screens, energy damping can be determined. The above porosity range is proved to be effective in dissipating hydrodynamic energy. (Dinakaran2002, Vijayalakshmi 2005). The baffles were placed at position where the velocity of the fluid is high. When the velocity of fluid is more the energy dissipation is also more. Usually, velocity would be maximum at $L/2$ distance for first sloshing mode. So, the most efficient location for placing of baffle is at $L/3$ and $2L/3$. In the present study, baffles were placed at $L/2$ location for first case and at $L/3$ and $2L/3$ locations for second case in rectangular tank. The staggered pores arrangement is shown in Figure 3.10 and the fabricated porous baffles are shown in the Figure 3.11.

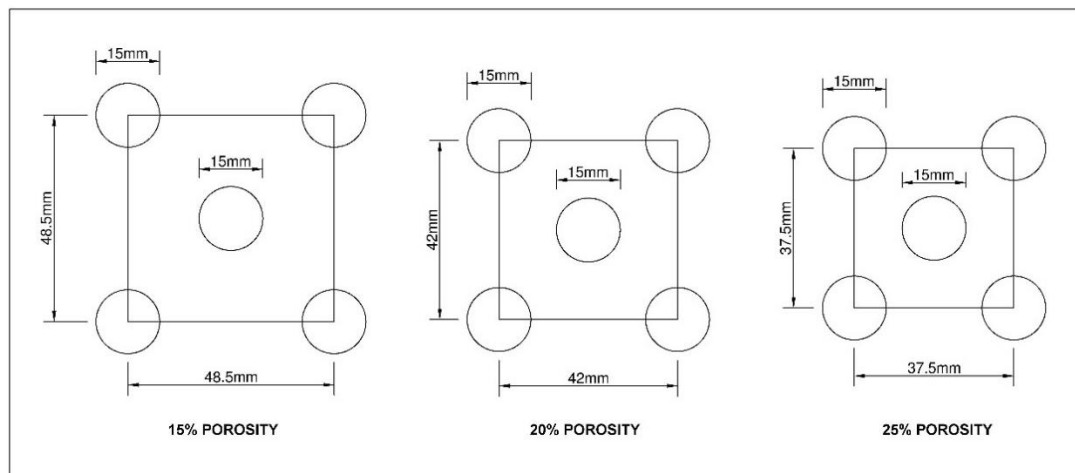


Figure 3.10 Size of pores in baffles wall for different staggered position of 15%, 20% and 25% porosities

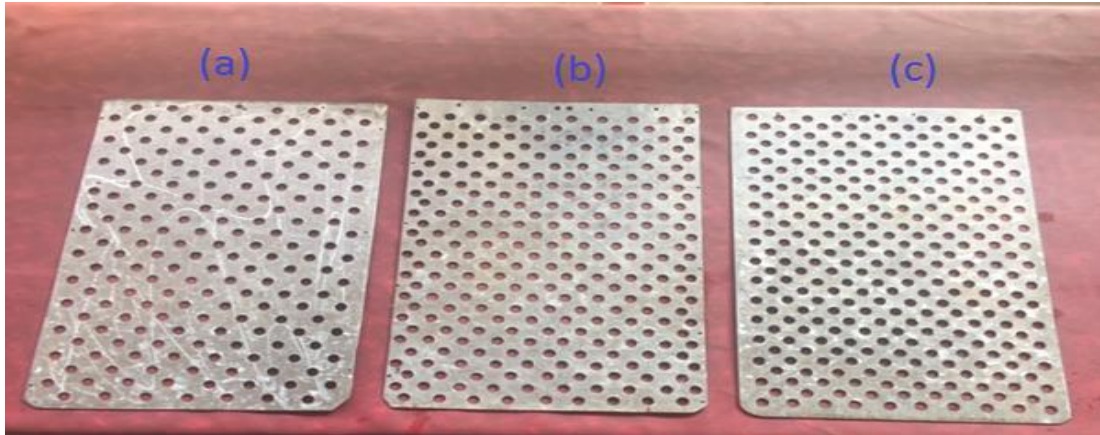


Figure 3.11 Photographic of porous baffles (a) 15%, (b) 20% and, (c) 25%

3.7 BASE SHEAR FORCE

As discussed earlier in section 3.2, platform1 and platform 2 are supported by the test frame through roller support and it is linked to respective load cells. During shake table experiments, the inertial forces are measured by respective load cells and acquired through data acquisition system. The sloshing forces and total base shear forces are calculated as follows, (Jamie, 2007):

$$F_1 = F_A + F_M + F_s \quad (3.3)$$

$$F_2 = F_A + F_M \quad (3.4)$$

$$F_s = F_1(t) - F_2 \quad (3.5)$$

$$F_b = F_1(t) - F_A(t) \quad (3.6)$$

Where,

$F_1(t)$ = inertial force measured by the platform 1 load cell

$F_2(t)$ = inertial force measured by the platform 2 load cell

$F_A(t)$ = force measured due to inertia of the empty tank

$F_M(t)$ = force measured due to inertia of the contained fluid

F_s = sloshing force

F_b = total base shear force

3.8 SHAKE TABLE MOTION

The shake table motion is measured with LVDT of displacement range -50 mm and $+50\text{ mm}$. The table is excited with seventeen discrete excitation frequencies to ensure proper resolution of the frequency-response curve. The table excitation amplitudes of 4 mm and 8 mm are considered for the present study. The excitation frequencies of the tanks are given below in Table 3.2.

Table 3.2 Excitation frequencies for shake table experiments

Mode (n)	Frequency (Hz)			Frequency ratio f/f_1			Amplitude (mm)
	$h_s/l=0.163$	$h_s/l=0.32$ 5	$h_s/l=0.488$	$h_s/l=$ 0.163	$h_s/l= 0.325$	$h_s/l= 0.488$	
	0.4566	0.4566	0.4566	0.7535	0.5887	0.5415	4 & 8
	0.4939	0.5363	0.5533	0.8151	0.6915	0.6561	
	0.5312	0.6160	0.6499	0.8767	0.7943	0.7707	
	0.5685	0.6957	0.7466	0.9382	0.8970	0.8854	
1 st	0.6059	0.7755	0.8432	1	1	1	
	0.7695	0.9266	0.9778	1.2700	1.1948	1.1596	
	0.9331	1.0777	1.1122	1.5400	1.3896	1.3190	
2 nd	1.0967	1.2287	1.2468	1.8100	1.5843	1.4786	
	1.2179	1.3281	1.3413	2.0100	1.7125	1.5907	
	1.3391	1.4275	1.4358	2.2101	1.8407	1.7027	
3 rd	1.4604	1.5270	1.5302	2.4103	1.9690	1.8147	
	1.5528	1.6069	1.6091	2.5628	2.0720	1.9083	
	1.6452	1.6868	1.6880	2.7153	2.1751	2.0018	
4 th	1.7376	1.7666	1.7671	2.8678	2.2780	2.0957	
	1.8130	1.8363	1.8366	2.9922	2.3678	2.1781	
	1.8884	1.9060	1.9061	3.1166	2.4577	2.2605	
5 th	1.9637	1.9757	1.9757	3.2409	2.5475	2.3430	

EXPERIMENTAL INVESTIGATION WITHOUT BAFFLES

This chapter describes the experimental setup used in the present study for no baffle condition. The chapter begins with the details of sloshing tanks used and followed by a discussion of sloshing oscillation time histories, maximum sloshing response, sloshing oscillation spectra and sloshing forces.

4.1 RESULTS AND DISCUSSION

This chapter presents the results obtained from the series of shake table experiments which are conducted for three different fill levels in a sway excited rectangular tank. The following sections detail the time histories of sloshing oscillation, maximum free surface response (η_{max}), root mean square elevation (η_{rms}), maximum sloshing force (F'_{max}), average of ten largest sloshing peaks (F'_{av}) and sloshing dynamics oscillation spectra.

4.1.1 Sloshing Oscillation Time Histories

Liquid sloshing oscillations due to the sway excited momentum in the partially filled rectangular tanks are reported herein. A tank with aspect ratios of 0.163, 0.325 and 0.488 is considered. In each case, the sloshing oscillation responses for the wave excitation $f = f_1, f_3$ and f_5 are superposed. Sloshing oscillation for excitation amplitudes of 4 mm and 8 mm are considered. Figure 4.1 presents the sloshing oscillation time histories for 25%, 50% and 75% fill levels subjected to excitation amplitude of 4 mm and 8mm respectively. It is learnt that non-linear behavior is evident from the time evolution of free surface of the liquid even for the sinusoidal excitation. The position of wave probes is placed at both ends of the sloshing tank for measuring free surface elevations.

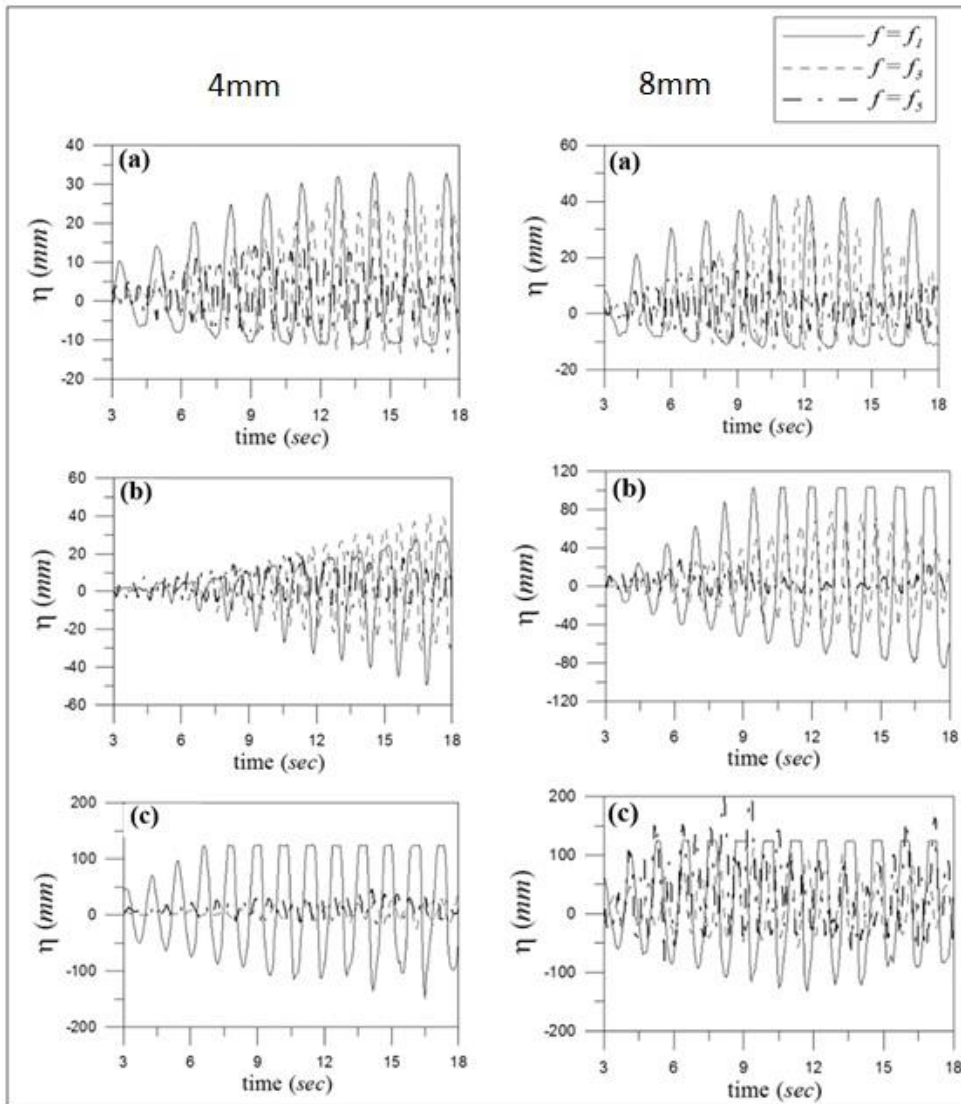


Figure 4.1 Time histories of sloshing oscillation corresponding to excitation amplitudes of 4 mm and 8 mm: (a) $h_s/l = 0.163$, (b) $h_s/l = 0.325$, (c) $h_s/l = 0.488$.

Comparison of the sloshing oscillation time histories of three fill levels leads to the following observations:

- Higher sloshing oscillations are observed in the order of $f = f_1$, $f = f_3$ and $f = f_5$ i.e., at odd mode sloshing frequencies irrespective of the fill levels and excitation amplitudes.
- It is seen from graphs that, $f = f_1$ is the critical mode of sloshing for sway excited rectangular tanks of partially filled liquid depths.

- As seen from the graphs, sloshing oscillation is higher for 8 mm excitation amplitude compared with 4 mm excitation amplitude irrespective of the fill levels.
- For three different fill levels, the higher sloshing oscillation are observed in the order of 50%, 75% and 25% fill levels.

4.1.2 Maximum Free Surface Response (η_{max})

The maximum sloshing run-up in the sway excited rectangular sloshing tank is determined by the maximum free surface response within the steady-state oscillation for a particular excitation frequency and excitation amplitude. The variation of maximum free response is normalised with the wave amplitude. The Normalised maximum free surface response (η_{max}/A) for the different frequency ratios (f/f_1) for three fill levels are projected in figure 4.2. The excitation frequencies vary from 0.4566 Hz to 1.9757 Hz respectively. Variation of η_{max}/A with different frequencies ratio (f/f_1) for different fill levels are shown in figure 4.3. Sloshing is a resonance phenomenon and highly non-linear in characteristics. There are three fill levels selected based on the study of Nasar et al. (2008). The fill depth of 50% is critical fill level which delineating between soft spring and hard spring characteristics of sloshing phenomenon [Waterhouse (1994); Nasar et al. (2013)]. Sloshing is sensitive to excitation frequency than excitation amplitude. However, it is sensitive to amplitude around resonance because of jumping phenomenon [Faltinsen et al., 2000; Faltinsen and Timokha, 2001; Faltinsen and Timokha, 2002]. Hence two different excitation amplitudes are considered based on the limitation of shake table set-up.

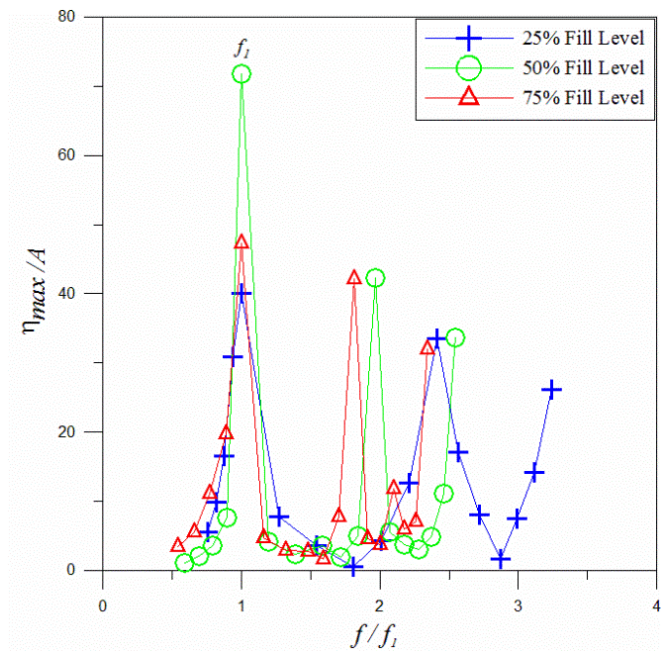


Figure 4.2 Variation of η_{max}/A no porous baffle with various frequencies ratio for $h_s/l = 0.163, 0.325$ and 0.488

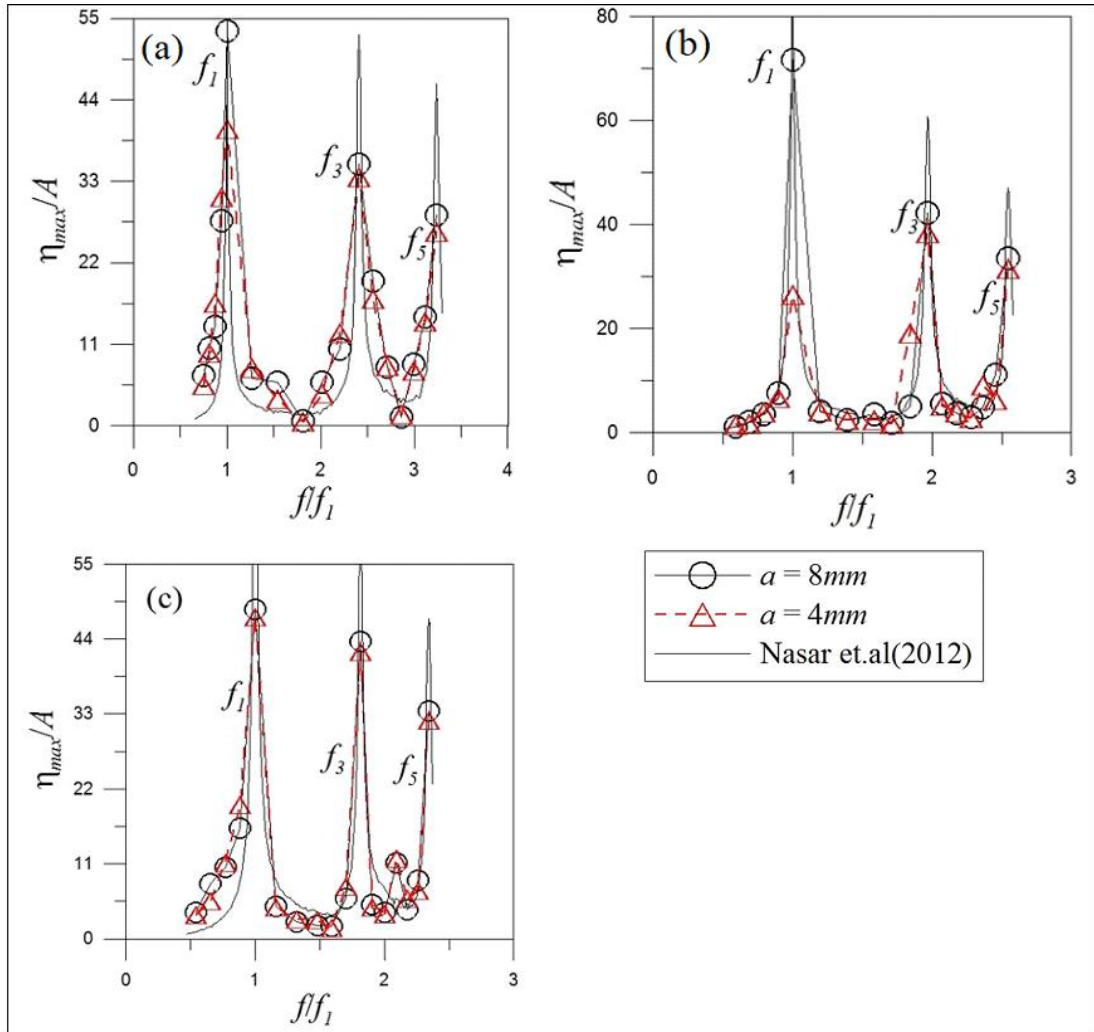


Figure 4.3 Variation of η_{max}/A with different frequencies ratio (ff_1) for a) $h_s/l = 0.163$; b) $h_s/l = 0.325$ and (c) $h_s/l = 0.488$

Comparison of the maximum free surface response elevation of different fill levels leads to the following observations:

- Experimental results are compared with the numerical works of Nasar et al., (2012). Maximum responses and a good correlation are precisely predicted for odd mode sloshing frequencies.
- For the maximum free surface response is higher for 50% fill level ($h_s/l = 0.325$) than the maximum free surface response obtained for 75% fill level ($h_s/l = 0.488$) and 25% fill level ($h_s/l = 0.163$).

- Graphs show that the critical mode of sloshing for sway excited rectangular tanks with partially filled water depths is at the first mode natural frequency ($f = f_1$).
- Maximum free surface response is observed in the order $f = f_1, f = f_3$ and $f = f_5$ i.e., at odd mode sloshing frequencies.
- On comparison of three different fill levels, the higher sloshing oscillations are observed in the order of 50%, 75% and 25% fill levels.

4.1.3 Root Mean Square Surface Elevation (η_{rms})

The normalized root mean square of sloshing (η_{rms}/A) for various excitation frequency ratio (f/f_1) are presented in Figure 4.4.

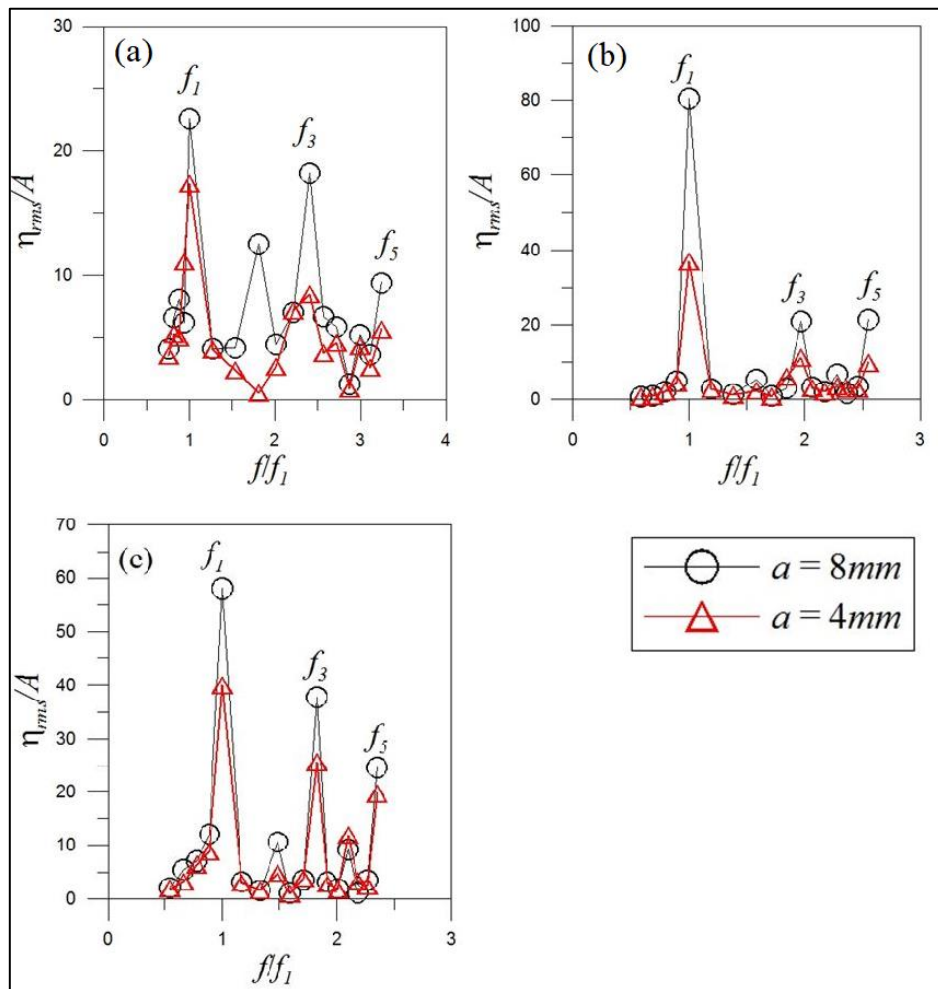


Figure 4.4 Comparison of η_{rms}/A with different frequencies ratio (f/f_1) for (a) $h_s/l=0.163$; (b) $h_s/l=0.325$, (c) $h_s/l=0.488$

Comparison of the root mean square surface elevation of different fill depths leads to the following observations:

- By considering all the normalized root mean square surface elevation which is higher for 50% fill level ($h_s/l = 0.325$) than the response obtained for 75% ($h_s/l = 0.488$) and 25% fill level ($h_s/l = 0.163$).
- Normalized root mean square surface elevation is observed in the decreasing order of $f = f_1, f = f_3, f = f_5$ i.e., at odd mode sloshing frequencies.
- The trend is same as that of normalized maximum free surface response.

4.1.4 Sloshing Dynamics

In this section, sloshing dynamics is discussed by identifying the harmonics available in the energy spectrum of sloshing oscillations of 25%, 50% and 75% fill levels. Figure 4.5(a) 4.5(b) and 4.5(c) illustrates the sloshing oscillation spectra subjected to excitations at $f = f_1, f = f_3, f = f_5$ for $h_s/l = 0.163$ subjected to excitation amplitude of 4 mm. Figure 4.5(d) 4.5(e) and 4.5(f) illustrates the sloshing oscillation spectra subjected to excitations at $f = f_1, f = f_3, f = f_5$ for $h_s/l = 0.325$ subjected to excitation amplitude of 4 mm. In the similar manner of representation, Figure 4.5(g), 4.5(h) and 4.5(i) illustrates the sloshing oscillation spectra subjected to excitations at $f = f_1, f = f_3, f = f_5$ for the excitation amplitude of 4 mm for $h_s/l = 0.488$. The spectral results of above said experimental conditions are compared with the results of relative liquid depths of 0.325 and 0.488. Odd modes contributions are dominating even modes and hence comparison of sloshing oscillation spectra of $f = f_1, f = f_3, f = f_5$ is projected in this section for different relative liquid depths and scaled tanks. Similar trends are followed for the sloshing oscillation spectra subjected to excitations at $f = f_1, f = f_3, f = f_5$ for $h_s/l = 0.163$ subjected to excitation amplitude of 8 mm shown in figure 4.6(a) 4.6(b) and 4.6(c). Figure 4.6(d) 4.6(e) and 4.6(f) illustrates the sloshing oscillation spectra subjected to excitations at $f = f_1, f = f_3, f = f_5$ for $h_s/l = 0.325$ subjected to excitation amplitude of 8 mm. In the similar manner of representation, Figure 4.6(g), 4.6(h) and 4.6(i) illustrates the sloshing oscillation spectra subjected to excitations at $f = f_1, f = f_3, f = f_5$ for the excitation amplitude of 8 mm for $h_s/l = 0.488$.

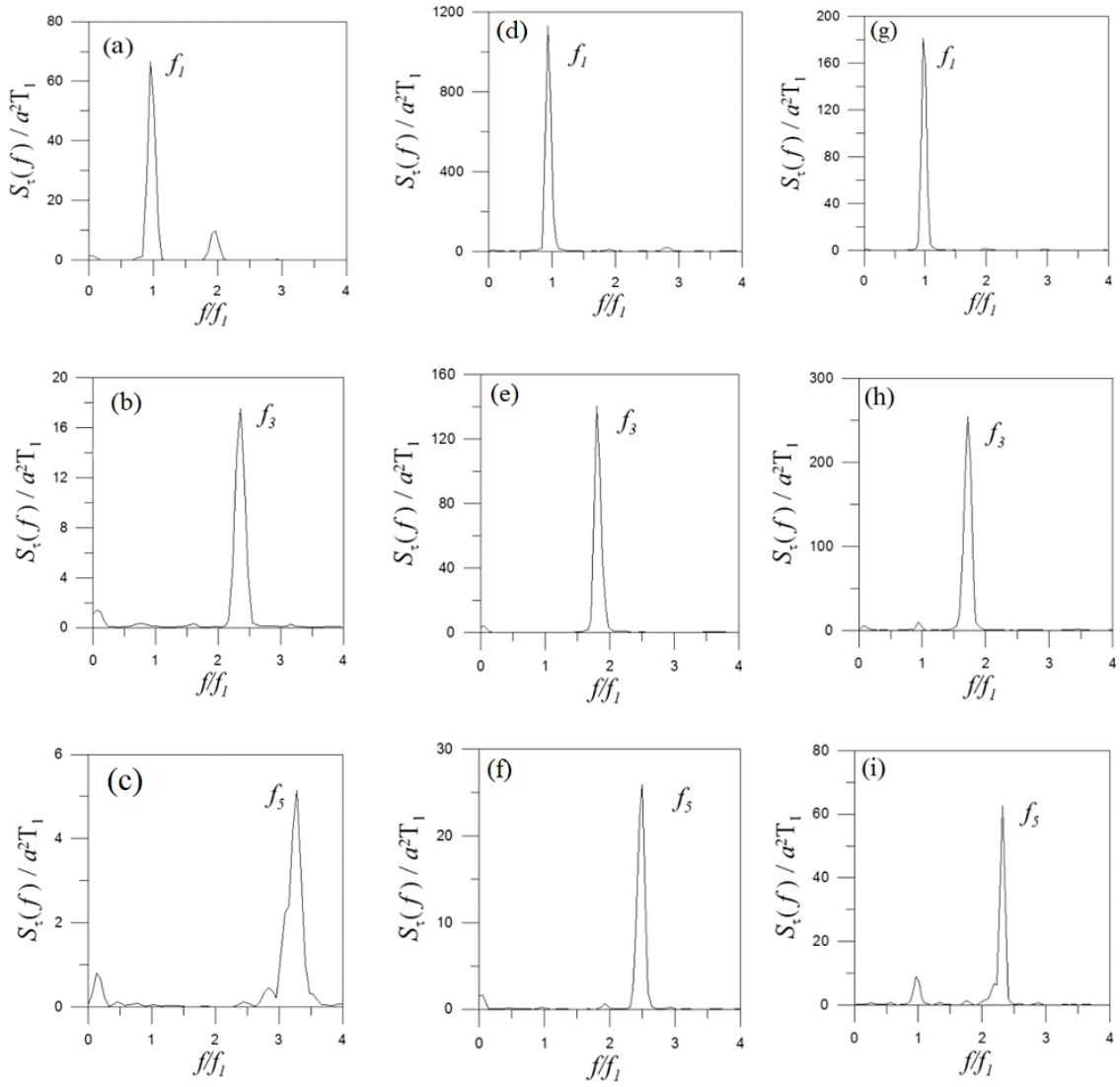


Figure 4.5 Sloshing oscillation spectra corresponding to excitation amplitude of 4 mm for $h/l = 0.163$; (a) $f = f_1 = 0.6059$, (b) $f = f_3 = 1.4603$, (c) $f = f_5 = 1.9637$, $h/l = 0.325$; (d) $f = f_1 = 0.7755$ (e) $f = f_3 = 1.5270$, (f) $f = f_5 = 1.9757$ and $h/l = 0.488$; (g) $f = f_1 = 0.8432$, (h) $f = f_3 = 1.5302$, (i) $f = f_5 = 1.9757$

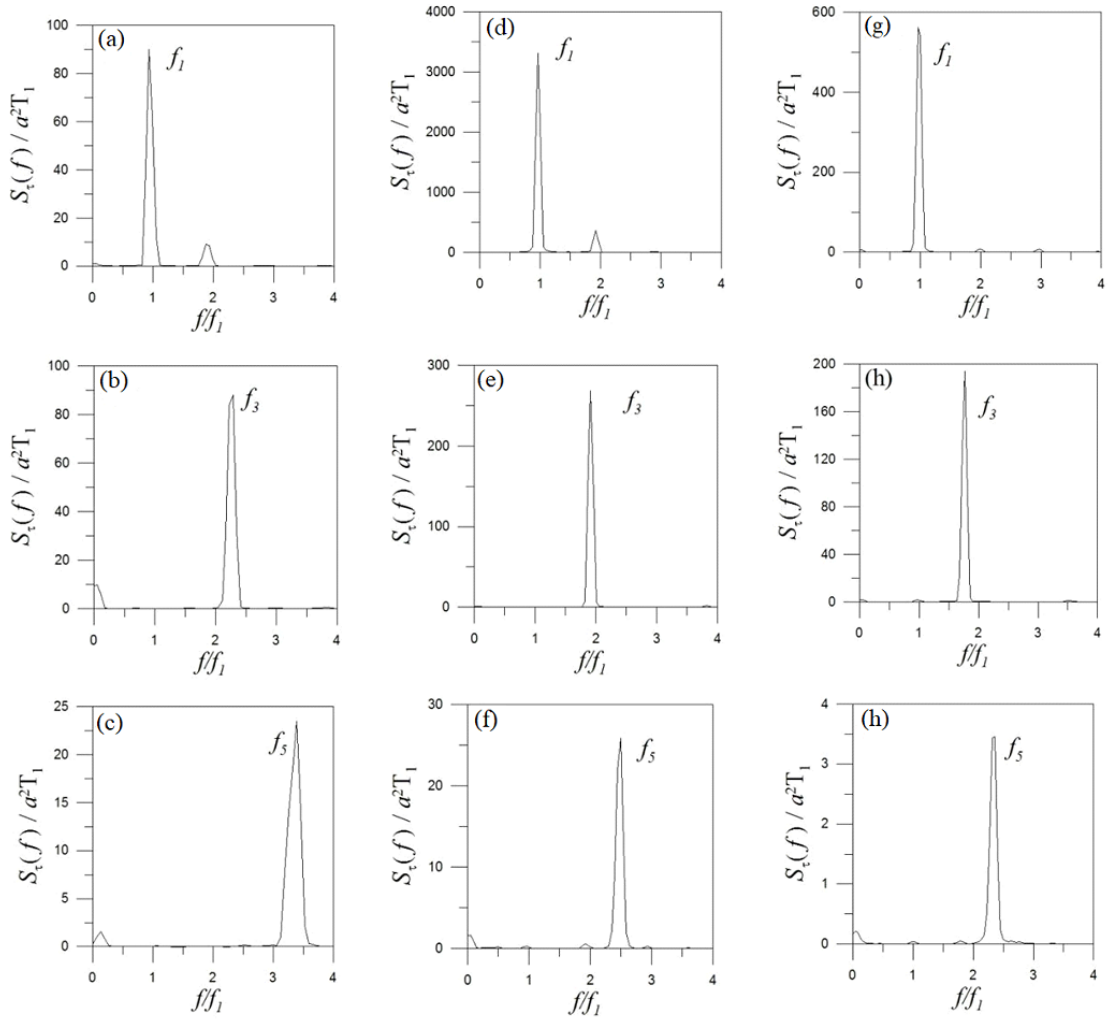


Figure 4.6 Sloshing oscillation spectra corresponding to excitation amplitude of 8 mm for $h_s/l = 0.163$; (a) $f = f_1 = 0.6059$, (b) $f = f_3 = 1.4603$, (c) $f = f_5 = 1.9637$, $h_s/l = 0.325$; (d) $f = f_1 = 0.7755$, (e) $f = f_3 = 1.5270$, (f) $f_5 = 1.9757$ and $h_s/l = 0.488$; (g) $f = f_1 = 0.8432$, (h) $f = f_3 = 1.5302$, (i) $f = f_5 = 1.9757$

For 25% fill level ($h_s/l = 0.163$), as the excitation amplitude increases from 4 mm to 8 mm, there is an increase in energy concentration. With the increase in sloshing frequency from first mode to fifth mode, the energy concentration decreases. When comparing for $h_s/l = 0.163$, the energy concentration is in the decreasing order of $h_s/l = 0.325$ and $h_s/l = 0.488$.

As observed for the 25% fill ($h_s/l = 0.163$), the effect of excitation amplitude is pronounced in increasing the energy spectrum as the amplitude of excitation increases

and energy concentration decreases as the sloshing frequency increases from first mode to fifth mode for the tanks and for 50% ($h_s/l = 0.325$) & 75% ($h_s/l = 0.488$) fill levels.

4.1.5 Sloshing Force

A proper estimation of sloshing force is the significant part of sloshing dynamics and it is the deciding parameter for the design and operation of any moving object which is carrying a tank with partially filled liquid. Sloshing force mainly depends on the frequency of the moving tank, excitation amplitude, geometry, size of sloshing tank and depth of liquid filled in the tank. By considering all above-mentioned factors, the sloshing force is measured using ballast mast concept for the shake table excitation frequencies.

The sloshing force is represented in normalized peak sloshing force (F'_{max}) and normalized average sloshing force (F'_{av}) of ten largest peaks. The variation in the maximum sloshing force is normalized with the inertial force of liquid as it is treated as solid mass. The normalized peak sloshing force and normalized average sloshing force are given as follows, (Jamie, 2007):

$$F'_{max} = \frac{F_{max}}{m_w (2\pi f)^2 A} \quad (4.1)$$

$$F'_{av} = \frac{F_{av}}{m_w (2\pi f)^2 A} \quad (4.2)$$

Where A is excitation amplitude, m_w is total mass of the fluid and f is excitation frequency.

The variation of F'_{max} and F'_{av} with different frequencies ratios (f/f_1) are projected for three different water depths, which are shown in Figure 3.12 and Figure 3.13. Each Figure shows the normalized sloshing force for three different fill levels with 4 mm and 8 mm excitation amplitudes.

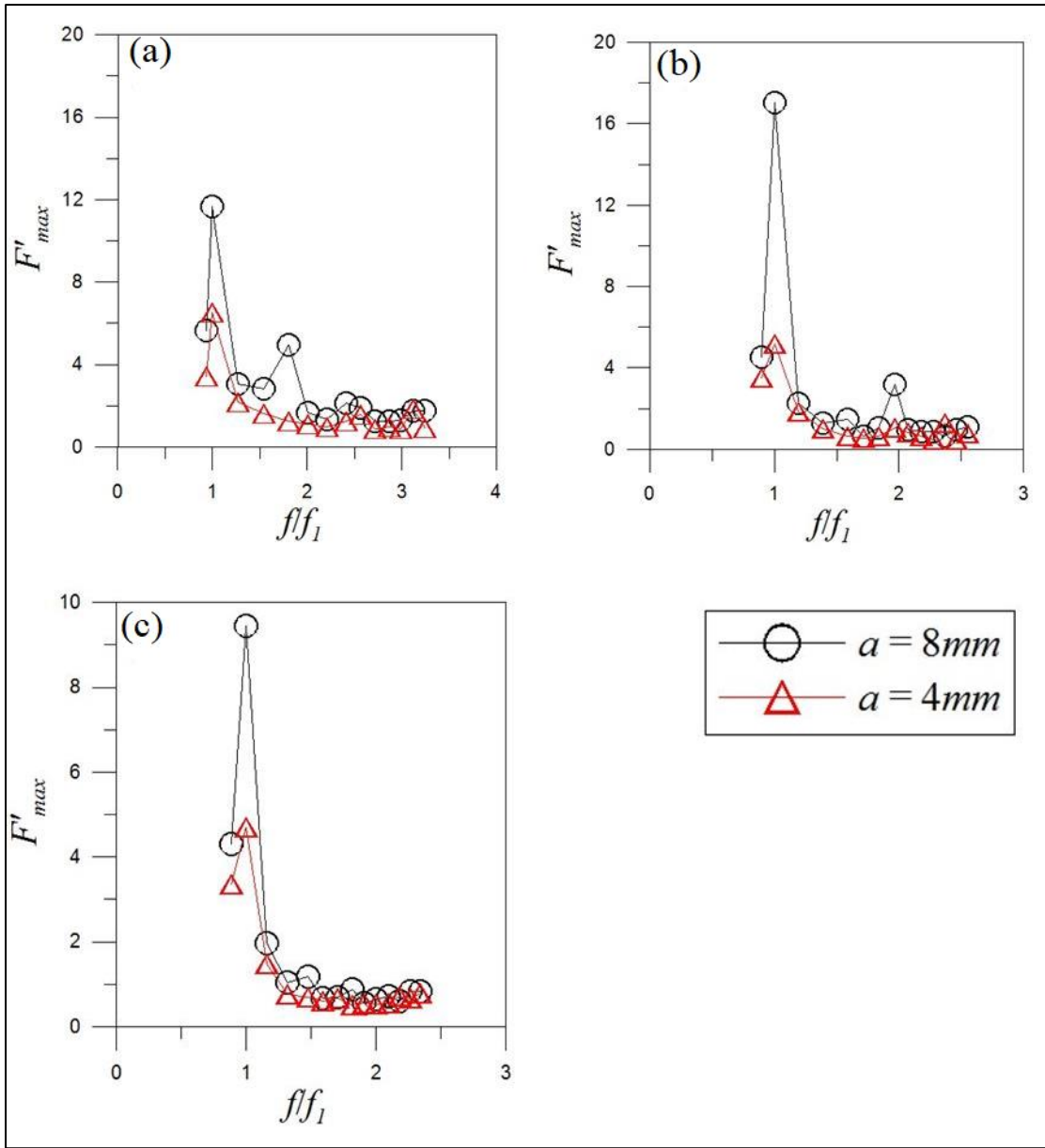


Figure 4.7 Comparison of F'_{max} with different frequency ratios (f/f_1) for (a) $h_s/l = 0.163$, (b) $h_s/l = 0.325$ and (c) $h_s/l = 0.488$

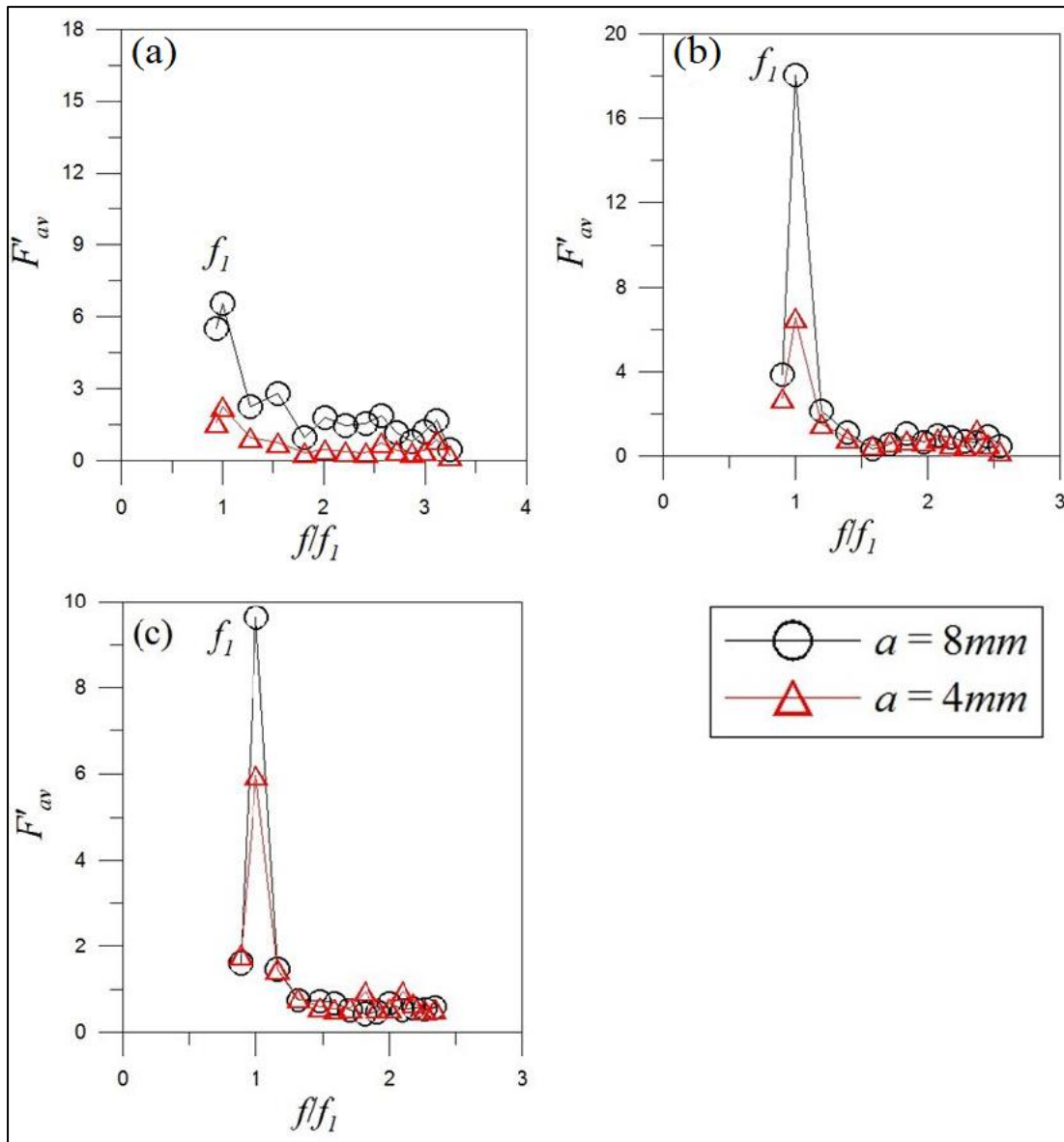


Figure 4.8 Comparison of average of 10 largest sloshing peaks, F'_{av} with different frequency ratios (f/f_1) for (a) $h_s/l = 0.163$, (b) 0.325 , and (c) 0.488

4.2 CLOSURE

The sloshing behaviour in the sway excited rectangular tank is presented by using shake table experiments. Three fill levels of 25% ($h_s/l = 0.163$), 50% fill ($h_s/l = 0.325$) and 75% fill ($h_s/l = 0.488$) are considered. The partially filled rectangular tank is subjected to excitation frequencies ranging between 0.4566 Hz to 2.794 Hz , which covers up to fifth mode sloshing frequency. Two excitation amplitudes of 4 mm and 8 mm are

considered. The experimental parameters such as sloshing oscillation and sloshing force are discussed for partially filled scaled sloshing tanks. The key conclusions drawn from the experimental study are given below:

- An experimental setup is designed and devised for measuring sloshing force using ballast mass concept.
- The experimental work iterates that first sloshing mode is the critical mode irrespective of sloshing tank and aspect ratios.
- As the dimensions of the sloshing tank increases, the number of peak responses, i.e; number of harmonics in the sloshing energy spectrum decreases.
- Sloshing oscillation time histories decreases in an order for 25% and 50% fill levels and for 75% fill level, sloshing oscillation increases in the order irrespective of excitation amplitudes.
- Normalised maximum free surface response ((η_{rms}/A)) and normalised root mean square of sloshing elevation ((η_{rms}/A)) is observed in the order $f = f_1, f = f_3$ and $f = f_5$ i.e; at odd mode sloshing frequencies.
- Maximum energy (sloshing dynamics) is obtained for 50% fill level irrespective of the tanks and excitation amplitudes. Energy concentration decreases in an order of for 25% fill level and for 50% and 75% fill level, energy concentration decreases in the order irrespective of excitation amplitudes.
- Sloshing force (F'_{max} and F'_{av}) is high at 25% fill level irrespective of the excitation frequencies and amplitudes.
- When the water depth is more than 50% fill level, sloshing force (F'_{max} and F'_{av}) is maximum irrespective of the excitation frequency and amplitude.
- It can be concluded that the 50% filled condition experiences violent sloshing irrespective of the excitation amplitudes and excitation frequencies.

EXPERIMENTAL INVESTIGATION WITH BAFFLES

5.1 RESULTS AND DISCUSSION

The sloshing dynamics, sloshing oscillation and sloshing force behaviour are presented in Chapter 4. In order to explore the effectiveness of porous baffle in comparison with no baffle case, herein, the porous baffles of different porosities are considered. This chapter presents the results obtained from the series of shake table experiments that were conducted in sway excited rectangular tank for two different types of flexible materials ie; acrylic and mild steel plate in order to assess the performance of the porous baffles. The following sections present the time histories of free surface elevation, maximum free surface response, energy dissipation, spectral moments and forces were presented for different porous baffles and placement conditions.

5.2 FREE SURFACE RESPONSE

5.2.1 Acrylic Sheet

Figure 5.1 to Figure 5.3 show the steady state time series of normalized free surface of sloshing oscillation for the excitation at natural sloshing frequency at excitation amplitude of 8mm. This graph represents the variations of free surface of water and magnitudes of the free surface of oscillation for no baffle and with porous baffles and for the baffle wall placed at a distance of $L/2$. The graph is plotted for (the frequencies of f_1, f_2, f_3, f_4 , and f_5 and considered excitation amplitude) for three different fill levels of 25%, 50% & 75% of the tank depth and porosities of 4.4%, 6.8% and 9.2% respectively. Figure 5.1 to Figure 5.3 explains the normalized free surface oscillation and demonstrate the comparison between no baffle and with baffle condition for 25%, 50% & 75% fill conditions. The free surface elevation is normalized with static water depth, h_s .

Figure 5.4 explains the normalized free surface oscillation at excitation of natural sloshing frequencies and demonstrates the comparison between no baffle and porous

baffles conditions for three different fill levels of 25%, 50% & 75% placed at $L/3$ & $2L/3$ locations at above said porosities for 25% filled condition ($h_s/l = 0.163$). Figure 5.5 demonstrates the same for 50% filled condition ($h_s/l = 0.325$). Free surface elevation of sloshing fluid with respect to time will be presented in this section for first five modes of frequencies with 75% fill level ($h_s/l = 0.488$) shown in figure 5.6. For both the conditions the amplitude of excitation is about 8 mm. Plots will be drawn to compare surface elevations with different porosities for ($L/3$ and $2L/3$) baffle configurations respectively. Free surface of the water, $\eta(0, t)$ is normalized with respect to the depth of the water and equation are shown below.

$$\eta' = \frac{\eta}{h_s} \quad (5.1)$$

Where η is free surface elevation of the water and h_s is the static water depth.

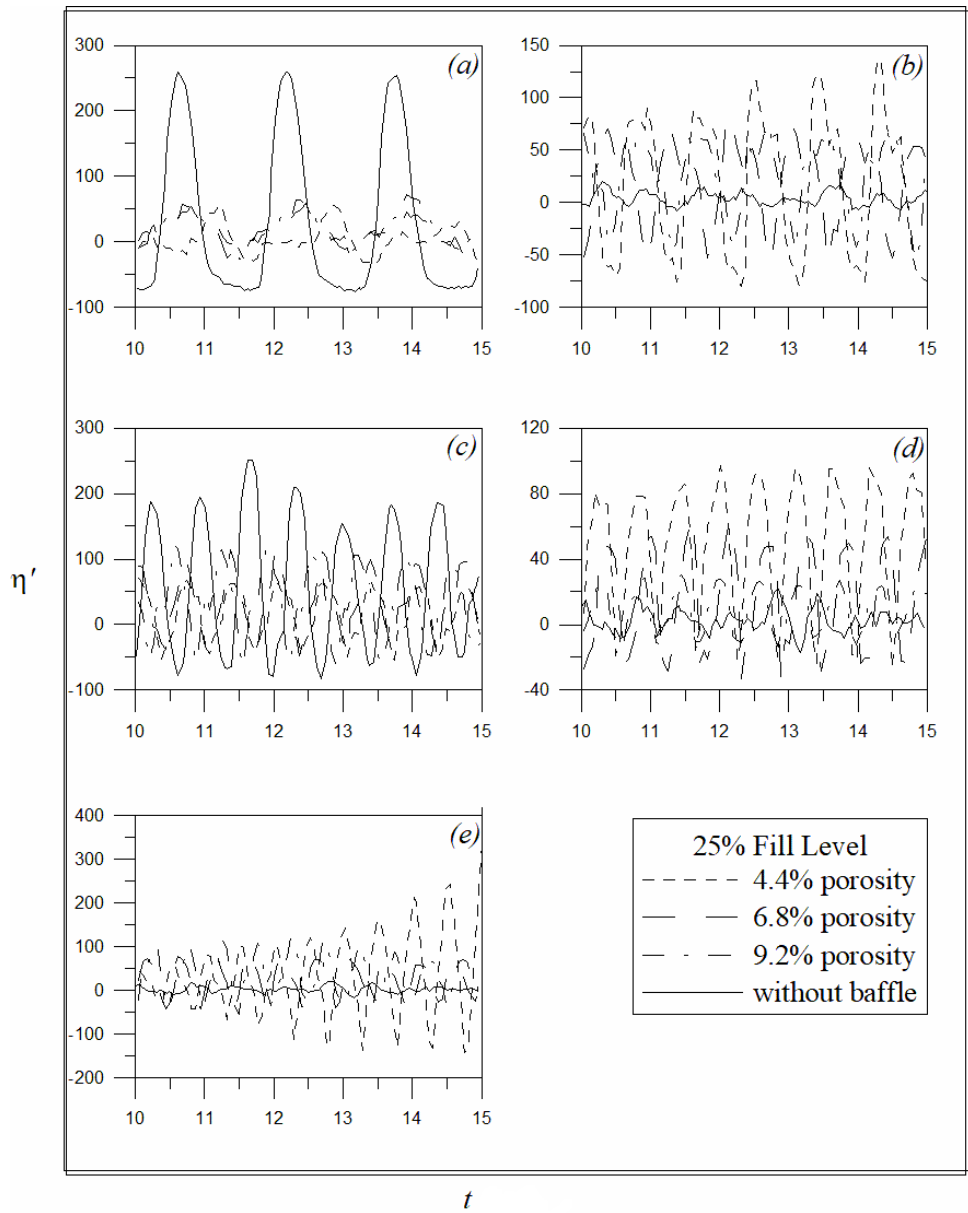


Figure. 5.1 Experimental free surface elevation response at $L/2$ location and excitation at natural sloshing frequencies $h_s/l = 0.163$, (a) $f = 0.6059 \text{ Hz}$ (f_1), (b) $f = 1.0967 \text{ Hz}$ (f_2), (c) $f = 1.4604 \text{ Hz}$ (f_3), (d) $f = 1.7376 \text{ Hz}$ (f_4) and (e) $f = 1.9637 \text{ Hz}$ (f_5)

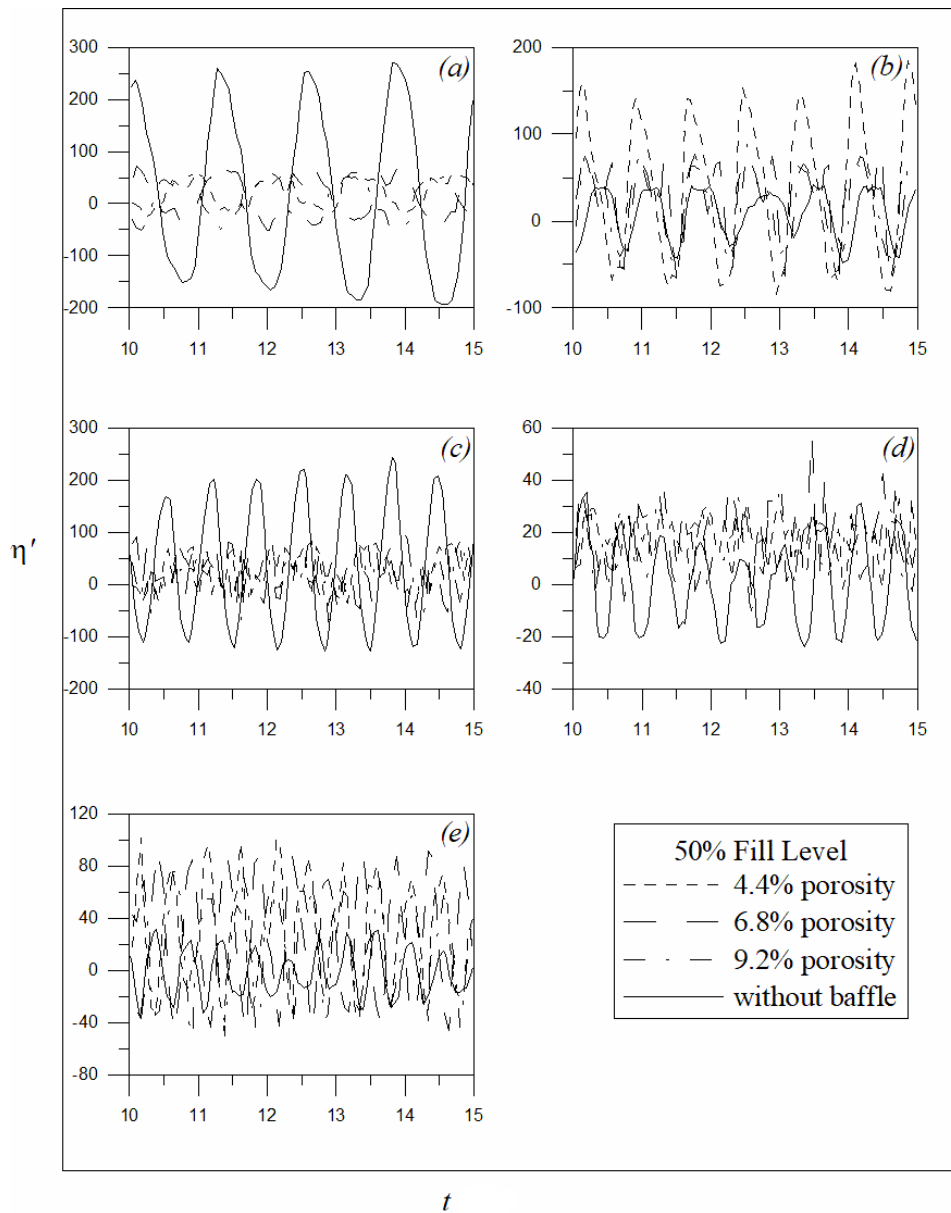


Figure 5.2 Experimental free surface elevation response at $L/2$ locations and excitation at natural sloshing frequencies $h_s/l = 0.325$, (a) $f = 0.7755 \text{ Hz}$ (f_1), (b) $f = 1.2277 \text{ Hz}$ (f_2), (c) $f = 1.5270 \text{ Hz}$ (f_3), (d) $f = 1.7666 \text{ Hz}$ (f_4) and, (e) $f = 1.9756 \text{ Hz}$ (f_5)

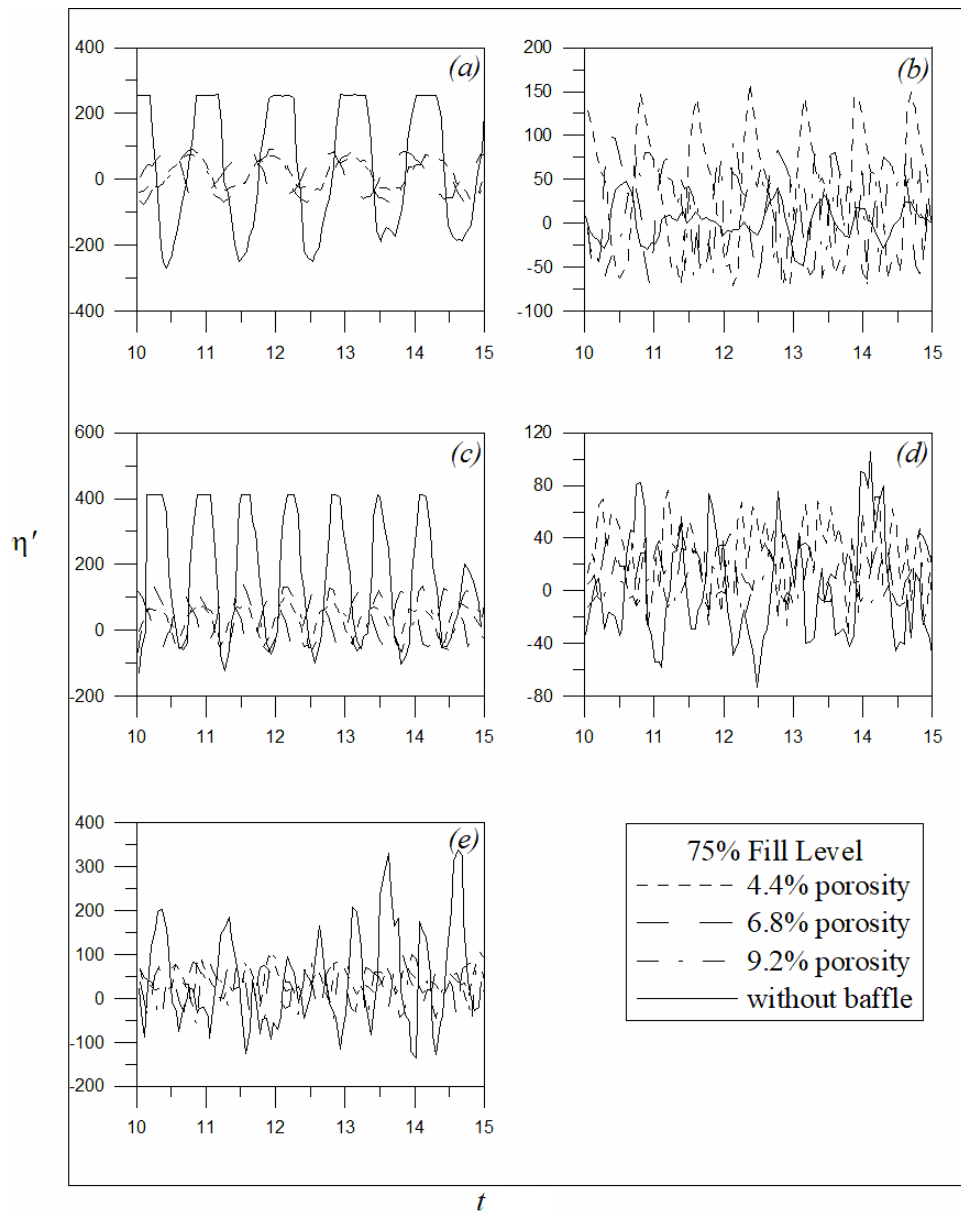


Figure 5.3 Experimental free surface elevation response at $L/2$ location and excitation at natural sloshing frequencies $h_s/l=0.488$, (a) $f= 0.8432 \text{ Hz}$ (f_1), (b) $f= 1.2468 \text{ Hz}$ (f_2), (c) $f= 1.5302 \text{ Hz}$ (f_3), (d) $f= 1.7671 \text{ Hz}$ (f_4) and, (e) $f= 1.9757 \text{ Hz}$ (f_5)

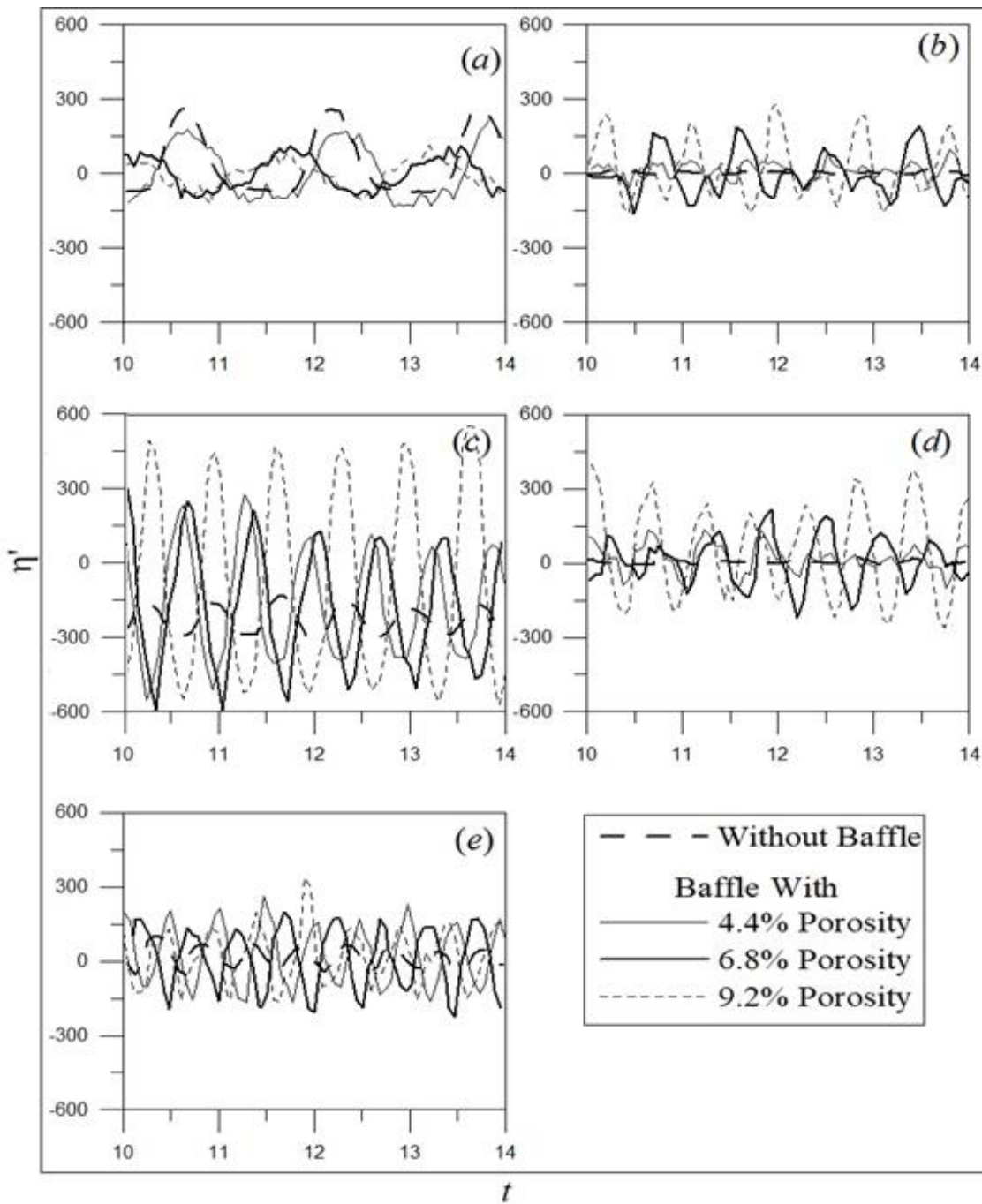


Figure 5.4 Experimental free surface elevation response at $L/3$ and $2L/3$ locations and excitation at natural sloshing frequencies $h_s/l = 0.163$, (a) $f = 0.6059 \text{ Hz}$ (f_1), (b) $f = 1.0967 \text{ Hz}$ (f_2), (c) $f = 1.4604 \text{ Hz}$ (f_3), (d) $f = 1.7276 \text{ Hz}$ (f_4) and, (e) $f = 1.9637 \text{ Hz}$

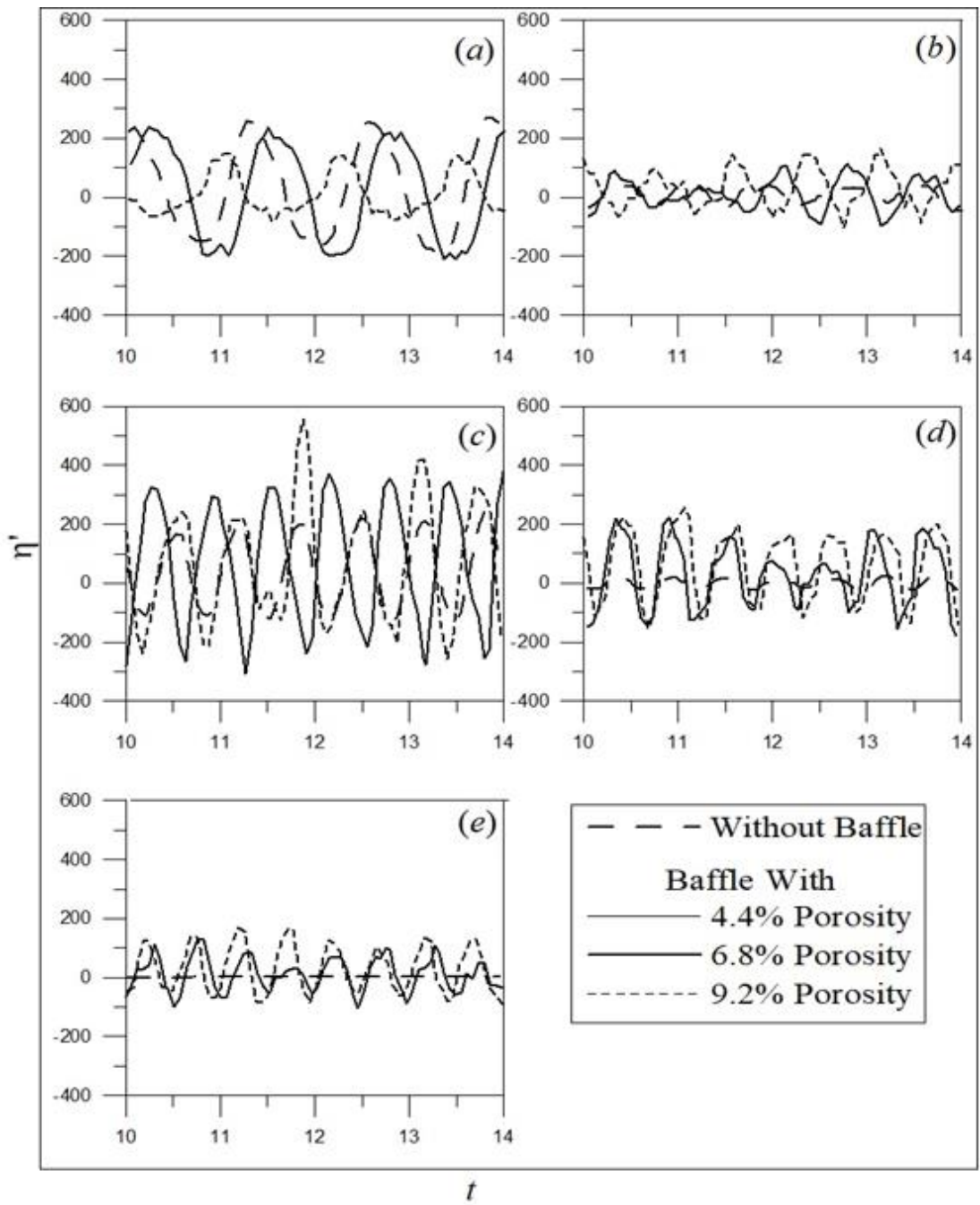


Figure 5.5 Experimental free surface elevation response for $L/3$ and $2L/3$ locations and excitation at natural sloshing frequencies $h_s/l = 0.325$, (a) $f = 0.7755 \text{ Hz}$ (f_1), (b) $f = 1.2277 \text{ Hz}$ (f_2), (c) $f = 1.5270 \text{ Hz}$ (f_3), (d) $f = 1.7666 \text{ Hz}$ (f_4) and, (e) $f = 1.9756 \text{ Hz}$ (f_5)

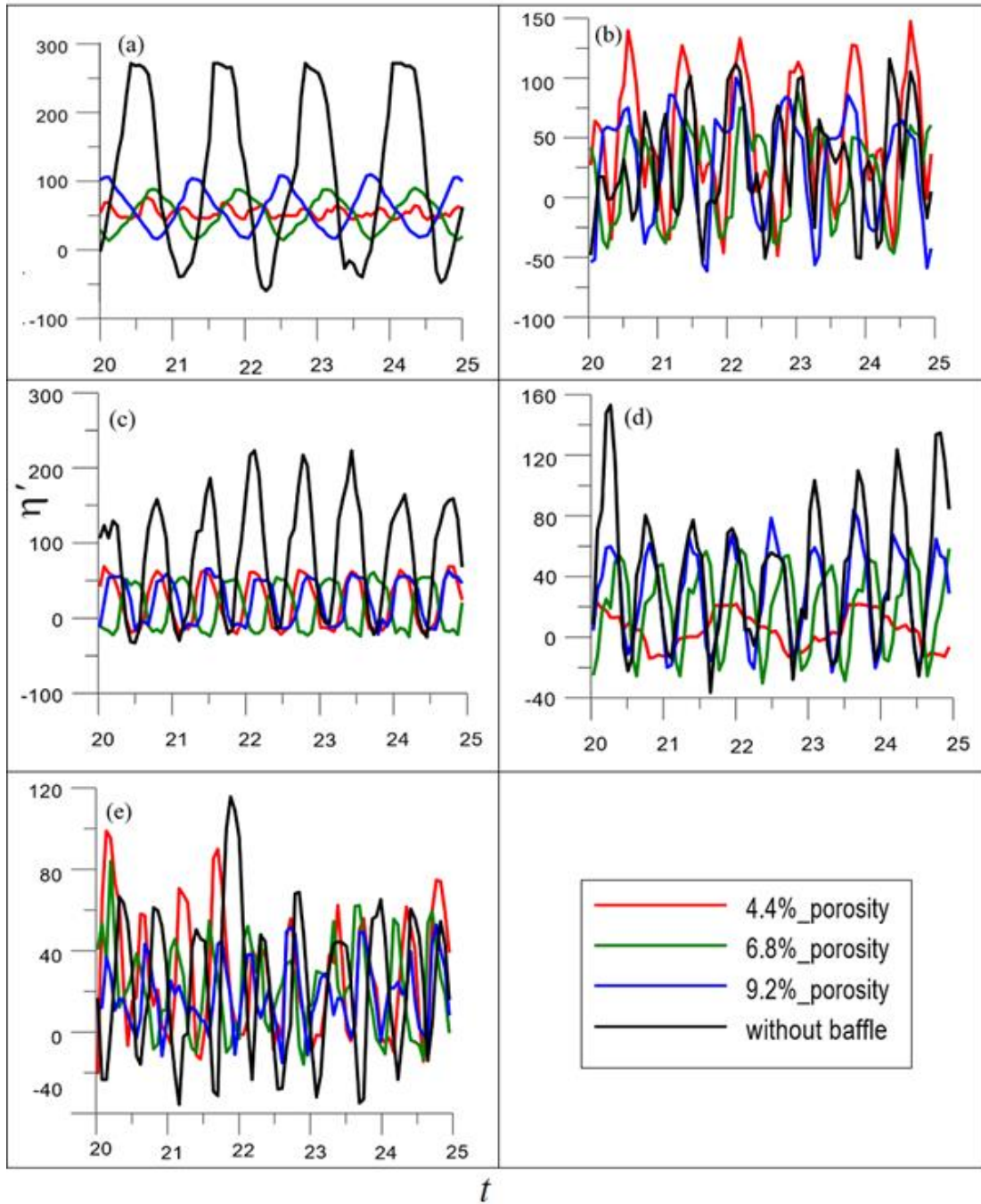


Figure 5.6 Experimental free surface elevation response for baffle at $L/3$ and $2L/3$ location and excitation at natural sloshing frequencies $h_s/l=0.488$, (a) $f= 0.8432 \text{ Hz}$ (f_1), (b) $f= 1.2468 \text{ Hz}$ (f_2), (c) $f= 1.5302 \text{ Hz}$ (f_3), (d) $f= 1.7671 \text{ Hz}$ (f_4) and, (e) $f= 1.9757 \text{ Hz}$ (f_5)

Comparison of above three fill levels with different porosities of free surface elevation response results with and no porous baffle leads to the following observations for $L/2$ conditions:

- As seen from graphs for both with and no baffle conditions, for the odd mode frequencies i.e, f_1 , f_3 , and f_5 the normalized free surface elevation is more compared to the even mode frequencies i.e, f_2 and f_4 for 25%, 50% & 75% fill levels.
- As in case of 50% of water depth there is slight changes, for the fifth mode frequency (f_5), the normalized free surface elevation is slightly lower than even mode frequencies.
- At the excitation of third mode sloshing, the normalized free surface sloshing elevation increases with increasing the porosity (4.4%, 6.8% and 9.2%) of the baffles for 25% water depth. And for 50% of water depth, 6.8% porosity gives η' is greater than 9.2% porosity.
- First mode frequency is the critical mode in both positions of baffles.
- In case of without baffle the normalized free surface elevation magnitude is keep decreasing with the increases in excitation frequency for the fill levels. But in case of with baffle the pattern is not same, the normalized free surface elevation for $h_s/l = 0.163$ condition is getting more respective at f_3 and in case of $h_s/l = 0.325$ condition more respective getting at f_1 .
- For third mode frequency (f_3), the normalized free surface sloshing amplitude is more compared to all other mode frequencies and it increases with increasing the porosity of the baffle for both 25% fill level and in case of 50% fill level it is occurring at first mode frequency (f_1).

Free surface elevation response results with and no porous baffle leads to the following observations for $L/3$ & $2L/3$ conditions:

- For both with and without baffle cases $h_s/l = 0.163$ tank has high free surface response amplitude than the $h_s/l = 0.325$ tank.
- For porous baffle third sloshing mode is the critical mode of sloshing.
- For second and fourth sloshing modes normalized free surface amplitude increases with increasing the porosity of the baffles.

- It is evident that the porous baffles show their inefficiency at the excitation of fifth mode sloshing ($f = f_5$) irrespective of the fill level considered.
- For both with and no baffle cases, $h_s/l = 0.163$ has high free surface response than the $h_s/l = 0.325$.
- Third sloshing mode is the critical mode of sloshing for porous baffles.
- For second and fourth sloshing modes, normalized free surface elevation increases with increasing the porosity of the baffles.
- As seen from the graphs the surface elevation in case of with porous baffle condition at odd mode frequencies ($f = f_1, f = f_3, f = f_5$) is lower than that of no baffle condition for porosities 4.4%, 6.8% and 9.2% respectively.
- In both baffle positions, the crucial mode is the first mode frequency for ($L/3$ and $2L/3$).
- Second and fourth mode frequencies does not show significant difference in surface elevation.

5.2.2 Mild Steel Plate

Figure 5.7 exhibits the steady state time histories of the normalized free surface oscillation at excitation of natural sloshing frequencies and demonstrates the comparison between no porous baffle and porous baffles conditions at $L/2$ location for 25% filled condition ($h_s/l = 0.163$). Similarly, Figure 5.8 and Figure 5.9 demonstrate the same for 50% filled condition ($h_s/l = 0.325$) and 75% filled condition ($h_s/l = 0.488$) respectively with the porosities considered is 15%, 20% and 25%. For all three conditions the amplitude of excitation is about 8 mm.

The oscillation of the free surface elevation is greatly enhanced by resonance when the frequency ratio is increased to ($f=f_1$), which corresponds to the first mode of the natural frequency in the rectangular tank as shown in Figure 5.7(a). This is due to the fact that when the oscillations of the tank coincide with the oscillations of the flow, the amount of energy that the flow absorbs is maximized. When the oscillations of the flow match the natural frequency of vibration of the system, the flow tends to absorb more energy than it does at other frequencies. However, the variation of the free surface elevation is not significant in comparison to the free surface elevations of the neighboring frequency ratios when $f = f_2$, which corresponds to the second mode of the natural frequency as

shown in Figure 5.7(b). At the excitation of $f=f_2$, a sudden increase in the amplitude of the free surface elevation does not occur. Very weak liquid sloshing at frequency ratio f_2 supports this, as illustrated in Figure 5.7(b). In this instance, a portion of the fluids oscillation energy is actually extracted by the opposing force as a result of the tanks oscillation. The frequency of excitation over a range around the natural frequencies also influences the rate of sloshing as the frequency rises beyond f_2 . Thus, when $f=f_3, f_4$, and f_5 , the free surface elevations are augmented compared with neighboring frequency ratios, as shown in Figures 5.7(c), 5.7(d) and 5.7(e), respectively. Based on the mentioned results for the free surface elevations for different frequency ratios, it is understood that the resonant frequency is definitely the first mode of the fluid's natural frequency in the rectangular tank. The same trend is observed for 50% fill conditions ($h_s/l = 0.325$) and 75% fill conditions ($h_s/l = 0.488$) as shown in Figure 5.8 and Figure 5.9 respectively. The free surface elevations are augmented compared with neighboring frequency ratios as shown in Figures 5.10, 5.11 and 5.12, respectively for $L/3$ and $2L/3$ conditions.

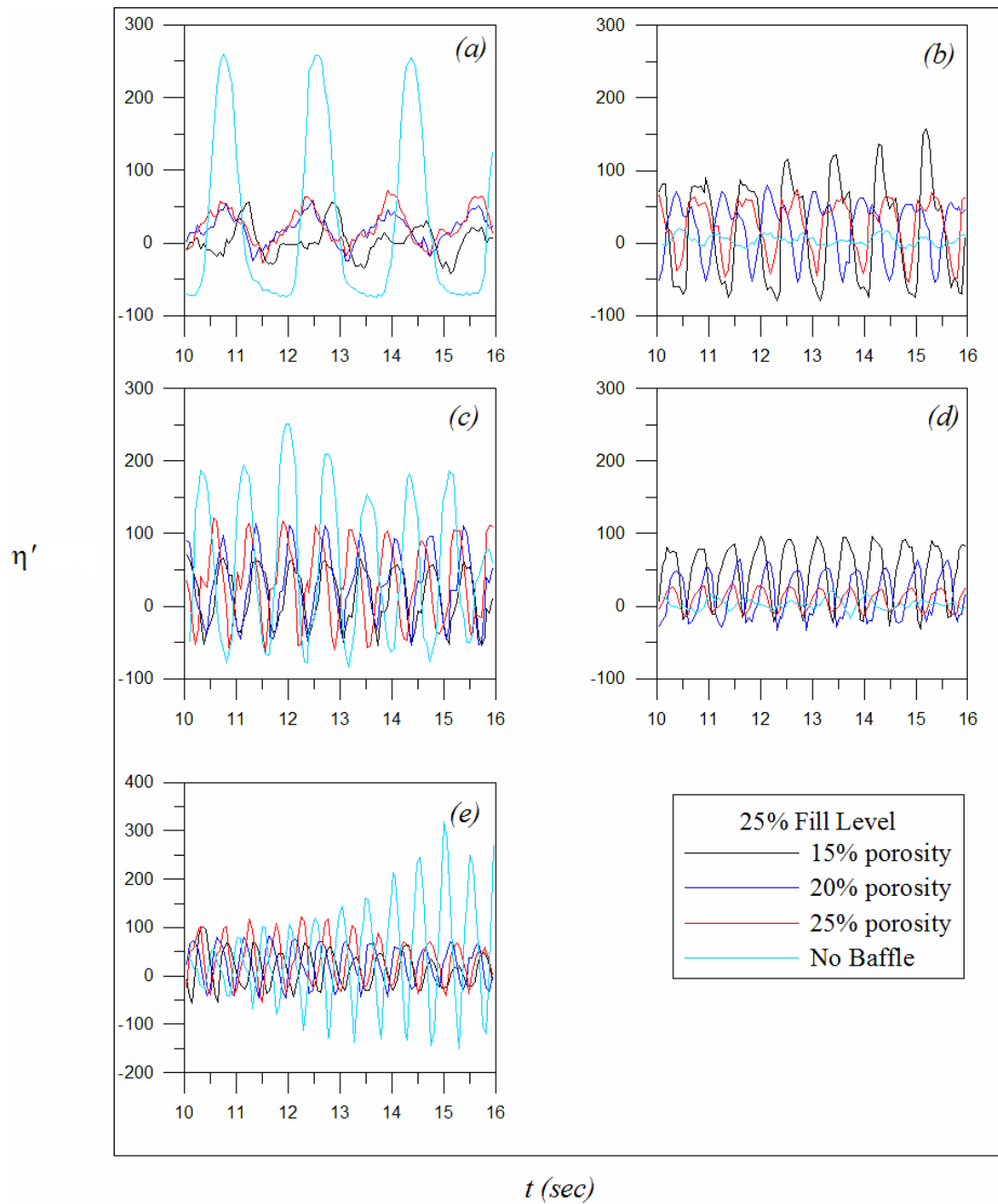


Figure 5.7 Time histories of free surface elevation with various frequency ratios at $L/2$ location for $h_s/l = 0.163$, (a) $f = 0.6059 \text{ Hz}$ (f_1), (b) $f = 1.0967 \text{ Hz}$ (f_2), (c) $f = 1.4604 \text{ Hz}$ (f_3), (d) $f = 1.7376 \text{ Hz}$ (f_4) and (e) $f = 1.9637 \text{ Hz}$ (f_5)

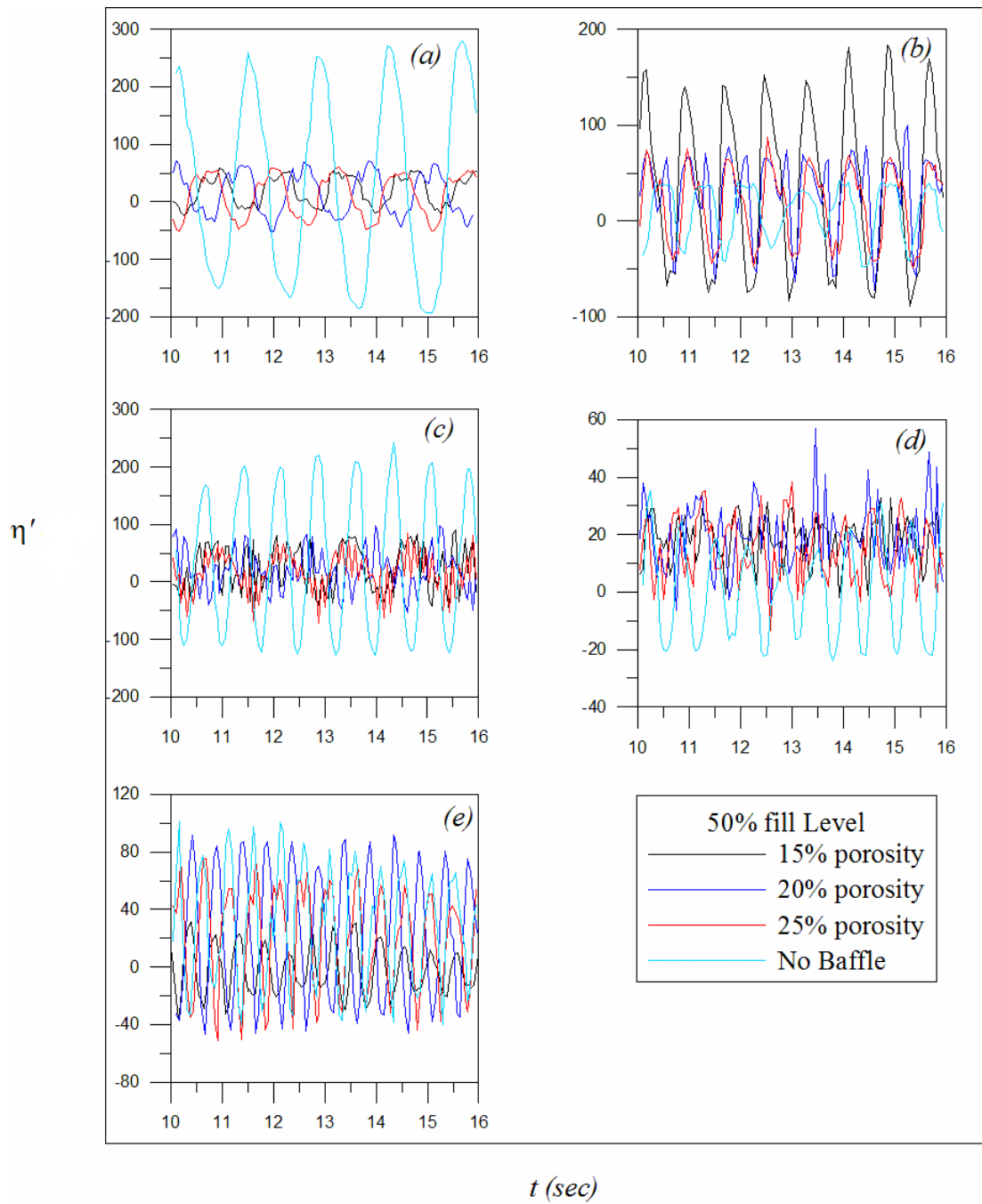


Figure 5.8 Time histories of free surface elevation with various frequency ratios at $L/2$ location for $h_s/l = 0.325$, (a) $f = 0.7755$ Hz (f_1), (b) $f = 1.2287$ Hz (f_2), (c) $f = 1.5270$ Hz (f_3), (d) $f = 1.7666$ Hz (f_4) and (e) $f = 1.9757$ Hz (f_5)

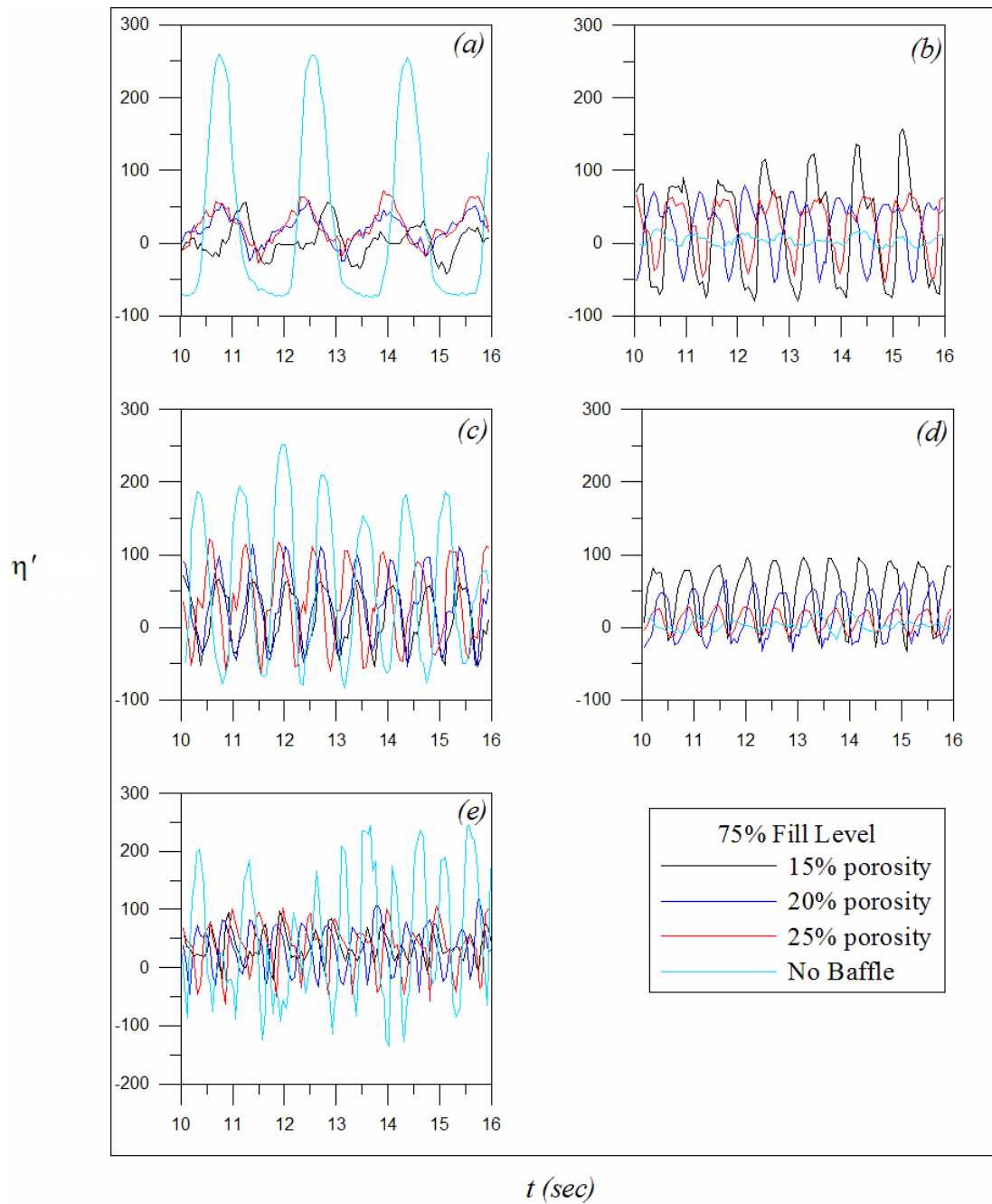


Figure 5.9 Time histories of free surface elevation with various frequency ratios at $L/2$ location for $h_s/l = 0.488$, (a) $f = 0.8432 \text{ Hz}$ (f_1), (b) $f = 1.2468 \text{ Hz}$ (f_2), (c) $f = 1.5302 \text{ Hz}$ (f_3), (d) $f = 1.7671 \text{ Hz}$ (f_4) and (e) $f = 1.9757 \text{ Hz}$ (f_5)

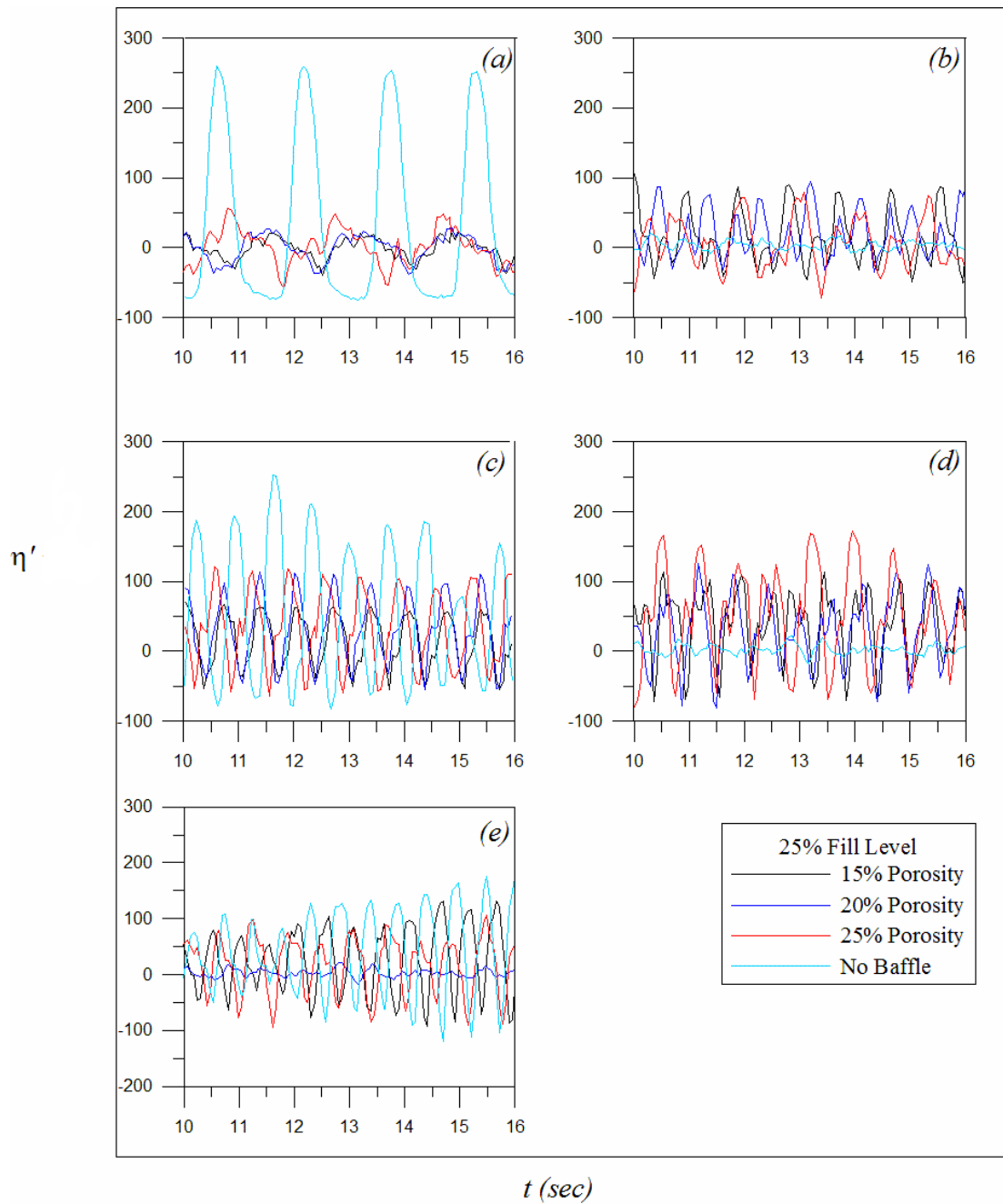


Figure 5.10 Time histories of free surface elevation with various frequency ratios at $L/3$ & $2L/3$ locations for $h_w/l = 0.163$, (a) $f = 0.6059 \text{ Hz}$ (f_1), (b) $f = 1.0967 \text{ Hz}$ (f_2), (c) $f = 1.4604 \text{ Hz}$ (f_3), (d) $f = 1.7376 \text{ Hz}$ (f_4) and (e) $f = 1.9637 \text{ Hz}$ (f_5)

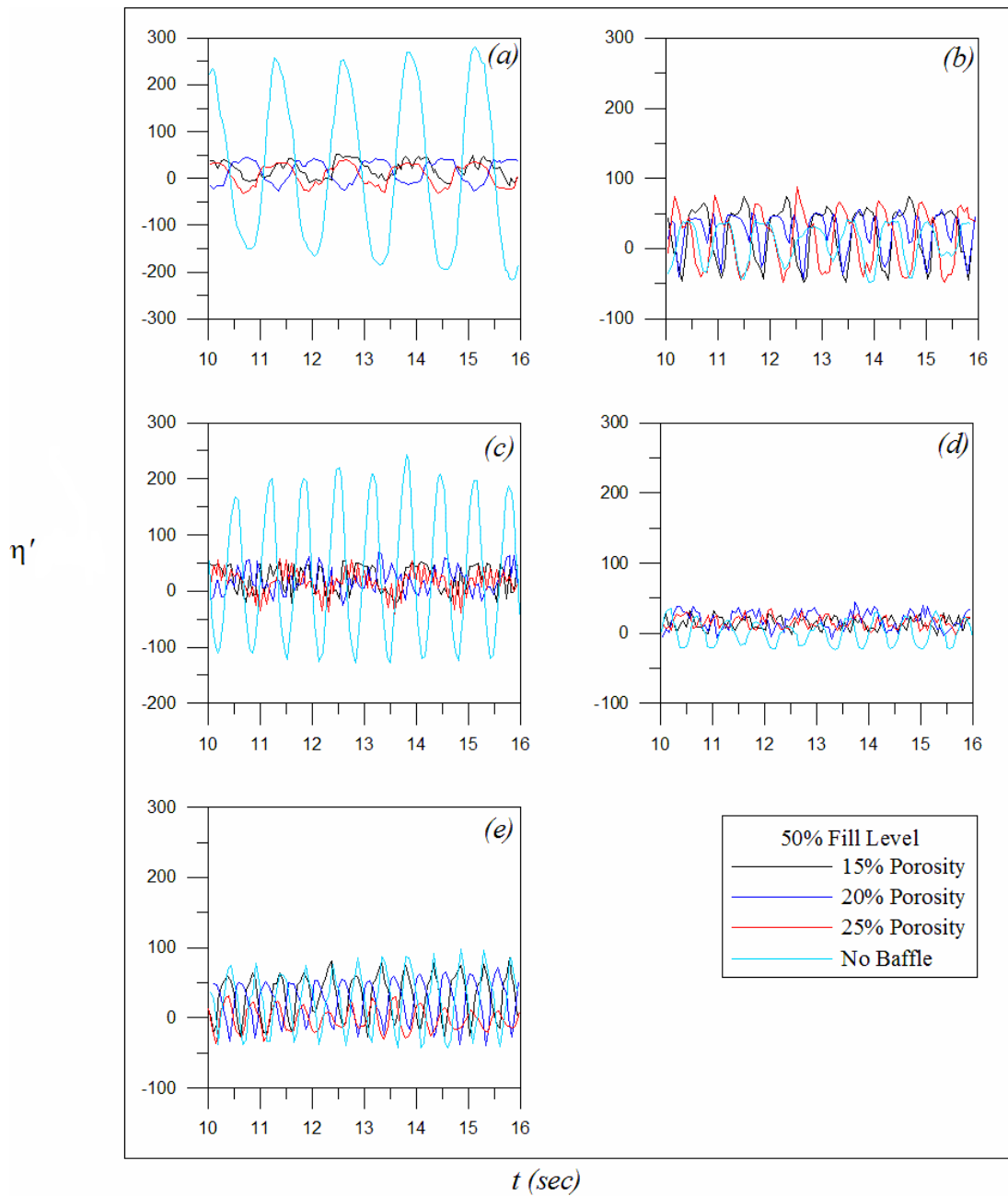


Figure 5.11 Time histories of free surface elevation with various frequency ratios $L/3$ & $2L/3$ locations for $h_s/l = 0.325$, (a) $f = 0.7755 \text{ Hz}$ (f_1), (b) $f = 1.2287 \text{ Hz}$ (f_2), (c) $f = 1.5270 \text{ Hz}$ (f_3), (d) $f = 1.7666 \text{ Hz}$ (f_4) and (e) $f = 1.9757 \text{ Hz}$ (f_5)

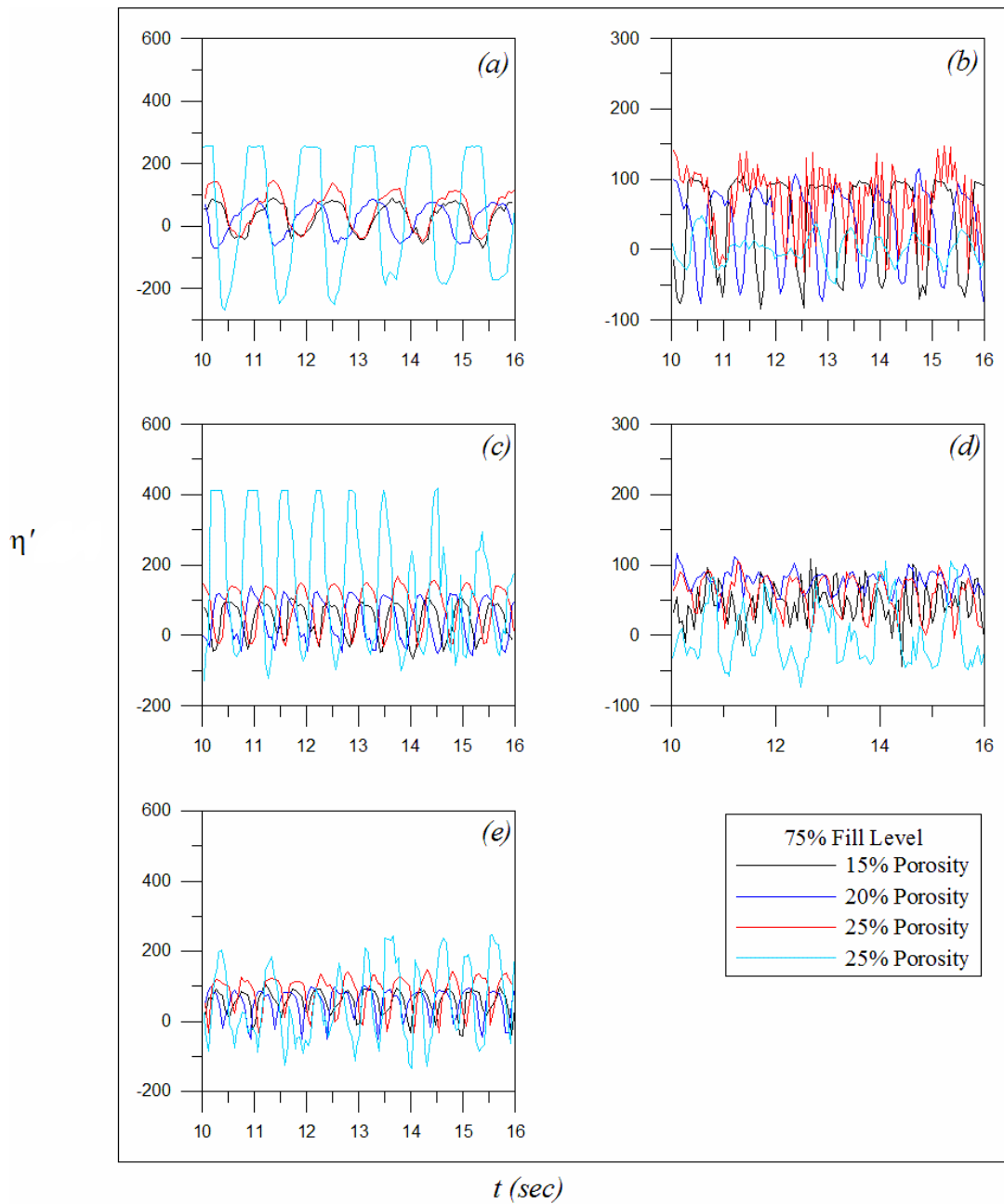


Figure 5.12 Time histories of free surface elevation with various frequency ratios $L/3$ & $2L/3$ locations for $h_s/l = 0.488$, (a) $f = 0.8432 \text{ Hz}$ (f_1), (b) $f = 1.2468 \text{ Hz}$ (f_2), (c) $f = 1.5302 \text{ Hz}$ (f_3), (d) $f = 1.7671 \text{ Hz}$ (f_4) and (e) $f = 1.9757 \text{ Hz}$ (f_5)

Comparing the free surface response elevation for with porous and no porous baffles of different porosities leads to the following observations.

- As seen from graphs for with baffle case, the normalized free surface elevation at $f=f_l$ is less than the no baffle condition for all 25%, 50% and 75% of water depths.
- At the excitation of third mode sloshing, the normalized free surface sloshing elevation increases with increasing the porosity (15%, 20% and 25%) of the baffles for 25% water depth and for 50% of water depth, 20% porosity gives higher fluid oscillation than 25% porosity.
- It is marked that the porous baffles show their inefficiency at the excitation of fifth mode sloshing ($f=f_5$) irrespective of the fill levels considered.
- For with porous baffle case, $h_s/l = 0.163$ has high free surface response than observed for $h_s/l = 0.325$ and $h_s/l=0.488$ and for no porous cases, $h_s/l = 0.488$ has high free surface response than observed for $h_s/l = 0.163$ and $h_s/l=0.325$.
- Third mode sloshing is the critical mode of sloshing for porous baffles in all the cases which can be seen from the results.
- It is marked that the porous baffles show their inefficiency at the excitation of fifth mode sloshing ($f=f_5$) irrespective of the fill levels considered.
- For with porous baffle case, $h_s/l = 0.163$ has high free surface response than observed for $h_s/l = 0.325$ and $h_s/l=0.488$ and for no porous cases, $h_s/l = 0.488$ has high free surface response than observed for $h_s/l = 0.163$ and $h_s/l=0.325$.
- Third mode sloshing is the critical mode of sloshing for porous baffles in all the cases which can be seen from the results.

5.3 MAXIMUM FREE SURFACE ELEVATION

5.3.1 Acrylic Sheet

The maximum free surface response gives the maximum free surface run-up in the sloshing tank for given excitation amplitude of 8mm and excitation frequencies. The excitation frequency modes and frequency ratios are given the Table 4.1. The excitation

frequencies ranging from 0.4566 Hz to 1.9637 Hz encompasses up to fifth mode sloshing frequency. The graph is plotted in between the normalized η_{max} versus frequency ratio (f/f_1). The shake table is operated with particular excitation amplitude and excitation frequencies.

$$f_n = \frac{1}{2\pi} \sqrt{\frac{n\pi g}{l} \tanh\left(\frac{n\pi h_s}{l}\right)} \quad n=1, 2, 3, \dots \quad (5.2)$$

Where,

l is the length of the tank,

h_s is the static liquid depth

n is the surface mode.

By the MATLAB coding the maximum wave amplitude (η_{max}) is found and η_{max} is normalized with the excitation amplitude (A) and this normalized η_{max} plotted with frequency ratio. The graphs are shown in figure 5.14 to 5.17 for both no baffle and with porous baffle.

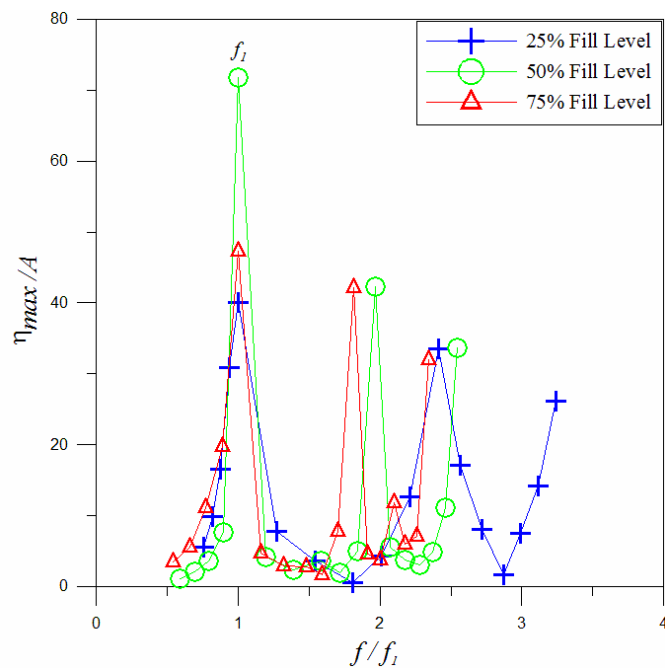


Figure 5.13 Variation of η_{max}/A no porous baffle with various frequencies ratio for $h_s/l = 0.163, 0.325$ and 0.488

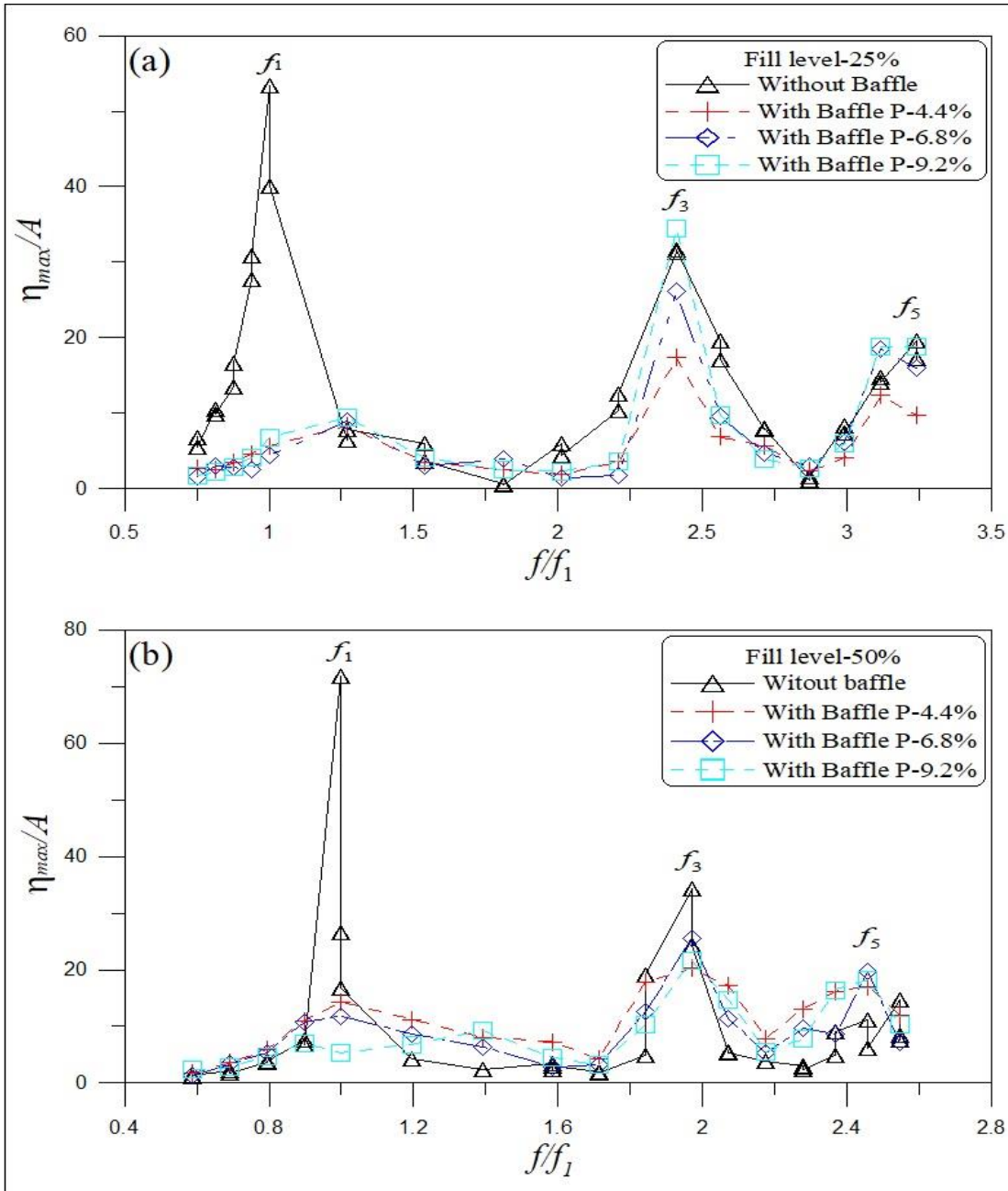


Figure 5.14 Variation of η_{max}/A with and without porous baffle for frequencies ratios (f/f_1), at $L/2$ location (a) $h_s/l = 0.163$ and, (b) $h_s/l = 0.325$

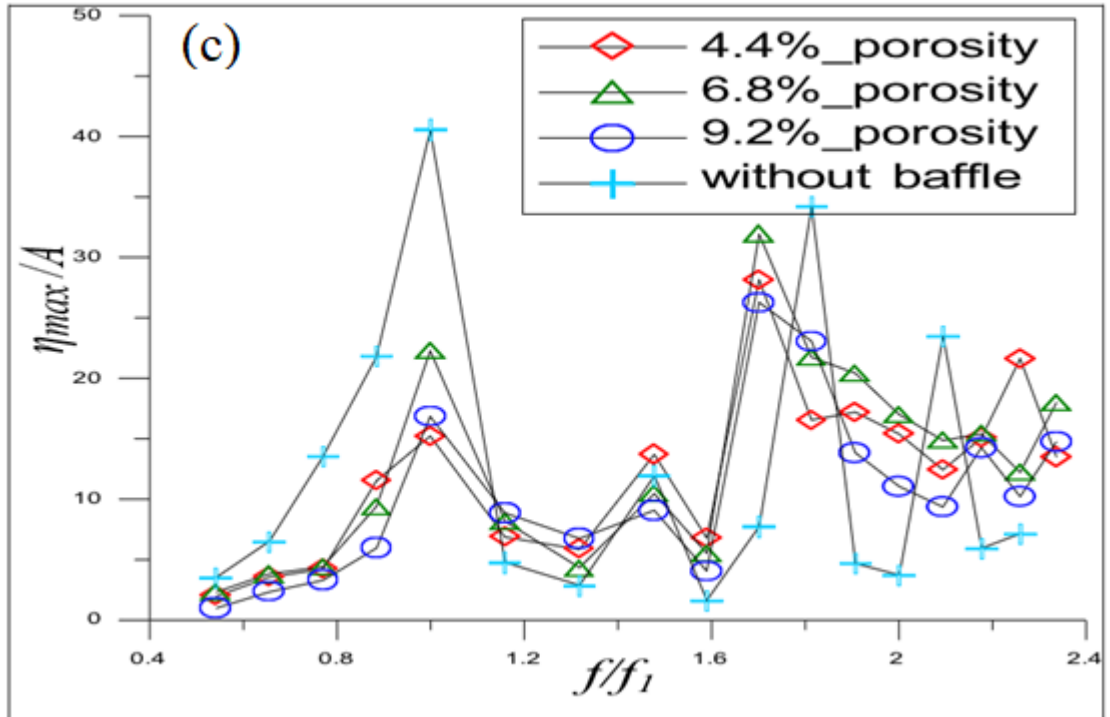


Figure 5.15 Variation of η_{max}/A with and without porous baffle for frequencies ratios (f/f_1), at $L/2$ location (c) $hs/l = 0.488$

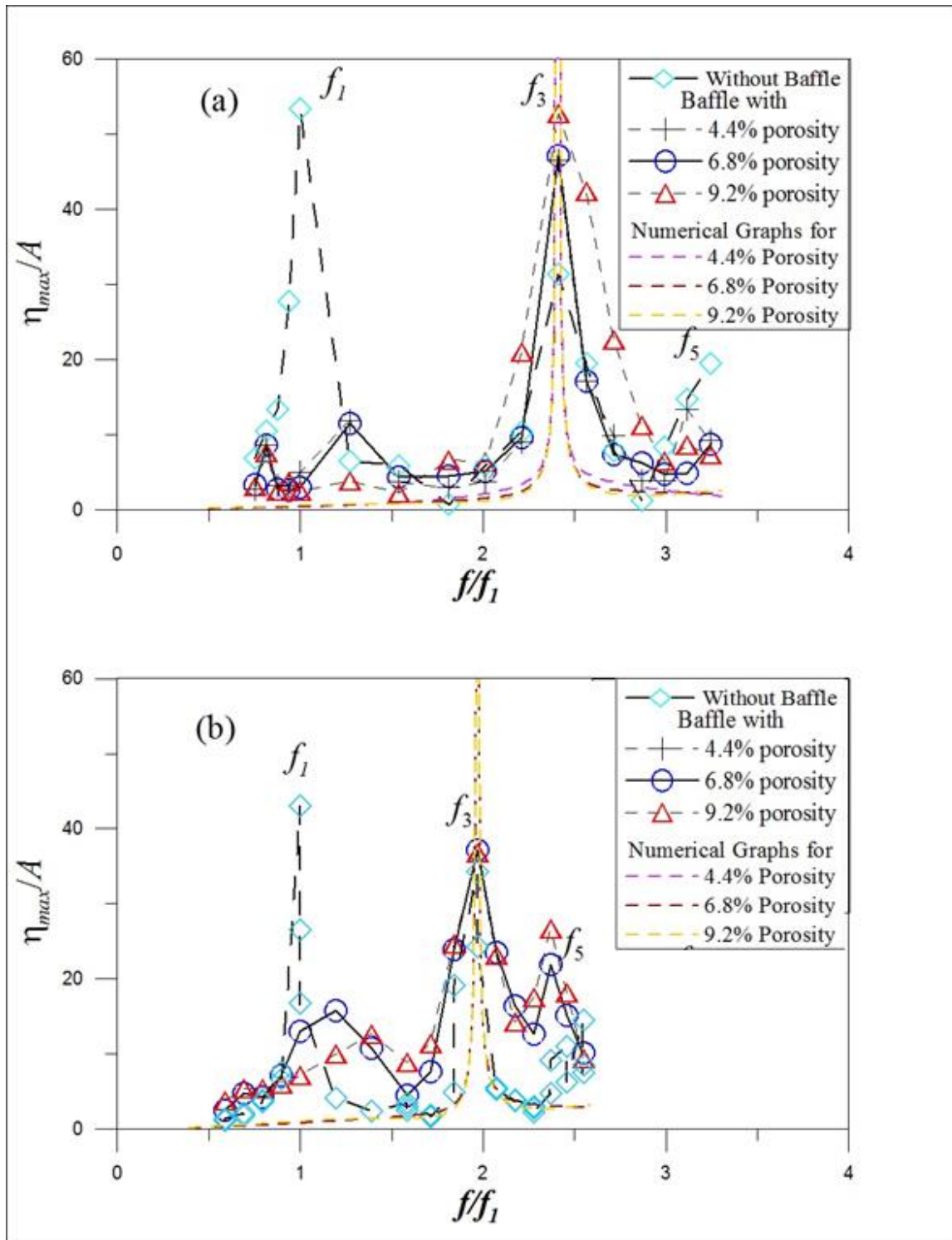


Figure 5.16 Variation of η_{max}/A with and without porous baffle to different frequencies ratio (f/f_1), at $L/3$ & $2L/3$ locations (a) $h_s/l = 0.163$ and, (b) $h_s/l = 0.325$

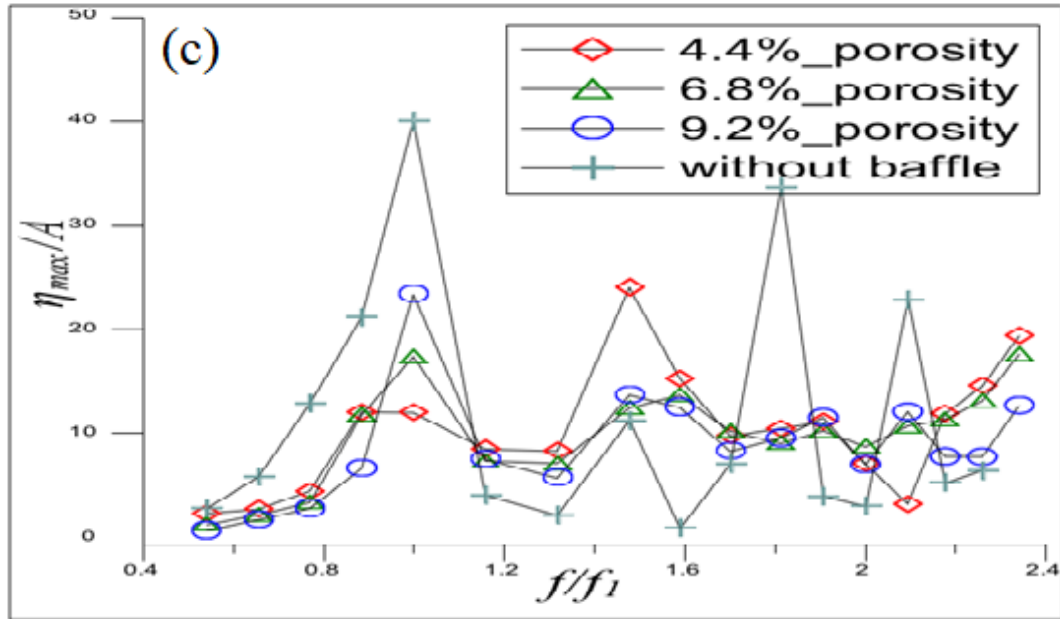


Figure 5.17 Variation of η_{max}/A with and without porous baffle to different frequencies ratio (f/f_1), at $L/3$ & $2L/3$ (c) $h_s/l = 0.488$

Comparing the above results of maximum free surface elevation obtained for with and without baffle condition leads to the following observations for $L/2$ locations:

- At excitation frequencies, the without baffle wall scenario demonstrates that free surface response for 25% fill condition ($h_s/l = 0.163$) is lower than 50% fill condition ($h_s/l = 0.325$)
- For both with and without a baffle wall conditions, higher responses are seen at odd mode frequencies in the following order of $f = f_1, f = f_3$ and $f = f_5$.
- Maximum sloshing response at $f = f_1$, is completely suppressed for all porous baffle conditions. However sloshing response is observed to be increased at $f = f_3$ and decreased at $f = f_5$, due to presence of the baffle.
- The maximum peak is getting at critical mode frequency i.e. f_1 and as frequency increases, the free surface amplitude goes on decreases for both condition.
- For the other mode frequency (f_3 and f_5) for both fill levels ($h_s/l = 0.325$ and $h_s/l = 0.163$) condition it is observed that, the free surface amplitude is higher for

with baffle compare to without Baffle. Because for this mode frequency the oscillation is less.

- Now comparing plots with and without porous baffles for both fill levels ($h_s/l = 0.163$ and $h_s/l = 0.325$), as we can see there is considerably reduction in amplitude for the first mode frequency (f_1) when we place the baffle. As in case of other mode frequencies, there is little reduction in the oscillation.
- Now coming to the porosity condition, it observed that as the porosity increases, the increase in the free surface response amplitude observed.
- By considering without baffle case at all excitation frequencies, it can be seen that free surface response is higher for 25% fill level ($h_s/l = 0.163$) than the response obtained for 50% fill level ($h_s/l = 0.325$)
- Comparing with and without porous baffles of $h_s/l = 0.163$, maximum free surface response elevation decreases for the excitation at first and fifth sloshing modes frequencies and increases for the excitation at third sloshing mode frequency.
- As said above similar observation is done for $h_s/l = 0.325$ condition.
- The free surface elevation increases with increasing the porosities for all excitation frequencies considered.

Free surface elevation obtained for with and without baffle condition leads to the following observations for $L/3$ & $2L/3$ locations:

- For all porous conditions, the maximum sloshing response is shown at $f = f_3$, as compared to $f = f_1$ for the no baffle condition.
- At odd mode sloshing frequencies $f = f_1$, $f = f_3$ and $f = f_5$, higher response is seen when considering the absence of the baffle conditions.
- Maximum sloshing response at $f = f_1$ is completely suppressed by all porous baffle conditions. However sloshing response is observed to be increased at $f = f_3$ and slightly decreased at $f = f_5$ due to the presence of porous baffle.
- Experimental results of porous conditions are compared with numerical work. It can be seen that a good correlation and maximum response at $f = f_3$ is predicted exactly.

- For both baffle conditions, the maximum surface elevation is lower in the case of the baffle condition for the first, third, and fifth modes ($L/3$ & $2L/3$).
- Since the first frequency mode is the critical mode, it has the highest maximum surface elevation.
- For all porosities, the second and fourth frequency mode maximum surface elevation reported under no baffle condition is lower than that of with baffle conditions.

5.3.2 Mild Steel Plate

Figure 5.18 shows the variation of normalized maximum free surface elevation η_{\max}/A as a function of the frequency ratio. When the frequency ratio is in the range of $0.6 \leq f/f_1 \leq 0.9$, the free surface elevation increases slightly. However, as f/f_1 increases from 0.8 to 1 (f_1), the free surface elevates significantly.

As f/f_1 increases further beyond $f=f_1$, the free surface elevation gradually drops until it hits and approaches the local minimum at f_2 . As f/f_1 keeps increasing from f_2 , the free surface elevation begins to rise again and reaches the second largest peak at f_3 . For further increase in f/f_1 resulting the free surface elevation decreases and increases alternatively and hence the local peaks at f_4 and f_5 correspond to the natural frequency modes. Similar trend is observed for the aspect ratio of 0.325 and 0.488 which is projected in Figure 5.19 and Fig. 5.20 respectively.

Fig. 5.21 shows the variation of normalized maximum free surface elevation η_{\max}/A as a function of the frequency ratio for $L/3$ and $2L/3$. When the frequency ratio is in the range of $0.6 \leq f/f_1 \leq 0.9$, the free surface elevation increases slightly. However, as f/f_1 increases from 0.8 to 1 (f_1), the free surface elevates significantly. Similar trend is observed for the aspect ratio of 0.325 and 0.488 which is projected in Figure 5.22 and Figure 5.23 respectively.

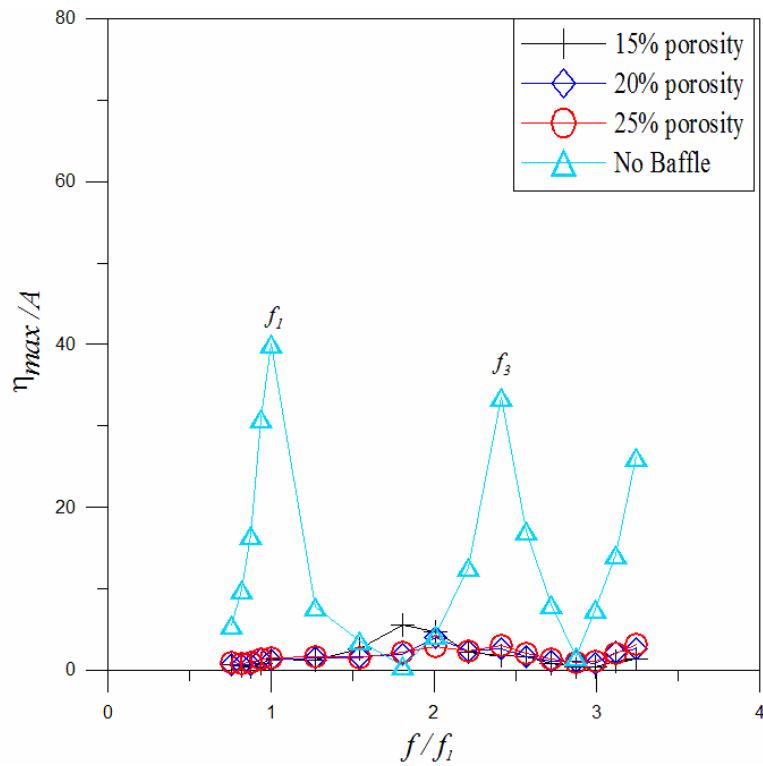


Figure 5.18 Variation of η_{max}/A with and no porous baffle with various frequencies ratio for $h_s/l = 0.163$ for $L/2$ locations

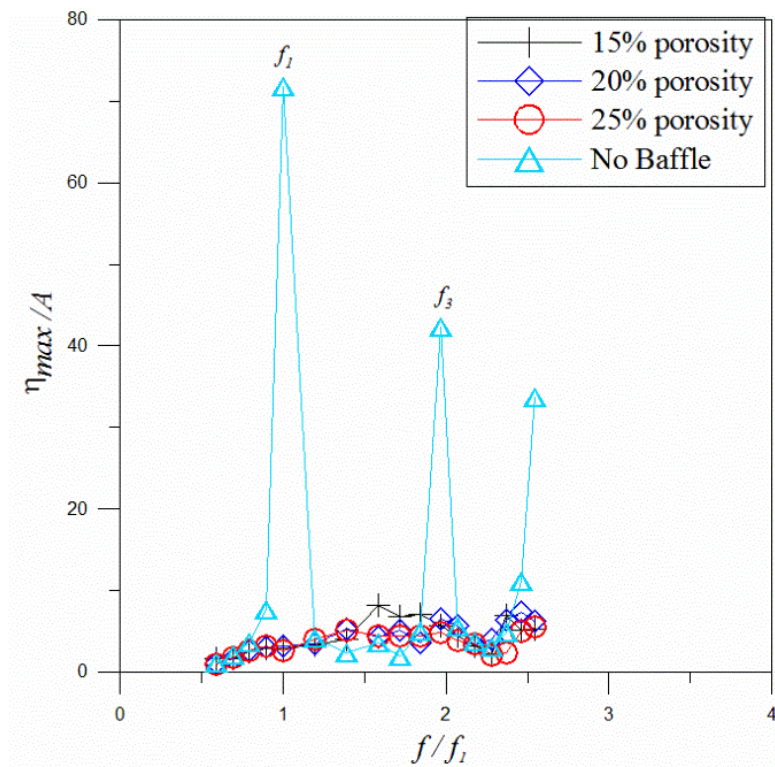


Figure 5.19 Variation of η_{max}/A with and no porous baffle with various frequencies ratio for $h_s/l = 0.325$ for $L/2$ locations

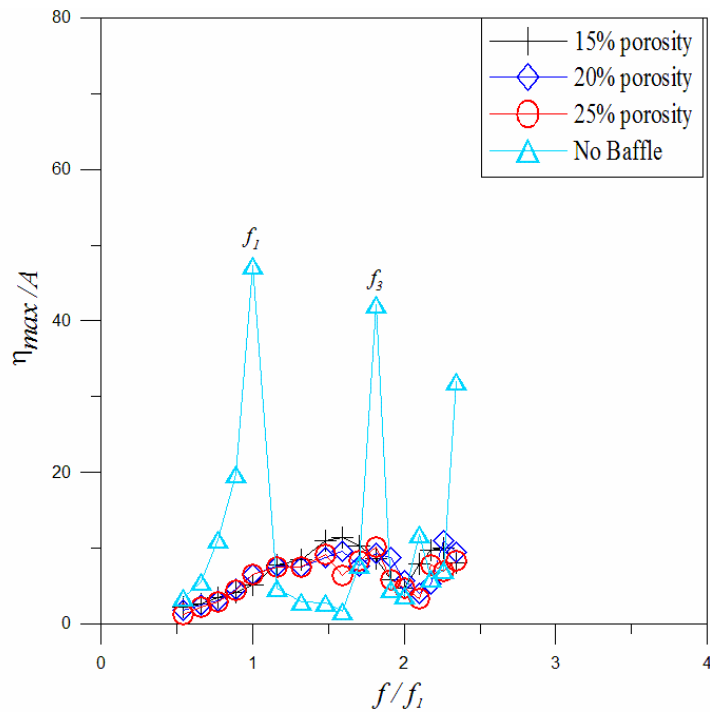


Figure 5.20 Variation of η_{max} / A with and no porous baffle with various frequencies ratio for $h_s/l = 0.488$ for $L/2$ locations

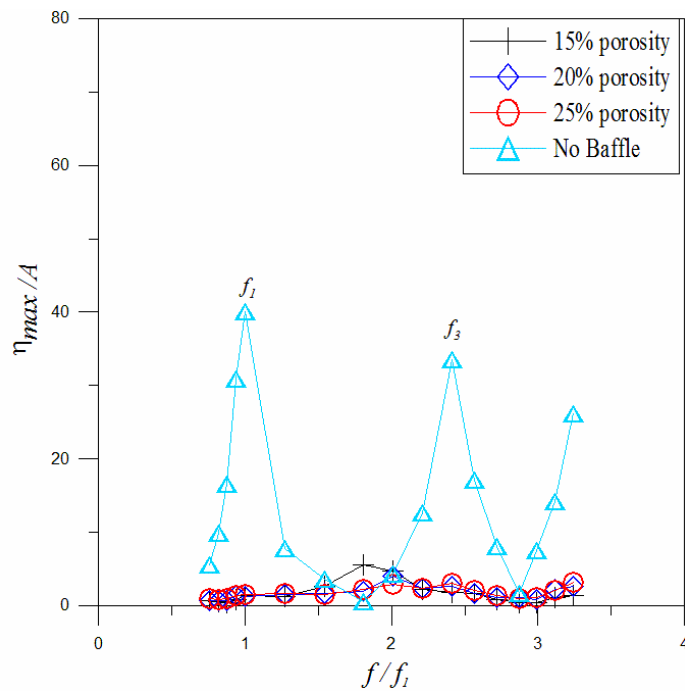


Figure 5.21 Variation of η_{max} / A with and no porous baffle with various frequencies ratio for $h_s/l = 0.163$ for $L/3$ and $2L/3$ locations

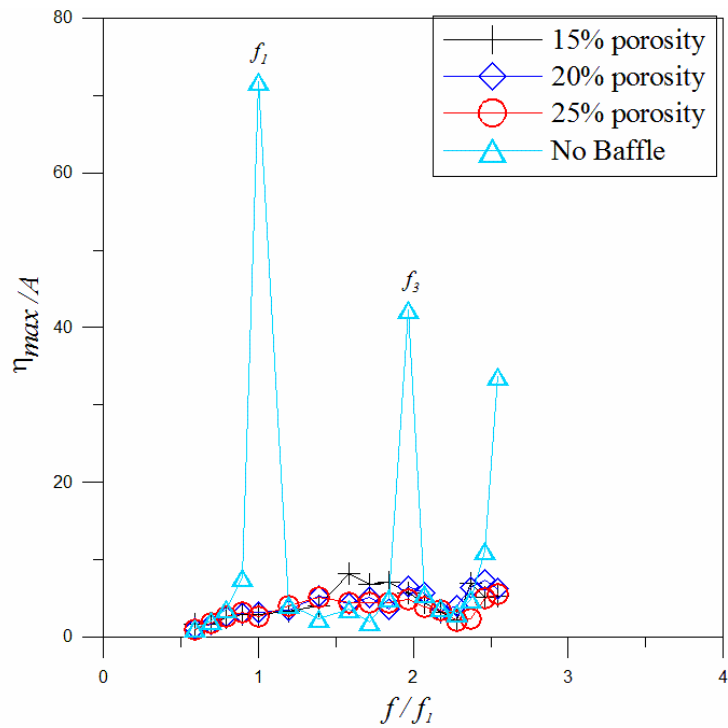


Figure 5.22 Variation of η_{max} / A with and no porous baffle with various frequencies ratio for $h_s/l = 0.325$ for $L/3$ and $2L/3$ locations

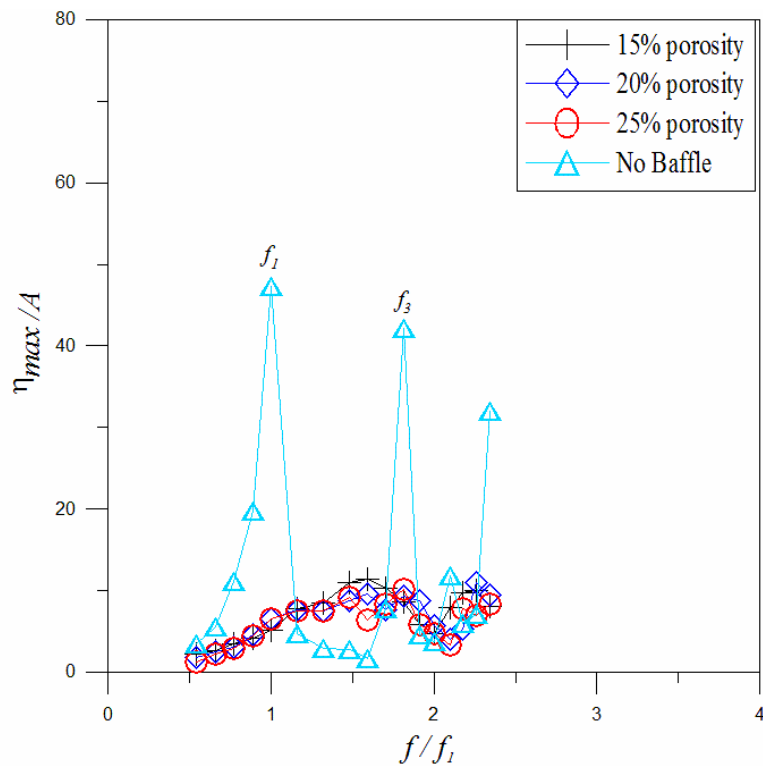


Figure 5.23 Variation of η_{max} / A with and no porous baffle with various frequencies ratio for $h_s/l = 0.488$ for $L/3$ and $2L/3$ locations

Comparing the maximum free surface response elevation of different porosities with and without porous baffles leads to following observations.

- In order to examine the effect of a natural frequency mode on liquid sloshing considering without baffle case at constant excitation frequencies, It has been found that the free surface response is higher for a liquid fill depth $h_s/l = 0.325$ than the response acquired by $h_s/l = 0.163$ and $h_s/l = 0.488$. Higher response is shown when the baffle scenario is not taken into account, specifically for odd mode sloshing frequencies in the order of $f=f_1$, $f=f_3$ and $f=f_5$.
- Maximum free surface elevation increases for the excitation of first mode frequency and decreases for the excitation at fifth sloshing mode frequency when compared to no baffle and with porous baffles of $h_s/l = 0.325$.
- In a similar manner, the observation was carried out for all the three conditions i.e., 25%, 50%, and 75% fill water depths. It is concluded that for all excitation frequencies taken into account, free surface elevation increases as porosities increase.
- For all three porous conditions, the maximum sloshing response is seen at $f = f_3$ for all the three porous conditions and $f = f_1$ which is for no baffled condition for all the water depth cases. Further it is clear that among all the filled conditions the sloshing oscillation is observed to be high for $h_s/l = 0.325$.
- All porous baffle conditions completely reduce the maximum sloshing response elevation at $f = f_1$. Though sloshing response is observed to be increased at $f = f_3$ and slightly decreases at $f = f_5$ due to the existence of porous baffle.

5.4 ENERGY DISSIPATION

Energy dissipation plots are plotted to know that how much energy is dissipated for one cycle of table motion. Energy dissipation is calculated by,

$$E_d = \int F dx \quad (5.3)$$

Where, F is the base shear force and x is the shake table displacement. For the normalization of energy,

$$E'_w = \frac{Ed}{\frac{1}{2}m_w(2\pi fA)^2} \quad (5.4)$$

Where,

- A Excitation amplitude
- m_w Total mass of the fluid
- f Excitation frequency

Equation 6 gives the normalized energy. The denominator represents the kinetic energy of the fluid if it is considered as a solid mass.

5.4.1 Acrylic Sheet

Graphs are plotted against normalized energy and frequency ratios. For with and without porous baffle cases the excitation frequency ranges from 0.4566 Hz to 1.9757 Hz, excitation amplitude of 8 mm and 4.4%, 6.8% and 9.2% porosities for 25%, 50% & 75% fill levels are considered. Figure 5.24 shows the dimensionless dissipated energy for no porous baffle conditions.

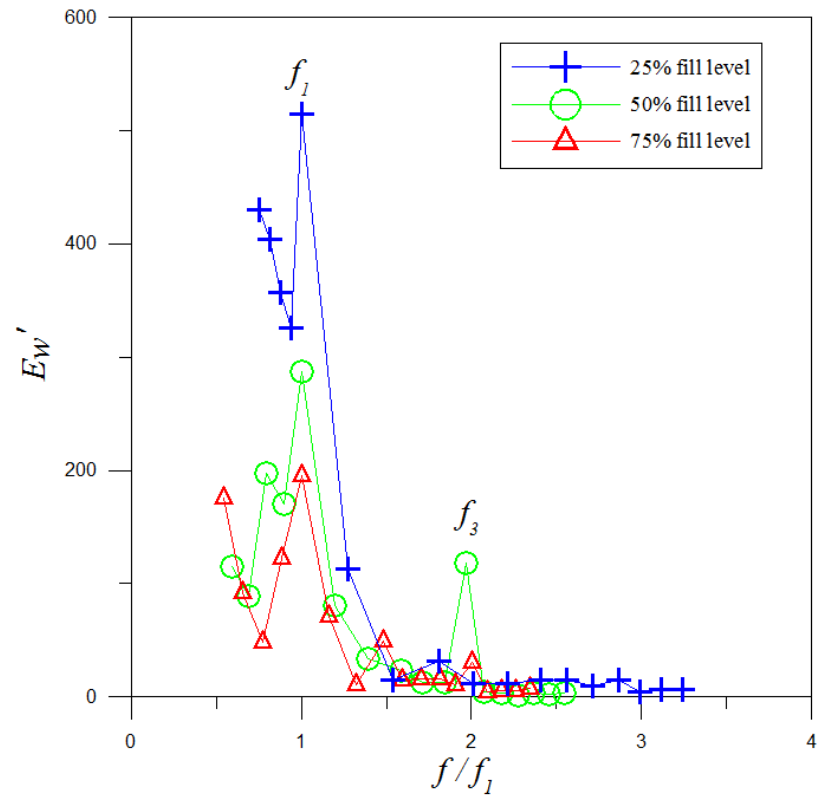


Figure 5.24 Dimensionless dissipated energy for excitation amplitude of 8 mm for no porous baffles for $h_s/l = 0.163, 0.325$ and 0.488

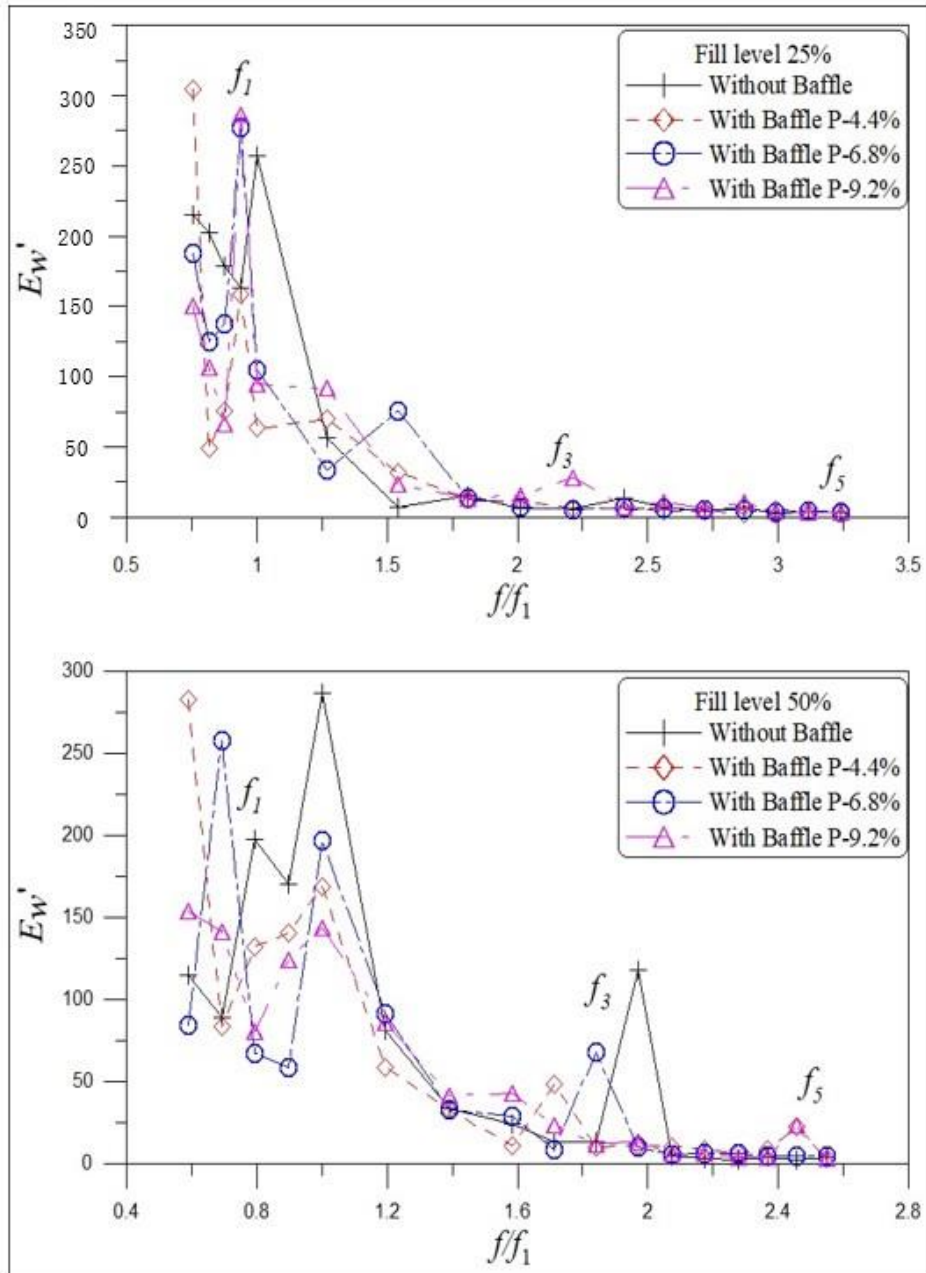


Figure 5.25 Comparison Of energy for with and without porous baffle at $L/2$ location for (a) $h_s/l = 0.163$ and, (b) $h_s/l = 0.325$

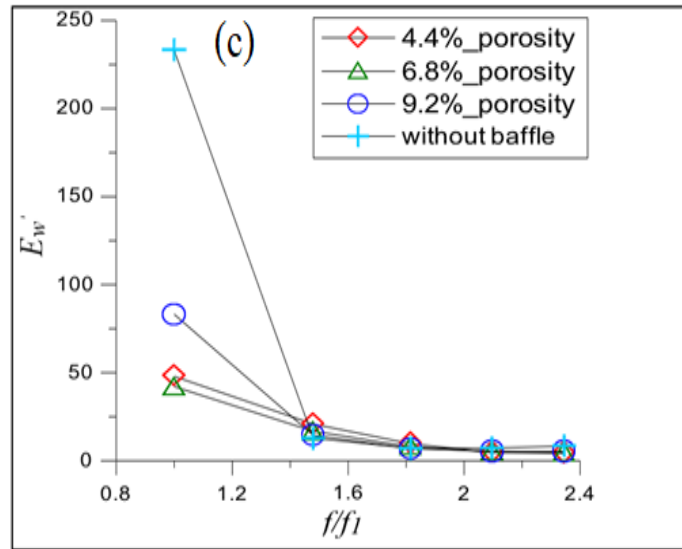


Figure 5.26 Comparison Of energy for with and without porous baffle at $L/2$ location for (c) $h_s/l = 0.488$

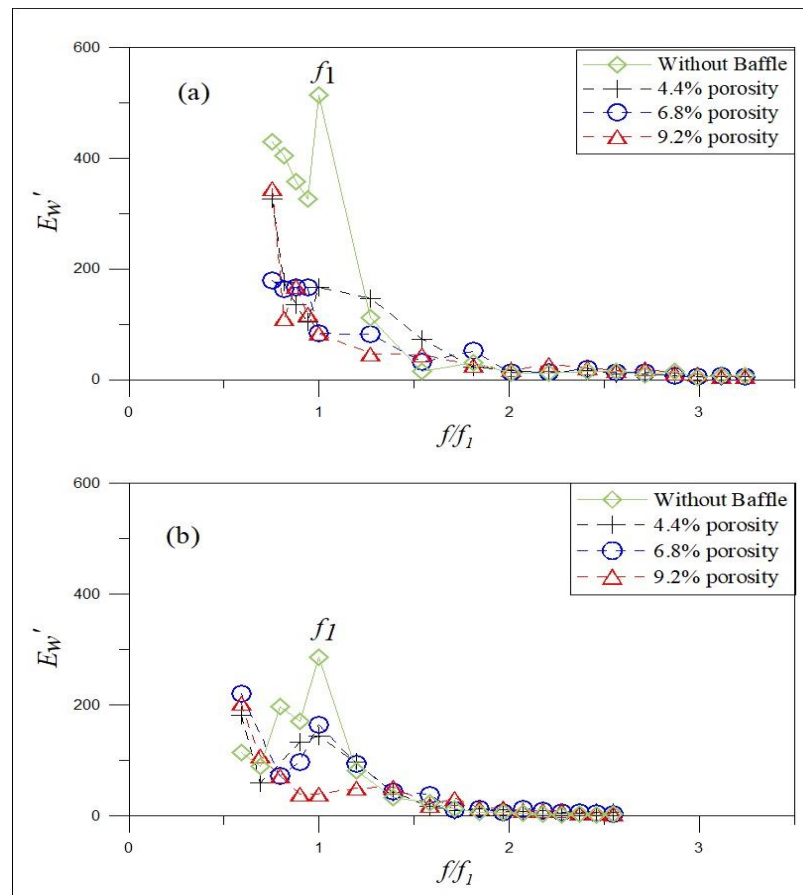


Figure 5.27 Comparison of energy for with and without baffle at $L/3$ & $2L/3$ locations for (a) $h_s/l = 0.163$ and (b) $h_s/l = 0.325$

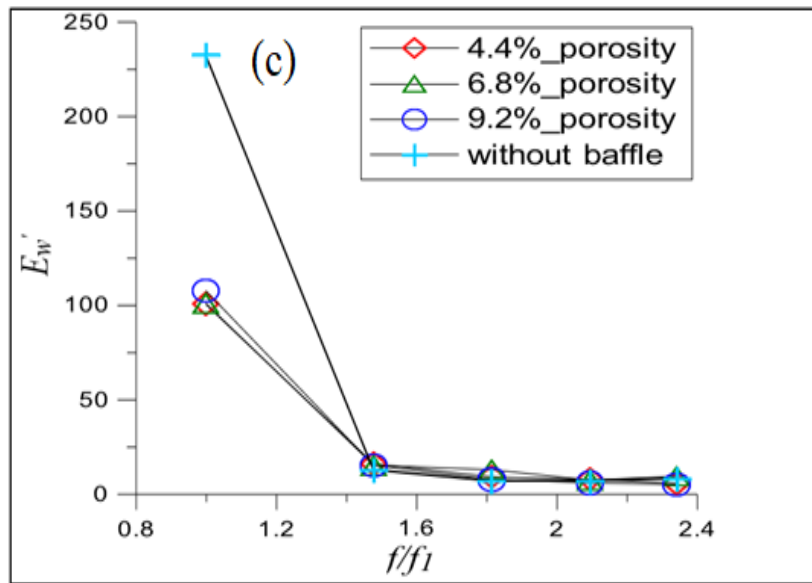


Figure 5.28 Comparison of Energy for with and without baffle at $L/3$ and $2L/3$ locations for (c) $h_s/l = 0.488$

From the above graphs the following points are observed for $L/2$ conditions:

- As increases in the fill level and excitation frequency, the normalized energy decreases for both with and without porous baffle condition.
- The dissipation of energy in case of $h_s/l = 0.163$ for porosity 4.4% is lesser compared to other two porous baffle. As in case of $h_s/l = 0.325$, the dissipation of energy for porous baffle 9.2% is lower compared to other two porous baffle.
- As we can see due to presence baffle for $h_s/l = 0.163$ condition, the energy dissipation is more compared to without baffle condition, for the first mode critical frequency.
- For first and fifth mode excitation frequencies the energy decreases from without baffle to higher porosities of the baffle.
- For third mode excitation frequency the energy dissipation increases with increasing the porosity of baffle and without baffle for $h_s/l = 0.325$ condition.

The following points are observed for $L/3$ & $2L/3$ conditions:

- For without baffle condition, first and fifth sloshing modes energy dissipation is higher compared with other porous baffles.

- At the excitation frequencies of first and fifth sloshing modes energy decreases as increasing the porosity of baffles.
- For third mode excitation frequency, energy dissipation increases with increasing the porosity of baffles.
- The energy dissipation for 25% fill level is more as compared with 50% fill level.
- The normalised energy is decreasing as the excitation frequency increases.
- The normalised energy is very high in case of no baffle condition compared to with baffle condition at first mode of frequency.
- The normalised energy is very close for the porosity in two baffle positions ($L/3$ & $2L/3$).

5.4.2 Mild Steel Plate

The total damping of a structure is increased by introducing some mechanism for energy dissipation. A liquid sloshing damper operates on the principle of energy dissipation through liquid sloshing and wave breaking of the free surface. As the baffle height increases, the obstruction effect of the baffle is enhanced causing increased viscosity and energy dissipation also known as hydrodynamic damping, which further suppresses the sloshing of the liquid. Porosities adopted for mild steel plate is 15%, 20% and 25% with three fill levels.

- The energy dissipation for 25% fill water depth is high compared with 50% and 75% fill depths of water.
- As the fill level increases normalized energy decreases for with porous and without porous baffle condition.
- For without porous baffle condition, first and third sloshing modes energy dissipation is higher compared with porous baffles.
- For third mode excitation frequency, energy dissipation increases with increasing the porosity of baffles.

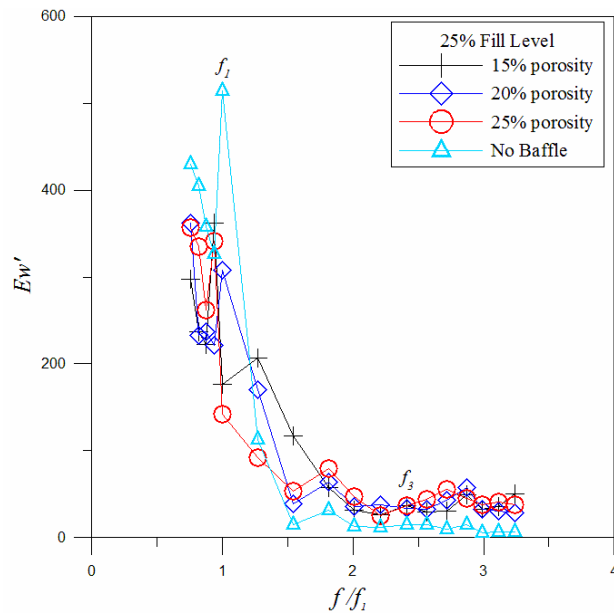


Figure 5.29 Dimensionless dissipated energy for excitation amplitude of 8 mm with and no porous baffles for $h_s/l= 0.163$ at $L/2$ location

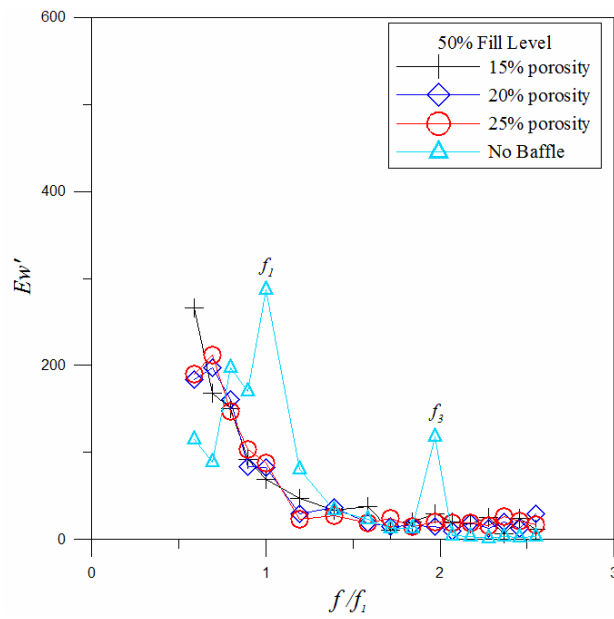


Figure 5.30 Dimensionless dissipated energy for excitation amplitude of 8 mm with and no porous baffles for $h_s/l= 0.325$ at $L/2$ location

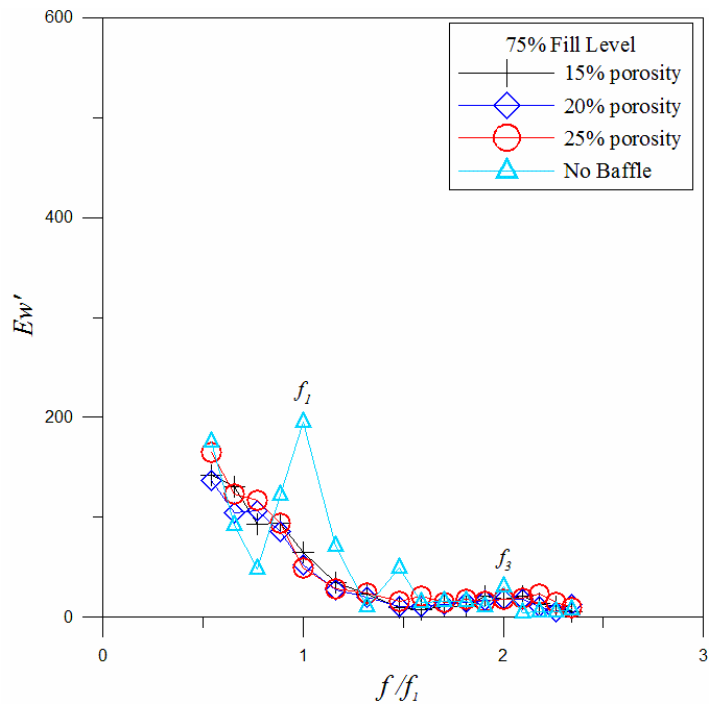


Figure 5.31 Dimensionless dissipated energy for excitation amplitude of 8mm with and no baffles for $h_s/l= 0.488$ at $L/2$ location

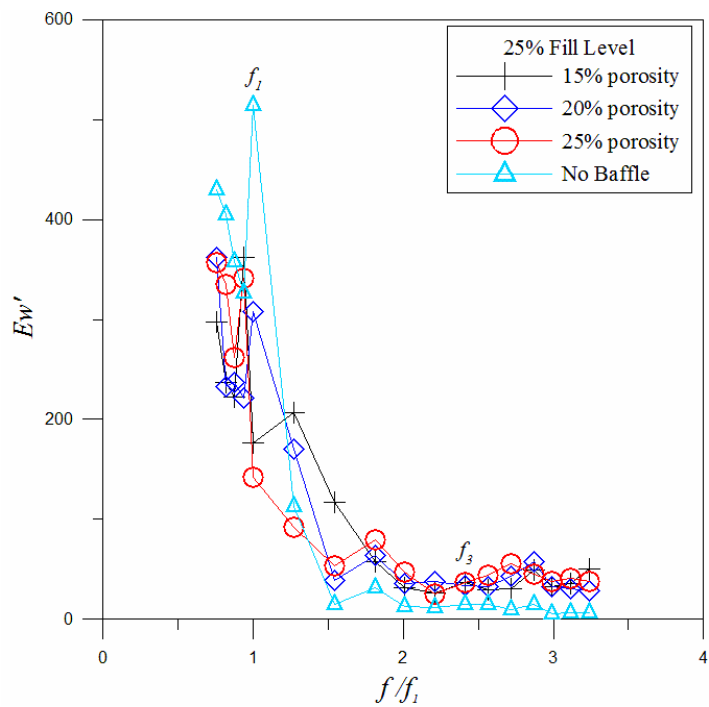


Figure 5.32 Dimensionless dissipated energy for excitation amplitude of 8 mm with and no porous baffles for $h_s/l= 0.163$ at $L/3$ & $2L/3$ locations

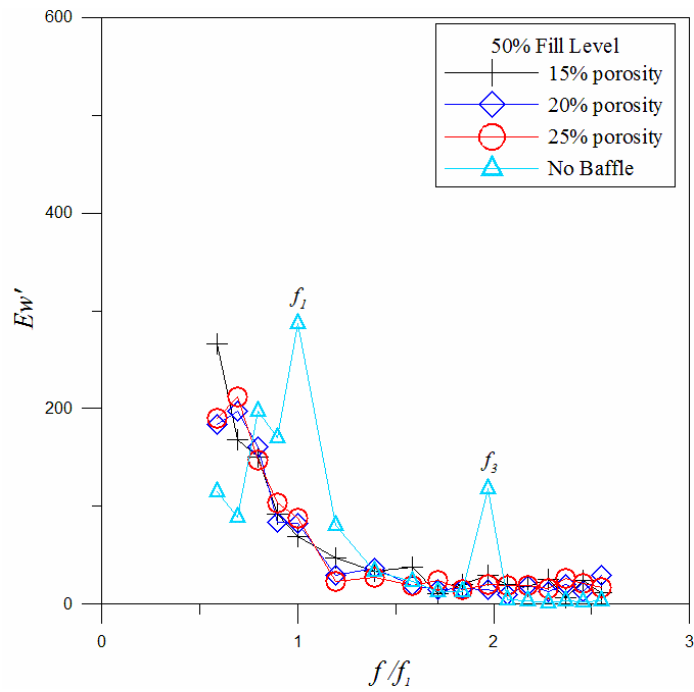


Figure 5.33 Dimensionless dissipated energy for excitation amplitude of 8 mm with and no porous baffles for $h_s/l= 0.325$ at $L/3$ & $2L/3$ locations

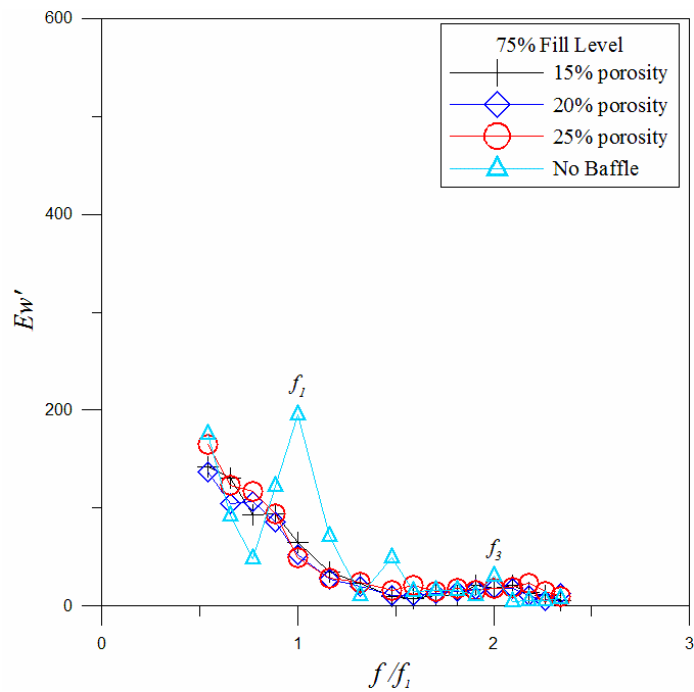


Figure 5.34 Dimensionless dissipated energy for excitation amplitude of 8 mm with and no baffles for $h_s/l= 0.488$ at $L/3$ & $2L/3$ locations

5.5 SCREEN FORCE

Screen force graphs are plots between screen forces (F_s) versus time period of oscillation (t). As seen from the Figure 5.36 and Figure 5.41, the plots are between screen forces and time period of oscillation. Which are important when determining the design forces on the porous baffle and on the damping devices. By using load cells screen forces are detailed. Baffle with Load Cell is shown in figure 5.35. The forces on the screen are measured using load cells with a 10 kgf capacity. The load cell is attached to the porous baffle on one end and on the other end is connected to the steel plate which is fixed to the cradle frame. This load cell values are taken to plot the screen force graphs. The graph is plotted for 25%, 50% & 75% fill level and for f_1 , f_2 , f_3 , f_4 , and f_5 excitation frequencies considered respective excitation amplitude.

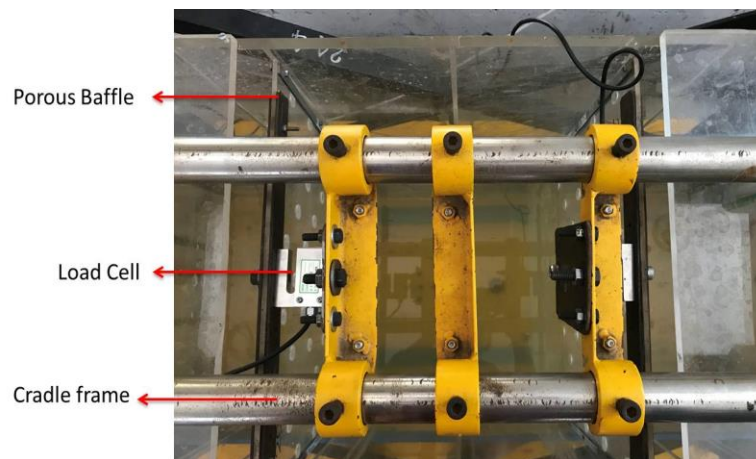


Figure 5.35 Baffle with Load Cell (top view)

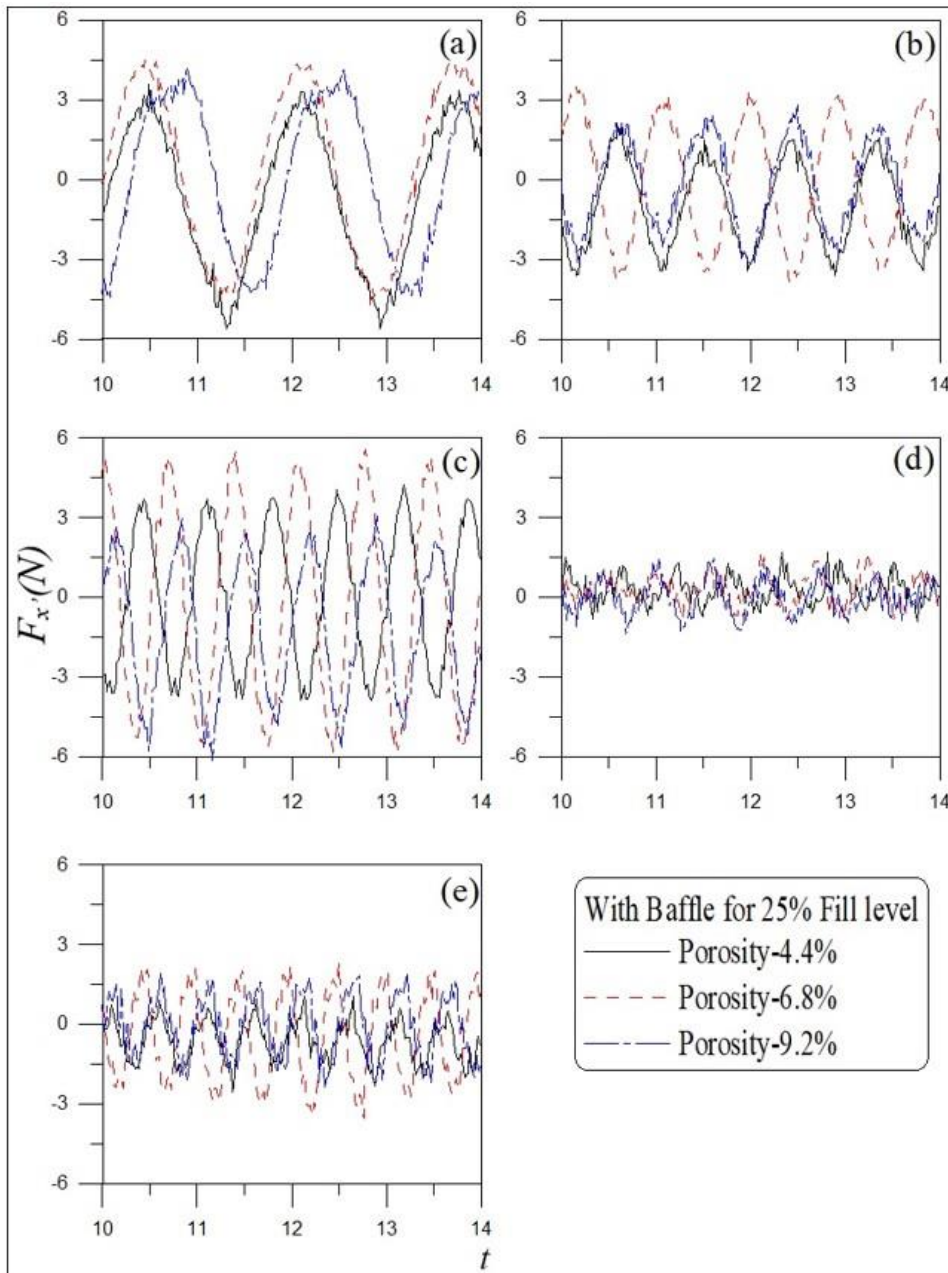


Figure 5.36 Experimental screen force for $h_s/l = 0.163$ and excitation at natural sloshing frequencies at $L/2$ location (a) $f = 0.6059$ Hz (f_1), (b) $f = 1.0967$ Hz (f_2), (c) $f = 1.4604$ Hz (f_3), (d) $f = 1.7276$ Hz (f_4) and, (e) $f = 1.9637$ Hz (f_5)

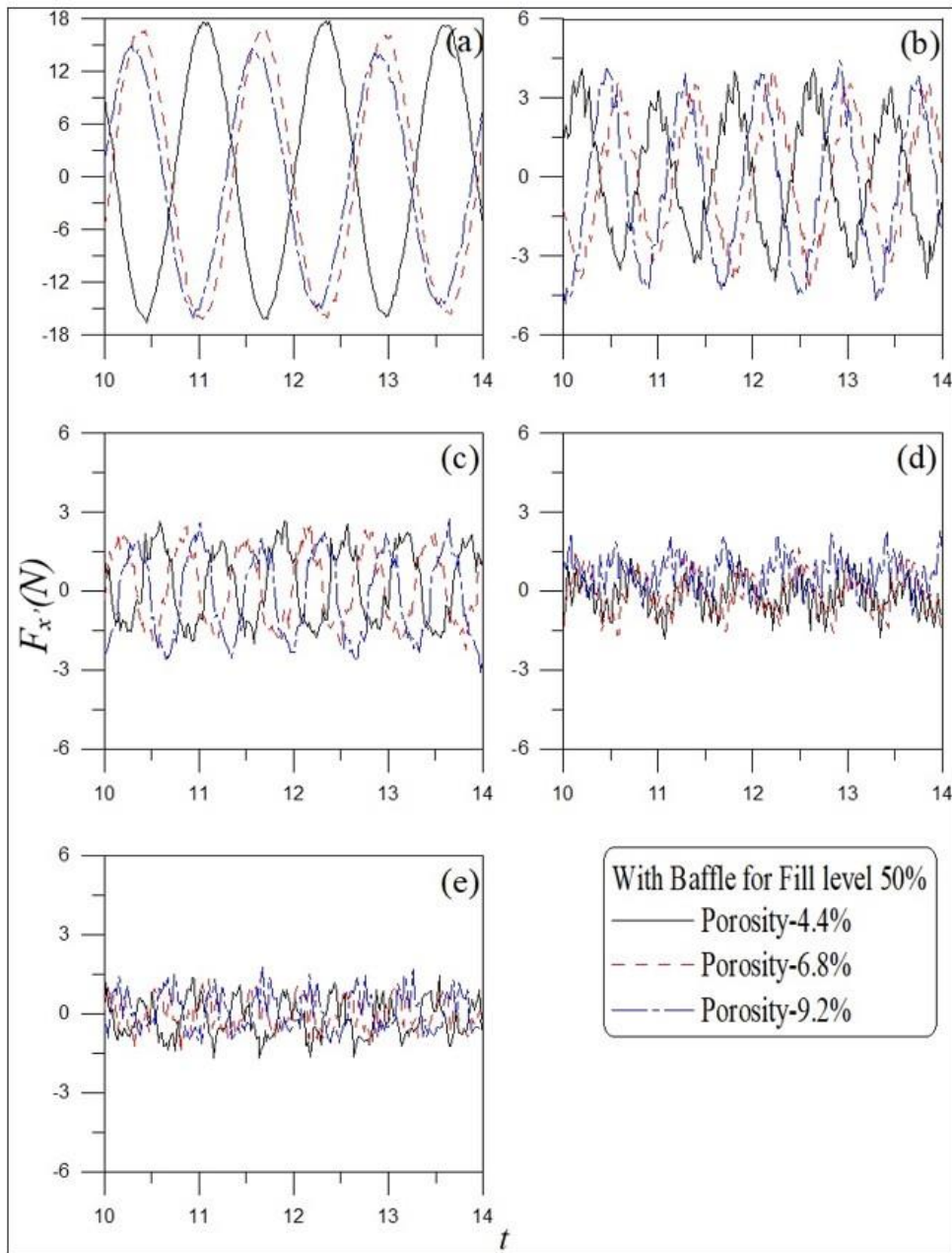


Figure 5.37 Experimental screen force for $h_s/l = 0.325$ and excitation at natural sloshing frequencies at $L/2$ location (a) $f = 0.7755$ Hz (f_1), (b) $f = 1.2277$ Hz (f_2), (c) $f = 1.5270$ Hz (f_3), (d) $f = 1.7666$ Hz (f_4) and, (e) $f = 1.9756$ Hz (f_5)

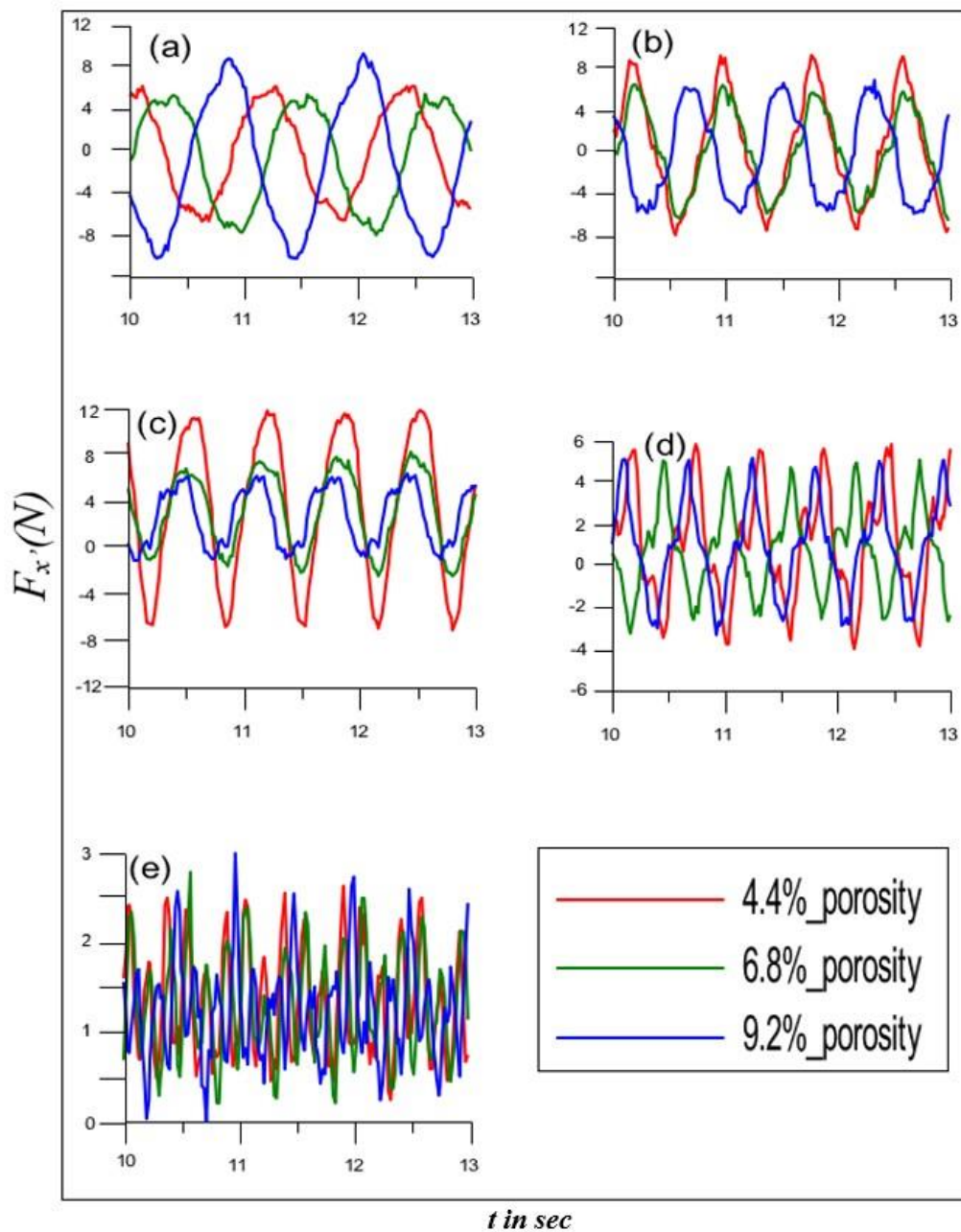


Figure 5.38 Experimental screen force for $h_s/l = 0.488$ and excitation at natural sloshing frequencies at $L/2$ location (a) $f = 0.8432 \text{ Hz}$ (f_1), (b) $f = 1.2468 \text{ Hz}$ (f_2), (c) $f = 1.5302 \text{ Hz}$ (f_3), (d) $f = 1.7671 \text{ Hz}$ (f_4) and, (e) $f = 1.9757 \text{ Hz}$ (f_5)

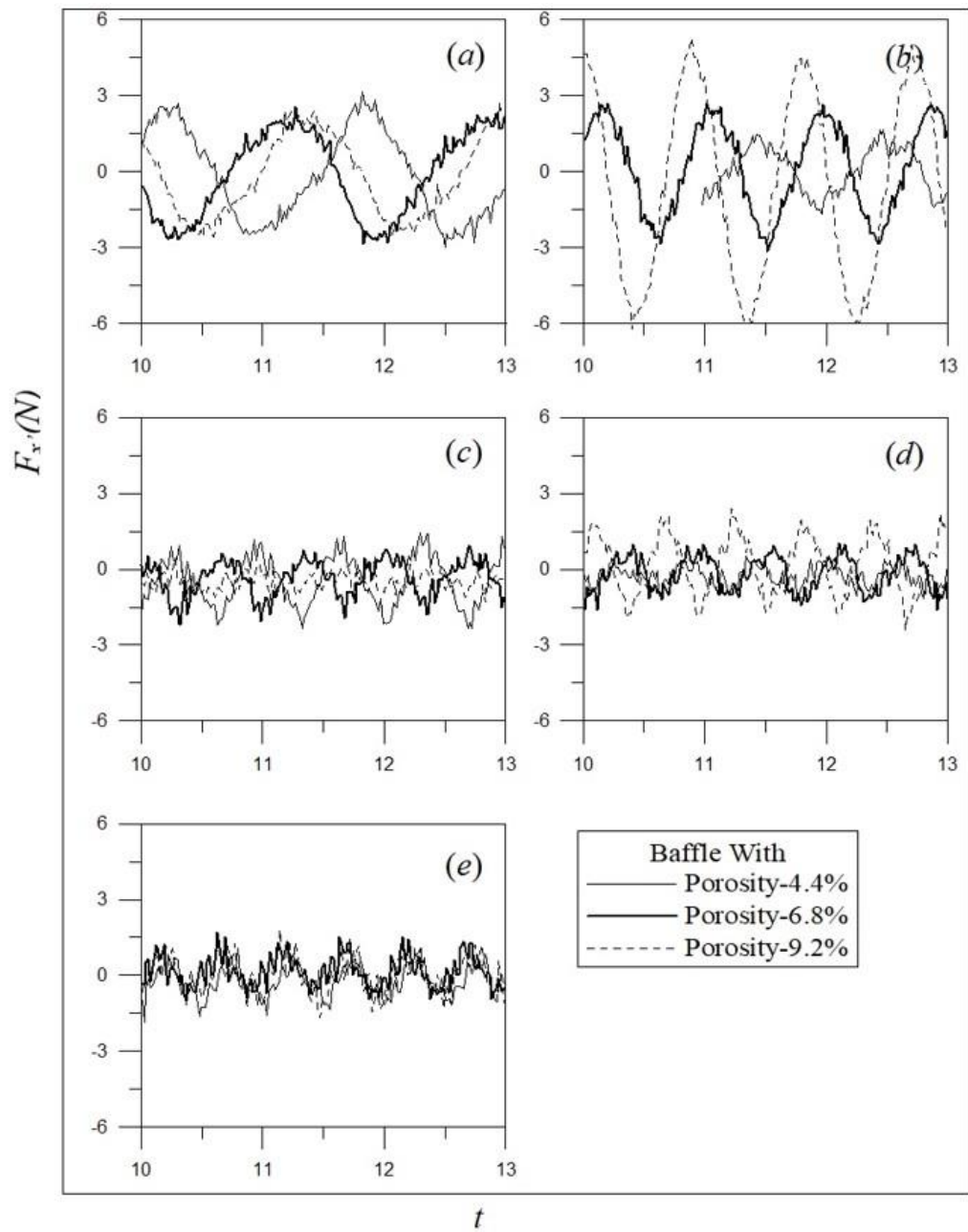


Figure 5.39 Experimental screen force for $h_s/l = 0.163$ and excitation at natural sloshing frequencies at $L/3$ & $2L/3$ locations (a) $f = 0.6059 \text{ Hz}$ (f_1), (b) $f = 1.0967 \text{ Hz}$ (f_2), (c) $f = 1.4604 \text{ Hz}$ (f_3), (d) $f = 1.7276 \text{ Hz}$ (f_4) and, (e) $f = 1.9637 \text{ Hz}$ (f_5)

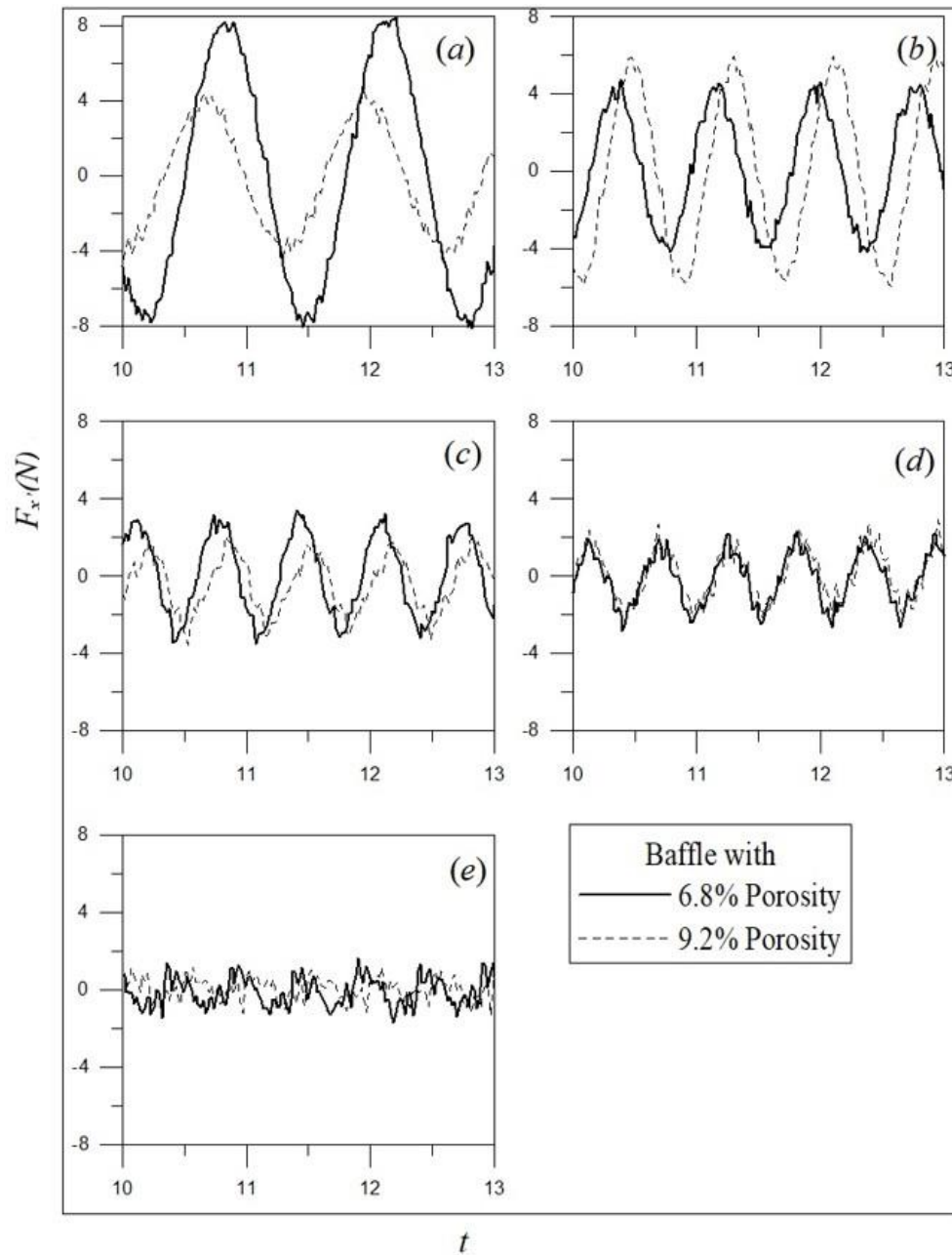


Figure 5.40 Experimental screen force for $h_s/l = 0.325$ and excitation at natural sloshing frequencies at $L/3$ & $2L/3$ locations (a) $f = 0.7755 \text{ Hz}$ (f_1), (b) $f = 1.2277 \text{ Hz}$ (f_2), (c) $f = 1.5270 \text{ Hz}$ (f_3), (d) $f = 1.7666 \text{ Hz}$ (f_4) and, (e) $f = 1.9756 \text{ Hz}$ (f_5)

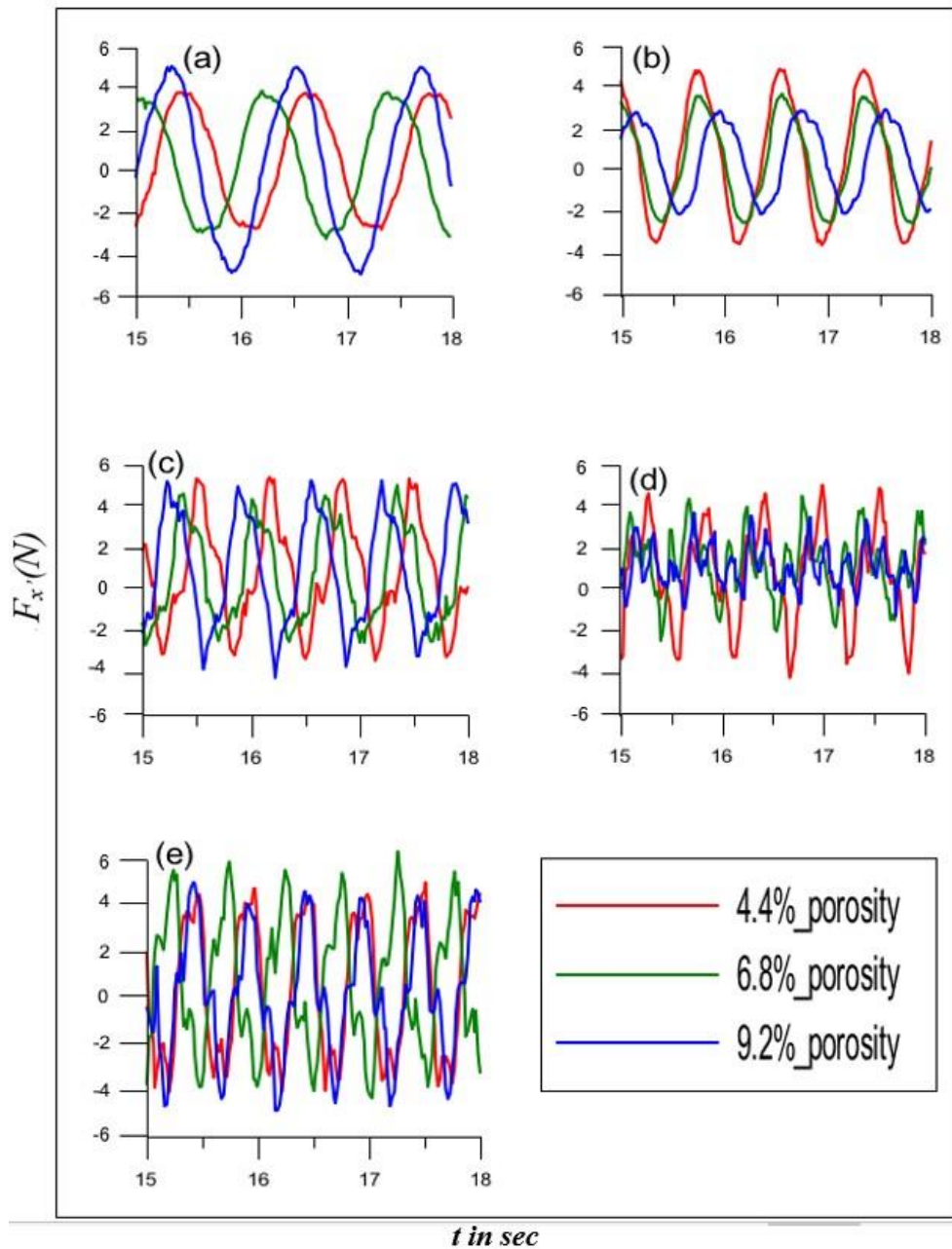


Figure 5.41 Experimental screen force for $h_s/l = 0.488$ and excitation at natural sloshing frequencies at $L/3$ & $2L/3$ locations (a) $f = 0.8432$ Hz (f_1), (b) $f = 1.2468$ Hz (f_2), (c) $f = 1.5302$ Hz (f_3), (d) $f = 1.7671$ Hz (f_4) and, (e) $f = 1.9757$ Hz (f_5)

Comparing the above plots of time series of screen force of with porous baffles of different porosities leads to the following observations for $L/2$ locations:

- In case of 25% fill level ($h_s/l = 0.163$), the maximum screen force is acting at third mode frequency (f_3). As in case of 50% fill level, it is occurring at first mode frequency (f_1).
- In case of 50% fill level as frequency increases, the screen force keep on decreasing for all percentage of porosity. As in case of 25% fill it is not same.
- In 25% fill level for all the modes of sloshing frequency, the screen force is for 6.8% porosity greater than 4.4% and this screen force is greater than 9.2% porosity.
- In 50% fill level first, third and fifth sloshing modes screen force for 4.4% porosity greater than 6.8% porous baffle and this screen force is greater than 9.2% porosity baffle. Second and fourth sloshing modes 9.2% porous baffle screen force is greater than 4.4% porosity and this force is greater than 6.8 porous baffle.
- The screen force values are close for all porosities in one baffle condition.

Screen force of with porous baffles of different porosities leads to the following observations for $L/3$ & $2L/3$ locations:

- In 25% fill level for odd sloshing modes, 6.8% porosity screen force is greater than 4.4% porosity, which is greater than 9.2% porosity baffles. In even sloshing modes, 9.2% porous baffle screen force is greater than 6.8% porous baffle, which is greater than the 4.4% porous baffles screen force.
- similarly, for 50% fill odd sloshing modes, 6.8% porosity screen force is greater than 9.2% porosity baffles. In the even sloshing modes, 9.2% porous baffle screen force is greater than 6.8% porous baffle screen force.
- In two baffle condition, the screen force for 4.4% baffle is higher than 6.8% and 9.2% porosity baffles at third frequency mode (baffles at $L/3$ and $2L/3$).

5.6 SLOSHING FORCE

Force due to the participating fluid is called as sloshing force. The portion of the fluid that generates the dynamic sloshing force is called as participating fluid. Sloshing forces is significant in design of containment walls of partially filled excited tanks and structural integrity with the main structure. Figure 5.42 represents the temporal evolution

of sloshing force for the excitation amplitude of 8 mm with no baffle conditions. Sloshing force time histories for 25%, 50% and 75% fill levels at no baffle locations with an excitation at odd mode sloshing frequencies (i.e. f_1, f_3 , and f_5) are shown in Fig. 5.43.

The sloshing force is primarily determined by the moving tank's frequency, excitation amplitude, geometry, tank size, and liquid depth. In the present study the sloshing force is measured using ballast mast concept for the shake table excitation frequencies as mentioned in Table 3.1. The inertial force of liquid, which is represented as solid mass, is used to standardize the variation in maximum sloshing force. A proper estimation of sloshing force is the significant part of sloshing dynamics and it is the deciding parameter for the design and operation of any moving object which is carrying a tank with partially filled liquid. A slosh forces prominent peak in the spectrum may be found close to the excitation frequency, the natural frequency, or the vibration frequency. The normalized peak sloshing force are given as follows, (Jamie, 2007):

$$F'_s = \frac{F_s}{m_w (2\pi f)^2 A} \quad (5.5)$$

Where A is excitation amplitude, m_w is total mass of the fluid and f is excitation frequency.

The variation of F'_s with different frequencies ratios (f/f_1) are projected for three different water depths, which are shown in Figure 5.44 to Figure 5.49 respectively. Each Figure shows the normalized sloshing force for different fill levels of sloshing tanks with 8mm excitation amplitude for both $L/2$ conditions and $L/3$ & $2L/3$ conditions.

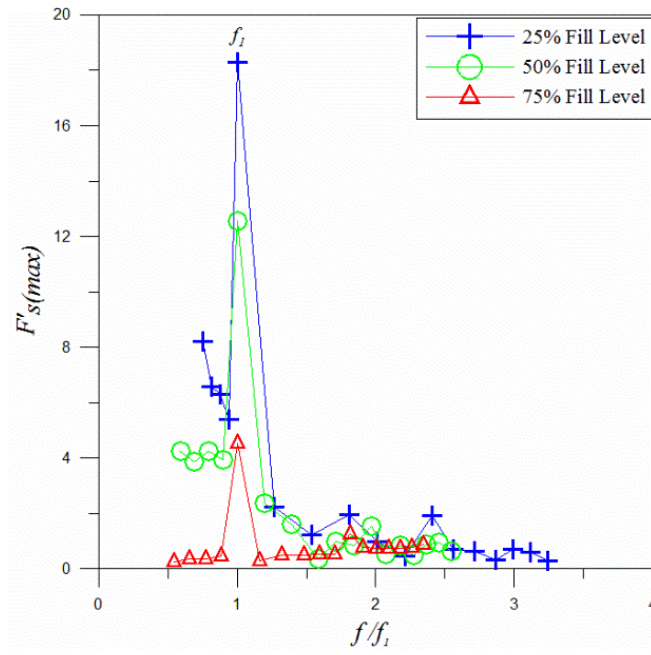


Figure 5.42 Dimensionless maximum sloshing force for excitation amplitude of 8mm no porous baffles for $h_s/l = 0.163, 0.325$ and 0.488

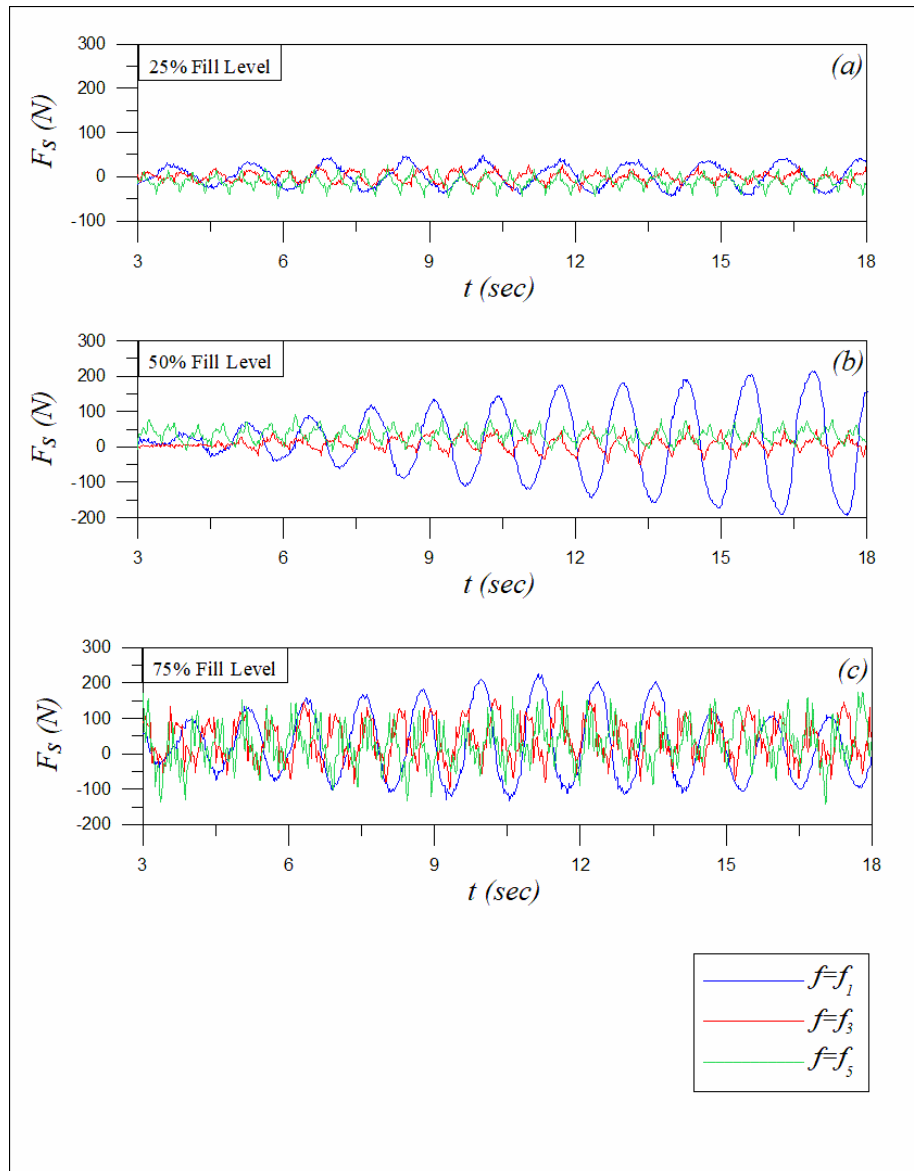
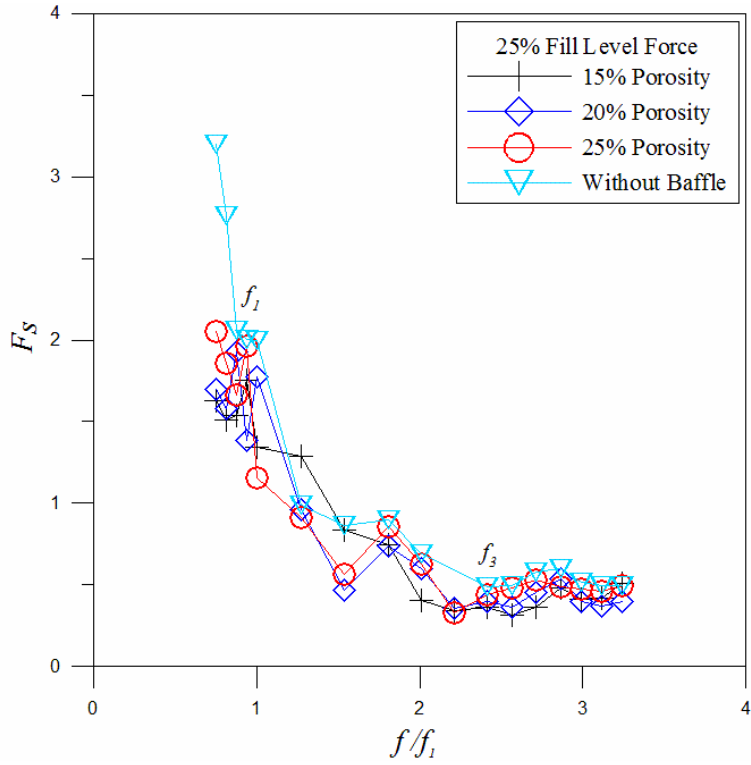


Figure 5.43 Time histories of sloshing force corresponding to excitation amplitude for no baffle $h_w/l = 0.163$ (a) $f = 0.6059 \text{ Hz}$ (f_1), $f = 1.4604 \text{ Hz}$ (f_3), $f = 1.9637 \text{ Hz}$ (f_5), $h_w/l = 0.325$ (b) $f = 0.7755 \text{ Hz}$ (f_1), $f = 1.5270 \text{ Hz}$ (f_3), $f = 1.9757 \text{ Hz}$ (f_5), and $h_w/l = 0.488$ (c) $f = 0.8432 \text{ Hz}$ (f_1), $f = 1.5302 \text{ Hz}$ (f_3), $f = 1.9757 \text{ Hz}$ (f_5)

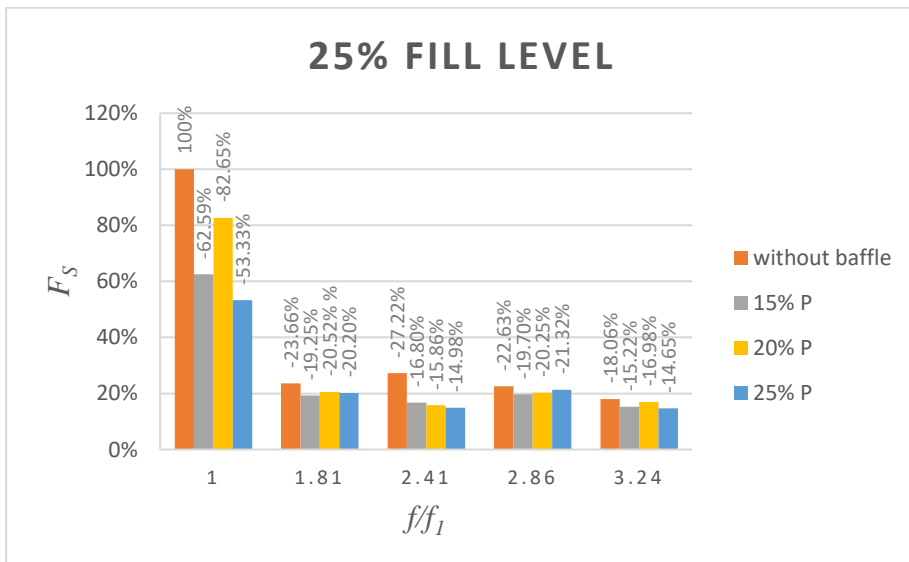
Comparison of the time histories of sloshing force leads to the following observations:

- It is evident that $f = f_1$ is the critical mode of sloshing frequency. It's because, regardless of the fill levels. The largest sloshing force is seen at $f = f_1$.
- The decreasing order of sloshing force is at $f = f_1$, $f = f_3$ and at $f = f_5$ mode sloshing frequencies irrespective of the fill levels.

- As seen from graphs, sloshing forces are maximum at 50% fill level in comparison with 25% and 75% fill levels.

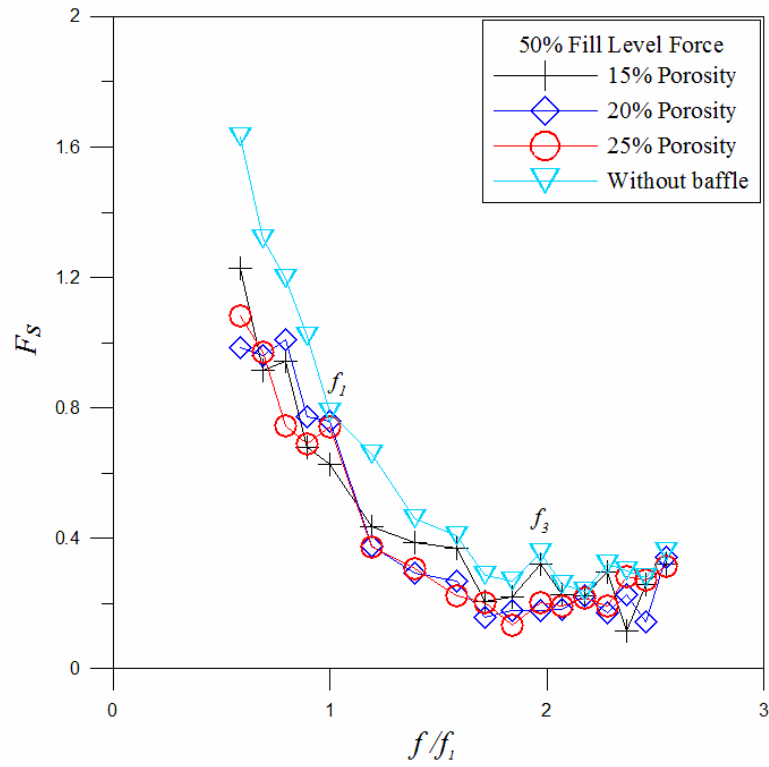


(a)

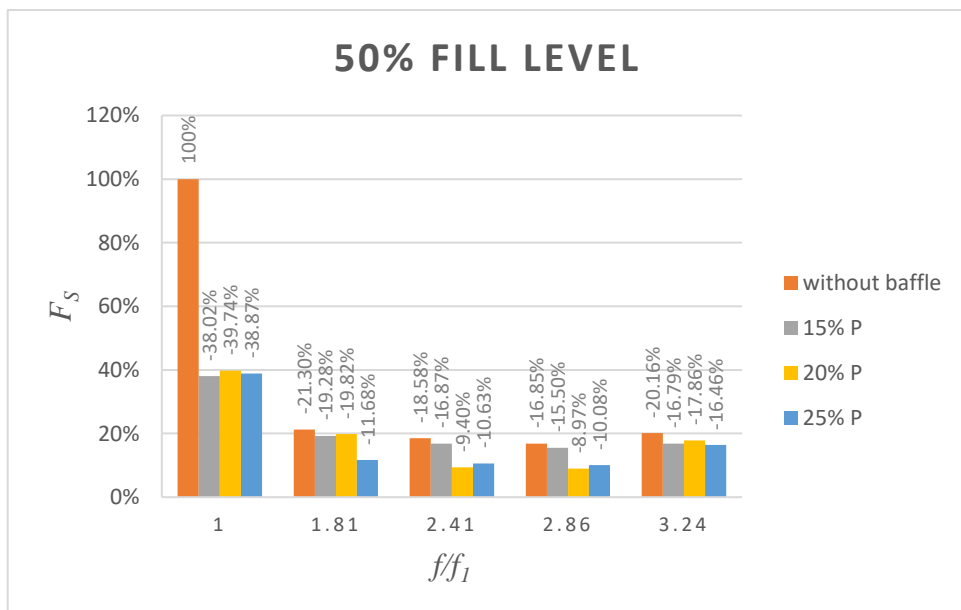


(b)

Figure 5.44 (a) and (b) Variation of sloshing forces for with baffle and no baffle for 25% fill level at $L/2$ location

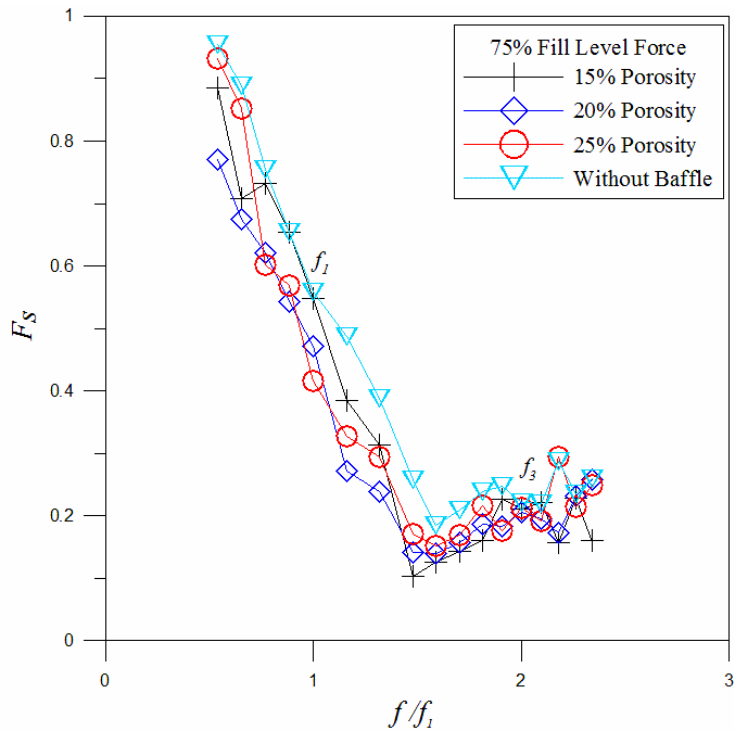


(a)

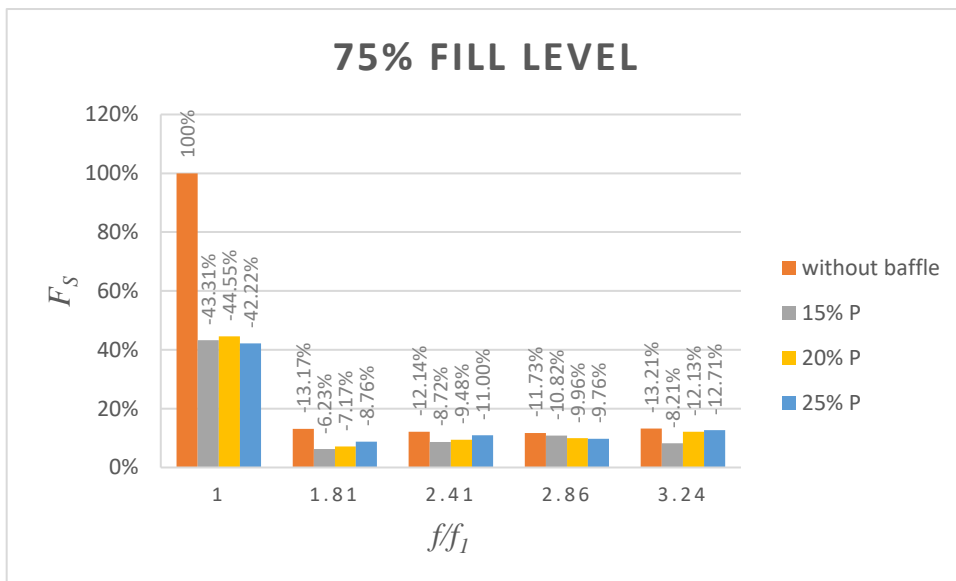


(b)

Figure 5.45 (a) and (b) Variation of sloshing forces for with baffle and no baffle for 50% fill level at $L/2$ location



(a)



(b)

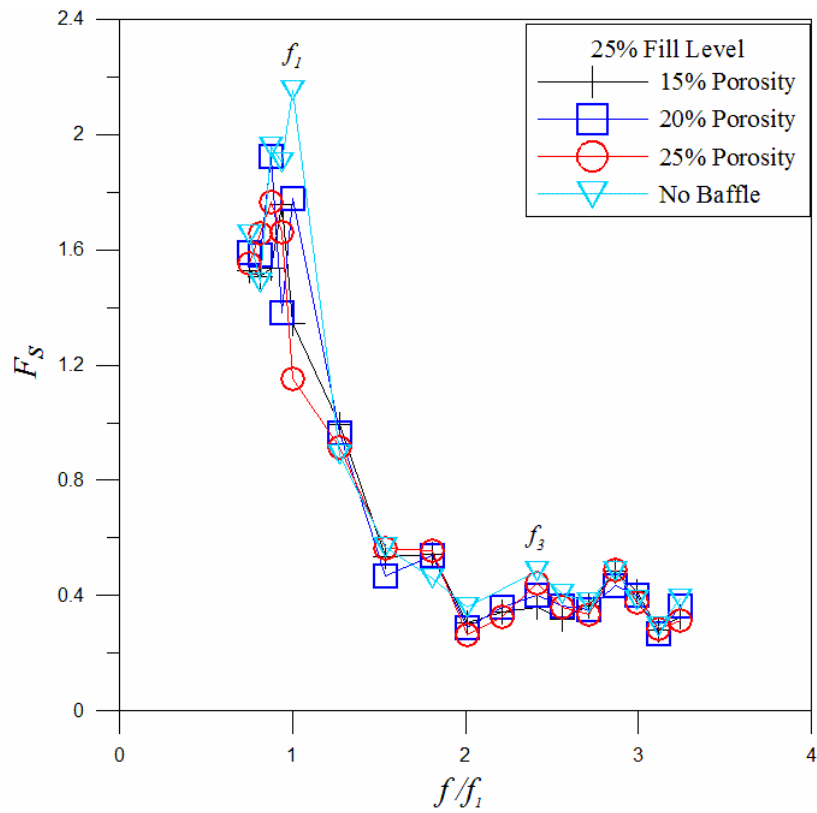
Figure 5.46 (a) and (b) Variation of sloshing forces for with baffle and no baffle for 75% fill level at $L/2$ location

The Figure 5.44 (a) and (b) represents the variation of sloshing force against non-dimensional frequency for the liquid depth of 25% fill level. As excitation frequencies increase the sloshing force decreases. In this case it is observed that the sloshing force

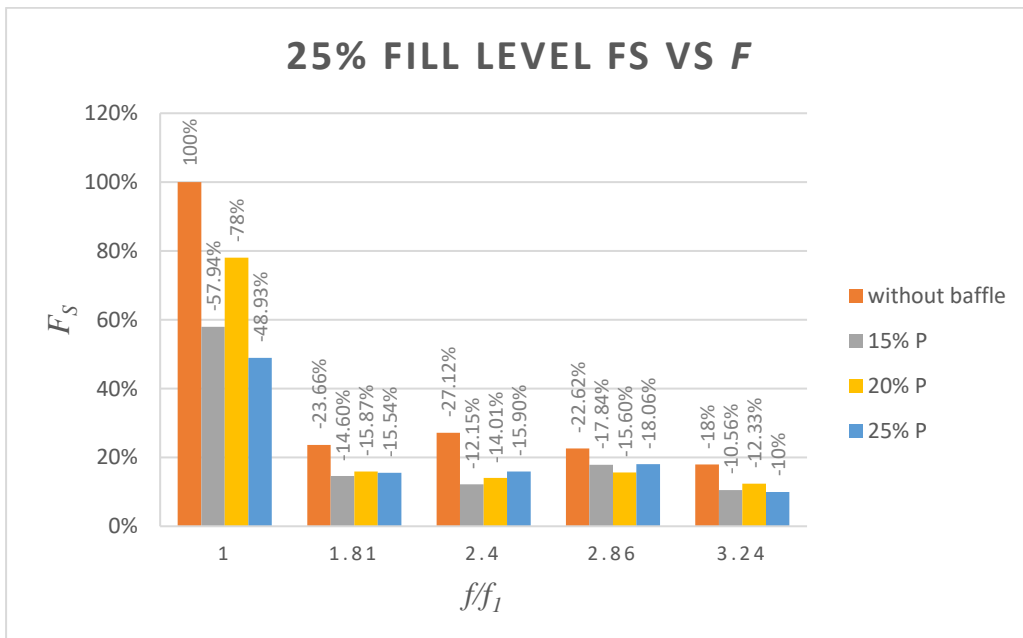
reduces slightly by use of 25% porosity of screen comparatively with 15% porosity and 20% porosity. The max sloshing force is observed at resonance condition ($f=f_1$) for both with and no baffles conditions of all three porosities. The tank with baffles of 25% porosity shows minimum of 53.33% at $f=f_1$ whereas the 15% and 20% porosity of baffles shows 62.59% and 82.65% with respect to no baffle case respectively.

The variation of sloshing force with normalized frequency is shown in Figure 5.45 (a) and (b) for the depth of 50% fill level. Sloshing force decrease when there is increase in excitation frequencies for f_3 . Beyond that the sloshing force slightly increases. The maximum sloshing force observed before resonance ($f=f_1$) for both baffle and no baffle i.e.; $f/f_1=0.59$. The tank with baffle of 15% porosity shows minimum values of 38.02% whereas the 20% and 25% porosities of baffles show 39.74% and 38.87% respectively including with no baffle conditions.

Similarly, the Figure 5.46 (a) and (b) shows the sloshing force with normalised frequency for the case of 75% fill level. Sloshing force decreases with the increase in excitation frequencies up to 1.96. Again, from that point the sloshing force slightly increases further. The maximum sloshing force observed before resonance ($f=f_1$) for both with and without baffle i.e.; $f/f_1=0.54$. It is observed that the sloshing force for the porosity of screen 25% porosity shows minimum values of 42.22% whereas the 15% and 20% porosities of baffles show 43.31% and 44.55% with respect to no baffle conditions.

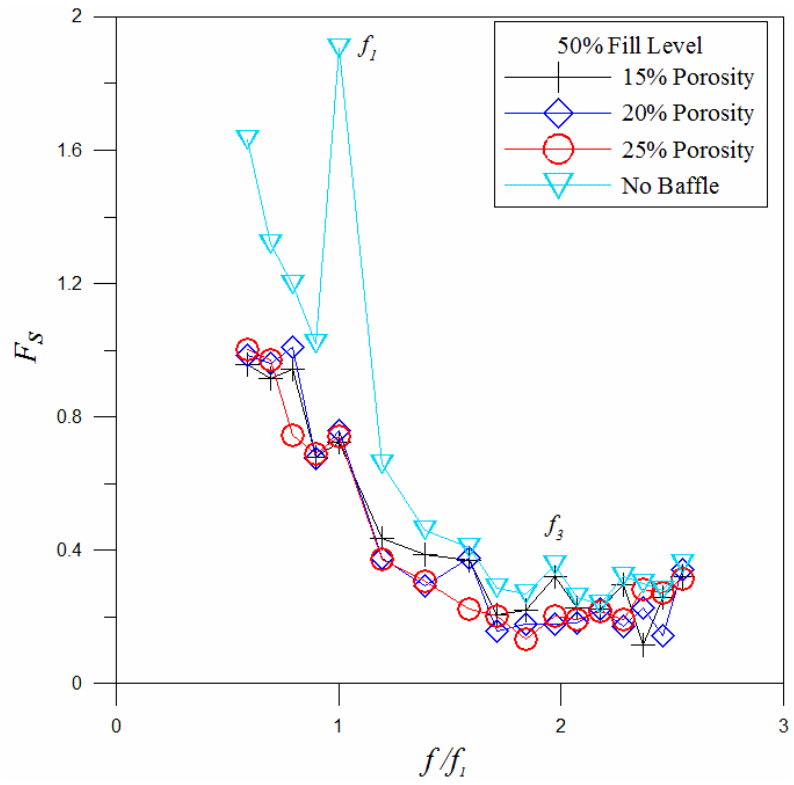


(a)

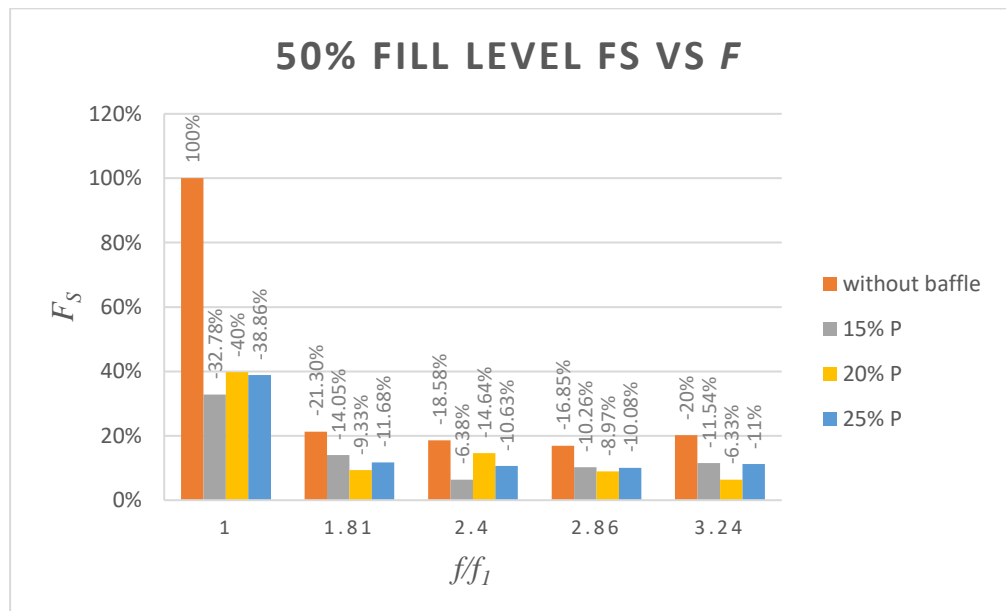


(b)

Figure 5.47 (a) and (b) Variation of sloshing forces for with baffle and no baffle for 25% fill level at $L/3$ & $2L/3$ locations

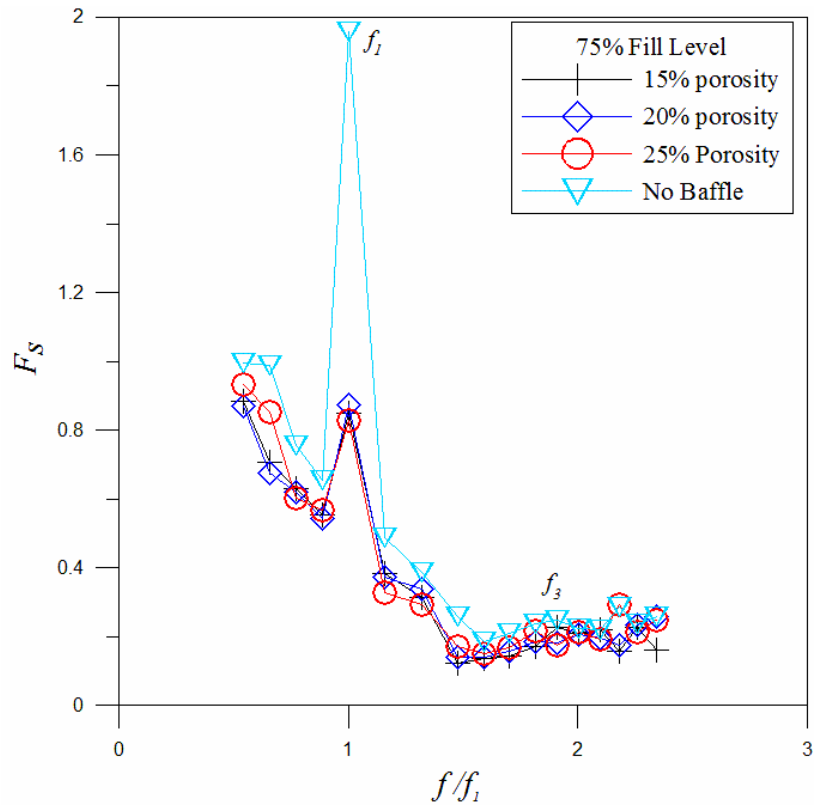


(a)

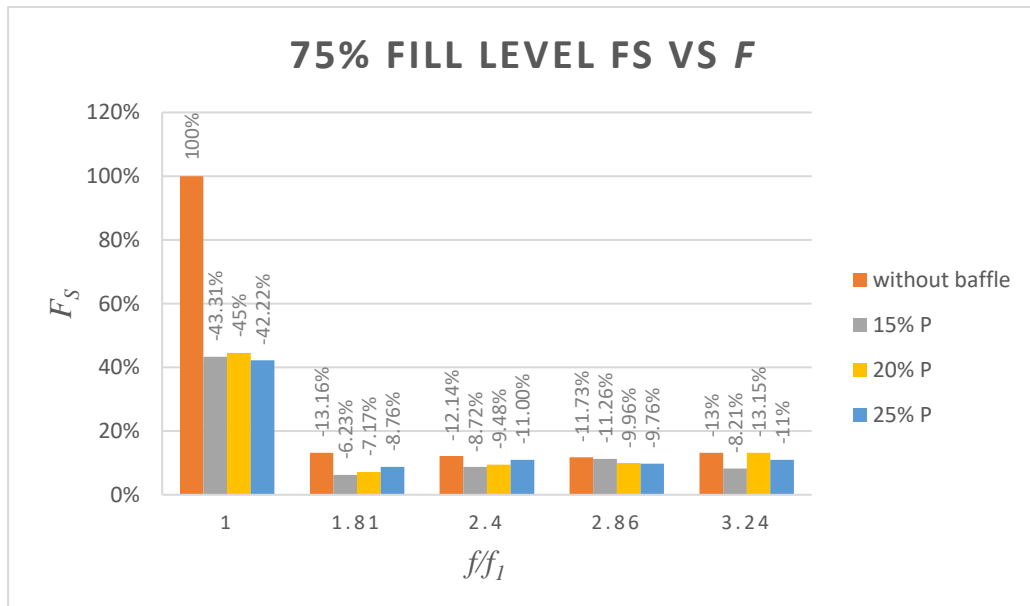


(b)

Figure 5.48 (a) and (b) Variation of sloshing forces for with baffle and no baffle for 50% fill level at $L/3$ & $2L/3$ locations.



(a)



(b)

Figure 5.49 (a) and (b) Variation of sloshing forces for with baffle and no baffle for 75% fill level at $L/3$ & $2L/3$ locations

The Figure 5.47 (a) and (b) represents the variation of sloshing force against non-dimensional frequency for the liquid depth of 25% fill level. As excitation frequencies increase the sloshing force decreases. In this case it is observed that the sloshing force reduces slightly by use of 20% porosity of screen comparatively with 15% porosity and 25% porosity. The max sloshing force is observed at resonance condition ($f=f_1$) for both with and no baffles conditions of all three porosities. The tank with baffles of 25% porosity shows minimum of 48.93% at $f=f_1$ whereas the 15% and 20% porosity of baffles shows 57.94% and 78.01% with respect to no baffle case respectively.

The variation of sloshing force with normalized frequency is shown in Figure 5.48 (a) and (b) for the depth of 50% fill level. Sloshing force decrease when there is increase in excitation frequencies for f_3 . Beyond that the sloshing force slightly increases. The maximum sloshing force observed before resonance ($f=f_1$) for both baffle and no baffle i.e.; $f/f_1=0.59$. The tank with baffle of 15% porosity shows minimum values of 32.78% whereas the 20% and 25% porosities of baffles show 39.74% and 38.86% respectively including with no baffle conditions.

Similarly, the Figure 5.49 (a) and (b) shows the sloshing force with normalised frequency for the case of 75% fill level. Sloshing force decreases with the increase in excitation frequencies up to 1.96. Again, from that point the sloshing force slightly increases further. The maximum sloshing force observed before resonance ($f=f_1$) for both with and without baffle i.e.; $f/f_1=0.54$. It is observed that the sloshing force for the porosity of screen 25% porosity shows minimum values of 42.22% whereas the 15% and 20% porosities of baffles show 43.31% and 44.55% with respect to no baffle conditions.

- As mode of frequency increases sloshing force decreases and also it is observed that first mode frequency which is the critical mode is giving higher sloshing force as compared with other modes of frequency.
- It was also observed that the existence of baffles has a considerable impact on the lateral slosh force and corresponding resonance frequencies.
- The baffles significantly decreased the longitudinal force amplifications during longitudinal acceleration excitations.

- It is proved that there are several spectrum components in the resulting forces that can be related to the excitation, resonance, and vibration.

5.7 SPECTRAL MOMENT (m_0)

The variance value of the water surface fluctuations about mean is provided by the area under the signal spectrum, which also includes the total energy of the irregular wave system per plan area. Spectral moment m_0 is calculated for the different excitation frequencies and excitation amplitude of $8mm$. Figure 5.50 to 5.55 shows the graph between the m_0 versus frequency ratio. The wave spectrum is defined as the graph of the spectral density function versus wave frequency. Sea surface elevation being considered at a point which is at a horizontal distance 'x' from any chosen origin and at time instant 't' ($\eta(x, t)$) is,

$$\eta(x, t) = \sum_{n=1}^M a_j \cos(k_j x - \omega_j t + \theta_j) \quad (5.6)$$

Where,

M Number of linear waves being added together.

A_j Amplitude of the j^{th} wave

K_j Wave number of the j^{th} wave ($(2\pi)/\text{Length of the } j^{\text{th}} \text{ wave}$)

Ω_j Angular wave frequency ($(2\pi) / \text{Period of the } j^{\text{th}} \text{ wave} = (2\pi) \times \text{frequency in cycles per second of the } j^{\text{th}} \text{ wave}$)

θ_j Phase of the j^{th} wave assumed to be uniformly distributed over the interval $(0, 2\pi)$

The amplitude (a_j) of the component wave is related to an important statistical function called the Spectral Density Function by the relationship.

$$a_j = \sqrt{2S_\eta(\omega_j)\Delta\omega} \quad (5.7)$$

Where,

$S\eta(\omega_j)$ Spectral density function corresponding to the frequency ω_j for sea surface (η)

$\Delta\omega$ frequency step or interval used in calculating above mentioned function.

Once a spectrum for a particular signal is known, a variety of information can be deduced from it. The significant information obtained is that of the wave frequency composition in a given wave sample. Additionally, the area under the wave spectrum provides both the variance of the fluctuations and the total energy of the irregular wave system per plan area about mean. Through the MATLAB coding m_o can be found for the different excitation frequencies and an excitation amplitude of $8mm$. The graph is plotted for 25%, 50% and 75% fill level and for $f_1, f_2, f_3, f_4,$ and f_5 excitation frequencies.

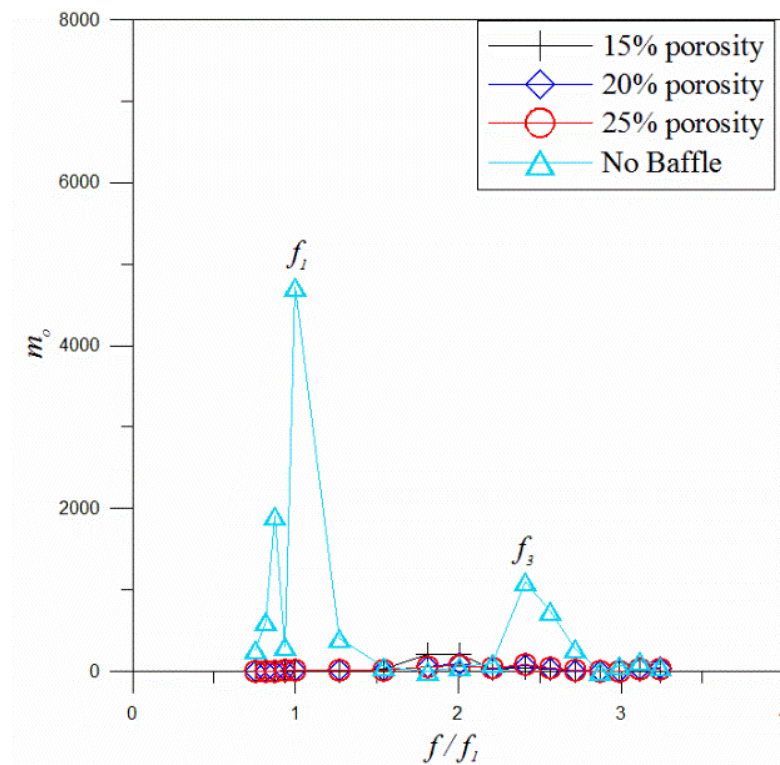


Figure 5.50 Variation of spectral energy (m_o) with different frequencies ratio (f/f_1); for $hs/l = 0.163$ for $L/2$ locations.

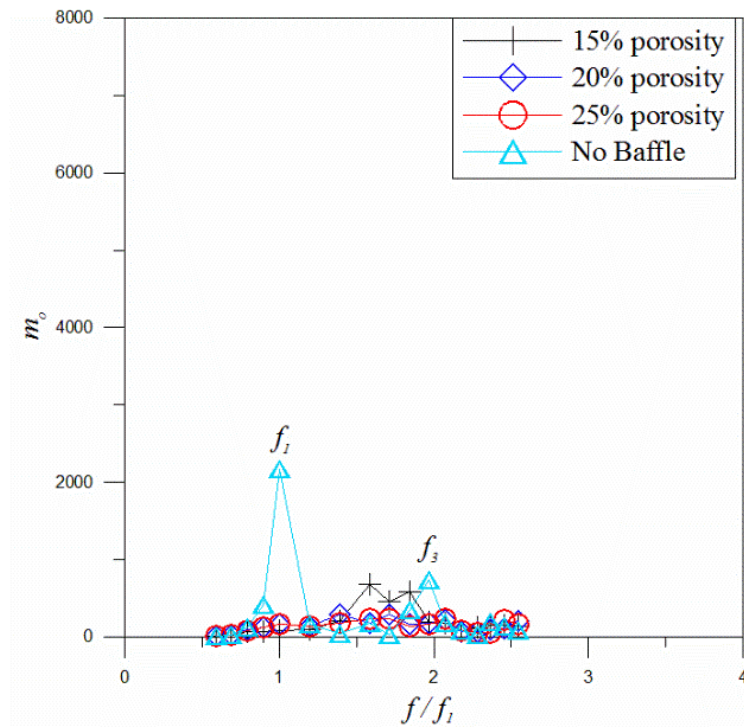


Figure 5.51 Variation of spectral energy (m_o) with different frequencies ratio (f/f_1); for (a) $hs/l = 0.325$ for $L/2$ locations

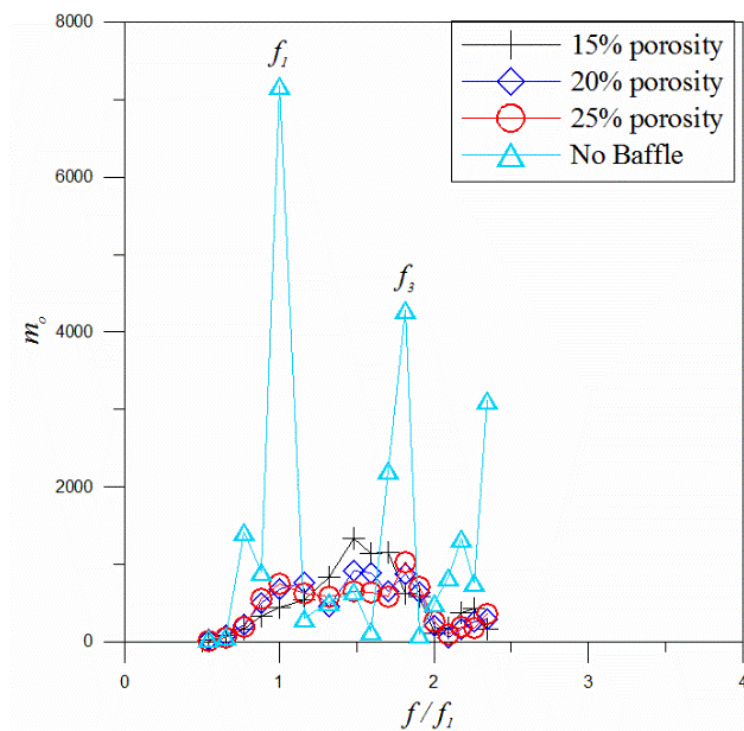


Figure 5.52 Variation of spectral energy (m_o) with different frequencies ratio (f/f_1); for (a) $hs/l = 0.488$ for $L/2$ locations.

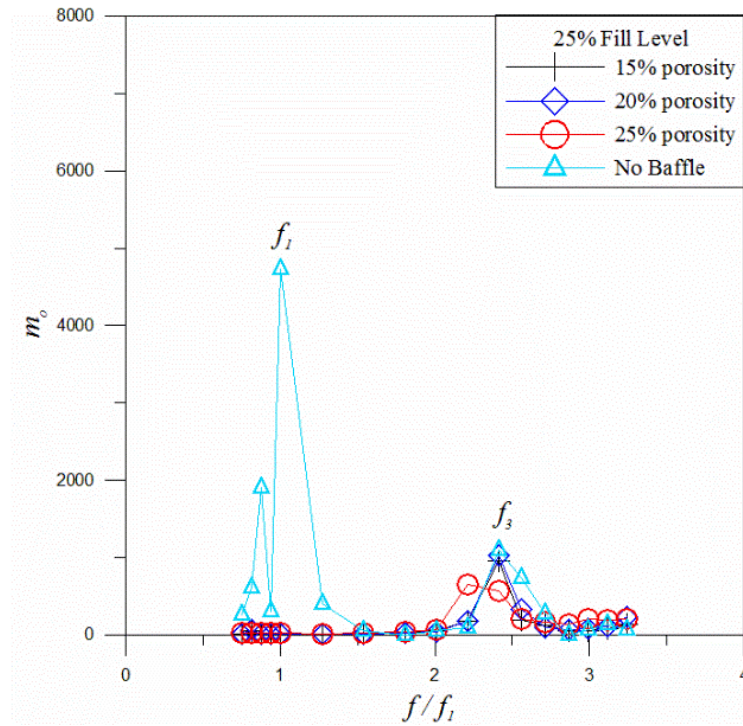


Figure 5.53 Variation of spectral energy (m_o) with different frequencies ratio (f/f_1); for $hs/l= 0.163$ for $L/3$ & $2L/3$ locations.

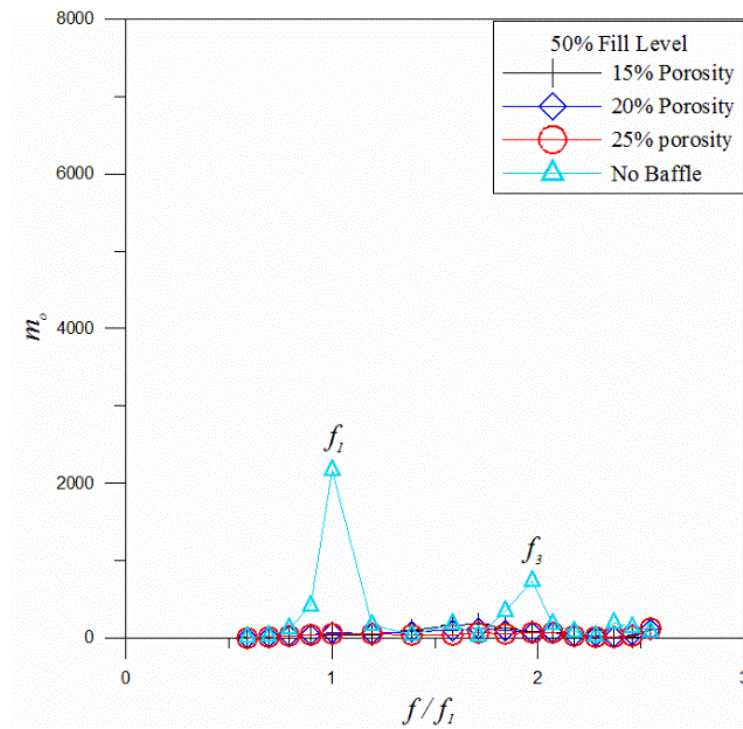


Figure 5.54 Variation of spectral energy (m_o) with different frequencies ratio (f/f_1); for $hs/l = 0.325$ for $L/3$ & $2L/3$ locations.

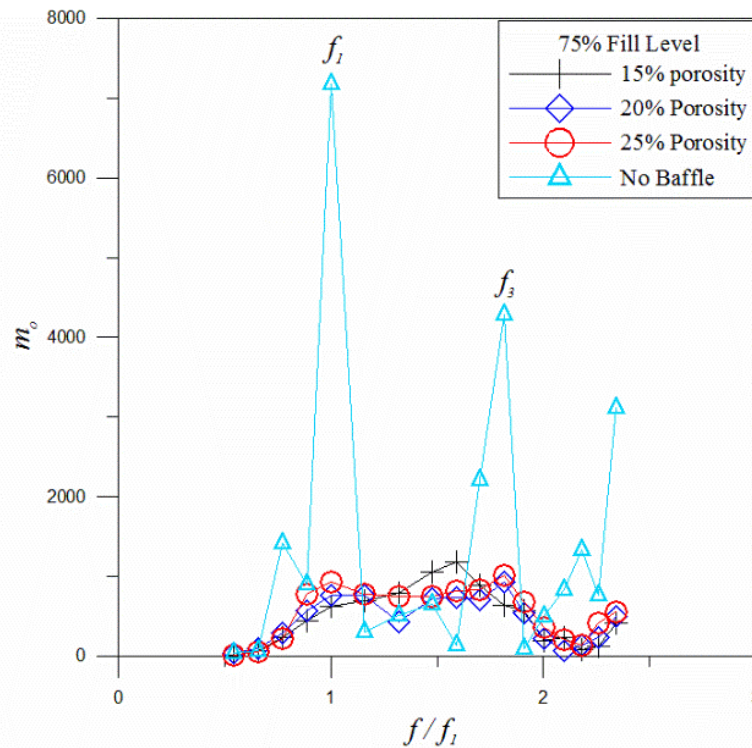


Figure 5.55 Variation of spectral energy (m_o) with different frequencies ratio (f/f_1); for (a) $h_s/l = 0.488$ for $L/3$ & $2L/3$ locations

Comparing the plots of m_o versus frequency ratio of no baffle and with porous baffles for different porosities leads to the following observations for $L/2$ conditions:

- In graphs it is observed that the maximum m_o value is at odd mode frequency i.e, f_1, f_3 and f_5 respectively.
- m_o value of no porous baffle is higher than the with baffle condition for both the 25% 50%, and 75% of water fill levels.
- In 25% fill level for 25% porosity, m_o value is greater than the 15% and 20% porosities.
- In case of the 50% fill level, m_o value for 15% porosities is greater than 20% of porosity and this value is greater than 25% porosity.
- As comparing three fill levels, 75% fill level m_o magnitude is greater than 25% and 50% fill levels. At the excitation frequency $f = f_3$, m_o value of with baffle condition is higher for 75% fill than compare with other 25% and 50% of fill levels.

m_o versus frequency ratio of no baffle and with porous baffles for different porosities leads to the following observations for $L/3$ & $2L/3$ conditions:

- In 25% fill level, highest porosity (25%) gives higher m_o than the other porosities (15% and 25%) for the excitation frequency of $f = f_3$.
- In case of 50% fill level, 20% porosity m_o value is greater than 25% porosity.
- m_o value of no porous baffle is greater than the with baffle condition for both the 25% 50%, and 75% of water fill levels.
- As comparing to three fill levels, 75% fill level m_o is greater than 50% and 25% fill levels.
- It may be deduced that the presence of porous baffles increases the energy of free surface oscillation.

NUMERICAL PERFORMANCE CHARACTERISTICS OF SLOSHING RECTANGULAR TANK

6.1 BACK GROUND

The structural interaction of sloshing tank and oscillation of liquid in a sway excited tank is studied using CFD solver. In addition, the presence of porous baffle in sloshing tank is explored by earlier researchers. The flexibility of baffle of a particular material with varying thickness on sloshing effect is also explored by using CFD solver.

Nema (2014) conducted a study to investigate the effects of earthquake frequency content on a water storage tank's seismic behavior. The study focused on the study of the effect of the frequency content on the tank's sloshing behavior. The results of the study were then analyzed using the ANSYS-FLUENT software. The different fill levels and the varying baffle heights were then adjusted to achieve the desired results. A two-phase flow simulation has been performed in a 3-D tank with a combination of baffles and incompressible, viscous fluid. The simulation was carried out using the FVM finite volume method. In the recent few researchers [*Kingsley and Craig (2007)* *Godderidge et al. (2009)*], studied the dynamics of a partially filled tank using a combination of computational fluid dynamics (CFD) and the VOF method. The latter allows them to predict the behavior of the tank's free surface. In the present study, the researchers are focused on developing a numerical model that takes into account the Reynolds Average Navier-Stokes equations. The results of the study are then validated by the experimental measurements.

6.2 COMPUTATIONAL FLUID DYNAMICS (CFD)

Chemical reactions, fluid flow, heat transfer, and other phenomena are studied through computational fluid dynamics (CFD), which is a type of mathematical technique used for simulating various problems. This is a powerful tool for analyzing and solving non-industrial and industrial issues. Partial differential equations in computational fluid

dynamics (CFD) are solved using various numerical techniques. These methods are used to discretize the equations in a linear manner. The results of these procedures are then analyzed using the Gauss-Seidel method. Over the years, computational fluid dynamics has been extensively used in various engineering fields. It is a powerful tool for analyzing and solving non-technical problems. This type of mathematical technique is mainly used for analyzing and solving fluid flow and heat transfer problems. Through its numerical and algorithm-based methods, the researcher can predict the nature of the flow and its chemical reactions. CFD predicts all of them by solving the set of following governing mathematical equations numerically:

- Conservation of mass
- Conservation of momentum
- Conservation of energy
- Conservation of species
- Effect of body forces

The goal of CFD is to solve the non-linear Partial differential equations. This technique can be used to perform complex physical problems and ideal conditions. However, it can also cause errors such as the truncation error. In order to minimize these errors, the equations are divided into linear algebra equations for each grid or cell. Then these linear equations are solved easily. There are three basic methods of discretization:

- **Finite Difference Method:** The domain is then discretized into a series of grid points, which are known as structured i, j, k , and grid is required. After that, the non-linear Partial Differential equations are given a linear algebra solution using Taylor series of expansion.
- **Finite Element Method:** In addition to performing structural problems, fluid dynamics can also be used to solve other non-linear problems. The domain is divided into various elements, and each element has its own equation.
- **Finite Volume Method:** The process of discretizing the domain is performed through a finite volume method known as FVM. After that, the Gauss divergence theorem is used to discretize the 26 partial differential equations. This method then allows the computational fluid dynamics to solve various non-linear equations.

6.2.1 Ansys- Fluent CFD Platform

ANSYS Fluent is a general-purpose software platform used for analyzing and solving various problems related to computational fluid dynamics. It can be used to model flow, heat transfer, and turbulence. The platform's physical prototypes allow engineers to perform precise analysis of complex problems. One of the most challenging computational fluid dynamics problems is the implementation of the Navier-Stokes equations. CFD software is commonly used to perform numerical solutions, which are validated with the results of the experimental work. Some of the popular packages include: ANSYS-FLUENT, CFX, FLOW-3D, and PHONICS. Most of these software's use the FVM method for discretization.

6.3 MATHEMATICAL FORMULATION AND NUMERICAL SIMULATION

This study presents a computational fluid dynamics model that is based on the Reynolds-Averaged Navier-Stokes method (RANS in equation 6.1 and 6.2). It is able to perform complex computational fluid dynamics problems by taking into account the various factors that affect the flow and pressure of fluids. The model is a multiphase multi-phase solver that takes into account the velocity component and the fluid pressure and fluid density. The parameters of two fluids are simultaneously solved in the computational domain using the governing equations. These include mass conservation, momentum conservation, and turbulence.

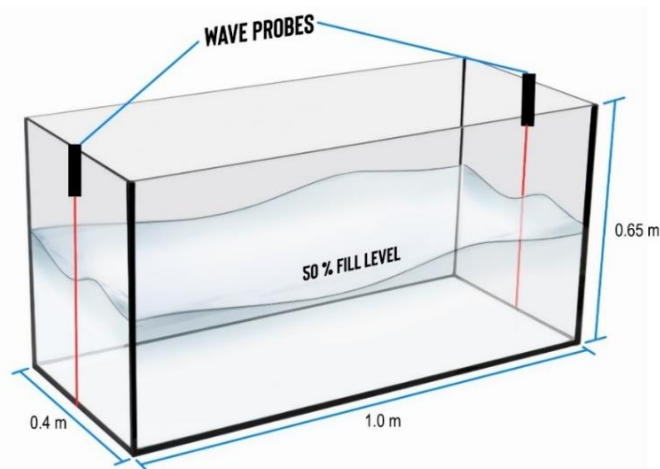


Figure 6.1 Geometry of the shake table model

For free surface wave motion and a nonlinear free surface wave motion problem that is based on the implementation of the Navier-Stokes equation (Eq. 6.3) and the continuity equation (Eq. 6.4). The water is incompressible and Newtonian, and its density does not change with time. The computational domain of the numerical 3-D Tank model and its dimensions are given in Figure 6.1. Reynolds stresses defined by $-\overline{u'_i u'_j}$; ν_T is the eddy viscosity and can be defined as $\nu_T = C_\mu k^2 / \epsilon$, k is the turbulence kinetic energy, and its rate of dissipation is ϵ . C_μ is a constant and is defined as 0.0845. (Ansys Fluent User's Guide, 2019).

$$\frac{\partial u_i}{\partial x_i} = 0 \quad (6.1)$$

$$\frac{\partial u_i}{\partial t} + u_j \frac{\partial u_i}{\partial x_j} = -\frac{\partial p}{\partial x_i} + \frac{\partial}{\partial x_j} \left[(\nu + \nu_T) \left(\frac{\partial u_i}{\partial x_j} + \frac{\partial u_j}{\partial x_i} \right) \right] + \frac{\partial}{\partial x_j} (-\overline{u'_i u'_j}) \quad (6.2)$$

$$\nabla \cdot \mathbf{u} = 0 \quad (6.3a)$$

$$\rho \left(\frac{\partial \mathbf{u}}{\partial t} \right) = -\nabla p + \nabla^2 \mu + F_e \quad (6.3b)$$

Navier-Stokes equation in two-Dimensional Cartesian coordinate systems can be rewritten as

$$\rho \left(\frac{\partial u}{\partial t} + u \frac{\partial u}{\partial x} + v \frac{\partial u}{\partial y} \right) = -\frac{\partial p}{\partial x} + \mu_w \left(\frac{\partial^2 u}{\partial x^2} + \frac{\partial^2 u}{\partial y^2} \right) + \rho g_x \quad (6.4a)$$

$$\rho \left(\frac{\partial v}{\partial t} + u \frac{\partial v}{\partial x} + v \frac{\partial v}{\partial y} \right) = -\frac{\partial p}{\partial y} + \mu_w \left(\frac{\partial^2 v}{\partial x^2} + \frac{\partial^2 v}{\partial y^2} \right) + \rho g_y \quad (6.4b)$$

Where u , v are components of the velocity field in the x and y -direction, respectively. P is the fluid pressure and ρ is density. μ_w is the kinematic viscosity and g_x and g_y are the gravitational acceleration components. In Eq. (6.3a), the first term corresponds to the inertial forces; the second term corresponds to pressure/forces; the third term corresponds to viscous forces; the fourth term corresponds to external forces applied to the fluid. Eqs. (6.4a) and (6.4b) represent the Navier-Stokes equation in a 2D Cartesian coordinate system. Eq. 6.5 presents the continuity equation, Eq. 6.6 presents the continuity equation for incompressible flow and Eq. 6.7, based on the conception of the control volume, the motion of the free surface is tracked by solving the transport equation of the VOF function.

$$\frac{\partial}{\partial x}(\rho x) + \frac{\partial}{\partial y}(\rho y) + \frac{\partial \rho}{\partial t} = 0 \quad (6.5)$$

$$\frac{\partial u}{\partial x} + \frac{\partial v}{\partial y} + \frac{\partial w}{\partial z} = 0 \quad (6.6)$$

$$\frac{\partial F}{\partial t} + u_i \frac{\partial F}{\partial x_i} = 0 \quad (6.7)$$

F is the volume fraction of fluid in the control volume, defined as 1 in the fluid, 0 in the void, and $0 < F < 1$ at the free surface. The primary focuses on the numerical generation and capture of free surface elevation. In order to solve the two-phase problems, the volume of fluid method was developed by Hirt and colleagues in 1981. This method was able to solve the problems by taking into account the various factors that affect the flow and pressure of fluids and also present dynamics and free surface boundary condition model. The work presents a framework for solving the governing equations of the computational domain using the relevant boundary conditions. The increase in the mesh densities at the water surface elevation helps in capturing the free surface elevation.

6.4 SOLVER CONTROLS

ANSYS Fluent has a wide variety of solvers that can affect the convergence and quality of the results of a given problem. One of the most common solutions used by the company is the segregated solution algorithm. This method allows the users to solve the governing equations in sequential steps. Since the equations are non-linear, multiple iterations of the solution are required before a complete solution can be obtained. Another technique that can be used to speed up the process of solving complex problems is the non-iterative time advancement (NITA). This method has been shown to improve the performance of the computational fluid dynamics process (ANSYS Fluent User Guide, 2020). The NITA scheme is designed to minimize the errors that are generated during the sequential steps of a given solution. It does not require the user to reduce the error from each step to zero. The computational flow of the scheme shows that only one global iteration is performed during a given time. The advantage of this method is that it allows the users to perform sub-iterations in sequential steps, but the outer velocity-pressure is only performed once in a given time step, which significantly speeds up the simulations. This method also eliminates the time discretization error, which is typically associated with the computation of multiple sub-iterations.

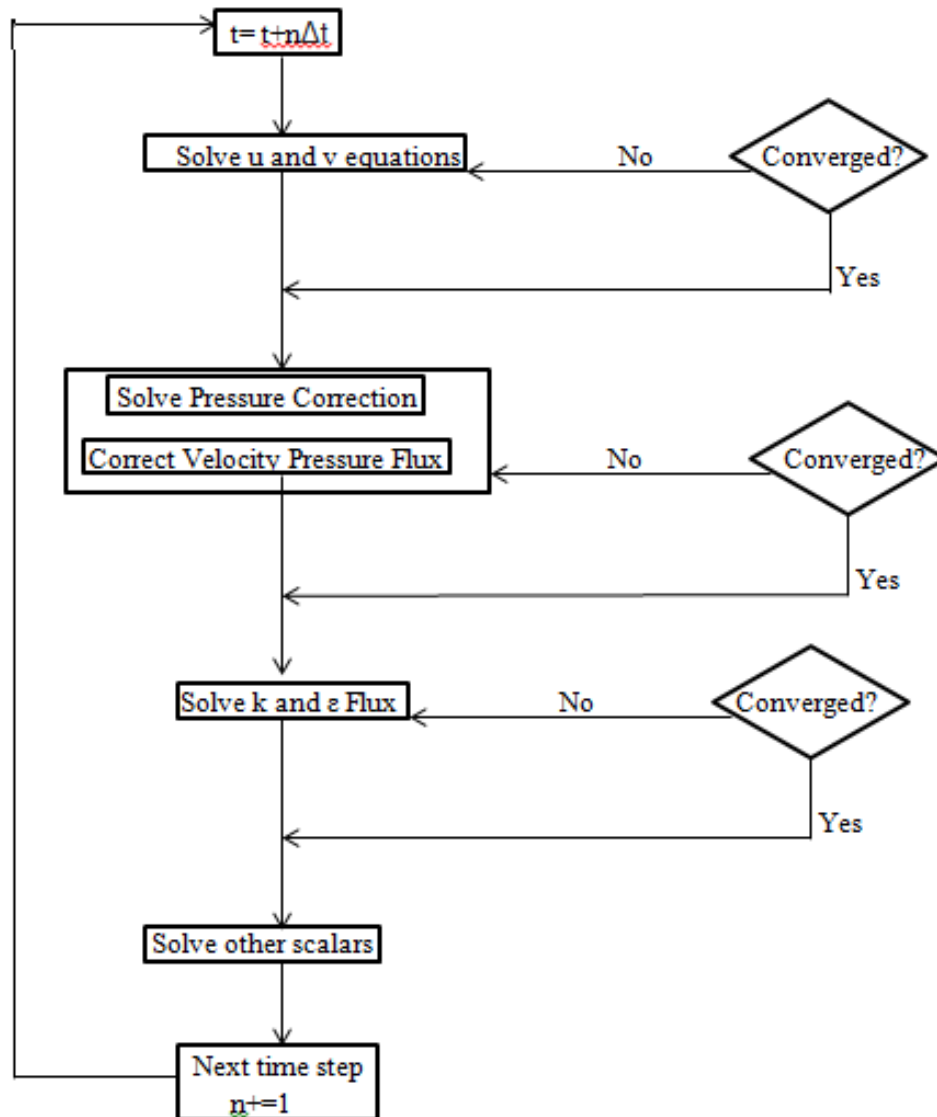


Figure 6.2 Non-Iterative Time Advancement flow chart (ANSYS Fluent User Guide, 2020)

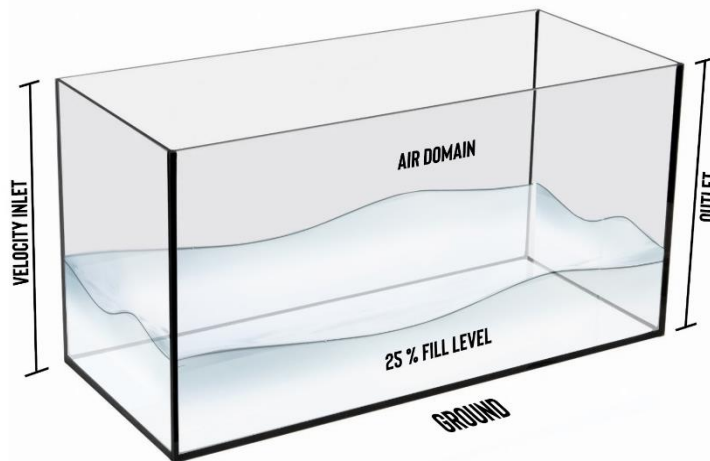
Since the equations are non-linear, it is necessary to control the variable change in the solution. This process is performed by implementing an under-relaxation factor. This method ensures that the change in the variable is minimal during each iteration. The new value of a variable is computed by taking into account the old value and the under-relaxation factor.

6.5 PRELIMINARY INVESTIGATION

The preliminary investigation is carried out to arrive at suitable sloshing tank length and mesh or grid size by using a numerical tool based on computational fluid dynamics (CFD). At first, a numerical sloshing tank is created with different mesh sizes to select the optimum mesh size. In the sub-sections, an elaborate discussion is discussed to arrive at an optimum numerical sloshing tank for the study.

6.5.1 Modelling of geometry

A three-dimensional numerical sloshing tank is modelled with dimensions of length, breadth and height as 1m x 0.4m x 0.65m respectively. The water depth is considered for three different fill levels wherein the test model is placed at a distance of two distinct locations with three different porosities. The geometry of the sloshing rectangular tank is modelled using the design modeler tool in ANSYS Fluent. The end probe is measured at positions $L/2$ and $L/3$ and $2L/3$ locations. The obtained data are used to calculate the free surface elevations for all the cases adopted.



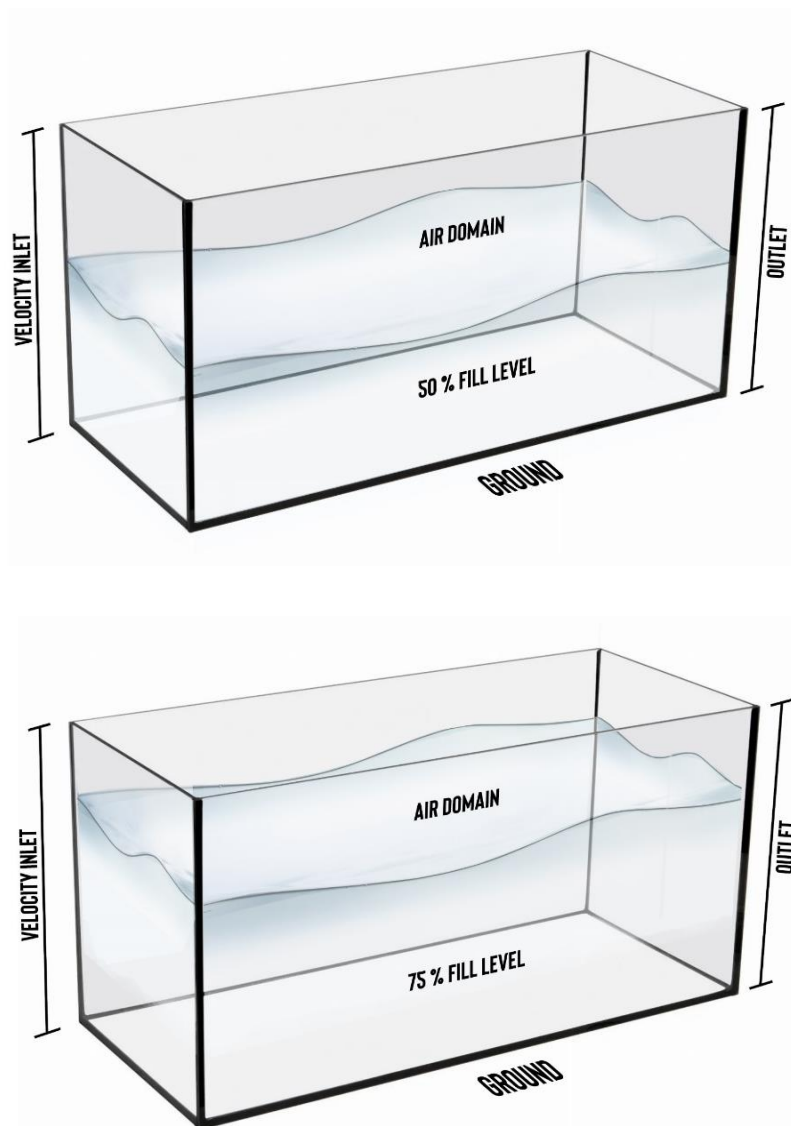


Figure 6.3 Schematic numerical sloshing tanks with three different fill levels with boundary conditions

The general steps involved in numerical simulation of ANSYS - FLUENT can be broadly classified into three. Pre-processing, Solver, and Post-processing. Pre-processing can be subdivided into Geometry building, Meshing, and defining the boundary conditions, as illustrated in Figure 6.4.

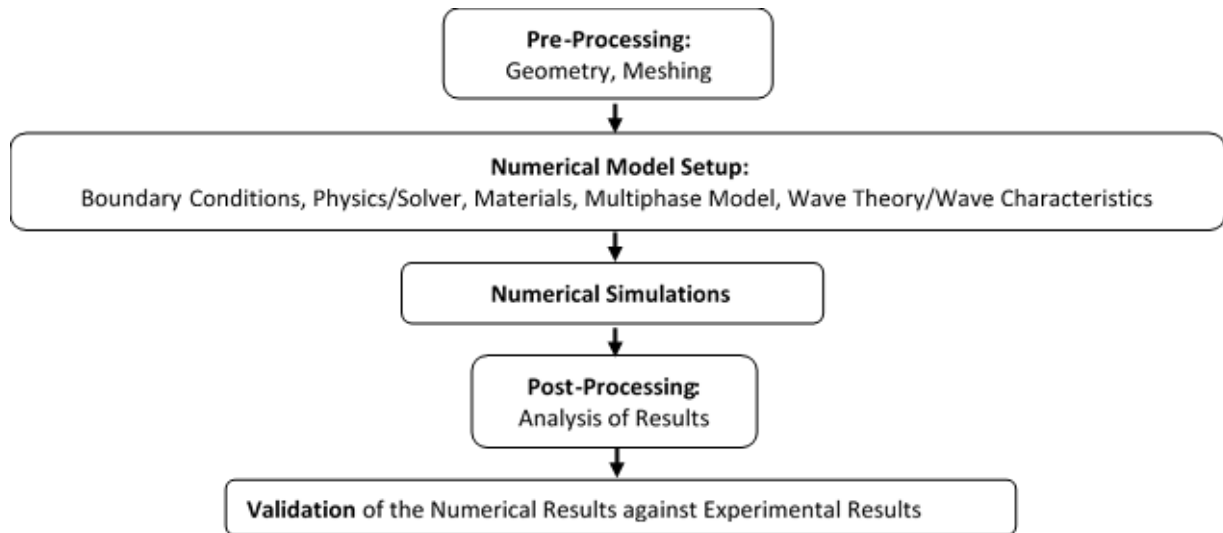


Figure 6.4 Workflow in numerical simulations Ansys-Fluent

6.5.2 Meshing details

The suitable mesh selection determines the solution's accuracy, stability, and computational efficiency. Hence in this segment, we devote a detailed discussion on the grid size or mesh details. The numerical grid pattern is created using the Ansys mesh tool. Using the face meshing method, the solution region is split into square elements of chosen dimensions, and then a structured mesh is created. Initially, to determine the effect of mesh size on the accuracy of ANSYS Fluent results, a three-dimensional numerical sloshing tank is modelled, and the wave surface elevations are obtained. Figure 6.5(a) illustrates the fluent meshing for mild steel plate single case porous baffles and double case porous baffle are shown in figure 6.5 (b). The computational simulations are carried out for three mesh sizes, viz. 0.005m x 0.005m, 0.006m x 0.006m and 0.007m x 0.007m as shown in Figures. 6.6 (a-c). Table 6.2 shows the base grid dimensions for which the trials are carried out. Havn (2011) and Kumaran (2022) recommended the criteria for sizing the mesh and time step for better accuracy. The mesh size parameters are illustrated in Table 6.2.

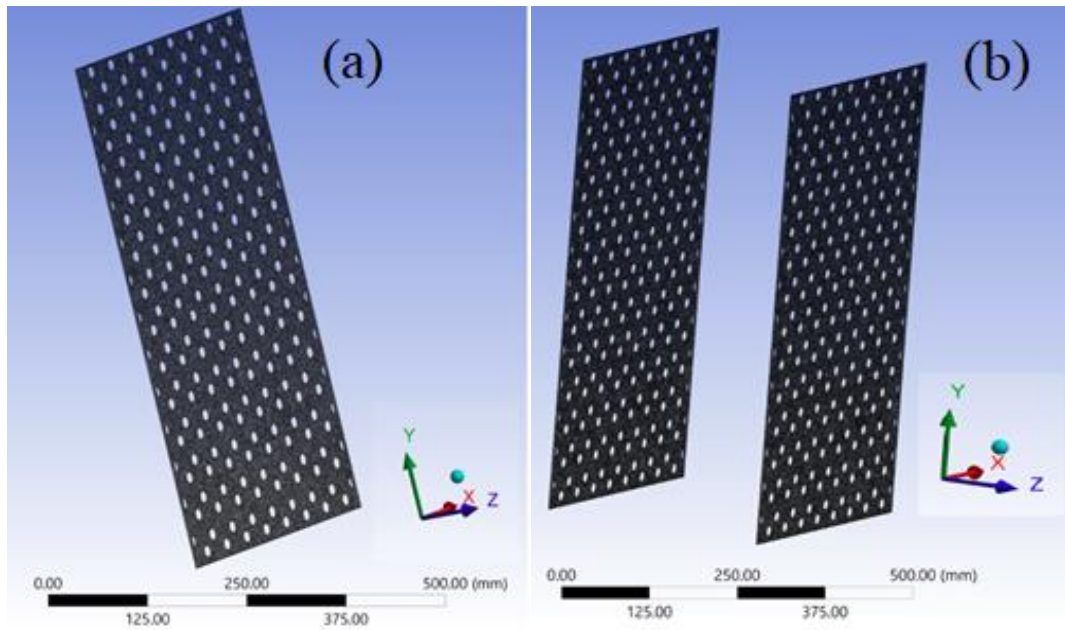


Figure 6.5 The fluent meshing for mild steel plate (a) Single case porous baffles and (b) Double case porous baffle.

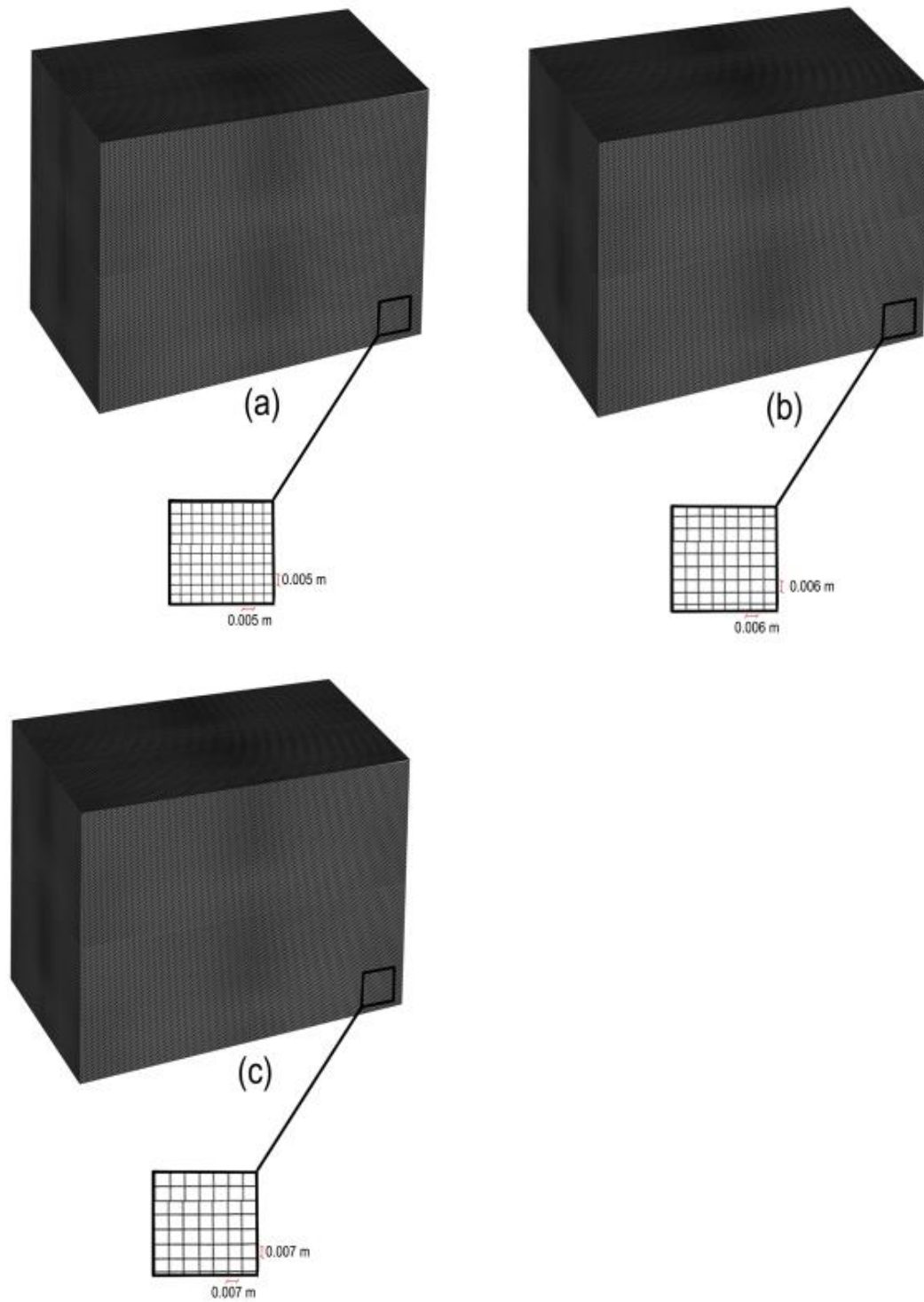


Figure 6.6 (a-c) Fluent meshing closer to the test model

Table 6.2 Grids Parameters

Mesh	ΔX (m)	ΔZ (m)	Grid cell density	No. of Elements	No. of Nodes
1.	0.007	0.007	400	9610713	9801564
2.	0.006	0.006	500	32500000	32929227
3.	0.005	0.005	800	24500000	25864789

From the mesh convergence results obtained for the cases mentioned above, inferences are drawn that higher grid cell density gives more accurate results. But the computational time is very high than the same. So, it can be inferences that higher grid cell density is preferred for more accurate results while increasing the nodes and elements in the computation domain with finer mesh results more in time. But from the mesh convergence study shown in Table 6.2, the grid size of 0.005m is observed with similar trends compared with the 0.006m and 0.0007m grid size. Hence, for the present study, the numerical sloshing tank meshes into structured square meshes of 0.005 m grid size, and the whole structure meshes uniformly into a square structured mesh of 0.005m x 0.005m. Due to that, the computational time reduces as fewer elements are used.

6.5.3 Boundary Conditions

As we solve the 2nd order governing equation in 3-D sloshing tank, we need four boundary conditions to get the solution mathematically. Here in the physical domain, we have the following four boundary conditions.

- (i) Inlet = velocity inlet
- (ii) Outlet = pressure outlet
- (iii) Bottom = ground
- (iv) Top = Air domain

The boundary conditions are illustrated schematically in Figure 6.3.

The numerical sloshing tank involves multiple phases, i.e., air and water. Flowing media (water) is always set as the secondary phase, and the medium over that is a primary phase (air). In order to ensure that the preliminary phase species are present in every cell, Fluent automatically generates the secondary phase within the domain. This method ensures that the fill level is equal to the chosen water depth (d). For clarity, the actual boundary conditions are shown in Figure 6.3. The ocean wave is generated using a User Defined Function (UDF) to the inlet velocity boundary within the Fluent analysis module. A unique UDF is created in the setup part for each water depth (d), length (L), height (H), and time period combination.

As an initial condition, static pressure is given for the liquid face, and the free surface between the air and water interface is generated by the volume of the fluid model (VOF). The implicit formulation is used for the volume fraction parameter.

6.5.4 Influence of the numerical wave sloshing tank

Numerical simulations are carried out for three different fill levels of depths with lengths 1m breadth 0.4m and height 0.65m. The results of this study are presented in the form of free surface elevation graphs. The rising height of the liquid does not affect the free surface elevation. However, the pressure from the surface does not allow the liquid to return to its original free surface. The free surface elevation is decreased dramatically when the frequency of the sloshing is near to the natural frequency. However, more violent sloshing phenomenon occurs at the new natural frequency $f=f_1$. The maximum free surface elevation can be reduced only if the excitation frequency is close enough to the first and third natural frequencies. It does not change significantly under the fourth and fifth natural frequencies.

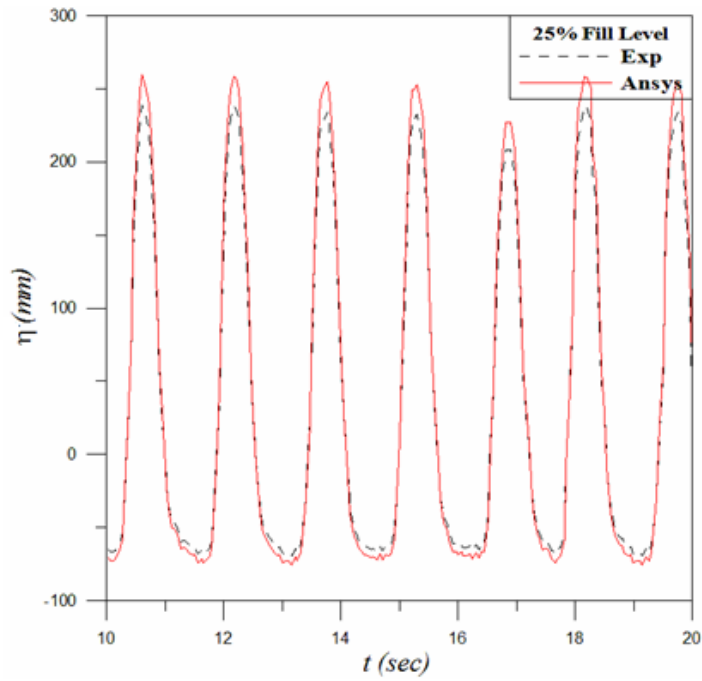


Figure 6.7 Variation of free surface elevation (η') between experimental and computational results for the aspect ratio of $h_s/l= 0.163$.

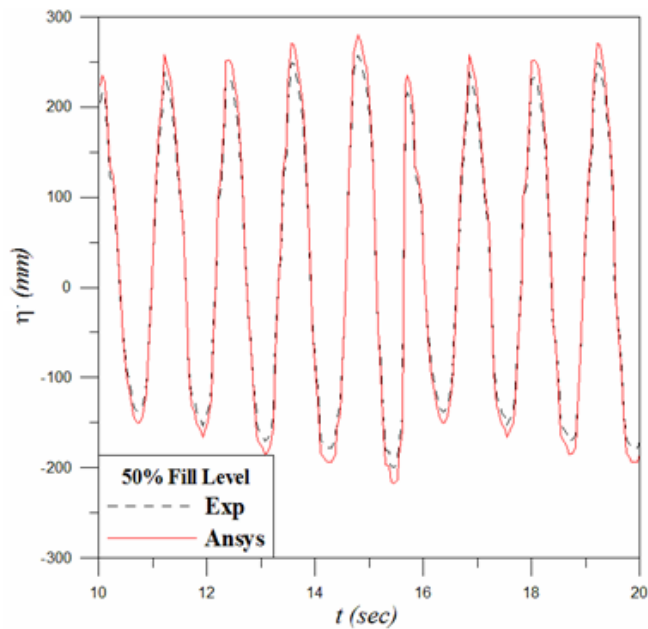


Figure 6.8 Variation of free surface elevation (η') between experimental and computational results for the aspect ratio of $h_s/l= 0.325$.

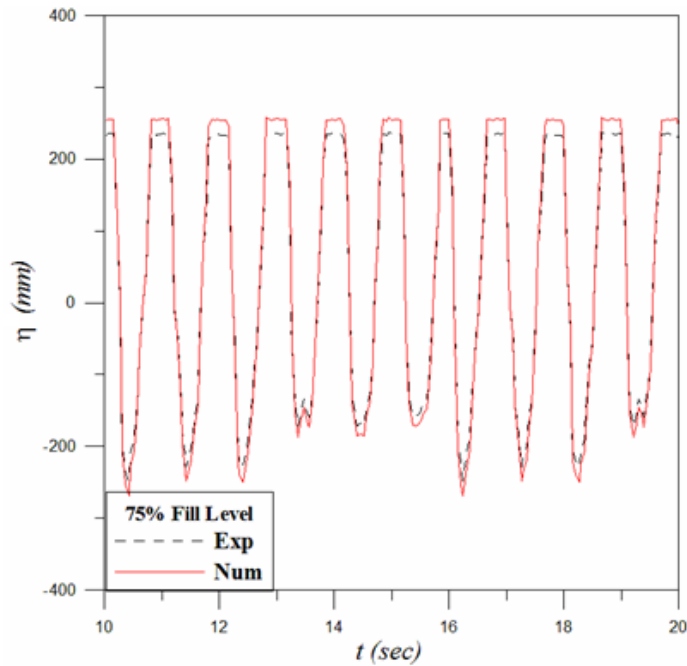


Figure 6.9 Variation of free surface elevation (η') between experimental and computational results aspect ratio of $h_s/l= 0.488$.

6.5.5 Validation between ANSYS Fluent and Experimental Results

In this study the use of the k-epsilon viscous model for the study of the effects of the water depth on the flow rate and the boundary conditions. In order to choose the appropriate wave theory for the given conditions, the user should first consider the relative water depth. DNV RP 205 (2010) provides a list of the suitable wave theories for different wave conditions. The simulations are performed on a workstation computer using an Intel CPU E5-2620v3 2.40 GHz processor. The typical time for a single combination is around 1 day. The results of the simulations are presented in the form of free surface elevation graphs. Since the rising height of the liquid does not affect the free surface elevation, the liquid will return to its original free surface. The impact of the pressure from the surface on the tank's sidewall is small. The minimum liquid filling depth of 25% is considered to be ideal for the study of the effects of the water depth on the flow rate and the boundary conditions. However, increasing the filling level can decrease the free board available for the movement of free surface elevation and cause the liquid to give impact on the top panel.

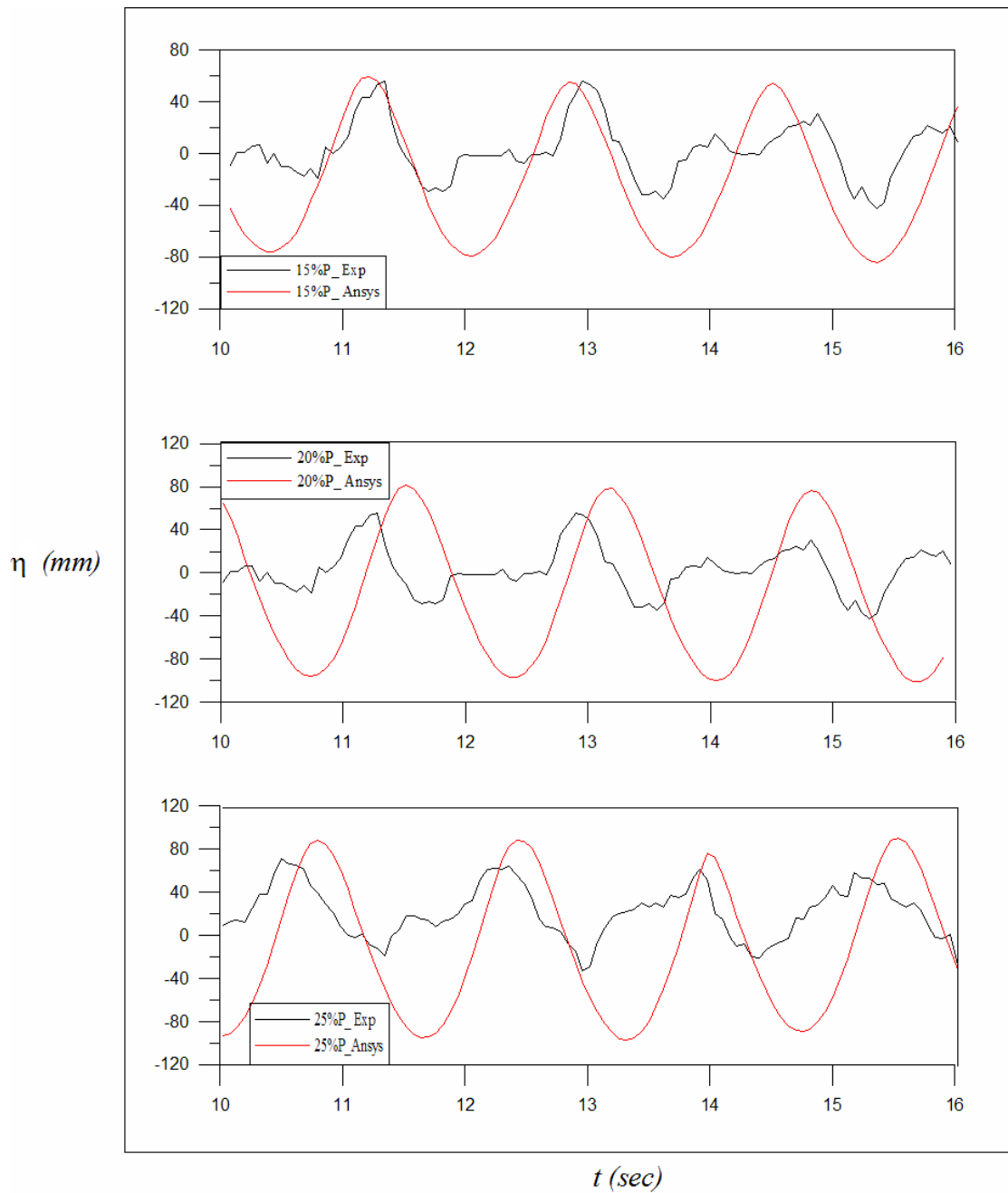


Figure 6.10 Time histories of free surface elevation with baffle frequency ratios 0.6059 $H_z(f_1)$ for $h_s/l = 0.163$ at single baffle condition ($L/2$).

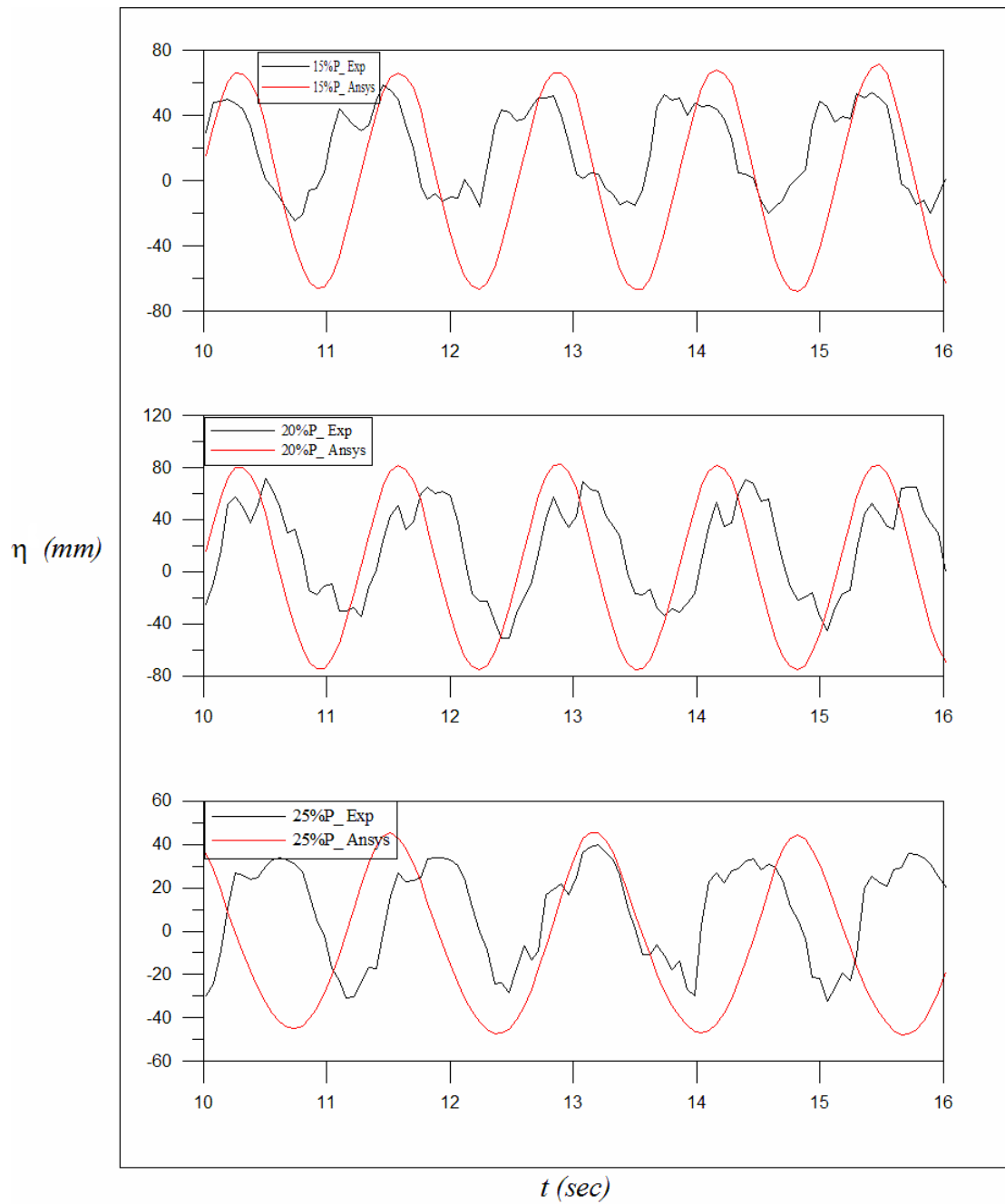


Figure 6.11 Time histories of free surface elevation with baffle frequency ratios 0.7755 $Hz (f_i)$ for $hs/l = 0.325$ at single baffle condition ($L/2$).

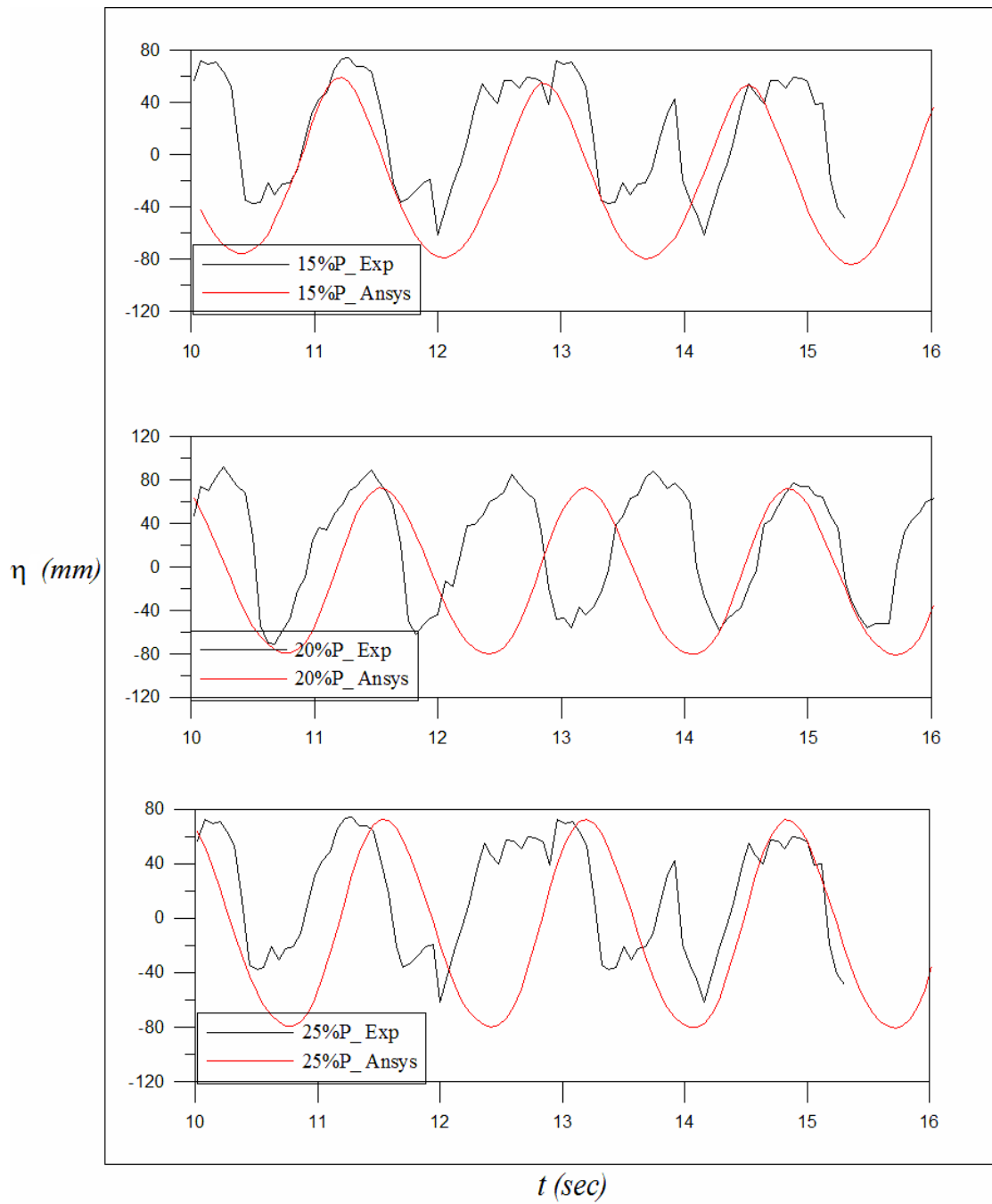


Figure 6.12 Time histories of free surface elevation with baffle frequency ratios 0.8432 $Hz (f_1)$ for $hs/l = 0.488$ at single baffle condition ($L/2$).

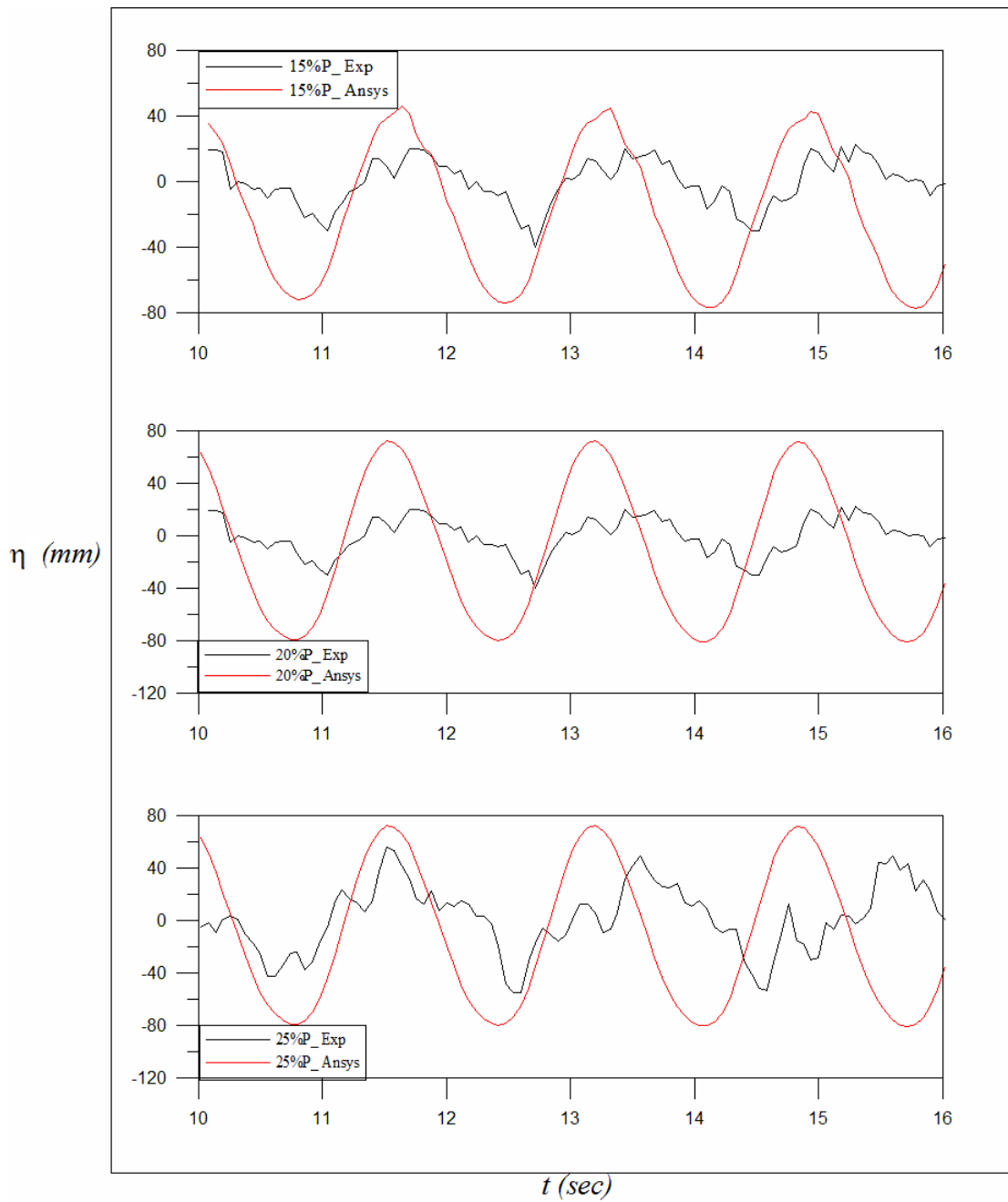


Figure 6.13 Time histories of free surface elevation with baffle frequency ratios 0.6059 $H_z(f_1)$ for $h_s/l = 0.163$ at double baffle conditions ($L/3$ and $2L/3$).

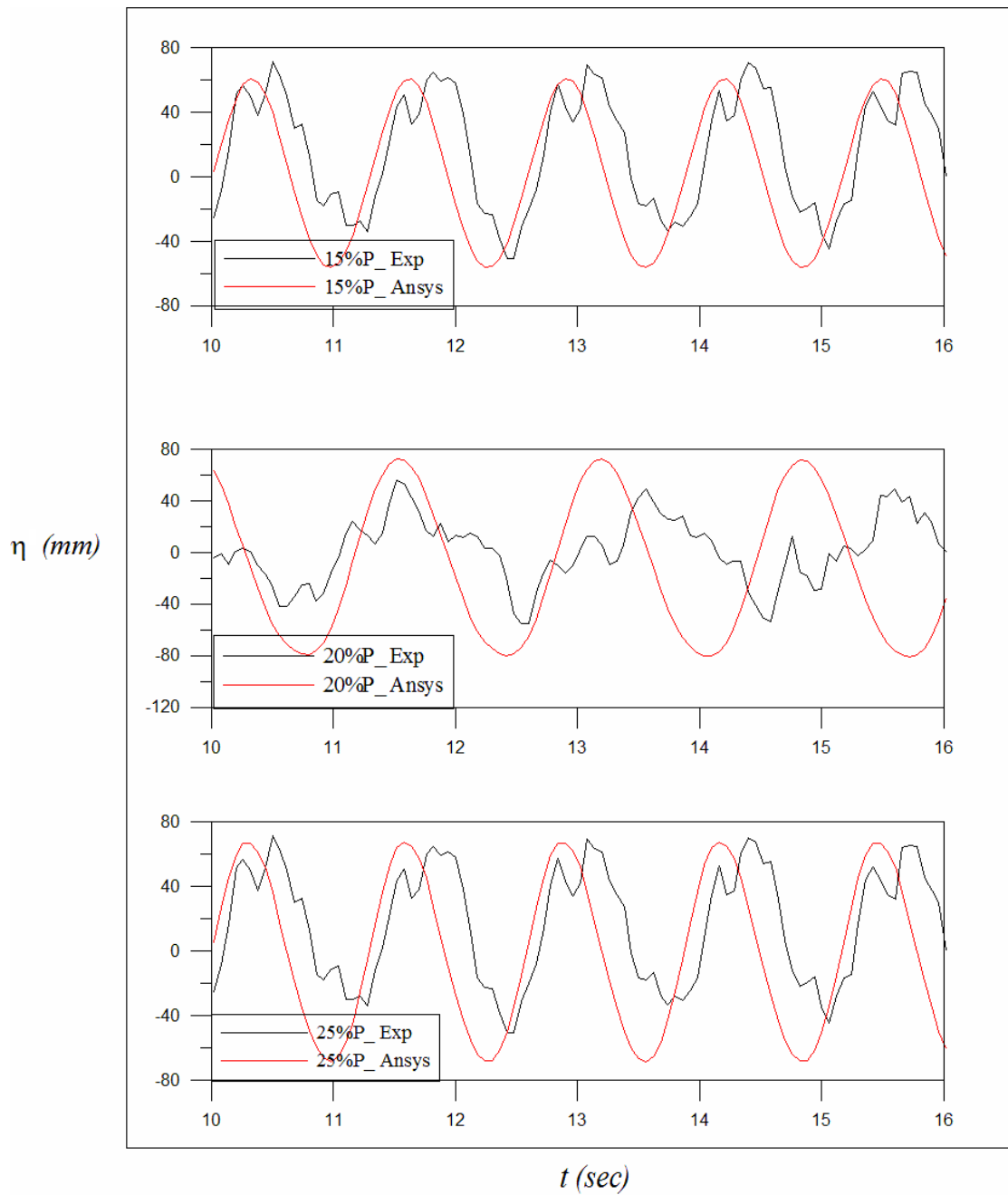


Figure 6.14 Time histories of free surface elevation with baffle frequency ratios 0.7755 $H_z(f_1)$ for $h_s/l = 0.325$ at double baffle conditions ($L/3$ and $2L/3$).

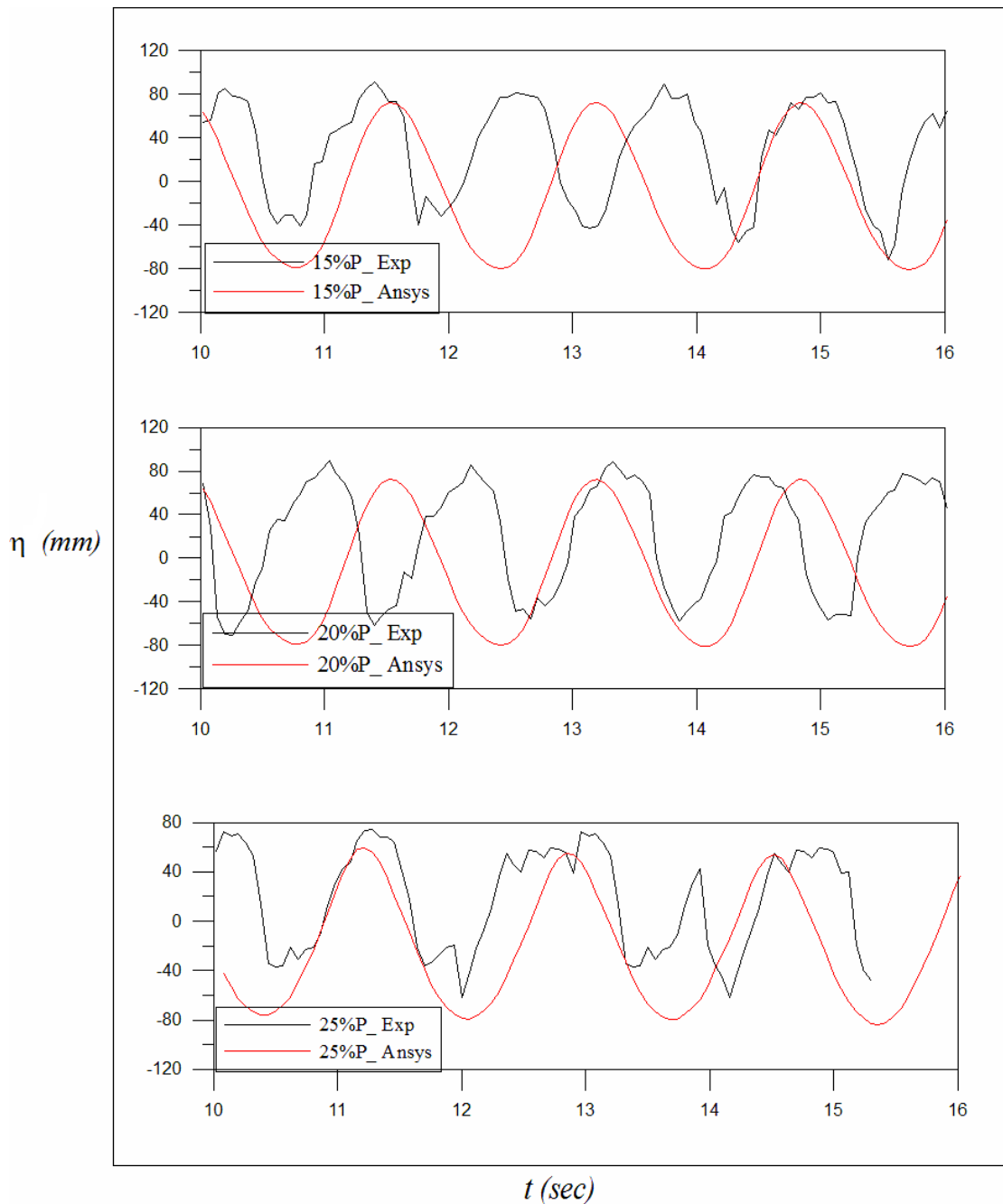


Figure 6.15 Time histories of free surface elevation with baffle frequency ratios 0.8432 $H_z (f_i)$ for $hs/l = 0.488$ at double baffle conditions ($L/3$ and $2L/3$).

A UDF is defined for the components of inlet velocity to generate waves numerically to simulate the wave theory. This numerical sloshing tank gave considerably good results in-line with the experimental results. For the time step of 0.03s ($T/200$), surface elevation in the wave crest and trough obtained from the numerical study closely

correlates with the experimental study. Hence the time step of 0.03s is considered for all CFD simulations.

Finally, it is concluded that the numerical simulations with a mesh size of 0.005m x 0.005 m, with time step 0.03s, 1m tank length and numerical beach condition, provide a good output, with an admissible correlation with experimental and theoretical approaches.

6.5.6 Relative error calculation

$$\text{Relative error} = \frac{E_p - N_p}{E_p} \times 100$$

Where E_p - Experimental results

N_p - Numerical results

The mean relative error in wave height measured by the wave probe is 9.24 %, and the free surface elevation variation shows correlations between experimental study and numerical solutions.

From the outcome of preliminary investigations. Here the various effects of sloshing in reducing the wave reflection characteristics, and the validation of the numerical model is done by comparing it with an experimental approach with an acceptable error for better numerical solutions. The following input parameters remain fixed throughout the numerical study, such as the Height ($h = 0.65m$), mesh size ($0.005m$), Numerical tank length ($1m$).

The conclusions arrived are:

1. Increasing the computational grid or mesh size results in wave damping and a small shift in the peak of results providing insignificant numerical solutions. To overcome these three mesh sizes (0.005×0.005 , $0.006m \times 0.006m$ and $0.007m \times 0.007m$) are considered. It is noted that ($0.05m \times 0.005m$) agrees with experimental and theoretical approaches and is effective in computational time compared to a upper mesh size.

2. To optimize the length and height of sloshing tank, several factors are considered. Finally, the numerical simulations with a mesh size of 0.005m x 0.005 m, with timestep 0.03s, for 1m tank length provide a better output with a good agreement with numerical and experimental results.

It is understood that when increasing the frequency ratio to ($f/f_1=1$) which corresponds to the first mode of the natural frequency of the fluid in the rectangular tank, the oscillation of the free surface elevation is dramatically amplified due to resonance as shown in Figure 6.6 -6.8. The energy that the flow takes in through its oscillations is greatly increased when the tank's oscillations coincide with the system's natural frequency. This phenomenon helps in maximizing the flow's energy efficiency.

As seen from graphs for no baffle case, the normalized free surface elevation at $f=f_1$ is always higher for all 25%, 50% and 75% of water depths. Physical model results seem to be in good agreement with the numerical simulations.

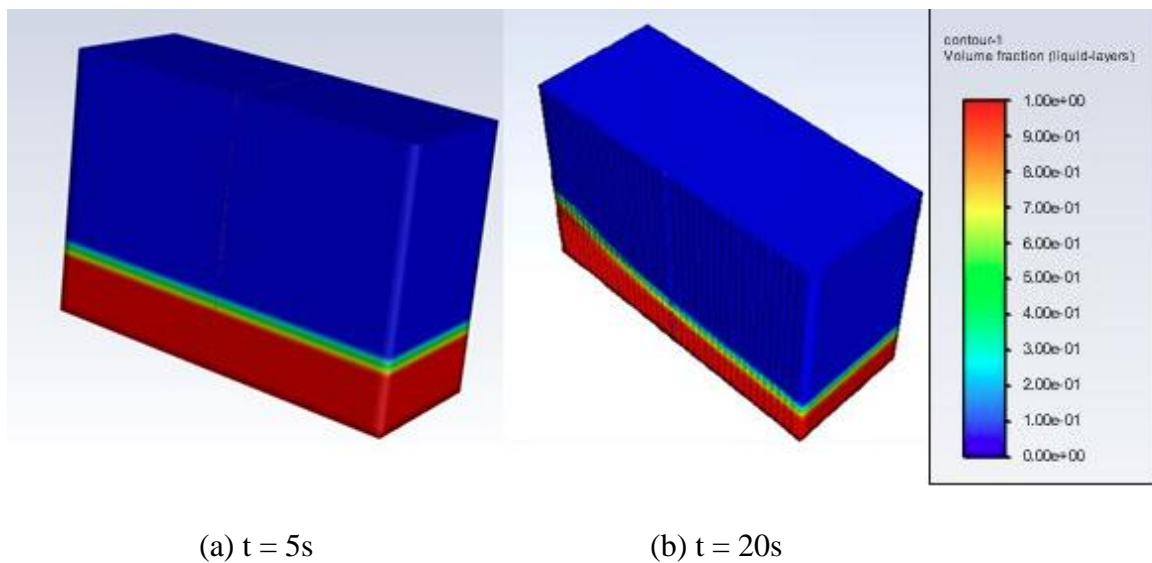
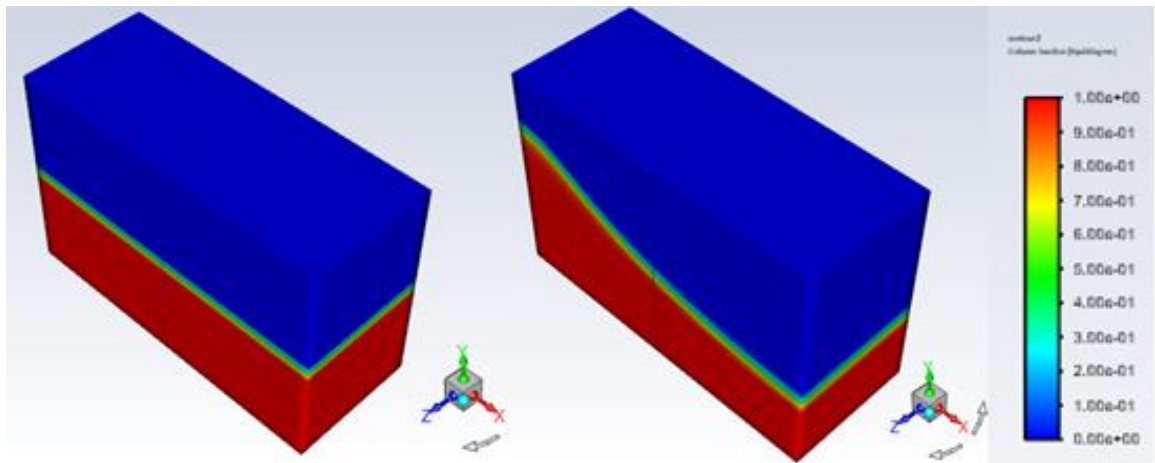


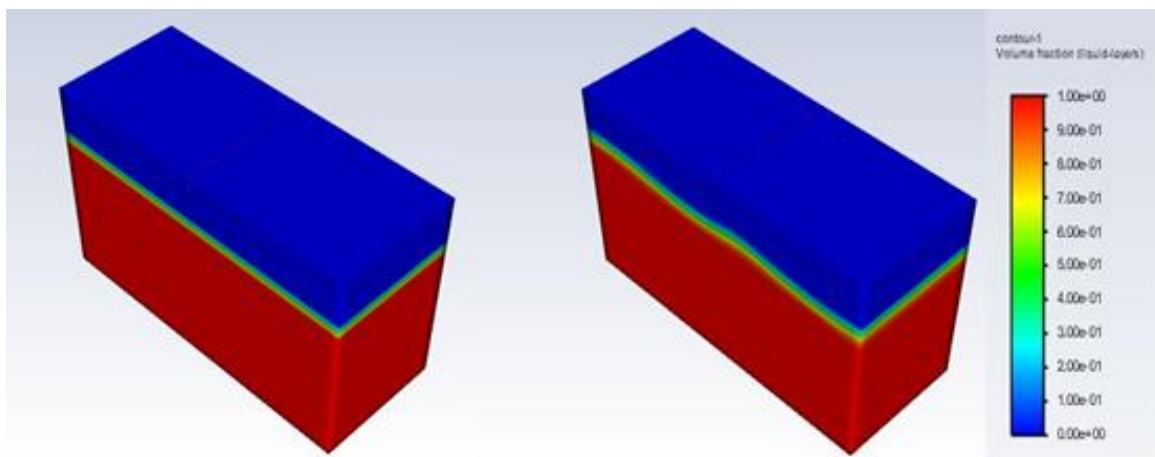
Figure 6.16 (a) Wave propagation in numerical sloshing oscillation at $t= 5sec$ (b) Peak sloshing oscillation at $t= 20sec$ for baffle at $L/2$ location for 25% fill level case.



(a) $t = 5s$

(b) $t = 20s$

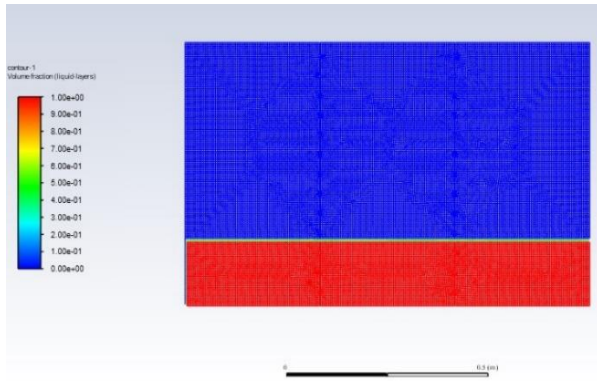
Figure 6.17 (a) Wave propagation in numerical sloshing oscillation at $t= 5sec$ (b) Peak sloshing oscillation at $t= 20sec$ for baffle at $L/2$ location for 50% fill level case.



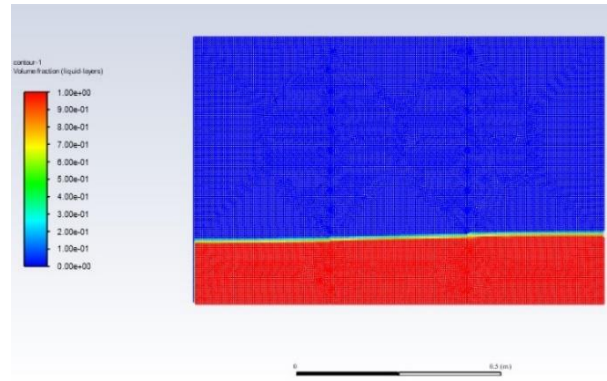
(a) $t = 5s$

(b) $t = 20s$

Figure 6.18 (a) wave propagation in numerical sloshing oscillation at $t= 5sec$ (b) Peak sloshing oscillation at $t= 20sec$ for baffle at $L/2$ location for 75% fill level case.

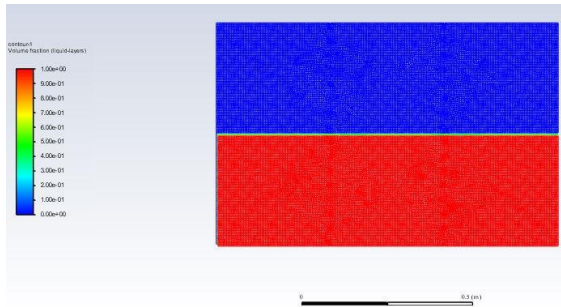


(a) $t = 5s$

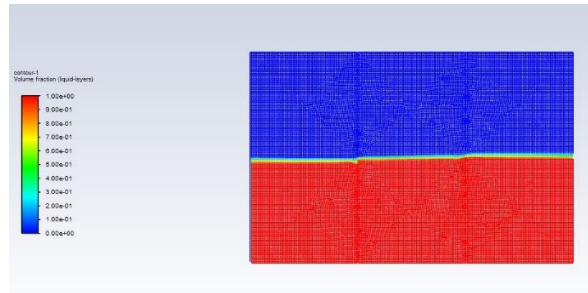


(b) $t = 20s$

Figure 6.19 (a) Wave propagation in numerical sloshing oscillation at $t= 5sec$ (b) Peak sloshing oscillation at $t= 20sec$ for baffle at $L/3$ & $2L/3$ locations for 25% fill level case.

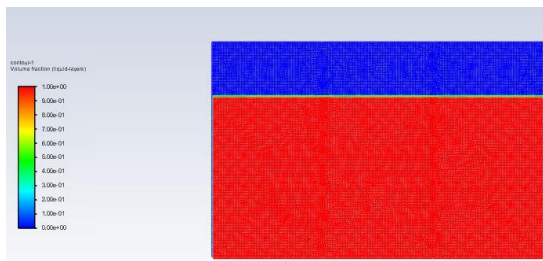


(a) $t = 5s$

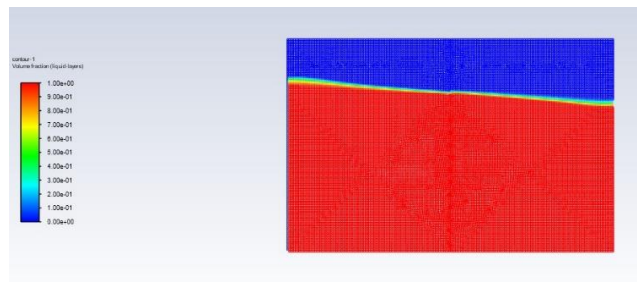


(b) $t = 20s$

Figure 6.20 (a) Wave propagation in numerical sloshing oscillation at $t= 5sec$ (b) Peak sloshing oscillation at $t= 20sec$ for baffle at $L/3$ & $2L/3$ locations for 50% fill level case.



(a) $t = 5s$



(b) $t = 20s$

Figure 6.21 (a) Wave propagation in numerical sloshing oscillation at $t= 5sec$ (b) Peak sloshing oscillation at $t= 20sec$ for baffle at $L/3$ & $2L/3$ locations for 75% fill level case.

The VOF model takes into account the non-interpenetrating properties of the two phases of the flow, namely, water and air. Since the two phases are not interpenetrating, they are assumed to be unsteady and are solved by the RANS and the Navier-Stokes

equations. The wave propagation and interaction of the wave with the test model shown in Figure 6.16 to Figure 6.21 represent the water volume fraction in a numerical sloshing tank during waves progress.

Figure 6.16 to 6.21 shows the initial sloshing oscillation at $t= 5s$ and peak maximum sloshing oscillation at $t= 20s$. The water volume fraction graph is the numerical evidence for sloshing elevation acting on the side wall at different instants of time with different fill levels.

6.6 CLOSURE

In the present chapter, an attempt is made to select the proper numerical model to study the performance of sloshing rectangular tank. The performances of the baffles are estimated using numerical modelling under wave conditions for different fill levels.

These conclusions have been drawn when the numerical results are validated by experimental data.

- The VOF model is appropriate for the study of the effects of the water depth on the flow rate and the boundary conditions. It can also be used with a permissible error to simulate the conditions in the experiment.
- When the excitation frequency of the liquid-water system is close to the natural frequency, the violent phase of the phenomenon occurs more frequently. The troughs and crests of the curve of the pressure and moment also change as the system's behavior changes.
- It has been known that the reduction in the fluid motion caused by the use of baffles can also contribute to the force response. However, the effect of the forcing frequency on the sloshing is not as pronounced as it is when the system is at the natural frequency.
- The goal of this study is to analyze the effects of the liquid-water system's forces acting on the tank and its various effects on the free surface elevation and the pressure and moment amplitude. In addition to the resonance condition, the excitation frequency also affects the moment and pressure amplitude.

- The numerical study shows a good correlation with the experiment results and the deviation of numerical simulation in comparison with experimental findings is found to be 9.24%

CHAPTER 7

CONCLUSIONS

7.1 SUMMARY

In the sloshing dynamics problem, analysis of sloshing oscillation characteristics and estimation of sloshing force are the important parameters to design a liquid containment in ship going vessels, liquid transporting vessel on highways and its application extends to various engineering disciplines. Further, porous baffle configurations are considered to understand the sloshing energy dissipating characteristics. The performance of porous screens of different porosities such as 4.4%, 6.8%, 9.2%, 15%, 20% and 25% are assessed. The effectiveness of two screen placements $L/2$ & $L/3$ and $2L/3$ positions in the sloshing tank are studied. Three different fill levels of 25%, 50% and, 75% which corresponds to aspect ratios, (h/L) of 0.163, 0.325, and 0.488 are considered to explore the effect of fill levels.

An uni-directional shake table is designed and devised to measure the sloshing force. The concept of ballast mass to measure the base shear force and sloshing force is tried for the patentability. The rectangular sloshing tank is subjected to sinusoidal excitations with frequencies ranging from 0.4566 Hz to 1.9757 Hz which covers up to fifth mode sloshing frequency to test the effectiveness of vertical screens in mitigating liquid sloshing. An sinusoidal excitation amplitude of 8 mm is considered. For no baffle condition experimental results are compared with numerical model of Nasar et al.(2012). Whereas, experimental results of porous baffle conditions are validated with simulation results obtained from ANSY-FLUENT. The experimental results are found to be good agreement with numerical results for no baffle conditions.

7.2 CONCLUSIONS

In the current work comparison of the sloshing effect (sloshing base shear forces, free surface elevation and screen forces) with and without porous baffles are done with two different fill levels. In present study, tank with and without baffle having excitation frequency and amplitude, from above calculation and analysis the following conclusion

is made. The study also focuses on the dynamic response and the performance of the porous baffles placed at $L/3$ and $2L/3$ locations for both acrylic plate and mild steel plate. The main objective of the investigation was to assess the sloshing effects in sway excited rectangular tank with and without porous baffles and validate same with the computational fluid dynamics. A series of shake table experiments were completed under sinusoidal excitation for an amplitude of 8 mm. In the present work comparison of the sloshing effect (sloshing base shear forces, free surface elevation and screen forces) with and without porous baffles (acrylic plate and Ms plate) are done with three different fill levels. The main objective of the investigation was to assess the effects of sloshing in sway excited rectangular tank with and no porous baffles.

- A range of excitation frequencies from 0.46 Hz to 3.2 Hz which encompasses up to fifth mode natural frequencies has been investigated by experimental work to test the efficiency of vertical screens in mitigating liquid sloshing.
- Due to the presence of the porous baffle the damping is increases in the partially filled sway excited rectangular tank. It can be concluded that porous baffle walls are very effective in reducing the sloshing effects compared to without baffle wall conditions.
- With graphical illustration, it is found that the increasing liquid filling level in the rectangular tank will increase the nonlinearity of the liquid motion during the sloshing.
- Installing a vertical baffle at the centre of the rectangular tank can greatly reduce the liquid sloshing motion and sloshing impact pressure on the wall and ceiling. The maximum impact pressure for the tank with baffle is reduced nearly 40% comparing with the cases without baffle on the bottom of the tank.
- In multiple baffled tanks, the baffle position at the mid possesses the most effective sloshing reduction in comparison with the $L/2$ location and $L/3$ & $2L/3$ locations.
- It has been known that the first mode of the fluid's natural frequency is the resonant frequency. This is because the results of the free surface elevation tests show that the fluid's free surface elevation can vary with the varying frequency ratios.

- It can be concluded that baffles significantly reduce the liquid motion and consequently the force response. Baffles alter the free surfaces sloshing mode shapes and reduce natural sloshing frequencies.
- The tank with a water depth of $h_w/l= 0.325$ and porous baffle of 15% porosity shows attenuation in sloshing force of about 32.78% whereas the 20% and 25% porosities of baffles show attenuation of 39.74% and 38.86% respectively in comparison with no baffle condition at $L/3$ & $2L/3$ locations.
- The sloshing tank with baffles placed at $L/3$ & $2L/3$ of $h_w/l= 0.325$ and with a porosity of 15% gives a better reduction in sloshing effect by 84%.
- It can be concluded that the use of baffles can reduce the fluid motion, and this effect is also reflected in the force response. However, the effect of the forcing frequency on the sloshing is not as pronounced when the system is at the natural frequency.
- The numerical study shows a good correlation with the experiment results and the deviation of numerical simulation in comparison with experimental findings is found to be 9.24%.

7.3 FUTURE SCOPES

- In the present study, vertical baffles are considered. Combination of horizontal and vertically placed baffles can be considered to study the sloshing effects, to reduce the run-up on the end the walls and to reduce the on the top panel.
- The flexibility of the baffle can be considered in simulating ANSYS-Fluent.
- Porosity with finer interval can be considered.
- Sloshing experiment can be carried out for random excitations to simulate the earthquake conditions.

REFERENCES

- Akyildiz, H. and Ünal, E. (2005). "Experimental investigation of pressure distribution on a rectangular tank due to the liquid sloshing." *Ocean Eng.*, 32(11), 1503-1516.
- Akyildiz, H., and Ünal, N. E. (2006). "Sloshing in a three-dimensional rectangular tank: numerical simulation and experimental validation." *Ocean Eng.*, 33(16), 2135-2149.
- Akyildiz, H. (2012). "A numerical study of the effects of the vertical baffle on liquid sloshing in two-dimensional rectangular tank." *J. of Sound and Vibration*, 331(1), 41-52.
- Armenio, V. and La Rocca, M. (1996). "On the analysis of sloshing of water in rectangular containers: numerical study and experimental validation." *Ocean Eng.*, 23(8), 705-739.
- Belakroum, R., Kadja, M., Mai, T. H. and Maalouf, C. (2010). "An efficient passive technique for reducing sloshing in rectangular tanks partially filled with liquid." *Mechanics Research Communications*, 37(3), 341-346.
- Biswal, K. C., Bhattacharyya, S. K. and Sinha, P. K. (2004). "Dynamic response analysis of a liquid-filled cylindrical tank with annular baffle." *J. of Sound and Vibration*, 274(1), 13-37.
- Cavalagli, N., Biscarini, C., Facci, A. L., Ubertini, F., and Ubertini, S. (2017). "Experimental and numerical analysis of energy dissipation in a sloshing absorber." *J. of Fluids and Structures*, 68, 466-481.
- Cho, J. R., Lee, H. W. and Ha, S. Y. (2005). "Finite element analysis of resonant sloshing response in 2-D baffled tank." *J. of Sound and Vibration*, 288(4), 829-845.
- Cho, I. H., Choi, J. S. and Kim, M. H. (2017). "Sloshing reduction in a swaying rectangular tank by an horizontal porous baffle." *Ocean Eng.*, 138, 23-34.
- Cho, I. H. (2021). "Liquid sloshing in a swaying/rolling rectangular tank with a flexible porous elastic baffle." *Marine Structures*, 75, 102865.

Dong, C. (2015). "Modelling and simulation of sloshing motion in partly filled tank." Master's thesis, *Aalesund University College*.

Evans, D. V. and McIver, P. (1987). "Resonant frequencies in a container with a vertical baffle." *J. of Fluid Mechanics*, 175, 295-307.

Frandsen, J. B. (2004). "Sloshing motions in excited tanks." *J. of Computational Physics*, 196(1), 53-87.

Faltinsen, O. M. and Timokha, A. N. (2011). "Natural sloshing frequencies and modes in a rectangular tank with a slat-type screen." *J. of Sound and Vibration*, 330(7), 1490-1503.

Godderidge, B., Turnock, S., Tan, M. and Earl, C. (2009). "An investigation of multiphase CFD modelling of a lateral sloshing tank." *Computers & Fluids*, 38(2), 183-193.

Goudarzi, M. A., Sabbagh-Yazdi, S. R. and Marx, W. (2010). "Investigation of sloshing damping in baffled rectangular tanks subjected to the dynamic excitation." *Bulletin of Earthquake Eng.*, 8(4), 1055-1072.

Goudarzi, M. A. and Sabbagh-Yazdi, S. R. (2012). "Analytical and experimental evaluation on the effectiveness of upper mounted baffles with respect to commonly used baffles." *Ocean Eng.*, 42, 205-217.

Hejazi, F. S. A., and Mohammadi, M. K. (2019). "Investigation on sloshing response of water rectangular tanks under horizontal and vertical near fault seismic excitations." *Soil Dynamics and Earthquake Eng.*, 116, 637-653.

Hu, Z., Zhang, X., Li, X. and Li, Y. (2018). "On natural frequencies of liquid sloshing in 2-D tanks using Boundary Element Method." *Ocean Eng.*, 153, 88-103.

Hou, L., Li, F. and Wu, C. (2012). "A numerical study of liquid sloshing in a two-dimensional tank under external excitations." *J. of Marine Science and Application*, 11(3), 305-310.

- Ibrahim, R. A. (2005). "Liquid sloshing dynamics: theory and applications." *Cambridge University Press*.
- Isaacson, M. and Premasiri, S. (2001). "Hydrodynamic damping due to baffles in a rectangular tank." *Canadian Journal of Civil Eng.*, 28(4), 608-616.
- Jin, H, Liu, Y. and Li, H. J. (2014). "Experimental study on sloshing in a tank with an inner horizontal perforated plate." *Ocean Eng.*, 82, 75-84.
- Jin X Tang J Tang X Mi S Wu J Liu M and Huang Z (2020). Effect of viscosity on sloshing in a rectangular tank with intermediate liquid depth. *Experimental Thermal and Fluid Science*, 118, 110-148.
- Jin X Liu M Zhang F and Li D (2022). Mitigation of liquid sloshing by multiple layers of dual horizontal baffles with equal/unequal baffle widths. *Ocean Engineering*, 263, 112184.
- Jung, J. H, Yoon, H. S, and Lee, C. Y. (2015). "Effect of natural frequency modes on sloshing phenomenon in a rectangular tank." *International J. of Naval Architecture and Ocean Eng.*, 7(3), 580-594.
- Jung, J. H., Yoon, H. S., Lee, C. Y. and Shin, S. C. (2012). "Effect of the vertical baffle height on the liquid sloshing in a three-dimensional rectangular tank." *Ocean Eng.*, 44, 79-89.
- Kamath A Grotle EL and Bihs H (2021). Numerical investigation of sloshing under roll excitation at shallow liquid depths and the effect of baffles. *Journal of Marine Science and Application*, 20(2), 185-200.
- Kumar, A. and Sinhamahapatra, K. P. (2016). "Dynamics of rectangular tank with perforated vertical baffle." *Ocean Eng.*, 126, 384-401.
- Kumaran, V., Neelamani, S., Vijay, K. G., Al-Anjari, N., and Al-Ragum, A. (2022). "Wave attenuation by multiple slotted barriers with a zig-zag arrangement-A physical and numerical approach." *Journal of Hydro-environment Research*, 41, 25-37.

- Kingsley, T. C. and Craig, K. J. (2007). "Design optimization of containers for sloshing and impact." *Struct. and Multidisciplinary Optimization*, 33(1), 71-87.
- Kim, S. P., Chung, S. M., Shin, W. J., Cho, D. S., and Park, J. C. (2018). "Experimental study on sloshing reduction effects of baffles linked to a spring system." *Ocean Eng.*, 170, 136-147.
- Liu, Z., Feng, Y., Lei, G., and Li, Y. (2019). "Fluid sloshing dynamic performance in a liquid hydrogen tank." *International Journal of Hydrogen Energy*, 44(26), 13885-13894.
- Liu, Z., Feng, Y., Lei, G., and Li, Y. (2019). "Hydrodynamic performance in a sloshing liquid oxygen tank under different initial liquid filling levels." *Aerospace Science and Technology*, 85, 544-555.
- Liu, Z., Feng, Y., Lei, G., and Li, Y. (2019). "Sloshing hydrodynamic performance in cryogenic liquid oxygen tanks under different amplitudes." *Applied Thermal Engineering*, 150, 359-371.
- Liu, Z., Feng, Y., Liu, Y., Lei, G., and Li, Y. (2020). "Fluid sloshing dynamic performance in a fuel storage tank under sinusoidal excitations." *Applied Thermal Engineering*, 168, 114814.
- Lin, B. H., Chen, B. F., and Tsai, C. C. (2019). "Method of fundamental solutions on simulating sloshing liquids in a 2D tank." *Computers & Mathematics with Applications*.
- Maleki, A. and Ziyaeifar, M. (2008). "Sloshing damping in cylindrical liquid storage tanks with baffles." *J. of Sound and Vibration*, 311(1), 372-385.
- Neves, M. A. S., Fonfach, J. M. and Manderbacka, T. (2016). "Numerical sloshing simulations: Comparison between lagrangian and lumped mass models applied to two compartments with mass transfer." *Ocean Eng.*, 114, 168-184.

- Nema, P. K. (2014). “Computational study of sloshing behaviour in 3-D rectangular tank with and without baffle under seismic excitation.” Master thesis, *National Institute of Technology, Rourkela*.
- Ning, D. Z., Song, W. H., Liu, Y. L. and Teng, B. (2012). “A boundary element investigation of liquid sloshing in coupled horizontal and vertical excitation.” *J. of Applied Mathematics*, 2012.
- Niraj K. (2013). “Study of Sloshing Effects in a Cylindrical Tank with and without Baffles under Linear Acceleration.” Doctoral dissertation, *National Institute of Technology, Rourkela*.
- Nasar, T., Sannasiraj, S. A. and Sundar, V. (2008). “Experimental study of liquid sloshing dynamics in a barge carrying tank.” *Fluid Dynamics Research*, 40(6), 427-458.
- Nasar, T., Sannasiraj, S. A. and Sundar, V. (2009). “Wave-induced sloshing pressure in a liquid tank under irregular waves.” *Proc., of the Institution of Mechanical Engineers, J. of Engineering for the Maritime Environment*, 223(2), 145-161.
- Nasar, T. and Sannasiraj, S. A. (2019). “Sloshing dynamics and performance of porous baffle arrangements in a barge carrying liquid tank.” *Ocean Engineering*, 183, 24-39.
- Nayak, S. K. and Biswal, K. C. (2015). “Fluid damping in rectangular tank fitted with various internal objects—An experimental investigation.” *Ocean Eng.*, 108, 552-562.
- Pal, N. C., Bhattacharyya, S. K., and Sinha, P. K. (2001). “Experimental investigation of slosh dynamics of liquid-filled containers.” *Experimental Mechanics*, 41(1), 63-69.
- Panigrahy, P. K., Saha, U. K. and Maity, D. (2009). “Experimental studies on sloshing behaviour due to horizontal movement of liquids in baffled tanks.” *Ocean Eng.*, 36(3), 213-222.
- Park, W. M., Choi, D. K., Kim, K., Son, S. M., Oh, S. H., Lee, K. H., and Choi, C. (2020). “Simple analytical method for predicting the sloshing motion in a rectangular pool.” *Nuclear Engineering and Technology*, 52(5), 947-955.

Qin, H., Mu, L., Tang, W., and Hu, Z. (2019). “Numerical study on structural response of anti-sloshing baffles of different configurations in a sloshing tank considering hydroelasticity.” *Ocean Eng.*, 188, 106290.

Qiu Y Bai M Liu Y Lei G and Liu Z (2022). Effect of liquid filling level on sloshing hydrodynamic characteristic under the first natural frequency. *Journal of Energy Storage*, 55, 105452.

Radnic, J., Grgic, N., Kusic, M. S, and Harapin, A. (2018). “Shake table testing of an open rectangular water tank with water sloshing.” *Journal of Fluids and Structures*, 81, 97-115.

Saghi, H. and Ketabdari, M. J. (2012). “Numerical simulation of sloshing in rectangular storage tank using coupled FEM – BEM.” *J. of Marine Science and Application*, 11(4), 417.

Saghi, H., Ning, D. Z., Cong, P. W., and Zhao, M. (2020). “Optimization of baffled rectangular and prismatic storage tank against the sloshing phenomenon.” *China Ocean Eng.*, 34(5), 664-676.

Saghi, H., Mikkola, T., and Hirdaris, S. (2021). “The influence of obliquely perforated dual-baffles on sway induced tank sloshing dynamics.” *Journal of Engineering for the Maritime Environment*, 235(4), 905-920.

Singal, V., Bajaj, J., Awalgaonkar, N. and Tibdewal, S. (2014). “CFD analysis of a kerosene fuel tank to reduce liquid sloshing.” *Proc., Eng.*, 69, 1365-1371.

Saoudi, Z., Hafsia, Z. and Maalel, K. (2013). “Dumping effects of submerged vertical baffles and slat screen on forced sloshing motion.” *J. Water Resource. Hydraulics. Engg*, 2(2), 51-60.

Stephen, J. J., Sannasiraj, S. A., and Sundar, V. (2019). “Numerical modeling of nonlinear sloshing of liquid in a container coupled with barge subjected to regular excitation.” *Journal of Hydrodynamics*, 31(5), 999-1010.

- Thuvanismai, N., Sannasi, S., and Vallam, S. (2012). "Liquid sloshing dynamics in a barge carrying container subjected to random wave excitation." *J. Naval Architecture and Marine Eng.*, 9(1), 43-65.
- Tsao, W. H., and Huang, Y. L. (2021). "Sloshing force in a rectangular tank with porous media." *Results in Engineering*, 11, 100250.
- Vijayalakshmi, K. (2005). "Hydrodynamic of a perforated circular caisson enriching a vertical cylinder." Ph.D. thesis, *Indian Institute of Technology, Madras, India*.
- Warnitchai, P., and Pinkaew, T. (1998). "Modelling rectangular Dampening of liquid sloshing in tanks with flowdevices." *Engineering Structures*, 20(7), 593-600.
- Wang, W. and Xiong, Y. P. (2014). "Minimising the sloshing impact in membrane LNG tank using a baffle." *University of Southampton, Highfield, Southampton SO17 1BJ, UK*.
- Wang, W., Peng, Y., Zhou, Y., and Zhang, Q. (2016). "Liquid sloshing in partly-filled laterally-excited cylindrical tanks equipped with multi baffles." *Applied Ocean Research*, 59, 543-563.
- Wang, W., Peng, Y., Zhang, Q., Ren, L., and Jiang, Y. (2017). "Sloshing of liquid in partially liquid filled toroidal tank with various baffles under lateral excitation." *Ocean Eng.*, 146, 434-456.
- Wang, W., Zang, Q., Wei, Z., and Guo, Z. (2019). "An isogeometric boundary element method for liquid sloshing in the horizontal eccentric annular tanks with multiple porous baffles." *Ocean Eng.*, 189, 106367.
- Xue, M. A., Lin, P. Z., Zheng, J. H., Ma, Y. X., Yuan, X. L., and Nguyen, V. T. (2013). "Effects of perforated baffle on reducing sloshing in rectangular tank: experimental and numerical study." *China Ocean Eng.*, 27(5), 615-628.
- Xue, M. A., Zheng, J., Lin, P. and Yuan, X. (2017). "Experimental study on vertical baffles of different configurations in suppressing sloshing pressure." *Ocean Eng.*, 136, 178-189.

Yu, L., Xue, M. A., and Zheng, J. (2019). “Experimental study of vertical slat screens effects on reducing shallow water sloshing in a tank under horizontal excitation with a wide frequency range.” *Ocean Eng.*, 173, 131-141.

Zhang, A. M., Cao, X. Y. and Ming, F. R. (2014). “Sloshing in a rectangular tank based on SPH simulation.” *Applied Ocean Research*, 47, 241-254.

Zheng JH Xue MA Dou P and He YM (2021). A review on liquid sloshing hydrodynamics. *Journal of Hydrodynamics*, 33(6), 1089-1104.

Zhang, G. Y., Zhao, W. W., and Wan, D. C. (2022). “Numerical simulations of sloshing waves in vertically excited square tank by improved MPS method.” *Journal of Hydrodynamics*, 34(1), 76-84.

Appendix A

ERROR ANALYSIS

A.1 General

The measured data from any experiment is subject to uncertainties due to a number of factors. These can be classified as those which can be eliminated, those which cannot be eliminated or minimized. The main objective of the error analysis is to quantify the unavoidable errors and to estimate gross errors. In other words, the uncertainties in the measurement system are to be estimated.

Errors in experimental observations are gross errors, systematic errors and random errors. Gross errors (also called blunders) are mostly human errors. These includes mistakes in reading instruments, using wrong settings, making wrong entries, and doing wrong calculations on measurement results. These errors do not follow any statistical description and cannot be easily eliminated. But these can be avoided by taking great care and repeating the measurements. Systematic errors are errors which could be evaluated and, in most cases, can be corrected. These can be instrumental errors, environmental errors, and observational errors. Instrumental errors occur due to defects in the instruments, improper use, loading errors etc. An example of improper use is that of using the instrument outside its range. Loading effect means the changes in the measured quantity due to the introduction of the measuring instrument. Environmental errors include the errors due to variations in temperature, pressure, humidity, and external magnetic fields. These errors can be eliminated or reduced keeping environmental parameters constant during the period of observation, using instruments like self-compensating gauges and vacuum sealed instruments. These can also be corrected by computing the errors due to the above factors. Observational errors occur due to errors in reading the instrument like parallax error. This also depends on the person taking the readings. In spite of the precision of the instrument, two persons may record different readings.

In the present experimental study, the various data from the different instruments were acquired through a computer-based system and hence most of the observational and recording errors are eliminated. The auto zero adjustment in the data acquisition system

minimizes the zero error to negligible values. The calibration factors were incorporated in the data acquisition program and thus, the possible mistakes in computation were also reduced. The uncertainties in the calibration and measurement stages for all the instruments in the system are estimated.

A.2 Most Probable Value and Confidence Interval

The total error in a measuring system occurs due to various factors and is found to be normally distributed. This is because due to the central limit theorem, the variation in the sum of several random variables, which may be having different distributions, (not necessarily normal) is normally distributed. The primary aim of error analysis is to estimate the reliability of the measurement. For this, one has to determine the most probable value of the measured parameter and the probability that it lies within a specified range. Normally, the results are reported as the most probable value of the measured parameter and the probability that it lies within a specified range. Normally the results are reported as the most probable value and the 95% confidence interval. The most probable value is the value around which the observation would fall and for infinite number of observations (termed as population); this value would be the arithmetic mean. The 95% confidence interval is the range in which the observations would lie with a probability of 95%. For large samples, this value ranges from -2σ to $+2\sigma$, where σ is the standard deviation.

A.3 Determination of Uncertainty for Linear Regression

The general method for determining the best fitting straight line for a set of data is the method of least squares or linear regression. The general form of the linear equation is given by;

$$y = a_0 + a_1x \tag{A.1}$$

where a_0 and a_1 represent the intercept and slope of the line, respectively. In linear regression, the value of a_0 and a_1 are found out such that the sums of the squares of the errors are minimum.

The linear regression methodology has been used to estimate the uncertainties in the estimation of the calibration factors for the run-up probes, LVDT and LOAD cells. The details are briefed in the following sections.

A.4 Example analysis

As an example, the details of error estimation for the calibration factor of a runup probe are illustrated in this section. The runup probes were calibrated by immersing them into the water by a known depth and the corresponding voltage variations were noted. A typical calibration reading for a runup probe is given in Table A.1.

The estimated uncertainties of each instrument expressed as percentage of their respective slope of the regression fit (a_1) with 95% confidence are given in Table A.2.

Table A.1 Calibration readings for a run-up probe

Depth of submergence (cm)	Voltage (mV)
16.5	480.23
19.5	516.46
22.5	551.18
25.5	578.7
28.5	605.56
31.5	634.69
34.5	666.2
37.5	691.77
40.5	725.13
43.5	754.98
46.5	785.34
49.5	819.13
52.5	853.41
55.5	890.8

Table A.2 Percentage error for various instruments

Instrument	Calibration factor (a_1)	Uncertainty as percentage of a_1 with 95% confidence
Runup probe 1	0.0782 m/V	0.0847%
Runup probe 2	0.0743 m/V	0.0698%
Accelerometer 1	2.392 m/s ² /V	0.193%
Accelerometer 2	2.576 m/s ² /V	0.145%
Load cell 1	0.0468 N/mV	0.1664%
Load cell 2	0.0512 N/mV	0.1668%
LVDT	0.0468 mm/mV	0.1489%

LIST OF JOURNAL PUBLICATIONS

1. **Sahaj K. V.**, T. Nasar and Vijay K. G. (2021) “Experimental Study on Liquid Sloshing with dual Vertical Porous Baffles in a Sway Excited Tank”. *Ocean Systems Engineering. Vol.11, No.4 (2021) 353-371.*
2. **Sahaj K. V.**, Shwetha shri and T. Nasar “Sloshing Dynamics in a Sway Excited Rectangular Scaled Tanks”. *Journal of Marine Science and Application* (under review).
3. **Sahaj K. V.**, Kumaran V. and T. Nasar “Sloshing dynamics with a Vertical Porous Baffle in a Sway Excited Tank- Physical and Numerical Approach”. *Ships and Offshore Structures* (Under review).
4. Chithuloori Pravallika., **Sahaj K. V.**, T. Nasar and Jin Man Kim “Liquid Sloshing in Laterally excited tank Equipped with single baffle”. *Journal of Hydrodynamics* (Under review).

NATIONAL/INTERNATIONAL CONFERENCES

1. **Sahaj K. V.** and T. Nasar “Experimental Study on Liquid Sloshing Dynamics in a Sway Excited Rectangular Tank” Proceedings of National Conference on Advances in Structural Technologies (CoAST-2019), 1st-3rd Feb, 2019. Department of Civil Engineering. NIT Silchar, Assam, India.
2. **Sahaj K. V.** and T. Nasar “Experimental and Numerical Study on Liquid Sloshing Dynamics with Single Vertical Porous Baffle in a Sway Excited Ship Tank, EGU General Assembly 2020, Online, 4–8 May 2020, EGU2020-929, <https://doi.org/10.5194/egusphere-egu2020-929>.
3. **Sahaj K. V.** and T. Nasar “Effectiveness of Porous Baffle on Resonance Sloshing Motion: An Experimental Study”, proceedings in 2nd International conference on recent advances in fluid and thermal science (ICRAFT 2020), 19th-21st March, 2021. BITS Pilani, Dubai.

4. **Sahaj K. V.**, Pavan Kumar and T. Nasar “Effect of porous baffle on sloshing dynamics placed at $L/2$ location in a sway excited rectangular tank”, HYDRO 2020 – International conference on hydraulics, water resources and coastal engineering, 26th – 28th March, 2021. NIT Rourkela, Odisha, India. (ISBN 978-93-90631-56-8).
5. **Sahaj K. V.**, Shwetha shri and T. Nasar “Experimental Study on Liquid Sloshing Dynamics in a Sway Excited Rectangular Tank”, 23rd Congress of the International Association for Hydro-Environment engineering and research Asia and Pacific Division 14th -17th December, 2022. Department of Ocean Engineering. IIT Madras, Chennai, India.
6. **Sahaj K. V.**, and T. Nasar “Effect of porous baffles on sloshing dynamics placed at $L/3$ and $2L/3$ locations in a sway excited rectangular tank”, 8th Asian conference on mechanics of functional materials and structures (ACMFMS 2022), 11th to 14th December 2022, IIT Guwahati, Assam, India.
7. **Sahaj K. V.**, Kesava Chatla and T. Nasar “Effect of Porous Baffle on Sloshing Dynamics in a Sway Excited Ship Tank”, HYDRO 2022 – International conference on hydraulics, water resources and coastal engineering, 22th – 24th December, 2022. Punjab engineering College, Chandigarh, India.

CURRICULUM VITAE



NAME: SAHAJ K V

PERMANENT ADDRESS: S/o Kanthappa Alangar,
Door No. 6-156/16, “Shravasthi”
1st Cross Abbakka Nagar Road,
Padubettu, Kottara
Mangaluru, Karnataka - 575006

EDUCATION: MASTER OF TECHNOLOGY
Discipline: Structural Engineering
Sahyadri College of Engineering and Management, Mangaluru,
Karnataka
Affiliated to: Visvesvaraya Technological University,
Belgaum.

BACHELOR OF ENGINEERING
Discipline: Civil Engineering
Vivekananda College of Engineering and Technology, Puttur
Mangaluru, Karnataka
Affiliated to: Visvesvaraya Technological University,
Belgaum.

CONTACT NO.: +91-9980083955

EMAIL ID: sahaj30.k.v@gmail.com

ORCID: <https://orcid.org/0000-0006-9727-523X>
